ANALYTICAL CHEMISTRY TO DECIPHER THE COLORS OF POMPEII BEFORE AND AFTER THE 79 AD MOUNT VESUVIUS ERUPTION

This PhD Thesis has been developed in the Analytical Chemistry Department from the University of the Basque Country

(Faculty of Science and Technology, Leioa, Spain)

IKER MARCAIDA ORMAZABAL

LEIOA, DECEMBER 2019

ANALYTICAL CHEMISTRY TO DECIPHER THE COLORS OF POMPEII BEFORE AND AFTER THE 79 AD MOUNT VESUVIUS ERUPTION

By

Iker Marcaida Ormazabal

Directors

Juan Manuel Madariaga Mota

Prof. of Analytical Chemistry

University of the Basque Country

Maite Maguregui Hernando

Prof. of Analytical Chemistry

University of the Basque Country

PhD manuscript presented to apply for Doctor Degree in the University of the Basque Country (UPV/EHU)

IKER MARCAIDA ORMAZABAL

LEIOA, DECEMBER 2019

AKNOWLEDGEMENTS

Iker Marcaida, the author of this PhD Thesis, is grateful to the Basque Government for funding his predoctoral fellowship.

This PhD Thesis has been funded by the Ministry of Economy and Competitiveness (MINECO) and the European Regional Development Fund (FEDER) through the project DISILICA-1930 (2014-59124-P) together with funding from the AEI, Agencia Estatal de Investigación (FEDER/UE), through the project MADyLIN (2017-87063-P).

I would like also to thank the Naples National Archaeological Museum and to the Archaeological Park of Pompeii, concretely to the Applied Research Laboratory, for the permissions given to perform the in situ measurements of the powdered pigments contained in their original bowls recovered from the burial, and also to analyze in situ the Pompeian wall paintings. In fact, this PhD Thesis has been developed within the framework of the two agreements signed between the Archaeological Park of Pompeii and the University of the Basque Country (UPV/EHU). Besides, I would also like to thank to the *Expeditio Pompeiana Universitatis Helsingiensis* (EPUH) for transfer us the wall painting fragments recovered from the burial of the House of Marcus Lucretius.

Moreover, I want also to thank to the “Cátedra Unesco de Paisajes Culturales y Patrimonio” for funding the three months international stay in the “Jozef Stefan Institut” (Ljubljana, Slovenia) and to the Basque Government for giving me the possibility of performing an additional stay of three months in the “Instituto de Estructura de la Materia” from the “Consejo Superior de Investigaciones Científicas (CSIC)” in Madrid (Spain).

TABLE OF CONTENTS

1. INTRODUCTION 1

1.1. The timeline of Pompeii: From the origins to the eruption of 79 AD 2

1.2. The discovery of Pompeii. Back to life of the ancient city 4

1.3. Distribution of the ancient city of Pompeii and the Roman *domus* 5

1.4. The wall decorations in Pompeii 9

1.5. The Pompeian pigment palette: Original colors, degradations and transformations 13

1.6. Evolution of the scientific interest in the characterization of the pigments used in the wall paintings of Pompeii 15

1.7. Traditional and emerging analytical techniques and methodologies to analyze powder pigments or those used in wall paintings 18

1.8. References 30

2. OBJECTIVES OF THE PhD THESIS 41

3. EXPERIMENTAL PART 45

3.1 Pompeian powdered pigments 48

3.1.1 Pigments preserved in the Naples National Archaeological Museum 48

3.1.2 Pigment powders from the Applied Research Laboratory of Pompeii 49

3.2 Standards, reagents and apparatus 50

3.2.1 Standards 50

3.2.2 Reagents 51

3.2.3 The muffle used for the thermal ageing experiments 52

3.3 Molecular handheld/portable spectroscopic instrumentation 52

3.3.1 Portable Raman spectrometers 52

3.3.2 Handheld Diffuse Reflectance Infrared Fourier Transform spectrometer 55

3.3.3 Field reflectance Visible-Near Infrared-Short Wave Infrared (VNIR-SWIR) spectroradiometer....56
3.4 Elemental handheld/portable spectroscopic instrumentation....57
3.4.1 Handheld energy dispersive X-ray fluorescence spectrometers (HH-EDXRF)....57
3.4.2 Laser induced breakdown spectrometer (LIBS)....59
3.5 Analytical techniques to determine the molecular composition of the pigments in the laboratory....61
3.5.1 Raman micro-spectroscopy....61
3.5.2 Infrared spectroscopy (IR)....63
3.5.3 X-ray diffraction (XRD)....64
3.6 Analytical techniques to determine the elemental composition of the pigments in the laboratory....65
3.6.1 Scanning electron microscope couple to energy dispersive X-ray fluorescence spectrometry (SEM-EDS)....65
3.6.2 Energy dispersive X-ray fluorescence spectrometry (EDXRF)....66
3.6.3 Inductively coupled plasma-mass spectrometry (ICP-MS)....68
3.6.4 Thermal Ionization Mass Spectrometry (TIMS)....69
3.6.5 Stable isotopes analysis through isotope ratio mass spectrometry coupled to an elemental analyzer (EA-IRMS)....70
3.7 Synthesis of Ag-NPs and verification of their usefulness for the SERS analysis....71
3.8 Data treatment by chemometrics....72
3.9 References....73

RESULTS AND DISCUSION....75

PART 1. IN SITU AND LABORATORY METHODOLOGIES TO CHARACTERIZE INORGANIC AND LAKE PIGMENT POWDERS FROM POMPEII....79

4. IN SITU CHARACTERIZATION OF INORGANIC AND LAKE PIGMENTS FROM POMPEII 83

4.1 Introduction 83
4.2 Samples 87
4.3 Green pigments 89
4.4. Pink pigments 91
4.5 Blue pigments 94
4.6 White pigment 98
4.7 Yellow pigments 100
4.8 Red pigments 103
4.9 Conclusions 107
4.10 References 109

5. LABORATORY CHARACTERIZATION OF RED AND YELLOW OCHRE PIGMENTS *113*

5.1 Introduction 113
5.2 Samples 116
5.3 Molecular characterization of the Pompeian ochres 117
5.3.1 Major mineral phases in red and yellow ochre pigments under study 117
5.3.2 Minor and trace mineral phases identified by Raman spectroscopy 120
5.3.3 Identification of possible contaminations by Raman microscopy 124
5.4 Elemental characterization of red and yellow ochre pigment powders and multivariate analysis 127
5.4.1 Multivariate analysis of the elemental data 128
5.4.2 Tungsten and tin as geochemical markers for provenance tracing 132
5.5 Lead isotopic ratio analysis 134
5.6 Conclusions 137
5.7 References 140

6. CHEMICAL-MINERALOGICAL CHARACTERIZATION OF THE INORGANIC MORDANT USED TO MANUFACTURE POMPEIAN PINK LAKE PIGMENTS 145

6.1 Introduction 145
6.2 Samples and sampling strategy 147
6.3 In situ HH-EDXRF analysis 147
6.4 Microscopic observations of the lake pigments in the laboratory 149
6.5 Laboratory non-invasive X-ray-based analytical techniques for the elemental characterization of the pink lake pigments 150
6.6 Major, minor, and trace elements quantification by ICP-MS and Pb isotope ratio analysis 155
6.7 Molecular analysis of the lake pigments in the laboratory 158
6.8 Conclusions 162
6.9 References 165

7. OPTIMIZATION OF A SERS-BASED METHODOLOGY TO IDENTIFY THE ORGANIC COLORANTS USED IN POMPEIAN PINK AND PURPLE LAKE PIGMENTS 169

7.1 Introduction 169
7.2 Samples and reagents 174
7.3 Evaluation of the synthesized silver nanoparticles (Ag-NPs) suitability for the SERS analysis and selection of the best analytical conditions 175
7.4. Sample treatment optimization 178
7.4.1 Study of the effectiveness of the organic solvents 181
7.4.2. Optimization of the volume of the organic solvent 183
7.4.3. Optimization of the mass 184
7.4.4. Selection of the laser excitation wavelength 185
7.5 SERS characterization of standards and Pompeian pink and purple lake pigments 186
7.6 Conclusions 190
7.7 References 191

PART 2. THE COLORS USED IN MOSAICS, TRANSFORMATION OF THE BINDER IN FRESCOES AND MODELLING OF THE YELLOW OCHRE PIGMENT TRANSFORMATION 197

8. MATERIALS USED TO OBTAIN THE COLORS IN POMPEIAN MOSAIC TESSERAE 203

8.1 Introduction 203
8.2 Mosaic description 207
8.3 Molecular characterization of the mosaics 208
8.3.1. Red and orange tesserae 209
8.3.2 White tesserae 210
8.3.3 Black tesserae 213
8.4 Elemental characterization of the mosaics 215
8.5 Conclusions 219
8.6 References 221

9. EVALUATION OF CALCIUM CARBONATE DEGRADATION IN THE WALL PAINTINGS THROUGH STABLE ISOTOPES ANALYSIS 225

9.1 Introduction 225
9.2 Description of the samples 228
9.3 Molecular characterization of the efflorescences 234
9.4 Stable isotope composition analysis 235
9.4.1 Carbon and oxygen isotopic composition analysis 235
9.4.2 Sulfur isotopic composition analysis 239
9.5 Conclusions 243
9.6 References 244

10. IN SITU EDXRF METHOD TO DIFFERENTIATE ORIGINAL RED OCHRES FROM TRANSFORMED YELLOW OCHRES INTO RED 247

10.1 Introduction 247

10.2 Description of the analyzed wall paintings 251

10.3 Raw pigments samples 255

10.4 In situ Raman analyses 255

10.5 In situ elemental analyses: HH-EDXRF vs. p-LIBS 256

10.6 Discrimination model based on Principal Component Analysis (PCA) of the HH-EDXRF results 261

10.7 EDXRF analysis of the red and yellow ochre raw pigments in the laboratory 265

10.8 Conclusions 267

10.9 References 269

11. MOLECULAR SPECTROSCOPIC TECHNIQUES TO CLASSIFY AND QUANTIFY THE THERMAL TRANSFORMATION DEGREE OF YELLOW OCHRE INTO RED 273

11.1 Introduction 273

11.2 Samples 277

11.3 Thermal ageing of the yellow ochre fragments 278

11.4 Classification model using reflectance spectroscopy 279

11.5 Transformation degree quantification using Raman imaging analysis 285

11.5.1 Elemental characterization of the fragments before the thermal ageing by means of μ-EDXRF imaging 285

11.5.2 Molecular characterization of the fragments before thermal ageing by means of Raman Imaging 288

11.5.3 Raman imaging quantification of goethite transformation degree as a function of thermal impact 289

11.6 Conclusions 297

11.7 References 300

12. FINAL CONCLUSIONS AND FUTURE WORKS 303

APPENDIX. SCIENTIFIC PUBLICATIONS 310

RESUMEN DE LA TESIS DOCTORAL

Esta tesis doctoral, titulada "**LA QUÍMICA ANALÍTICA PARA DESCIFRAR LOS COLORES DE POMPEYA ANTES Y DESPUÉS DE LA ERUPCIÓN DEL VOLCÁN VESUBIO EN EL AÑO 79 d. C**", se centra en la caracterización de los pigmentos y materiales que utilizaron los antiguos artistas de Pompeya para crear las pinturas murales y mosaicos, así como en el desarrollo de metodologías analíticas para determinar las transformaciones del color que se produjeron como consecuencia de la erupción del volcán Vesubio.

El yacimiento arqueológico de Pompeya es uno de los vestigios más representativos e importantes de la Antigua Roma que se conservan en la actualidad. Se trata de una antigua ciudad fundada en el siglo VII a. C., y que formó parte del Imperio Romano. Debido a la gran erupción del volcán Vesubio que tuvo lugar en el año 79 d. C., esta ciudad quedó enterrada bajo un manto de lapilli, cenizas volcánicas y depósitos piroclásticos, que hicieron que la ciudad se haya podido conservar durante los más de 17 siglos en los que ha estado enterrada. Fue en el año 1748 cuando Pompeya fue descubierta y, a raíz de este sorprendente hallazgo, dieron compiezo las excavaciones propiamente dichas para recuperar la ciudad arqueológica junto con diversos objetos escondidos de gran valor arqueológico. Entre ellos, se recuperaron diferentes elementos decorativos dentro de las casas o *domus* Pompeyanas como pinturas murales y mosaicos, o los pigmentos contenidos en sus boles originales de arcilla, utilizados para crear estas obras de arte.

Por un lado, para caracterizar qué materiales se emplearon para conseguir los diferentes colores y tonalidades que se pueden apreciar en las pinturas murales, en esta tesis se han analizado pigmentos en polvo recuperados del enterramiento en sus boles originales. Para su caracterización, se ha seleccionado principalmente instrumentación analítica portátil y no-invasiva. De este modo, los pigmentos se han podido analizar en el propio Parque Arqueológico de Pompeya o en el Museo Arqueológico de Nápoles, obteniendo

resultados concluyentes si se comparan con los que se pueden obtener en el laboratorio con equipos de sobremesa más costosos.

En este sentido, se determinó que la mayoría de los pigmentos usados provenían de materiales naturales, tales como tierras arcillosas ricas en hierro para obtener los ocres rojos y amarillos -principalmente compuestos por hematita (Fe_2O_3) y goethita (FeOOH) respectivamente- o de minerales con un color característico machacados hasta obtener un fino polvo, como por ejemplo la malaquita verde ($Cu_2CO_3(OH)_2$), el cinabrio rojo brillante (HgS) o la dolomita blanca ($CaMg(CO_3)_2$).

Además de estos, también se han identificado pigmentos producidos mediante procedimientos más sofisticados. De este modo, para la obtención del color azul, difícil de obtener en aquella época debido a la falta de disponibilidad de materiales naturales de dicho color, se llevaban a cabo reacciones químicas, como es el caso de la producción del pigmento azul egipcio ($CaCuSiO_4$), un silicato de calcio y cobre obtenido mezclando arena, minerales de cobre y fundentes a temperaturas mayores de 800 °C. Por último, un modo diferente de obtener polvos coloreados, era a partir de la tinción de tierras con un colorante orgánico. En este sentido, para obtener colores rosas o púrpuras, dicho colorante se extraía principalmente de las raíces de la planta *Rubia* o de la concha del molusco marino del género *Murex*. En esta tesis, se ha podido determinar el uso del colorante *madder lake*, extraído de las raíces de la planta *Rubia*. Además, se ha optimizado el procedimiento de tratamiento de muestra para el análisis SERS de dicho colorante con el objeto de obtener unos resultados concluyentes utilizando la menor masa posible de pigmento. Gracias a ello, utilizando 5 mg de pigmento se puede identificar inequívocamente la presencia en el pigmento del mencionado colorante orgánico.

En esta tesis doctoral se han podido identificar todos los pigmentos previamente mencionados, sin prácticamente tener que destruir muestra y devolviendo los polvos

analizados en su mismo estado de conservación. Se debe remarcar este último punto, ya que uno de los objetivos ha sido el desarrollo y aplicación de metodologías analíticas que permitieran la identificación de la composición química de los pigmentos analizados. Para tal fin, las técnicas analíticas que se han utilizado principalmente en esta tesis doctoral han sido la espectroscopia Raman y la fluorescencia de rayos X (XRF), en sus versiones de mano o portátiles, lo que permite la identificación en el propio depósito de los pigmentos. Para complementar los resultados obtenidos de manera *in situ*, también se emplearon la espectroscopia de plasma inducido por láser (LIBS) portátil y espectroscopia infrarroja (IR) en modo reflectancia total atenuada. En el laboratorio se emplearon técnicas variadas como IR, difracción de rayos X (XRD), espectrometría de masas con plasma acoplado inductivamente (ICP-MS) o espectrometría de masas con fuente de ionización térmica (TIMS).

A parte de pigmentos en polvo, uno de los objetivos de esta tesis fue caracterizar dichos materiales ya aplicados en diferentes soportes, para formar los famosos mosaicos o pinturas murales. Primeramente, antes de caracterizar los pigmentos ya aplicados, se ha estudiado el estado de conservación del soporte pictórico. Dado que la mayoría de pinturas murales presentes en Pompeya se realizaron utilizando la técnica de fresco, el responsable de cohesionar los granos de pigmento en el muro es la calcita ($CaCO_3$), la cual se forma tras carbonatarse con el CO_2 atmosférico. Para este propósito se realizaron diversos análisis isotópicos, sobre diversos fragmentos de mortero y pintura mural Pompeyana, de los elementos estables que forman dicha calcita, es decir, el C y O. Los resultados sobre la composición isotópica de C y O obtenidos de los fragmentos analizados deberían mostrar por tanto la composición isotópica del CO_2 antiguo responsable de fraguar el mortero. Las variaciones observadas desde el exterior hacia el interior indican que se han podido producir procesos de disolución y re-precipitación de la calcita debido a la exposición y contacto con el agua de lluvia/humedad actual, lo cual ha promovido la degradación del mortero original y la formación de carbonatos secundarios.

Además del análisis isotópico de C y O, también se realizado el de S, con el fin de determinar las fuentes responsables de la presencia de S en los morteros y también en las eflorescencias (sales cristalizadas en superficie) de reciente formación presentes en diferentes muros de casas Pompeyanas. En cuanto a las eflorescencias, se observaron dos grupos de valores diferentes, los cuales podrían indicar dos fuentes de S que promueven la formación de eflorescencias. Por un lado, la lixiviación de los compuestos de azufre presentes en el material volcánico que ha estado en contacto con los muros donde aparecen las sales, y por otro lado, la aplicación de morteros modernos de restauración, que pueden aportar y movilizar azufre que posteriormente cristaliza en la superficie. En cuanto a la composición isotópica de azufre en los morteros, se comprobaron también dos grupos diferentes con valores completamente dispares, lo cual indicaría el uso de diferentes materiales añadidos como agregados para formar los morteros de las casas Pompeyanas.

Una vez estudiado el estado de degradación del soporte pictórico, se ha procedido a investigar los pigmentos aplicados. De este modo, se han caracterizado las teselas que forman dos mosaicos independientes presentes en la *Casa de los Amorcillos Dorados*, dentro del Parque Arqueológico de Pompeya. En dichos mosaicos se apreciaban colores tales como el blanco, naranja, rojo y negro. Para la determinación de la composición química de cada uno de ellos, se utilizaron la técnica XRF de mano y LIBS portátil anteriormente mencionada. En este estudio se pudo concluir que, para producir las teselas blancas, se utilizó roca caliza cortada en piezas cúbicas, sin aplicación alguna de capa pictórica. Para conseguir el color rojo y naranja, sobre estas piezas, se utilizando ocre rojo como pigmento. Para alcanzar la tonalidad naranja, este pigmento fue diluido en la capa aplicada con calcita. Finalmente, para las teselas negras, en cambio, se emplearon rocas volcánicas negras, principalmente aluminosilicatos, las cuales estaban fácilmente disponibles en las cercanías de Pompeya debido a la naturaleza volcánica de la zona. Como se pudo comprobar, los antiguos artistas Pompeyanos explotaban al máximo

los recursos naturales disponibles en la época para obtener los materiales que necesitaban para crear sus obras de arte.

Además de los mosaicos, también se han estudiado las pinturas murales. Concretamente, paneles que presentan la transformación del color más evidente y notoria que se puede apreciar hoy día en Pompeya, la del color amarillo a rojo, causada por el impacto térmico de los materiales emitidos durante la erupción del 79 d.C. En concreto, se trata de la deshidratación del pigmento ocre amarillo, el cual es un óxido de hierro hidratado (FeOOH), que al ser impactado por los flujos de las diversas corriente piroclásticas emitidos por el volcán Vesubio, se deshidrató, transformándose a rojo (ocre rojo, Fe_2O_3). Dicha deshidratación puede darse en un rango de temperaturas entre 200-300 °C, temperatura que sin duda pudo alcanzarse en los eventos eruptivos del 79 d.C.

Actualmente, en algunas áreas de pinturas murales del Parque Arqueológico de Pompeya es bastante difícil diferenciar, a primera vista, entre las áreas rojas originales y las obtenidas de la transformación del pigmento amarillo. Para ello, se han desarrollado diferentes modelos de discriminación y cuantificación con objeto de diferenciar áreas pintadas originalmente en rojo o presentes debido a la transformación del amarillo a rojo. Estos modelos se basan en el análisis elemental o molecular de tres zonas diferentes: zonas pintadas originalmente en amarillo que no han sido transformadas, zonas pintadas originalmente en amarillo transformadas a rojo y zonas pintadas originalmente en rojo que no se han transformado. De este modo, mediante la aplicación de quimiometría a los datos obtenidos, se han podido desarrollar modelos de discriminación que permiten diferenciar los rojos que provienen de un amarillo de los que son originales. En este sentido, gracias a un modelo basado en el análisis elemental mediante XRF portátil, se ha determinado que la presencia de As trazaría la discriminación entre el rojo original (presencia) frente al rojo obtenido por transformación del amarillo (ausencia).

Por otro lado, se ha desarrollado un nuevo modelo basado en el tratamiento quimiométrico de los resultados moleculares obtenidos mediante espectroscopia de reflectancia en el Visible-Infrarrojo cercano-Infrarrojo de onda corta (Vis-NIR-SWIR) en su versión portátil. Este modelo no solo fue capaz de diferenciar rojos originales de los obtenidos por transformación del amarillo, sino que también permitió clasificar las zonas transformadas en función a la temperatura de impacto. Para este propósito se emplearon fragmentos de ocre amarillo reales recuperados del enterramiento de Pompeya, los cuales fueron expuestos a diferentes temperaturas en el rango entre 200 °C y 400 °C para simular el impacto que se produjo en la erupción del 79 dC. Estos mismos fragmentos envejecidos térmicamente también fueron empleados para el desarrollo de una metodología basada en imagen Raman a escala microscópica. Dicha metodología, totalmente cuantitativa, permitió determinar el grado de transformación del ocre amarillo en función a la temperatura de impacto. En este caso se pudo también confirmar que la transformación comienza a 200 °C y esta se completa a 275°C.

De este modo, gracias a la combinación de estos modelos se puede determinar mediante el análisis de las zonas de amarillo transformado a rojo, no solo el porcentaje de transformación, sino también la temperatura concreta que impactó en el año 79 d.C. y que promovió dicho cambio de color. Por lo tanto, estas pinturas murales que presentan la transformación de color actúan hoy día como testigos de la erupción acaecida hace 2000 años, pudiéndose emplear para construir un mapa del impacto térmico que tuvo lugar en la antigua Pompeya en función al análisis de los diferentes murales impactados.

1. INTRODUCTION

Pompeii is one of the most important archaeological sites in the world. Located in southern Italy, in Campania region, near Naples and on the slopes of Mount Vesuvius, this ancient Roman city is worldwide known for the catastrophe that took place in the year 79 AD, when the volcano erupted violently, burying the entire ancient city until 1738, when the first excavations started in Pompeii.

In 1997 Pompeii was added to the UNESCO World Heritage List[1] together with Herculaneum and Torre Annunziata considering "*the impressive remains of the towns of Pompeii, Herculaneum and their associated villas, buried by the eruption of Vesuvius in 79 AD, provide a complete and vivid picture of society and daily life at a specific moment in the past that is without parallel anywhere in the world"*.

Nowadays Pompeii is one of the most visited archaeological sites in the world, which attracted more than 3.5 million visitors[2] in the year 2018. According to the data offered by the Archaeological Park of Pompeii, until 2015 already 49 out of 66 hectares from the ancient city have been dug out[3]. However, only one third of the excavated area can be

visited. Pompeii still keeps secrets under the volcanic deposits. Hopefully, in the coming decades these archaeological records (Roman *domus*, wall paintings, sculptures, potteries…) will come to light and they will not only be enjoyed by visitors, but also they will be object of study of many researches belonging to different scientific fields such as chemistry, geology, archaeology, anthropology, etc. In this sense, it will be crucial to develop analytical methodologies useful to study the original materials used to create the recovered archaeological records and to diagnose possible deteriorations and/or transformations. All these information turn out to be crucial also to define suitable conservation strategies and materials to ensure the preservation of the valuable heritage hidden in this ancient Roman city.

1.1. The timeline of Pompeii: From the origins to the eruption of 79 AD

It is not completely known when Pompeii was founded. However, it is more than likely that a site so well adapted for a city was occupied in an early date. In this sense, the history of Pompeii seems to start in the 7th century BC according to *Geography*, the encyclopedia of geographical knowledge written by Strabo[4], a Greek geographer, philosopher and historian. As described in *Geography*, Oscans -Italic people from Campania- occupied Pompeii and Herculaneum in the mentioned century. After Oscans, other civilizations (Etruscans, Pelasgians and Samnites) settled in Pompeii until it was conquered by the Roman Empire in 89 BC. It is believed that local civilizations settled the area due to the convenient location as a crossroad between regions, its prosperous local and foreign commerce, its excellent naval and land transport connections and the fertility of its land for the agriculture. These factors were already known in that period, as Strabo described in his encyclopedia[4].

Because of that, in the year 89 BC, under the dictatorial period of Publio Cornelio Silla, Pompeii became a Roman colony called "*Veneria Cornelia Pompeianorum*". From this period, Pompeii was inevitably influenced by the Roman architecture and culture[5]. For some time, due to its closeness to the seacoast, Pompeii, together with Herculaneum, functioned as a summer resort for Roman wealthy people[6]. Apart from that, it was also used as a military colony. Under Roman control, lot of *domus* (Roman houses), the amphitheatre, Temples of Jupiter, Isis and Venus, Sarno and Stabian Baths, etc. were constructed. However, in the year 62 AD, a premonitory event took place. A massive earthquake toppled a big part of the city, promoting the flood of sophisticated mountain spring waterworks and the partial collapse of some buildings[7]. A sequence of seismic events, probably with similar magnitude, characterized the life of this Roman town from this year until the eruption of Mount Vesuvius in 79 AD. Although an inscription found last year dated the 79 AD eruption in the month of October[8], historically, this event has been placed in the 24th of August. This is the date mentioned in the transcription of the letters of *Pliny the Younger.* His uncle, *Pliny the Elder*, a Roman author, naturalist and naval commander of the early Roman Empire army, decided to go with a ship to take notes about this natural event and to help the inhabitants of Pompeii. Unfortunately, he died in his attempt, suffocated by the noxious vapors emitted by Mount Vesuvius. His nephew, *Pliny the Younger,* who watched the scene from the other side of the Bay, described the volcanic events in detail in his letters[9]. The information gathered from this description of the eruption gives modern scientists and volcanologists an idea about the type of the eruption. Although at that moment, *Pliny the Younger* was only a teenager, his description matches with what scientists have concluded later. Because of Pliny's accuracy in describing the eruption, these types of volcanic eruption have been named as "Plinian" eruptions. Whatever it is the real date, the truth is that Pompeii was buried, hidden and frozen for centuries under ashes, lapilli, and tephra deposits emitted by Mount Vesuvius.

1.2. The discovery of Pompeii. Back to life of the ancient city

In the year 1711, during the Austrian period in the Kingdom of Naples, some workers discovered an ancient statue when they were performing a well near Mount Vesuvius. However, when Austrian domination of Naples finished, the excavations were abandoned.

After the war and the Bourbon invasion[10], Charles of Bourbon (Carlo di Borbone in Italian) was proclaimed the King of Naples (as Charles VII) between year 1731 and 1759. In those years, he tried to reform and to modernize the kingdom, unifying it and conquering the affection of the citizens together with his wife Maria Amalia of Saxony.

One of the most important events under his mandate was the resumption of the excavations that shyly started in Pompeii and Herculaneum under Austrian domination in 1711. The results exceeded everything it was planned. All the new findings recovered in the excavations started in 1748 eclipsed the previous ones. At that time, it was not known all the treasures hidden under the trepha deposits. Although the luckiness was an important factor, the tenacity of the monarch and his vision of the future by promoting the works again allowed coming to light the amazing heritage of the ancient Pompeii and Herculaneum[10]. Surprisingly, all the recovered records were in a great conservation state. Actually, the volcanic material that buried the ancient city kept Pompeii in these great conditions, isolating the entire city from the present atmosphere and its negative impact. In fact, most of the artifacts recovered from the burial were preserved mainly due to the presence of hardened layers of “tuono”, a material associated with the later phases of ash fall and pyroclastic density currents, which acted as protection barrier.

Thanks to that protection, the entire city can show nowadays the context of an ancient Roman city's daily life and this was one of the main reasons for including the Archaeological Park of Pompeii in the UNESCO World Heritage List[1] in 1997.

Since the first discoveries until nowadays excavations have been continuously carried out. In this sense, Pompeii left in view not only all the archaeological records with great value, but also a representative vestige of the ancient life. In this sense, all type of archaeological objects of great value such as pigments in their original bowls[11], wall paintings, mosaics[12], potteries[13,14], bones[15], carbonized loafs of bread[16]… have been recovered.

1.3. Distribution of the ancient city of Pompeii and the Roman *domus*

Thanks to the performed excavations it was possible to reveal the structure of the ancient Roman city of Pompeii. The urban development of Pompeii relies primarily on different districts within the ancient city, the so-called *Regio.* In addition, the street network and organization of city blocks were known as *Insula*. In this sense, ancient Pompeii was distributed in nine different *Regios* as shown in Fig. 1.1

Although there is an open debate among scholars about how precisely we should understand and define the term *Insula*, this could be considered as a high-rise building that could occupy an entire block or be a portion of a larger structure. The *Insulae* of ancient Roman cities provided housing for the bulk of the urban populace as apartment blocks, which differ significantly from the townhouse (*domus*). The *domus* (house in Latin) is essentially a dwelling for a single, extended family unit, while the *Insula* contains multiple units.

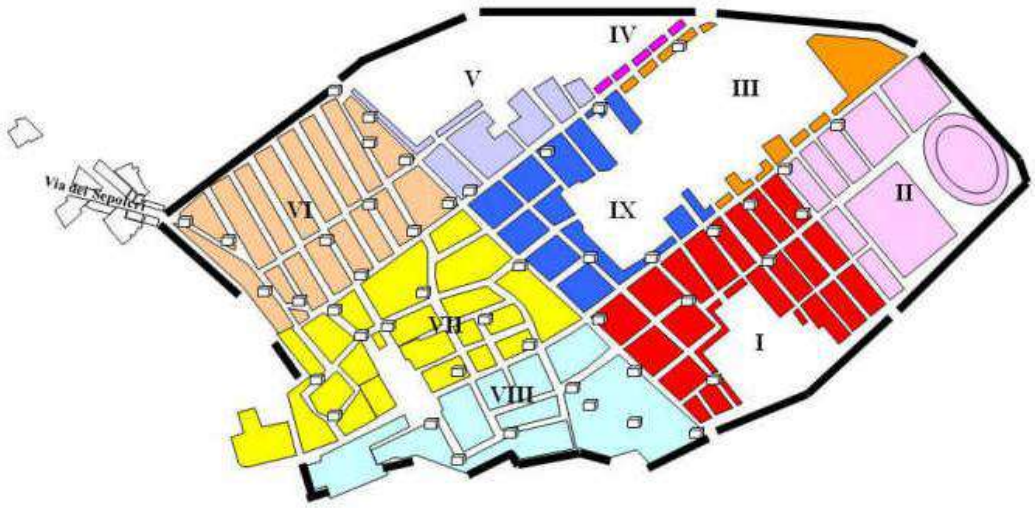

Fig. 1.1. Map of Pompeii showing the nine different *Regios*.
Source: http://pompeiiinpictures.com/pompeiiinpictures/index.htm

In the Roman world the best apartments were located at ground level, while the lower quality units were to be found on the upper floors of the structure[17]. In this way, a set of various different *Insulae* next to each other forms the previously mentioned *Regio*, which could be similar to the nowadays known as district of a city.

Most of the houses that came to light in Pompeii showed a characteristic Roman domestic architecture. The house type referred to as *domus* is a structure designed for either a nuclear or extended family, and located in a city or town. This typology was widespread in the Roman world and concretely, the sites of Pompeii and Herculaneum provide the best surviving evidence of *domus* architecture[18].

Vitruvius describes the Roman *domus* in the sixth and seventh book of his ten books of architecture[19]. In addition to the building and its foundations, the area on which it was built was part of the *domus*. He also considered important a perfect symmetry and the relationship between the proportions of the different living spaces[20]. To understand the organization of a Pompeian *domus* (see Fig. 1.2), it must be taken into account that it was

far from privacy. During a typical day, the spaces of the domus had to accommodate household religious rituals, the visits of invited and uninvited individuals, dinner guests, and the work of the intimates of the household. For this reason, we can think on the *domus* in terms of different rooms for different users. The shape, location, size, lighting, and decoration of each space often suggested the behavior of the person who entered or circulated through the domus[21].

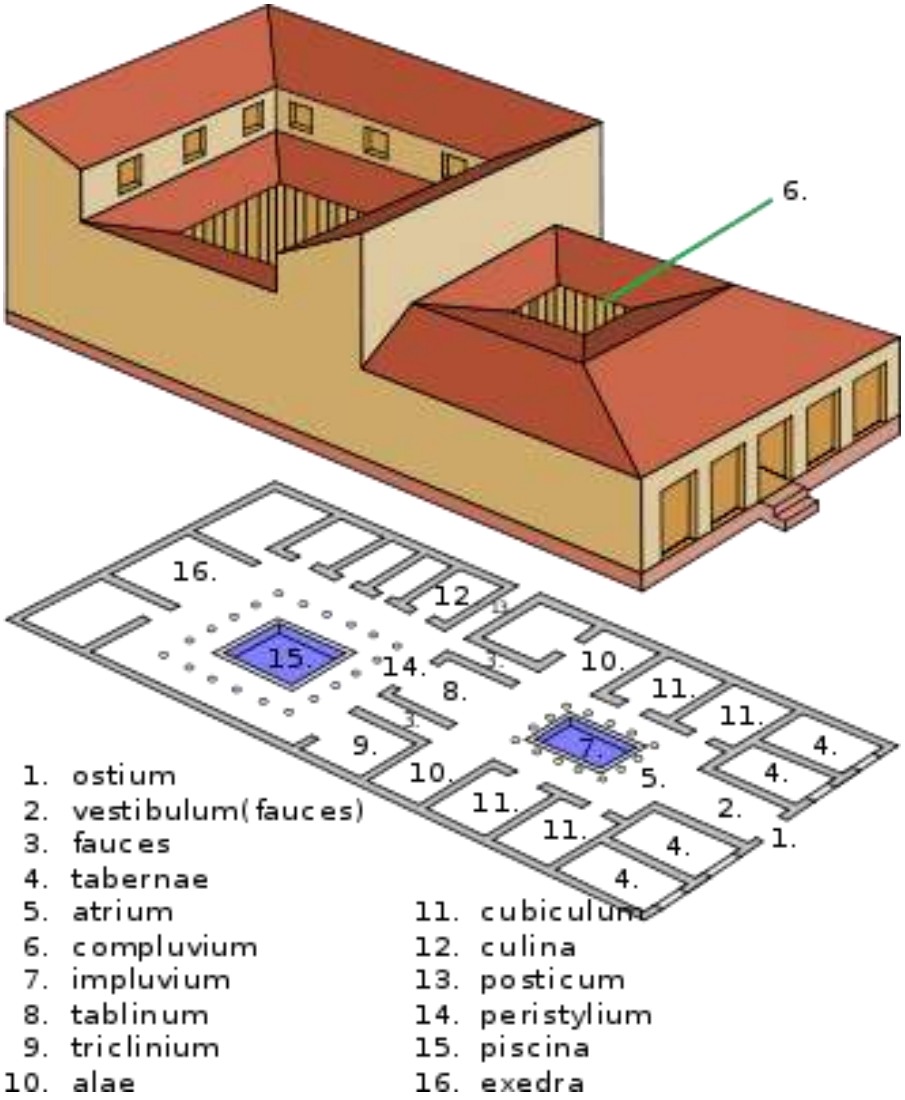

Fig. 1.2. Plan of a typical Roman *domus*.
Source: https://commons.wikimedia.org/wiki/File:Domus_suomi.png

The Romans employed two classes of nomenclature, one to describe the furnishing or the activity that went on in a room (*triclinium, cubiculum, peristylum*) and another to describe the structure or form, such as *exedra.*

Since there is not a completely standard *domus,* and some variations can be noticed in each, it is possible to discuss the primary features of a generic example (Fig. 1.2). The ancient architectural writer Vitruvius provided a wealth of information on the potential configurations of *domus* architecture. The entrance of the *domus* was the *fauces,* which begin the articulation of a long axis running through the *atrium*, or central hall, to the *tablinum*, or principal reception space. In particular, the main room of the *domus* was the *atrium.* In the classic layout of the Roman *domus*, the atrium served as the focus of the entire house plan. As the main room in the public part of the house, the atrium was the center of the house's social and political life[18]. The *tablinum* was such a kind of an office for the business of the owners.

A downward-sloping roof covered most of the space of the atrium, but the center of the roof was open. The *compluvium*, a square or rectangular opening in the center of the roof of the atrium, funneled rainwater from the roof into a catch basin directly beneath it, called the *impluvium*. The collected rainwater flowed into a cistern beneath the atrium floor. The rooms usually designated by the term *cubiculum* surround the atrium and had a single doorway opening to the atrium, their only source of light and air[18]. Finally, the *perystilum* was a continuous porch formed by a row of columns surrounding the perimeter of a courtyard.

1.4. The wall decorations in Pompeii

Wall paintings are one of the most impressive archaeological decorative objects that came to light during the excavations. They can be appreciated in major or less extent depending on the house. There are houses with magnificent wall paintings such as the "*Vila dei Misteri*", while other houses do not show or show more mediocre decorations. The wall paintings made by ancient artists involve the application of different plaster layers on the wall to end with the application of the pigments.

In this sense, according to Vitruvius[19], the Romans applied up to six preparation layers of plaster before painting a fresco, the most used painting technique in Pompeii. For that, the first layer of rendering, known as *arriccio* (see layer 2 in Fig. 1.3), was applied onto the surface of the brick/stone wall (see layer 1 in Fig. 1.3), to avoid any irregularities and holes. The *arriccio* is composed of a mortar of slaked lime and clean river sand of a large grain[19]. In this sense, three medium-fine grained layers of *arriccio* could be prepared. Afterwards, the entire compositional drawing known as the *sinopia* (after the red sinoper pigment used in the process) is executed on this layer (see red line in the right of Fig. 1.3)[19]. When this has completely dried out, the *intonaco* (see layer 3 in Fig. 1.3) is applied (the layer to be painted), which is composed of slaked lime mixed with clean river sand of a finer grain or marble powder, upon which the painting is executed. This was sometimes followed by a thinner layer known as the *intonachino*, which contains slightly more lime than the mortar[19] (see Fig. 1.3).

The renderings were applied in progressively thinner layers, with more lime added to the mortar with each successive layer, and the use of sand or marble powder of a progressively finer grain. These plasters only conserve their optimal characteristics for use as a background in fresco painting for a very short time (6–8h), also called 'golden-hour', during which they have a high degree of humidity.

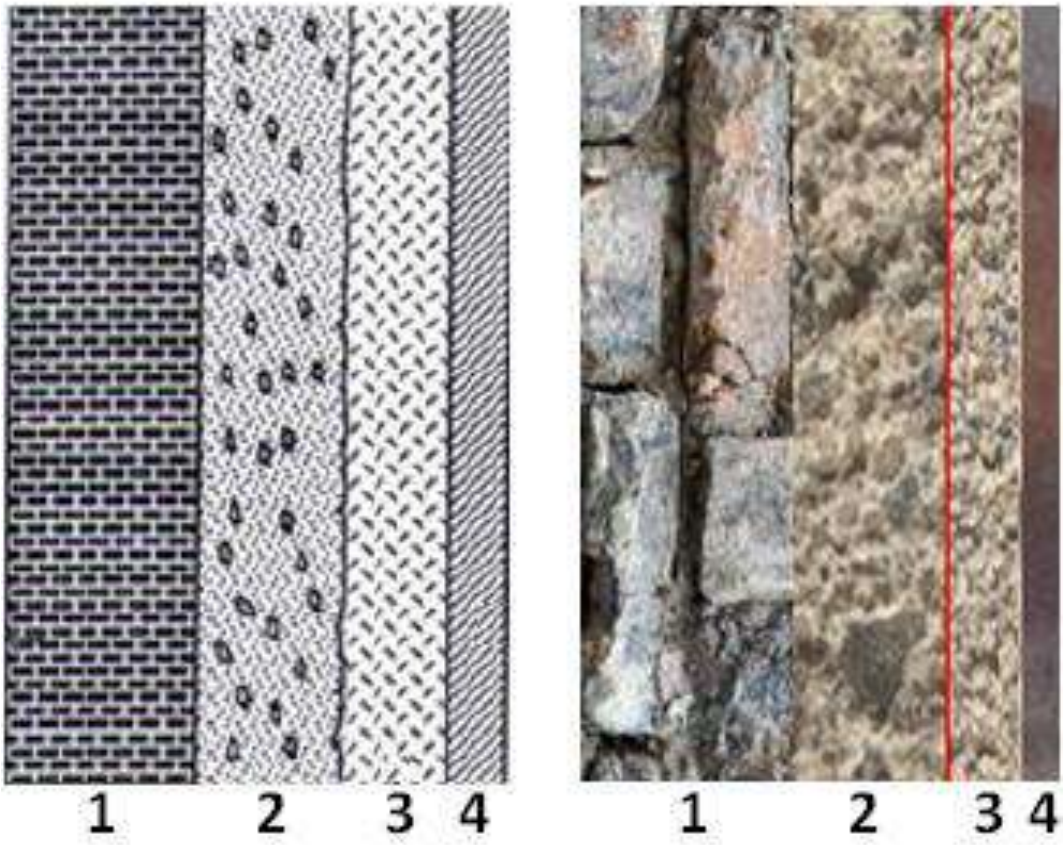

Fig. 1.3. Representation of an ancient fresco cross-section (1: Brick/stone wall; 2: arriccio; 3: intonaco; 4: pictorial layer).

The last layer of rendering, the *intonaco* (and if present the *intonachino*), was applied in relatively small sections which were predetermined according to the composition of the drawing. For this reason, the plaster is only applied to the portion of the wall to be painted on the same day. The calcium carbonate formed in the plaster by reaction between limewater (saturated in calcium hydroxide) and dissolved atmospheric carbon dioxide guarantees the binding of the applied pigment grains to the surface[22–24] (see layer 4 in Fig. 1.3).

The wall paintings from Pompeii were classified according to the specific pictorial decorations or styles used in each period of time. The German archaeologist August Mau defined four different styles: *First Style*, *Second Style*, *Third Style* and *Fourth Style*[25]. These painting styles were not unique for the city of Pompeii, since they are connected to the Roman period, naming them as *Roman pictorial styles*.

However, Pompeii and the surrounding cities buried by the Mount Vesuvius contain the largest source of evidences of that period. *First* and *Second* styles were popular in the Republican period (which ended in 27 BC) and grew out of Greek artistic trends, while *Third* and *Fourth* styles became fashionable in the Imperial period (20 BC-79 AD) for the particular case of Pompeii and Herculaneum.

First Style or *Structural, Incrustation or Masonry Style*, was used from year 200 BC to 80 BC. Its main feature is the simulation of marble (marble veneering), with other simulated elements such as suspended alabaster discs in vertical lines, wooden beams in yellow, and pillars and cornices in white. The used colors were vivid, being a sign of wealth (see Fig. 1.4)[26].

Second style, also called *Architectural Style*, dominated the 1st century BC and was developed out of the First Style incorporating elements of the *First Style*, such as faux marble blocks along the base of walls. It attempted to trick the viewer into believing that they were looking through a window by painting illusionistic images (see Fig. 1.4). This technique consisted of highlighting elements to pass them off as three dimensional realities, such as columns dividing the wall into zones[27].

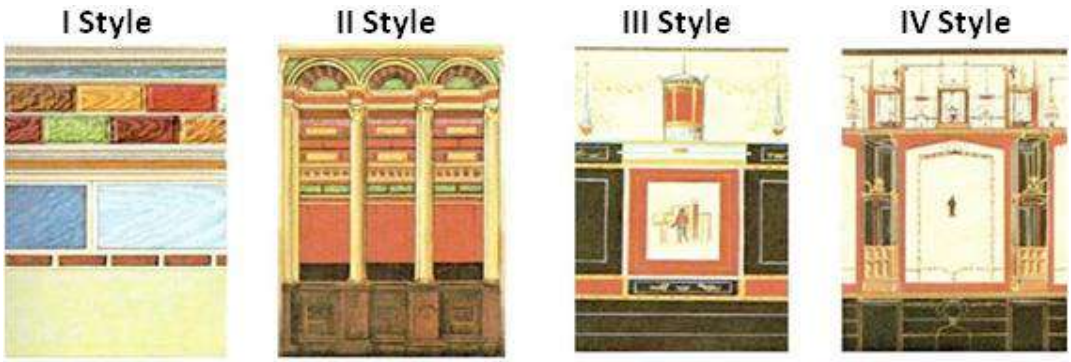

Fig. 1.4. Examples of Pompeian paintings of I, II, III and IV Styles.
Source: http://www.pompeiin.com/en/Painting_styles.html

Third style or *Ornate Style* came about in the early 1st century AD and was popular from around 20–10 BC until 50 AD. This style embraced the flat surface of the wall through the use of broad, monochromatic planes of color, such as black or dark red, punctuated by minute, intricate details. The *Third Style* was still architectural but, rather than implementing plausible architectural elements that viewers would see in their everyday world, it incorporated fantastic and stylized columns and pediments that could only exist in the imagined space of a painted wall (see Fig. 1.4).

Finally, *Fourth Style*, or *Intricate Style*, came in around 50 AD and represents with its involved and fantastic designs, the last stage in the development of Pompeian decoration. It can be best described as a combination of the three styles that came before. However, this style also incorporates central panel pictures on a much larger scale than in the *Third Style* and with a much wider range of themes, incorporating mythological, genre, landscape and still life images (see Fig. 1.4).

1.5. The Pompeian pigment palette: original colors, degradations and transformations

The used pigment palette by the Pompeian artists to create the magnificent wall paintings has been studied last years[11,28–32]. The used pigments had different natures depending on the source that they were taken from. On the one hand, the most accessible and cheap source was the local colorful iron-rich clays, which varied from yellow to red and brown. The pigments obtained from these materials, ochre pigments, were the ones already known and used since the prehistory, being hematite (α-Fe_2O_3) and goethite (α-FeOOH) the main compounds present in red and yellow ochres respectively[11,31,32]. On the other hand, in order to obtain a different range of colors that these local earths could not offer, minerals with a specific color were crushed to obtain a fine powder that may be used as pigment. Examples of these mineral pigments are the green malachite ($Cu_2CO_3(OH)_2$), red cinnabar (α-HgS), calcite ($CaCO_3$) or dolomite ($CaMg(CO_3)_2$), last both used as white color. All these pigments have been identified in Pompeii[11].

Another way of obtaining pigments was through a chemical reaction, like the preparation of Egyptian Blue ($CaCuSi_4O_{10}$). This reaction, described already by Vitruvius in the first century BC, consisted in mixing copper compounds with calcareous sand and a flux such as soda (Na_2O), natron ($Na_2CO_3 \cdot 10H_2O$) or plant ash[19,33].

Finally, the last way of pigment manufacture was achieved through a more sophisticate procedure, such as the mixture of organic and inorganic compounds, which lead to the so-called lake pigments. A lake pigment is formed by the precipitation of an organic colorant upon an insoluble inorganic substrate, usually called mordant, which forms the matrix of the pigment. In the Roman time, the organic colorant was usually obtained from plants or mollusks and the extracted dye was usually mixed with clays. Example of lake pigments used in Pompeii are the pinkish *madder lake*, which its organic colorant was

obtained from the roots of *Rubia* plant, or Tyrian purple, a purple dye obtained from the marine gastropod of genus Murex (such as *Murex brandaris*). In this last case, the obtained lake pigment was called *purpurissum*[34].

To determine the composition of the materials used as pigments, physico-chemical analyses are usually applied. This kind of analyses allows identifying not only their original elemental and molecular compositions, but also if they have suffered any kind of degradation or transformation during time. In this sense, up to now, many degradations have been identified in Pompeii. On the one hand, in previous works[35,36] the blackening of the red ochre pigments was studied. Thanks to this research it was determined that the attack of atmospheric SO_2 was the responsible in the transformation of the hematite present in red ochre (α-Fe_2O_3) into black magnetite (Fe_3O_4) together with the formation of gypsum ($CaSO_4 \cdot H_2O$).

An additional blackening process, in this case of the red pigment cinnabar (α-HgS), has been also studied and identified in Pompeii[37]. Some authors explained this color transformation due to a photoinduced conversion of α-HgS into black Hg^0. However, metallic mercury has been detected only in experiments using synthetic cinnabar[38], but never in real samples from Pompeii. Other authors claim that metacinnabar is formed, although metacinnabar neither was detected. On the other hand, degradation products such as corderoite ($Hg_3S_2Cl_2$), calomel (HgCl), terlinguaite (Hg_2ClO) and gypsum ($CaSO_4 \cdot H_2O$) were also detected in blacked areas[37]. Some authors mention that the photodegradation of cinnabar induced by the UV radiation can be assisted by chlorines[39]. Nevertheless, up to now it was not defined which is the minimum chlorine concentration necessary to promote the process and the real origin of this halide in the wall paintings of Pompeii.

Apart from these blackenings, one of the color transformations most present and noteworthy in the wall paintings of Pompeii is the one involving the yellow ochre transformation into red. This transformation had worldwide impact, since it has been published in diverse international media[40] and specialized scientific journals[41]. Although up to now there are not experimental evidences that demonstrated the mechanism of this transformation in Pompeii or Herculaneum, it is supposed that it took place when the pyroclastic density currents at high temperatures emitted by Mount Vesuvius in the year 79 AD impacted the yellow ochre areas of wall paintings, producing a dehydration reaction of the yellow ochre into red (hematite). In this sense, according to the literature, the dehydration temperature of goethite is set around 250°C.[42–45] and, concretely, this temperature was reached during the emissions of pyroclastic density currents in the 79 AD eruption[46].

1.6. Evolution of the scientific interest in the characterization of the pigments used in the wall paintings of Pompeii

The interest of the research groups in analyzing the chemical composition of the pigments in Pompeii has dramatically increased in the last years. In this sense, the IBeA (*Ikerkuntza eta Berrikuntza Analitikoa*) research group, from the Analytical Chemistry Department of the University of the Basque Country (UPV/EHU) in which this PhD Thesis has been developed, started researching in Pompeii in the year 2009. Although small samples were analyzed in 2008-2009 in the laboratory, the main objective of IBeA in Pompeii has been to develop non-invasive methodologies based on the use of portable instruments useful not only to determine the composition of the materials used in Pompeian wall paintings, but also to diagnose their conservation state.

This main objective has been developed since 2010 inside the *Analytica Pompeiana Univesitatis Vasconicae* (APUV) project (http://www.apuv-ibea.com).

Nowadays, Pompeian pigments and mural paintings are object of study of many worldwide research groups. To assess this evolution, two different bibliographic searches have been conducted in Scopus. The search has been delimited from 2000 up to now, since only few papers (less than four) can be found in previous years. In the first search, the keywords "Pompeii" and "pigments" have been considered. Altogether, two conference papers and one review not related with chemical or physico-chemical studies were found. Regarding papers, in total 28 were found, being two of them out of this field of application (conservation science). Among the rest of the papers (26), ten belong to IBeA research group, that is, the 38% of the total of the published papers, or 36% if the additional conference papers are considered. In Fig. 1.5 the number of paper published per year for this first search is represented to observe better the progression.

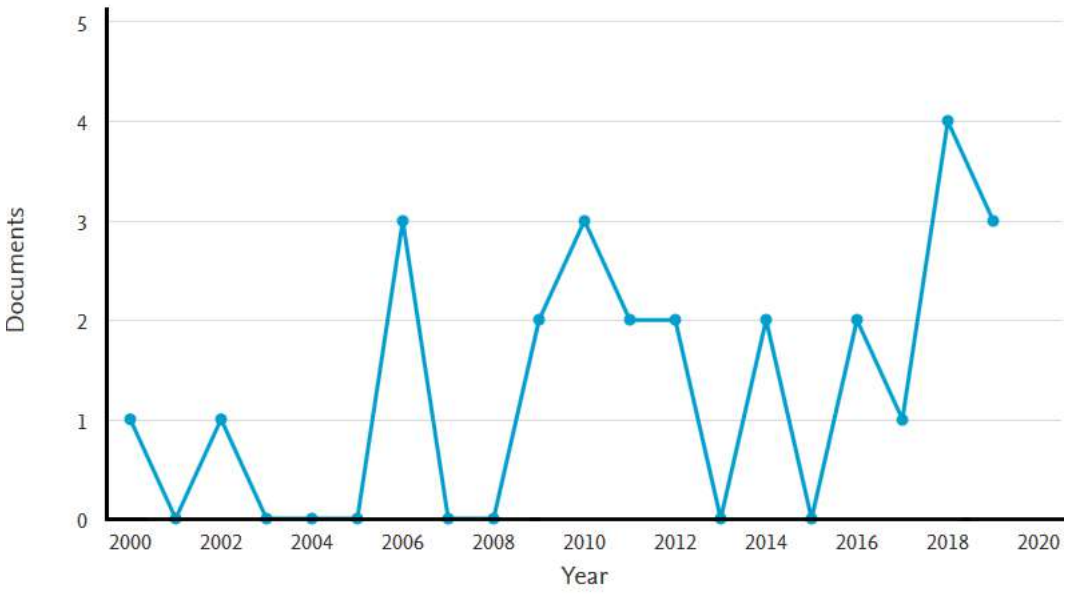

Fig. 1.5. Number of documents published by year since 2000 including the keywords "Pompeii pigments" (source: Scopus).

In the second search, the keywords "Pompeii" and "wall painting" have been considered. In this case, 7 conference papers, 15 book chapters, 5 reviews and 2 books were found. Among all, only four conference papers belong to the previously mentioned field of application. Additionally, 43 papers were also found. Among them, ten are not related with the field of application. Thus, among the total of 33 papers, 10 belong to IBeA, that is, more than the 30% of the total. If the four conference papers are included, the contribution of IBeA is set close to 27%. In Fig. 1.7 the number of papers published each year for this second search is represented.

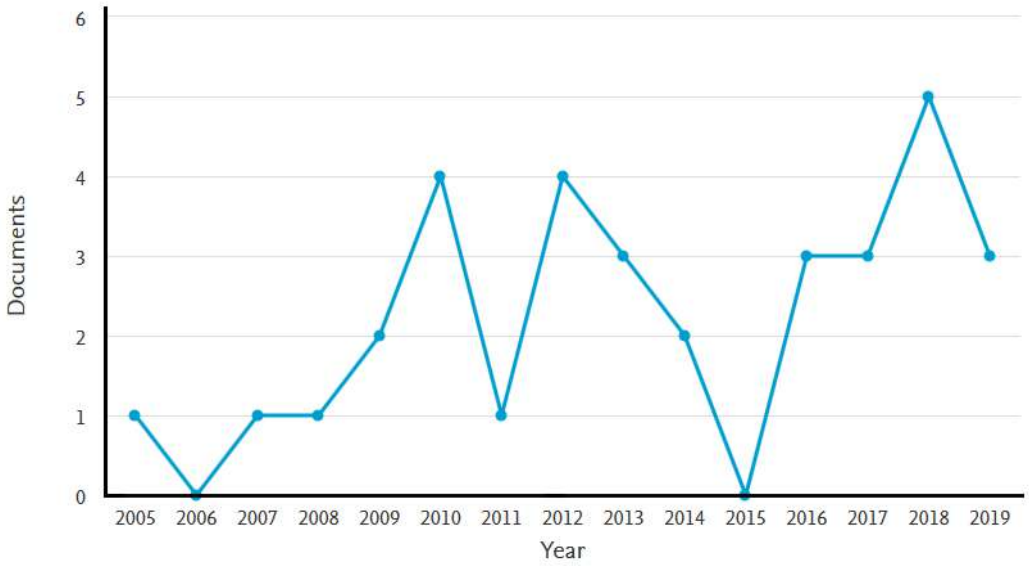

Fig. 1.6. Number of documents published by year since 2000 including the keywords "Pompeii" and "wall paintings" (source: Scopus).

In Fig. 1.5 and 1.6 it can be noticed that the increase in the publications took place around the yeas 2008-2010 reaching the maximum in 2018 in both searches. The dates seems to come in agreement with the launch of "*The Great Pompeii Project*"[47], which started in 2012 as an initiative of the Italian government to enhance the effectiveness of the actions and interventions for the protection of the archaeological area of Pompeii by developing a special urgent program of conservation, maintenance, and restoration. Considering

these events, the management of the park has invested most of its funds to support conservation projects instead of conducting new excavations. In this sense, the project is accompanied by a suitable plan for scientific and technical study aimed to both, diagnose the conservation state of the different archaeological items from Pompeii and expand the scientific knowledge. However, it must be remarked that IBeA proposed a similar objective since 2009, independently of the interests of *The Great Pompeii Project.* Under this frame, the Archaeological Park has established different collaboration agreements with diverse research groups. In this case, two agreements (2015-2017 and 2018-2021) between the Archaeological Park of Pompeii and the University of the Basque Country (UPV/EHU), including the collaboration with IBeA, have been signed. In the first agreement, the Archaeological Park highlights the interest to characterize the pigments present in its collection preserved in the Applied Research Laboratory of Pompeii (ARLP). In the second agreement, one of the objectives was to develop an analytical methodology to discriminate original red ochres from yellow ochres transformed into red. Both objectives established in the mentioned agreements have been developed in the framework of this PhD Thesis.

1.7. Traditional and emerging analytical techniques and methodologies to analyze powder pigments or those used in wall paintings

Traditionally, to analyze either pigment powders or pigments applied in wall paintings, it has been necessary to extract a sample of some milligrams or grams in the case of pigment powders[11,32] and a small fragment in the case of wall paintings[48,49]. The information was obtained mainly by means of microscopic observations. Some years later, thanks to the coupling of microscopy to spectroscopic techniques, it was possible to determine the nature of the used pigments in the stratigraphic section of wall painting

samples. The technological developments and the miniaturization of spectrometers that have taken place in the last years allow to use in situ the analytical instrumentation. In this sense, although a laboratory analysis can offer information about the different layers (stratigraphy) that compose a wall painting, in some cases the modern portable instrumentation allow obtaining enough information to extract conclusive results useful to answer specific objectives/questions. Taking into account that in the Archaeological Park of Pompeii the sampling of pigments in wall paintings or even powdered pigments preserved in their original bowls recovered from the burial of Pompeii is limited, and very often forbidden, the use of portable instrumentation becomes indispensable for the non-invasive analysis.

In this sense, elemental and molecular spectroscopic techniques are crucial to determine the chemical composition of the pigments. Among the molecular ones, infrared spectroscopy (IR) was the main analytical technique used in the 20th century[50]. In fact, in the literature from that period a wide variety of works dealing with the molecular characterization of pigments using IR spectroscopy as reference technique can be found[50–53]. This analytical technique uses IR radiation, which interacts with the sample and excites the molecules present on it, generating a spectrum of the energy absorbed by a molecule as a function of the frequency. Concretely, IR spectroscopy measures transitions between molecular vibrational energy levels as a result of the absorption of mid-IR radiation (4000-400 cm^{-1}). The vibrations that an excited molecule can suffer are stretching (changes in the bond lengths) or bending vibrations (change bond angles)[54], among others.

Traditionally, benchtop instruments measured the transmission of the emitted radiation to obtain the characteristic spectrum of the sample, which was usually prepared as pressed pellet[55]. This type of IR measurements is still employed, but nowadays measurements can also be conducted in reflectance mode. In this way, by coupling different modules to benchtop IR spectrometers the diffuse reflectance (DRIFT), the attenuated total reflectance (ATR) and the specular reflectance (ER) coming from the

sample can be collected. Moreover, thanks to these measuring modes, portable IR spectrometers were developed and they can be used in situ for pigment identification purposes[56,57]. These IR measuring modes do not need a previous preparation of the sample as a pressed pellet. In this sense, portable infrared spectrometers incorporate DRIFT, ATR and ER sample interfaces that are placed in contact with the material/surface to be analyzed collecting the IR spectrum in a non-invasive way. In this sense, since the ATR interface could leave a mark in the analyzed area due to the contact of its crystal, DRIFT or ER are usually used because they do not promote any alteration on the surface. Thereby, one of the main advantages of these portable spectrometers in the analysis of pigments and artworks is that IR spectra from a wall painting can be collected in situ[58–60], which was impossible to do years ago with the use of benchtop spectrometers working in transmission mode. In fact, these various measuring modes prove to be very effective in characterizing both the inorganic and organic constituents of a wide variety of artworks, giving an insight into the materials and techniques of execution[61–63]. Concretely, in the literature some works used portable DRIFT spectrometers aiming to characterize the pigments of Roman[64,65] and Pompeian wall paintings[66]. Normally, in the field of cultural heritage analysis, DRIFT samples interfaces are usually used since this kind of materials reflect fairly the light.

From 21st century onwards, the use of Raman has exceeded IR spectroscopy and during the last two decades, it can be considered one of the most used techniques in the analysis of materials belonging to the field of art and archaeology. In this sense, in the literature many works dealing with the characterization of pigments by means of benchtop Raman micro-spectrometers can be found[11,67–70]. This non-invasive analytical technique is based on the inelastic scattering of photons. A source of monochromatic light, usually from a laser in the visible, near infrared, or near ultraviolet range is used. The laser light interacts with molecular vibrations, phonons or other excitations in the system, resulting in the energy of the laser photons being shifted up or down. The shift in energy gives information about the vibration modes in the system[71].

The technological development of last decades allowed introducing in the market commercial portable Raman spectrometers able to offer high quality spectra with a good signal-to-noise ratio. Thanks to that, Raman spectroscopy has turned into one of the main analytical techniques used for the pigments identification in cultural heritage field due to the advantage of performing non-invasive and in situ analyses[72–76]. Last works showed the robustness of portable Raman spectroscopy in pigment identification, which also has been used in the case of wall paintings from Pompeii[66,77].

Nevertheless, in some cases Raman bands registered in the spectra are so weak that they cannot be detected or they are completely masked by the fluorescence phenomenon. In these cases, to enhance the Raman scattering signals and quench the fluorescence, metallic nanoparticles (NP) can be used. This variation to traditional Raman spectroscopy is called Surface Enhanced Raman Spectroscopy (SERS). The addition of NPs promotes a nanoscale roughened metal surfaces, typically made of gold (Au) or silver (Ag). Laser excitation of these roughened metal nanostructures resonantly drives the surface charges creating a highly localized plasmonic light field. When a molecule is absorbed or lies close to the enhanced field at the surface, a large enhancement in the Raman signal can be observed[78]. Indeed, it can be incremented up to 10^{15} times[79]. In the recent years SERS has been widely used for pigment identification purposes[80–84] and also in other applications such as in biomedicine, food analysis, pesticides detection in agriculture, etc.[85–89]. The most used NPs are based on silver (AgNP). However, depending on the sample and the aim of the analysis, gold (AuNP) and copper (CuNP) nanoparticles can also be used[90]. Besides, other metallic nanoparticles based on cobalt (CoNP), nickel (NiNP) and bismuth (BiNP) that show promising potential have been recently tested for the development of SERS-based sensors[91]. Therefore, although AgNP are the most common and used ones, there are many alternatives. And even more, since the morphology of the generated nanoparticles can be tuned controlling the growth mechanism by following different recipes, reaching to other structures such as silver nanostars instead the common nanoparticles[92].

Apart from that, laser ablation sampling method has been also combined with SERS (LA-SERS), in which laser ablation is used as a micro-sampling method onto a SERS-active film to characterize samples belonging to art with microscopic precision and sensitivity comparable to many mass spectrometry measurements[93]. As can be inferred, most of the SERS applications involve the extraction of samples.

Regarding IR and Raman spectroscopies, different spectral databases have been created with the aim of interpreting the spectra obtained by the users. In this sense, Infrared and Raman Users Group (IRUG) promoted the creation of a public database of IR and Raman reference spectra of materials, contributed by individuals and institutions in the international cultural heritage community and academia. Early compilations of IR spectra[94] were distributed in 1993 and 1995. On the other hand, it was not until 2009 when IRUG began to build a Raman counterpart to the IR database. After IRUG, additional infrared spectra databases were published, such as the "FTIR Spectra Database of Inorganic Art Materials"[95] in 2003 or RRUFF[96] a project containing an integrated database of Raman, X-ray diffraction and infrared (mainly ATR) spectra together with chemistry data for minerals.

In addition to Raman and IR spectroscopies, another conventional analytical technique that offers information about the molecular composition is X-ray diffraction (XRD). In this analytical technique, a crystal diffracts an emitted X-ray passing through it to produce beams at specific angles depending on the X-ray wavelength, the crystal orientation, and the structure of the crystal. Thus, a diffraction pattern is produced, which gives information on the structure of the crystal or the identity of a crystalline substance[97]. It can be considered a non-invasive technique because the sample is not destructed and it can be recovered after its measurement. However, if solid samples have to be analyzed, to improve the results and to obtain representative evidences, a grinding before its analysis should be conducted. Therefore, in these cases, XRD is considered destructive since the physical state of the sample is transformed.

In the literature some works used XRD for the characterization of archaeological pigments from Ancient Rome[98] and Pompeii[11,99,100]. Thus, it is a suitable analytical technique since raw pigments are already in powder form and no pre-treatment should be done for the analysis, recovering them in the same state after its measurement. In the last years, as an alternative to classical benchtop XRD instruments, portable XRD spectrometers have been developed and used for different purposes (e.g., pigments and archaeological materials analysis)[101,102]. One of the commercial portable XRD spectrometers is the TERRA Mobile XRD System[103], which all the instrument is contained in a box, like a suitcase, and it needs a little amount of powder sample to be placed in a holder to obtain the diffractograms. For this reason, wall paintings cannot be analyzed with this instrument. To conduct direct measurements on the wall, other XRD equipments mounted on a tripod supports to stabilize the spectrometer should be necessary.

Whenever it is possible, molecular analyses are combined with elemental measurements to obtain a full chemical characterization of the material under study. Elemental analysis is usually performed by means of energy dispersive X-ray fluorescence spectroscopy (EDXRF)[104–107], since the energy dispersion does not require mandatorily to prepare the samples as pressed pellets like in the case of wavelength dispersive XRF (WDXRF). XRF is a non-invasive analytical technique based on the emission of characteristic secondary fluorescent X-rays from a material (sample) that has been excited by being bombarded with high-energy X-rays emitted by the source of the instrument. This technique has been also used to carry out studies about origin and provenance of the pictorial materials[108] or technological and production issues[109]. However, last generation benchtop XRF spectrometers allow measuring at spatial resolutions down to 25 μm thanks to the use of polycapillary X-ray optics, which is a very good option in order to obtain high resolution elemental distribution images[110–112]. This is of great importance for the analysis of the distribution of pigments in an artwork and, it also enables investigation of the chemical composition of complicated paint layering[113].

Since 2002, handheld XRF spectrometers are also available to perform in situ non-invasive elemental measurements of artworks[114] or wall paintings[115]. Most of them belong to gun configuration instruments. Apart from this option, other portable XRF spectrometers mounted on tripods such as Elio of XGlab (part of Bruker), can be mentioned. This instrument offers the option of acquiring distribution maps in situ. A work published this year used this spectrometer to investigate *Old Woman Praying* artwork of Rembrandt[116], which suggests the potential of this kind of portable spectrometers and their increase in the use by researchers in the near future.

Almost four decades ago, Laser Induced Breakdown Spectroscopy (LIBS) technique was introduced to determine the elemental composition of diverse kind of material. In the field of art, archaeology and cultural heritage different objects such as polychromes[117], ceramic materials[118], metallic objects[119], and stone monuments[120], among others, have been analyzed by this technique. This analytical technique uses a highly energetic laser pulse as the excitation source that is focused in the sample. After the laser impact, sample ablation is produced. Thanks to the production of the plasma, atomization of the sample and excitation of the atoms present in the measuring area are produced. After that, the characteristic emission of the elements in the plasma is recorded in the spectrometer. The great potential attributed to LIBS technique lies in the fact that a stratigraphic analysis of the materials can be conducted since consecutive laser pulses can be applied at the same measured area, which allows performing a depth profiling analysis[121–123]. Benchtop LIBS spectrometers that can work under vacuum are capable to detect signals of C, N and O coming from the sample. On the contrary, the discrimination of the presence of these elements in the sample from the contribution of the atmosphere becomes difficult in the portable/handheld LIBS spectrometers, since measurements are usually acquired on air. On the other hand, portable LIBS spectrometers offer the advantage with respect to portable XRF ones of detecting light elements such as F, Na and Mg. For example, Na and Mg are difficult to be detected and quantified by portable/handheld XRF due to their high detection limits (higher than 1% in weight).

However, portable XRF spectrometers such as Tracer® from Bruker have recently incorporated detectors based on graphene entrance windows, which have higher transmission of X-rays throughout the energy spectrum and improves the transmission for light elements detection.

Another elemental technique that, in contrast to XRF and LIBS, does not offer the possibility of performing in situ analyses is scanning electron microscope coupled to energy dispersive X-ray fluorescence spectroscopy (SEM-EDS). In this analytical technique, the SEM uses an electron beam excitation in order to acquire microscopic images. Moreover, since the microscope can be coupled with an EDS analyzer, the X-ray fluorescence emitted by the elements present in the sample induced by the electron beam is detected obtaining spectra similar to those offered by XRF. SEM-EDS has been widely used in pigment analysis, in which samples are usually prepared as cross sections and the different layers are characterized[124,125]. This technique has been also used to identify in previous works[11,36,46] pigments from Pompeii.

In the last years, the main challenge proposed in the field of spectroscopic techniques is to achieve hyphenated instruments (combinations of instrumental techniques) useful to obtain the elemental and molecular information in the same area of analysis. Among the last developments, the coupling of Raman spectroscopy to SEM-EDS can be mentioned[126]. The structural and chemical analysis (SCA) introduced more than ten years ago by Renishaw offered the option of acquiring the Raman and the EDS spectra in the same microscopic area. Apart from that, the XRaman® (XGLab from Bruker) portable spectrometer, recently launched into the market, should be mentioned[127]. It is a combined EDXRF and Raman portable analyzer which allows obtaining elemental and molecular information in the same measurement area. In this case, the instrument is mounted on a tripod allowing to measure directly all kind of materials and surfaces. The same company also commercialized recently HYDRA®, a portable spectrometer designed to perform in situ the elemental and mineralogical analyses, by the combination of EDXRF

and XRD techniques. In particular, the instrument has been developed mainly for cultural heritage applications[128]. Nowadays, a prototype of this instrument is working in the laboratory of the Louvre museum. On the other hand, a similar XRF-XRD spectrometer called DUETTO® has been developed by the company ExaminArt[129] for its use in the analysis of artworks, wall paintings and all kind of items belonging to the field of art. This instrument has been inspired by the previously mentioned TERRA portable XRD.

As it can be observed, the development of these portable devices that combine different analytical techniques demonstrates the potential that in the near future, or even nowadays, will have these hybrid analytical techniques in the cultural heritage field.

Apart from commercial instruments, different research groups developed other hybrid benchtop instruments in the last years. For example, a new laser based technique "Tandem Laser Ablation (LA)-LIBS" that combines LA for ICP-MS and LIBS into one integrated laser ablation system has been also presented the last year[130]. This instrument allows analyzing elements from ppb to % level in a single ablation experiment. Elements that are difficult or impossible to measure with LA-ICP-MS are now possible to be analyzed with LIBS down to low ppm levels with CCD and/or ICCD detection. Considering that this instrument is of recent creation, still there are not applications in the field of cultural heritage.

On the other hand, within the framework of the European Research Infrastructure for Heritage Science (E-RIHS), LIBS technique has been combined with Raman and Laser Induced Fluorescence (LIF) in the same portable spectrometer[131]. This LIBS/LIF/Raman portable instrument associates the three lasers based on analytical methods for a more global and precise characterization of the heritage objects taking into account their precious characters and their specific constraints. Although this spectrometer is portable, its dimensions are too large to be carried on site easily. In this sense, an example of miniaturization is the SuperCam instrument mounted in the rover developed for the Mars

2020 mission, which in about 3 meters long, 2.7 meters wide, and 2.2 meters height. In this case, several analytical techniques such as Raman spectroscopy and LIBS are integrated.

Apart from the home-made or commercial regular benchtop instruments, big installations such as modern synchrotron facilities can be mentioned. The high energy flux (brilliant radiation) achieved in these installations offers the possibility of performing analyses in the sub-micrometric scale, which cannot be carried out with conventional benchtop instruments. A synchrotron is a particular type of cyclic particle accelerator in which the accelerating particle beam travels around a fixed closed-loop path. Thanks to this, the synchrotron radiation (SR) can be coupled to diverse analytical techniques that led into new possibilities of measurements, such as SR-XRF[132–134], SR-IR[134,135], X-ray absorption near edge structure (XANES)[133], X-ray absorption spectroscopy (XAS) or μ-XRD[133,134]. As these works demonstrated, the synchrotron based techniques are suitable for the characterization of pigments belonging to the field of art or archaeology, in particular in order to reveal degradation pathways or to identify different painted layers. Concretely, a previous work[37] used SR-XRF and XANES with the aim of decipher the mechanism of the blackening of the brilliant red cinnabar pigment used in Pompeii.

Apart from non-invasive and/or portable techniques, destructive analytical techniques such as gas (GC) or liquid chromatography (HPLC) for the molecular characterization and Inductively Coupled Plasma Mass Spectrometry (ICP-MS) for the elemental analysis can also be used to complement in situ analyses or non-invasive ones in the laboratory. However, the use of these techniques involves that samples cannot be recovered in their original state after the analyses. Therefore, in the case of archaeological pigments the main used techniques should be non-invasive, and they might be assisted by laboratory destructive instrumentation only when the sample amount allows performing this kind of analyses. Concretely, HPLC has been usually used with the aim of detecting organic

colorants present in pigments[136–138], while ICP-MS to analyze the minor and trace elemental composition in pigments[139,140].

To identify sources or provenances of the materials under study, isotope ratio analyses are usually conducted, which involves applying destructive techniques. For this purpose, Thermal Ionization Mass Spectrometry (TIMS) and ICP-MS can be used. In this sense, the most widely used element is Pb. Historically, Pb was among the first ore-extracted metals, thus, ore-derived Pb is found abundantly in the composition of many ancient artifacts at many archaeological sites. Pb has four stable isotopes (^{204}Pb, ^{206}Pb, ^{207}Pb and ^{208}Pb), three of which are radiogenic, which results in a wide range of natural variation in the isotopic composition of this element that makes it a good tracer for sourcing materials. TIMS has been the analytical technique of reference for archaeological lead isotope provenance studies[141,142]. However, since the introduction of multicollectors (MC) coupled to ICP-MS spectrometers around the year 2000, it has been possible to measure several isotopes simultaneously, with a high mass resolution[143–145]. These new spectrometers permit notable advances in geochemistry, and more recently in archaeology too. Therefore, it has now become the instrument of choice for measurement of high-precision isotope ratios. Nowadays precise and accurate measurements by means of MC-ICP-MS improve the tracing by increasing the analytical precision by a factor of 10 over that obtainable with routine TIMS. MC–ICP–MS also allows the measurements of new isotopic tracers such as Cu, Fe, Sn[146].

In addition to the chemical characterization, chemometrics can also be applied to differentiate the geological source of pigments according to the variation in the major, minor and trace element patterns. Multivariate statistical treatment of elemental data also allows understanding the variance within a sample set and calculating probabilities for sample grouping. In this sense, displaying the samples in principal component (PC) space helps to identify patterns or groups within the data. Thus, Principal Component Analysis (PCA) is probably the most used chemometric tool that allows classifying and

discriminating samples according, in this case, to their chemical composition[147–149]. In fact, PCA is an effective variable reduction technique for spectroscopic data. In the PCA, the scores plot on new principal components evidence the correlations among samples or spectra. Similar samples appear grouped in the score plot, while different samples appear segregate from each other. Similarly to scores, the loadings plot distributes the variables among PCs. Therefore, a bi-plot that combines the sample scores and variable loadings could give insights about the distribution of samples in the PC space according to their chemical composition.

For example, in the literature[108] the elemental composition of ochre pigments from Missouri (USA) was analyzed by means of XRF and compared with the composition of near iron ore formation materials that could postulate to be the source of these ochre pigments. Thereby, similarities or differences in the minor/trace elemental composition between samples and source materials could give useful information regarding their possible provenance or origin. This kind of data treatment can be applied similarly to obtain clues about the provenance of original raw pigments recovered from the burial of ancient Pompeii. However, as stated before, for this kind of applications the possible ore candidates should be accessible. An example of this is the work of Mazzocchin *et al.*[150] in which the origin of the Pompeian cinnabar pigment from the *Insula del Centenario* and the *House of Gold Bracelet* was traced through Pb isotopic analysis and comparing the results with different cinnabar ores.

1.8. REFERENCES

1. https://whc.unesco.org/en/list/829/ [Last accessed: 13th October].

2. http://pompeiisites.org/en/archaeological-park-of-pompeii/visitor-data/ [Last accessed: 13th October].

3. http://pompeiisites.org/wp-content/uploads/A-Guide-to-the-Pompeii-Excavations-2.pdf [Last accessed: 13th October].

4. Roller, D. W. The Geography of Strabo: An English Translation, with Introduction and Notes. (Cambridge, Cambridge University Press, 2014).

5. Laurence, R. Roman Pompeii: space and society. (London, Routledge, 2010).

6. La Boda, S. International Dictionary of Historic Places: Southern Europe. (London, Taylor & Francis, 1994).

7. Ruggieri, N. Seismic vulnerability of the ancient Pompeii through the evaluation of the 62 AD earthquake effects. *Int. J. Archit. Herit.* **11**, 490–500 (2017).

8. https://www.bbc.com/news/world-europe-45874858 [Last accessed: 13th October].

9. Jones, N. F. Pliny the Younger's Vesuvius "Letters" (6.16 and 6.20). *Class. World* **95**, 31–48 (2001).

10. Caridi, G. Carlos III: un gran rey reformador en Nápoles y España. (Madrid, La Esfera de los Libros, 2015).

11. Aliatis, I. *et al.* Pigments used in Roman wall paintings in the Vesuvian area. *J. Raman Spectrosc.* **41**, 1537–1542 (2010).

12. Arletti, R. *et al.* Glass mosaic tesserae from Pompeii: an archeometrical investigation. *Period. Mineral.* **75**, 25–38 (2006).

13. Pena, J. T. *et al.* The production and distribution of pottery at Pompeii: A review of the evidence; Part 1, Production. *Am. J. Archaeol.* **113**, 57–79 (2009).

14. Peña, J. T. *et al.* The production and distribution of pottery at Pompeii: a review of the evidence; part 2, the material basis for production and distribution. *Am. J. Archaeol.* **113**, 165–201 (2009).

15. Guarino, F. M. *et al.* Bone preservation in human remains from the Terme del Sarno at Pompeii using light microscopy and scanning electron microscopy. *J. Archaeol. Sci.* **33**, 513–520 (2006).

16. https://www.telegraph.co.uk/history/pompeii/9850077/Pompeii-exhibition-the-food-and-drink-of-the-ancient-Roman-cities.html [Last accessed: 13th October].

17. https://www.khanacademy.org/humanities/ancient-art-civilizations/roman/beginners-guide-rome/a/roman-domestic-architecture-insula [Last accessed: 13th October].

18. https://www.khanacademy.org/humanities/ancient-art-civilizations/roman/beginners-guide-rome/a/roman-domestic-architecture-domus [Last accessed: 13th October].

19. Rowland, I. D. *et al.* Vitruvius: Ten Books on Architecture. (Cambridge, Cambridge University Press, 1999).

20. Castrén, P. A. *et al.* Domus Pompeiana: una casa a Pompei. (Helsinki, Otava, 2008).

21. Ulrich, R. B. *et al.* A companion to Roman architecture. (New Jersey, Wiley, 2014).

22. Mora, P. *et al.* The conservation of wall paintings. (Oxford, Butterworth & Co., 1984).

23. Moropoulou, A. *et al.* Investigation of the technology of historic mortars. *J. Cult. Herit.* **1**, 45–58 (2000).

24. Giordani, M. *et al.* Effect of vaporization rate on calcium carbonate nucleation from calcium hydrogen carbonate aqueous solutions. *J. Cryst. Growth* **84**, 679–682 (1987).

25. Mau, A. Pompeii, its life and art. Vol. 1 (Alexandria, Library of Alexandria, 2007).

26. von Hesberg, H. The First Style in Pompeii: Painting and Architecture. (Munchen ,Gnomon, 1989).

27. Foss, P. W. The world of Pompeii. (London, Routledge, 2009).

28. Augusti, S. I colori Pompeiani. (Rome, De Luca Editore, 1967).

29. Aliatis, I. *et al.* Green pigments of the Pompeian artists' palette. *Spectrochim. Acta. A. Mol. Biomol. Spectrosc.* **73**, 532–538 (2009).

30. Canevali, C. *et al.* A multi-analytical approach for the characterization of powders from the Pompeii archaeological site. *Anal. Bioanal. Chem.* **401**, 1801-1814 (2011).

31. Cottica, D. *et al.* Pots with colored powders from the Forum of Pompeii. *Proceedings of the conference EMAC '07. 9th European Meeting on Ancient Ceramics. Budapest, Hungary* (2007).

32. Giachi, G. *et al.* Raw Materials in Pompeian Paintings: Characterization of Some Colors from the Archaeological Site. *Mater. Manuf. Process.* **24**, 1015–1022 (2009).

33. Mazzocchin, G. A. *et al.* A short note on Egyptian blue. *J. Cult. Herit.* **5**, 129–133 (2004).

34. Clarke, M. *et al.* Pompeii purpurissum pigment problems. *Proceedings of Art'05–8th International Conference on "Non Destructive Investigations and Microanalysis for the Diagnostics and Conservation of the Cultural and Environmental Heritage", Lecce, Italy* (2005).

35. Maguregui, M. *et al.* Thermodynamic and spectroscopic speciation to explain the blackening process of hematite formed by atmospheric SO_2 impact: the case of Marcus Lucretius House (Pompeii). *Anal. Chem.* **83**, 3319–3326 (2011).

36. Maguregui, M. *et al.* Multianalytical approach to explain the darkening process of hematite pigment in paintings from ancient Pompeii after accelerated weathering experiments. *Anal. Methods* **6**, 372–378 (2014).

37. Cotte, M. *et al.* Blackening of Pompeian cinnabar paintings: X-ray microspectroscopy analysis. *Anal. Chem.* **78**, 7484–7492 (2006).

38. Keune, K. *et al.* Analytical imaging studies clarifying the process of the darkening of vermilion in paintings. *Anal. Chem.* **77**, 4742–4750 (2005).

39. Radepont, M. *et al.* Thermodynamic and experimental study of the degradation of the red pigment mercury sulfide. *J. Anal. At. Spectrom.* **30**, 599–612 (2015).

40. https://www.theguardian.com/science/2011/sep/22/pompeii-red-yellow [Last accessed: 13th October].

41. Angelini, I. *et al.* The pigments of the frigidarium in the Sarno Baths, Pompeii: Identification, stratigraphy and weathering. *J. Cult. Herit.* (2019). DOI: 10.1016/j.culher.2019.04.021

42. de Faria, D. L. A. *et al.* Heated goethite and natural hematite: can Raman spectroscopy be used to differentiate them? *Vib. Spectrosc.* **45**, 117–121 (2007).

43. Prasad, P. S. R. *et al.* In situ FTIR study on the dehydration of natural goethite. *J. Asian Earth Sci.* **27**, 503–511 (2006).

44. Ruan, H. D. *et al.* Infrared spectroscopy of goethite dehydroxylation: III. FT-IR microscopy of in situ study of the thermal transformation of goethite to hematite. *Spectrochim. Acta. A. Mol. Biomol. Spectrosc.* **58**, 967–981 (2002).

45. Pomies, M. P. *et al.* TEM observations of goethite dehydration: application to archaeological samples. *J. Eur. Ceram. Soc.* **19**, 1605–1614 (1999).

46. Cioni *et al.* Temperatures of the AD 79 pyroclastic density current deposits (Vesuvius, Italy). *J. Geophys. Res. Solid Earth.* **109**, B02207, (2004).**46.**

47. http://pompeiisites.org/en/the-great-pompeii-project/ [Last accessed: 13th October].

48. Duran, A. *et al.* X-ray diffraction studies of Pompeian wall paintings using synchrotron radiation and dedicated laboratory made systems. *Appl. Phys. A* **99**, 333–340 (2010).

49. Duran, A. *et al.* Determination of pigments and binders in Pompeian wall paintings using synchrotron radiation–high-resolution X-ray powder diffraction and conventional spectroscopy–chromatography. *Archaeometry* **52**, 286–307 (2010).

50. Casadio, F. *et al.* The analysis of polychrome works of art: 40 years of infrared spectroscopic investigations. *J. Cult. Herit.* **2**, 71–78 (2001).

51. Bruni, S., *et al*. Spectrochemical characterization by micro-FTIR spectroscopy of blue pigments in different polychrome works of art. *Vib. Spectrosc.* **20**, 15–25 (1999).

52. Christensen, P. A. *et al.* Infrared spectroscopic evaluation of the photodegradation of paint Part I The UV degradation of acrylic films pigmented with titanium dioxide. *J. Mater. Sci.* **34**, 5689–5700 (1999).

53. Carbó, M. D. *et al.* Fourier transform infrared spectroscopy and the analytical study of works of art for purposes of diagnosis and conservation. *Anal. Chim. Acta* **330**, 207–215 (1996).

54. Larkin, P. Infrared and Raman spectroscopy: principles and spectral interpretation. (Elsevier, 2017).

55. Vetter, W. *et al.* Azurite in medieval illuminated manuscripts: a reflection-FTIR study concerning the characterization of binding media. *Herit. Sci.* **7**, 21-30 (2019).

56. Pięta, E. *et al.* Application of ATR-FTIR mapping to identification and distribution of pigments, binders and degradation products in a 17th century painting. *Vib. Spectrosc.* **113**, 102928 (2019).

57. Steger, S. *et al.* A complementary spectroscopic approach for the non-invasive in-situ identification of synthetic organic pigments in modern reverse paintings on glass (1913–1946). *J. Cult. Herit.* **38**, 20–28 (2019).

58. Manfredi, M. *et al.* Non-invasive characterization of colorants by portable diffuse reflectance infrared Fourier transform (DRIFT) spectroscopy and chemometrics. *Spectrochim. Acta. A. Mol. Biomol. Spectrosc.* **181**, 171–179 (2017).

59. Steger, S. *et al.* Capabilities and limitations of handheld Diffuse Reflectance Infrared Fourier Transform Spectroscopy (DRIFTS) for the analysis of colourants and binders in 20th century reverse paintings on glass. *Spectrochim. Acta. A. Mol. Biomol. Spectrosc.* **195**, 103–112 (2018).

60. Manfredi, M. *et al.* Portable diffuse reflectance infrared Fourier transform (DRIFT) technique for the non-invasive identification of canvas ground: IR spectra reference collection. *Anal. Methods* **7**, 2313–2322 (2015).

61. Vagnini, M. *et al.* Handheld new technology Raman and portable FT-IR spectrometers as complementary tools for the in situ identification of organic materials in modern art. *Spectrochim. Acta. A. Mol. Biomol. Spectrosc.* **176**, 174–182 (2017).

62. Saviello, D. *et al.* Non-invasive identification of plastic materials in museum collections with portable FTIR reflectance spectroscopy: reference database and practical applications. *Microchem. J.* **124**, 868–877 (2016).

63. Miliani, C. *et al.* Reflection infrared spectroscopy for the non-invasive in situ study of artists' pigments. *Appl. Phys. A* **106**, 295–307 (2012).

64. Amato, S. R. *et al.* A Multi-Analytical Approach to the Study of the Mural Paintings in the Presbytery of Santa Maria Antiqua Al Foro Romano in Rome. *Archaeometry* **59**, 1050–1064 (2017).

65. De Oliveira, L. F. *et al.* Caput mortuum: spectroscopic and structural studies of an ancient pigment. *Analyst* **127**, 536–541 (2002).

66. Madariaga, J. M. *et al.* Portable Raman, DRIFTS, and XRF analysis to diagnose the conservation state of two wall painting panels from pompeii deposited in the Naples national archaeological museum (Italy). *Appl. Spectrosc.* **70**, 137–146 (2016).

67. Kamińska, A. *et al.* Pigment identification of a XIV/XV c. wooden crucifix by means of the Raman spectroscopic technique. *J. Raman Spectrosc.* **37**, 1125–1130 (2006).

68. Gutiérrez-Neira, P. C. *et al.* Raman spectroscopy analysis of pigments on Diego Velázquez paintings. *Vib. Spectrosc.* **69**, 13–20 (2013).

69. Tuñón, J. A. *et al.* Micro-Raman spectroscopy on Iberian archaeological materials. *J. Raman Spectrosc.* **47**, 1514–1521 (2016).

70. Bredal-Jørgensen, J. *et al.* Striking presence of Egyptian blue identified in a painting by Giovanni Battista Benvenuto from 1524. *Anal. Bioanal. Chem.* **401**, 1433-1439 (2011).

71. Krishna, R. *et al.* Reference Module in Materials Science and Materials Engineering (Amsterdam, Elsevier, 2016).

72. Pozzi, F. *et al.* Evaluation and optimization of the potential of a handheld Raman spectrometer: in situ, noninvasive materials characterization in artworks. *J. Raman Spectrosc.* **50***,* 861-872 (2019).

73. Rousaki, A. *et al.* On-field Raman spectroscopy of Patagonian prehistoric rock art: Pigments, alteration products and substrata. *TrAC Trends Anal. Chem.* **105**, 338–351 (2018).

74. de Ferri, L. *et al.* In situ non-invasive characterization of pigments and alteration products on the masonry altar of S. Maria ad Undas (Idro, Italy). *Archaeol. Anthropol. Sci.* **11**, 609–625 (2019).

75. Barone, G. *et al.* In situ Raman and pXRF spectroscopic study on the wall paintings of Etruscan Tarquinia tombs. *Dyes Pigments* **150**, 390–403 (2018).

76. Colomban, P. On-site Raman study of artwork: Procedure and illustrative examples. *J. Raman Spectrosc.* **49**, 921–934 (2018).

77. Veneranda, M. *et al.* In-situ multianalytical approach to analyze and compare the degradation pathways jeopardizing two murals exposed to different environments (Ariadne House, Pompeii, Italy). *Spectrochim. Acta. A. Mol. Biomol. Spectrosc.* **203**, 201–209 (2018).

78. Moskovits, M. Surface-enhanced Raman spectroscopy: a brief retrospective. *J. Raman Spectrosc.* **36**, 485–496 (2005).

79. Nie, S. *et al.* Probing single molecules and single nanoparticles by surface-enhanced Raman scattering. S*cience* **275**, 1102–1106 (1997).

80. Neugebauer, W. *et al.* Naphthol Green–a forgotten artists' pigment of the early 20th century. History, chemistry and analytical identification. *J. Cult. Herit.* **36**, 153–165 (2019).

81. Pozzi, F. *et al.* Recent advances on the analysis of polychrome works of art: SERS of synthetic colorants and their mixtures with natural dyes. *Front. Chem.* **7**, 105-116 (2019).

82. Nardo, V. M. *et al.* SERS and DFT study of indigo adsorbed on silver nanostructured surface. *Spectrochim. Acta. A. Mol. Biomol. Spectrosc.* **205**, 465–469 (2018).

83. Shabunya-Klyachkovskaya, E. V. *et al.* Surface enhanced Raman scattering of inorganic microcrystalline art pigments for systematic cultural heritage studies. *Spectrochim. Acta. A. Mol. Biomol. Spectrosc.* **222**, 117235 (2019).

84. Sessa, C. *et al.* Towards a Surface Enhanced Raman Scattering (SERS) spectra database for synthetic organic colourants in cultural heritage. The effect of using different metal substrates on the spectra. *Microchem. J.* **138**, 209–225 (2018).

85. Tsoutsi, D. *et al.* Common aspects influencing the translocation of SERS to biomedicine. *Curr. Med. Chem.* **25**, 4638–4652 (2018).

86. Cañamares, M. V. *et al.* Raman, SERS, and DFT Analysis of the Main Alkaloids Contained in Syrian Rue. *J. Phys. Chem. C* **123**, 9262–9271 (2019).

87. Ai, Y. *et al.* Rapid qualitative and quantitative determination of food colorants by both Raman spectra and Surface-enhanced Raman Scattering (SERS). *Food Chem.* **241**, 427–433 (2018).

88. Kubackova, J. *et al.* Sensitive surface-enhanced Raman spectroscopy (SERS) detection of organochlorine pesticides by alkyl dithiol-functionalized metal nanoparticles-induced plasmonic hot spots. *Anal. Chem.* **87**, 663–669 (2014).

89. Canamares, M. V. *et al.* Surface-enhanced Raman scattering study of the adsorption of the anthraquinone pigment alizarin on Ag nanoparticles. *J. Raman Spectrosc.* **35**, 921–927 (2004).

90. Mosier-Boss, P. A. Review of SERS substrates for chemical sensing. *Nanomaterials* **7**, 142-171 (2017).

91. Thaler, J. *et al.* SERS activity of Co, Ni and Bi nanoparticles. *Proceedings of SBFoton International Optics and Photonics Conference, Campinas, Brazil* (2018).

92. Garcia-Leis, A. *et al.* Morphological tuning of plasmonic silver nanostars by controlling the nanoparticle growth mechanism: Application in the SERS detection of the amyloid marker Congo Red. *Colloids Surf. Physicochem. Eng. Asp.* **535**, 49–60 (2017).

93. Londero, P. Laser Ablation Surface-Enhanced Raman Spectroscopy (LA-SERS) for the Characterization of Organic Colorants in Cultural Heritage. *Proceedings of American Physical Society Bulletin, Louisiana, USA (2017).*

94. Price, B. *et al.* An infrared spectral library of naturally occurring minerals. *IRUG* **2**, 103–126 (1995).

95. Castro, K., *et al.* FTIR Spectra Database of Inorganic Art Materials. *Anal. Chem*. **75**, 214A-221A (2003).

96. Downs, R. T. The RRUFF Project: an integrated study of the chemistry, crystallography, Raman and infrared spectroscopy of minerals. *Proceedings of the 19th General Meeting of the International Mineralogical Association, Kobe, Japan,* (2006).

97. James, R. W. *et al.* The Optical Principles of the Diffraction of X-rays. (London, G. Bell & Sons, 1948).

98. Clark, R. J. *et al.* The identification by Raman microscopy and X-ray diffraction of iron-oxide pigments and of the red pigments found on Italian pottery fragments. *J. Mol. Struct.* **440**, 105–111 (1998).

99. Asscher, Y. *et al.* Combining multispectral images with X-ray fluorescence to quantify the distribution of pigments in the frigidarium of the Sarno Baths, Pompeii. *J. Cult. Herit.* (2019). DOI: 10.1016/j.culher.2019.04.014

100. Rovella, N. *et al.* Tituli Picti in the archaeological site of Pompeii: diagnostic analysis and conservation strategies. *Eur. Phys. J. Plus* **133**, 539-552 (2018).

101. Beck, L. *et al.* First use of portable system coupling X-ray diffraction and X-ray fluorescence for in-situ analysis of prehistoric rock art. *Talanta* **129**, 459–464 (2014).

102. Rotondo, G. G. *et al.* Non-destructive characterization of fifty various species of pigments of archaeological and artistic interest by using the portable X-ray diffraction system of the LANDIS laboratory of Catania (Italy). *Microchem. J.* **96**, 252–258 (2010).

103. https://www.olympus-ims.com/en/xrf-xrd/mobile-benchtop-xrd/terra/ [Last accessed: 13th October]

104. Sawczak, M. *et al.* Complementary use of the Raman and XRF techniques for non-destructive analysis of historical paint layers. *Appl. Surf. Sci.* **255**, 5542–5545 (2009).

105. Appolonia, L. *et al.* Combined use of FORS, XRF and Raman spectroscopy in the study of mural paintings in the Aosta Valley (Italy). *Anal. Bioanal. Chem.* **395**, 2005–2013 (2009).

106. Pitarch, À. *et al.* In situ characterization by Raman and X-ray fluorescence spectroscopy of post-Paleolithic blackish pictographs exposed to the open air in Los Chaparros shelter (Albalate del Arzobispo, Teruel, Spain). *Anal. Methods* **6**, 6641–6650 (2014).

107. Liritzis, I. *et al.* X-ray fluorescence spectrometry (XRF) in geoarchaeology (New York, Springer, 2011).

108. Popelka-Filcoff, R. S. *et al.* Trace element characterization of ochre from geological sources. *J. Radioanal. Nucl. Chem.* **272**, 17–27 (2007).

109. Samal, S. *et al.* Integrated XRD, EPMA and XRF study of ilmenite and titania slag used in pigment production. *J. Alloys Compd.* **474**, 484–489 (2009).

110. Haschke, M. *et al.* Fast elemental mapping with micro-XRF. *Adv X Ray Anal* **55**, 286–298 (2012).

111. Nakano, K. *et al.* Visualizing a black cat drawing hidden inside the painting by confocal micro-XRF analysis. *Microchem. J.* **126**, 496–500 (2016).

112. Wouters, B. *et al.* Characterization of archaeological metal remains in micromorphological thin sections using µXRF elemental mapping. *Geoarchaeology* **32**, 311–318 (2017).

113. Reiche, I. *et al.* Toward a three-dimensional vision of the different compositions and the stratigraphy of the painting L'Homme blessé by G. Courbet: coupling SEM–EDX and confocal micro-XRF. *Appl. Phys. A* **121**, 903–913 (2015).

114. Lehmann, R. *et al.* Klimt artwork: red-pigment material investigation by backscattering Fe-57 Mössbauer spectroscopy, SEM and p-XRF. *STAR Sci. Technol. Archaeol. Res.* **3**, 450–455 (2017).

115. Gebremariam, K. F. *et al.* Application of a portable XRF analyzer to investigate the medieval wall paintings of Yemrehanna Krestos Church, Ethiopia. *X-Ray Spectrom.* **42**, 462–469 (2013).

116. Uhlir, K. *et al.* Rembrandt's Old Woman Praying, 1629/30: A look below the surface using X-ray fluorescence mapping. *X-Ray Spectrom.* **48**, 293–302 (2019).

117. Pospíšilová, E. *et al.* Influence of laser wavelength and laser energy on depth profiling of easel painting samples. *Chem. Pap.* **73**, 2937-2943 (2019).

118. Lasheras, R. J. *et al.* Quantitative analysis of roman archeological ceramics by laser-induced breakdown spectroscopy. *Anal. Lett.* **50**, 1325–1334 (2017).

119. Tankova, V. *et al.* Investigation of archaeological metal artefacts by laser-induced breakdown spectroscopy (LIBS). *J. Phys. Conf. Ser.* **992**, 012003 (2018).

120. Senesi, G. S. *et al.* Application of a laser-induced breakdown spectroscopy handheld instrument to the diagnostic analysis of stone monuments. *Appl. Geochem.* **96**, 87–91 (2018).

121. Ke, C. *et al.* Application of laser induced breakdown spectroscopy for fast depth profiling analysis of type 316 stainless steel parts corroded by liquid lithium. *Fusion Eng. Des.* **136**, 1647–1652 (2018).

122. Senesi, G. S. *et al.* Depth profile investigations of surface modifications of limestone artifacts by laser-induced breakdown spectroscopy. *Environ. Earth Sci.* **76**, 565-573 (2017).

123. Gaudiuso, R. Calibration-free inverse method for depth-profile analysis with laser-induced breakdown spectroscopy. *Spectrochim. Acta Part B At. Spectrosc.* **123**, 105–113 (2016).

124. Valadas, S. *et al.* Study of mural paintings using in situ XRF, confocal synchrotron-μ-XRF, μ-XRD, optical microscopy, and SEM-EDS—The case of the frescoes from Misericordia Church of Odemira. *Microsc. Microanal.* **17**, 702–709 (2011).

125. Irazola, M. *et al.* In situ Raman spectroscopy analysis combined with Raman and SEM-EDS imaging to assess the conservation state of 16th century wall paintings. *J. Raman Spectrosc.* **43**, 1676–1684 (2012).

126. http://www.renishaw.es/es/sistema-sem-raman--6639 [Last accessed: 13th October]

127. https://www.xglab.it/combined-xrf-spectrometer-raman-analyzer-xraman.shtml [Last accessed: 13th October]

128. https://www.xglab.it/edxrf-xrd-spectrometer-hydra.shtml [Last accessed: 13th October]

129. Duetto 2 – eXaminArt. http://examinart.com/products/duetto-2/ [Last accessed: 13th October]

130. Colucci, M. T. *et al.* Tandem LA-ICP-MS & LIBS; A New Micro-Analytical Technique for the Measurement of Every Element in the Periodic Table. *Proceedings of Goldschmidt Conference Boston, USA* (2018).

131. Detalle, V. *et al.* LIBS-LIF-Raman: a new tool for the future E-RIHS. *Proceedings of Optics for Arts, Architecture, and Archaeology*, *Munchen, Germany* (2017).

132. Dik, J. *et al.* Visualization of a lost painting by Vincent van Gogh using synchrotron radiation based X-ray fluorescence elemental mapping. *Anal. Chem.* **80**, 6436–6442 (2008).

133. Van der Snickt, G. *et al.* Combined use of synchrotron radiation based micro-X-ray fluorescence, micro-X-ray diffraction, micro-X-ray absorption near-edge, and micro-fourier transform infrared spectroscopies for revealing an alternative degradation pathway of the pigment cadmium yellow in a painting by Van Gogh. *Anal. Chem.* **84**, 10221–10228 (2012).

134. Salvadó, N. *et al.* Shades of green in 15th century paintings: combined microanalysis of the materials using synchrotron radiation XRD, FTIR and XRF. *Appl. Phys. A* **111**, 47–57 (2013).

135. Salvadó, N. *et al.* Identification of copper-based green pigments in Jaume Huguet's Gothic altarpieces by Fourier transform infrared microspectroscopy and synchrotron radiation X-ray diffraction. *J. Synchrotron Radiat.* **9**, 215–222 (2002).

136. Pauk, V. *et al.* Characterization of natural organic colorants in historical and art objects by high-performance liquid chromatography. *J. Sep. Sci.* **37**, 3393–3410 (2014).

137. Degano, I. *et al.* HPLC-DAD and HPLC-ESI-Q-ToF characterization of early 20th century lake and organic pigments from Lefranc archives. *Herit. Sci.* **5**, 7 (2017).

138. Karapanagiotis, I. *et al.* Identification of red natural dyes in post-byzantine icons by HPLC. *J. Liq. Chromatogr. Relat. Technol.* **28**, 739–749 (2005).

139. Scadding, R. *et al.* An LA-ICP-MS trace element classification of ochres in the Weld Range environ, Mid West region, Western Australia. *J. Archaeol. Sci.* **54**, 300–312 (2015).

140. Green, R. L. *et al.* Trace element fingerprinting of Australian ocher using laser ablation inductively coupled plasma-mass spectrometry (LA-ICP-MS) for the provenance establishment and authentication of indigenous art. *J. Forensic Sci.* **52**, 851–859 (2007).

141. Clemenza, M. *et al.* Development of a multi-analytical approach for the characterization of ancient Roman lead ingots. *J. Radioanal. Nucl. Chem.* **311**, 1495–1501 (2017).

142. Degryse, P. *et al.* Tracing the resources of iron working at ancient Sagalassos (south-west Turkey): a combined lead and strontium isotope study on iron artefacts and ores. *Archaeometry* **49**, 75–86 (2007).

143. Baron, S. *et al.* Archaeological reconstruction of medieval lead production: Implications for ancient metal provenance studies and paleopollution tracing by Pb isotopes. *Appl. Geochem.* **24**, 2093–2101 (2009).

144. Baron, S. *et al.* Medieval lead making on Mont-Lozère Massif (Cévennes-France): tracing ore sources using Pb isotopes. *Appl. Geochem.* **21**, 241–252 (2006).

145. Iñañez, J. G. *et al.* Romita pottery revisited: a reassessment of the provenance of ceramics from Colonial Mexico by LA-MC-ICP-MS. *J. Archaeol. Sci.* **37**, 2698–2704 (2010).

146. Mason, T. F. *et al.* Zn and Cu isotopic variability in the Alexandrinka volcanic-hosted massive sulphide (VHMS) ore deposit, Urals, Russia. *Chem. Geol.* **221**, 170–187 (2005).

147. Medeghini, L. *et al.* Evaluation of a FTIR data pretreatment method for Principal Component Analysis applied to archaeological ceramics. *Microchem. J.* **125**, 224–229 (2016).

148. Awasthi, S. *et al.* Study of archaeological coins of different dynasties using libs coupled with multivariate analysis. *Opt. Lasers Eng.* **79**, 29–38 (2016).

149. Hazenfratz, R. *et al.* Study of exchange networks between two Amazon archaeological sites by INAA. *J. Radioanal. Nucl. Chem.* **309**, 195–205 (2016).

150. Mazzocchin, G. A *et al.* Isotopic analysis of lead present in the cinnabar of Roman wall paintings from the Xth Regio "(Venetia et Histria)" by ICP-MS. *Talanta* **74**, 690–693 (2008).

2. OBJECTIVES OF THE PhD THESIS

The main goal of this PhD Thesis has been to acquire knowledge about the composition of the pigments and materials used to give color to the Pompeian wall paintings and mosaics, trying also to approach the origin of some of the used materials. In addition to this, classification and quantification models of the yellow ochre pigment transformation into red caused by the thermal impact promoted by the emitted pyroclastic materials in the 79 AD eruption have been developed, since this is the most noteworthy and evident transformation of color in Pompeii. These methodologies will allow not only to discriminate original red ochre pigments from the reds caused by this transformation, but also to determine the degree of transformation and the impact temperature on each affected area.

Apart from the characterization of the colors (pigments) of Pompeii, this PhD Thesis also aimed to provide experimental evidences about the transformation of the calcium carbonate, the binder of the pigment grains in the fresco paintings of Pompeii, which could lead to the loss of cohesion of the pictorial layer to the wall, giving rise to the loss of the polychromy.

To attain these main objectives, seven operational objectives have been defined:

1. To develop portable non-invasive analytical methodologies useful to characterize in situ the composition of the materials used as pigments recovered from the burial of Pompeii. In this sense, inorganic pigments (blue, green, red, yellow and white) and lake pigments (pink and purple) have been analyzed.

2. To characterize in the laboratory the chemical composition of red and yellow ochre pigments and pink lake pigments using elemental and molecular techniques, together with chemometric analysis of the information to ascertain the possible source of the materials used to create certain pigments.

3. To optimize a sample pretreatment, which allows determining the nature of the dyes/colorants used to create the mentioned pink and purple lake pigments by means of SERS analysis developed using portable Raman spectrometers.

4. To characterize in situ the pictorial layer and the substrate used to manufacture Pompeian mosaic tesserae and to approach the source of the used materials.

5. To conduct carbon, oxygen and sulfur isotope ratio analysis to clarify if the atmospheric SO_2 from the current atmosphere, the one emitted during the eruption of 79 AD or the sulfates present in the modern restoration mortars are the responsible of the carbonate transformation into secondary carbonates or sulfates in the *intonachino*, *intonaco* and/or *arriccio* of the Pompeian walls and wall paintings, which could lead to the loss of cohesion of the pigment grains in the pictorial layers.

6. To design a model able to discriminate original Pompeian red ochre from the nowadays visible red areas painted originally using yellow ochre, based on the elemental composition determined by a handheld EDXRF spectrometer and Principal Component Analysis.

7. To develop classification and quantification models based on reflectance spectroscopy and Raman spectral imaging able to determine the percentage of transformation of the Pompeian yellow ochre pigment into red as a function of the impact temperature of the volcanic emissions.

3. EXPERIMENTAL PART

This chapter presents the samples of powdered pigments considered to develop this PhD Thesis, while the mosaics and wall paintings will be presented in each respective chapter. Besides, the used standards and reagents, the sample pretreatments required for the destructive analysis and the benchtop and portable/handheld instruments used for the characterization of materials are also described.

Considering the sampling restrictions in the Archaeological Park of Pompeii, portable/handheld instrumentation has been primarily selected to develop this PhD Thesis. However, when sampling permission from the Naples National Archaeological Museum was obtained, additional non-invasive and/or destructive studies were conducted in the laboratory to complete the experimental evidences obtained in situ.

For the molecular characterization of the powdered pigments, mosaic tesserae and polychromy of wall paintings, non-invasive spectroscopic techniques in their portable/handheld versions were mainly used. As it has been mentioned in the introduction, these techniques are widely employed in the field of conservation science[1]. Concretely vibrational spectroscopies such as Raman and infrared have been selected as the main techniques to extract conclusions. In this sense, many are the publications that show the usefulness of Raman spectroscopy technique in different fields of knowledge such as medicine[2], biology[3], forensics[4], conservation[5], art and archaeology[6,7], cultural

heritage analysis[8], etc. However, in some cases the results that can be obtained using Raman spectroscopy are limited by the influence of the fluorescence phenomena, which mask all the signals (bands) that represent the presence of a specific compound. In these cases, and also to achieve a complete mineralogical characterization of the samples, X-ray Diffraction can be used as an adequate option if samples can be extracted. Another alternative can be the use of metallic nanoparticles to promote the Surface Enhanced Raman effect (SERS), able to increase the Raman signal and quench the fluorescence, becoming the signals visible mainly for the identification of organic molecules.

Reflectance measurements in the Visible-Near Infrared-Short wave infrared (VNIR-SWIR) spectral range were also applied to verify its applicability in a specific study (Chapter 11).

To achieve a comprehensive study of pigments, apart from the molecular characterization, the elemental composition must be also investigated. In this PhD Thesis, laboratory based and portable/handheld instruments were also used for this purpose. For the non-invasive elemental characterization X-ray based analytical techniques have been widely used. When sampling process is not allowed, handheld X-ray fluorescence spectrometers (HH-XRF) are a good choice to determine the presence of major, minor and even trace elements up to the ppm ($\mu g \cdot g^{-1}$) level. In these cases, the area under study is usually set around 8-9 mm in diameter. Sometimes, lower lateral resolutions (around 3 mm in diameter) can be achieved using mechanical collimators, which was not the case of the instruments used in this PhD Thesis. For a preliminary screening in some cases, and to extract conclusive results in others, pigment powders and wall paintings polychromy were investigated using HH-XRF devices. When it was possible to extract samples, additional studies at lower lateral resolutions were conducted in the laboratory using Scanning Electron Microscope coupled to Energy Dispersive X-ray fluorescence spectrometry (spot size of some microns) and Energy Dispersive XRF (EDXRF at 1 mm and 25 μm lateral resolutions). All these studies were conducted qualitatively, since to obtain reliable and accurate results a previous optimization of quantitative methodologies should be

conducted. It is quite difficult to find certified pigment powders that will allow constructing empirical calibrations. Taking into account the thickness of the polychromy in the Pompeian wall paintings (around 10-20 μm), the direct HH-XRF measurements will show information about the elements composing both the paint layer and underlying mortar. Thereby, in this case homogeneous pressed pellets of the pigment do not represent the real matrix of the stratified sample. To overcome this limitation and to obtain accurate quantitative results, in some cases (Chapter 6), pigments powders were subjected to an acid extraction to perform a quantification of the trace elements (up to ppb, $ng \cdot g^{-1}$, level) by ICP-MS. Moreover, to study the lead isotopic ratio, useful to evaluate the possible provenance of specific pigments considered in this PhD Thesis, Thermal Ionization Mass Spectrometry (TIMS) analysis of ochre pigments was selected as the most adequate analytical technique. ICP-MS has been used also for this purpose. Moreover, for the stable isotopes analysis, an elemental analyzer coupled to an isotope ration mass spectrometer (EA-IRMS) was used.

All the analyses presented in this PhD Thesis have been conducted in the laboratories of IBeA of the Analytical Chemistry Department in the UPV/EHU, except SEM-EDS, XRD, TIMS and EA-IRMS analyses. These last analyses have been conducted in the Advanced Research Facilities (SGIKer) from the UPV/EHU. For the EA-IRMS analyses, an international doctorate internship in the Isotope Biogeochemistry group of the Department of Environmental Sciences of the Jozef Stefan Institute in Slovenia has been carried out.

3.1 Pompeian powdered pigments

Original raw powdered pigments have been recovered during the excavations campaigns in the archaeological site of Pompeii. These pigments were recovered in their original containers (mainly ceramic bowls) and they have been deposited and preserved in the Naples National Archaeological Museum (MANN) and in the Applied Research Laboratory of Pompeii (ARLP).

3.1.1 Pigments preserved in the Naples National Archaeological Museum

Most of the pigment powders analyzed in this PhD Thesis belong to the collection of the MANN. In Fig. 3.1 an assortment of pigments that were put to our disposal is shown. Concretely, one green, red, and white pigment, together with two yellow and different blue pigments from the MANN were analyzed in situ using portable instrumentation (Chapter 4). In addition, to perform deeper analyses in the laboratory of the red and yellow ochre pigments using benchtop instruments, we were allowed to extract some milligrams from five red and three yellow ochres (Chapter 5). Finally, four different pink lake pigments were also analyzed in situ, and after their analysis, some powders were also extracted to perform further analyses in the laboratory (Chapter 6 and 7).

Fig. 3.1. Some of the raw pigments preserved in the bowls deposited in the MANN and considered in this PhD Thesis.

3.1.2 Pigment powders from the Applied Research Laboratory of Pompeii (ARLP)

Apart from the previously described pigments, additional pigments from the collection preserved in the ARLP were also analyzed in situ (see Fig. 3.2). Concretely, one green and red pigment, two pink lake pigments and four blue pigments were considered.

Fig. 3.2. A green (left) and blue pigment (right) contained in their original bowls belonging to the deposit of ARLP.

3.2 Standards, reagents and apparatus

3.2.1 Standards

For the identification of the organic colorant in the Pompeian pink lake pigments (Chapter 7), alizarin (97%), and purpurin (90%) standards, both purchased from Sigma Aldrich (San Luis, USA) together with madder root lake pigment standard, purchased from Kremer (New York, USA), were used.

For the $\delta^{13}C$ and $\delta^{18}O$ isotopic analysis of Chapter 9, IAEA-CO1 Carrara marble, IAEA-CO8 natural carbonatite from Schelingen (Kaiserstuhl, Germany), and IAEA-CO9 barium carbonate powder reference materials were used for calibration of measurements. On the other hand, for the $\delta^{34}S$ isotopic analysis, IAEA-SO5 and IAEA-SO6, both barium sulfates obtained by precipitation from sulfate solution, and NBS-127 barium sulfate prepared by ion exchange of sulfate from seawater reference materials with $\delta^{34}S_{VCDT}$ values of 0.5‰, -34.1‰, and 20.3‰, respectively, were used for calibration.

To validate the Raman imaging-based quantitative method developed in the Chapter 11 of this PhD Thesis, goethite (Y-464 series, Nubiola, Spain) and hematite (99.99% metal basis, Alfa Aesar, MA, USA) standards were used to prepare the synthetic pellets based on the mixture of both iron oxides.

3.2.2 Reagents

To synthesize the Ag-nanoparticles (Ag-NPs) that were used in the Surface Enhanced Raman spectroscopy (SERS) analyses described in Chapter 7, silver nitrate (99.9999% trace metal basis) and trisodium citrate dihydratate (>99%), both from Sigma Aldrich (San Luis, Missouri, USA), were used.

For the acid digestion of the lake pigments considered in the PhD Thesis, HCl (37%, Pro Analysis, Merck) was used. For the subsequent liquid-liquid extraction hexane (95%, HPLC grade) and ethyl acetate (HPLC grade), both purchased from LAB-SCAN Analytical Sciences, were used.

For the lead isotopic analysis of ochre pigments, HCl (37%, Merck EMSURE®) and HNO_3 (67%, Merck EMSURE®) were used for the sample treatment before TIMS measurements. For the dissolution of the residue after the evaporation, HBr (TraceSELECT® Ultra, Fluka Analytical) was added. Finally, for the purification of Pb, PFA microcolumns for chromatography (Savillex) and AG 1X8 ionic exchange resin (Eichrom) were used.

For the $\delta^{13}C$ and $\delta^{18}O$ isotopic analysis of the samples, 100 % H_3PO_4 was prepared in the laboratory by the addition of 840 g of P_2O_5 (≥98.0%) to a 1.5 L of 85% H_3PO_4 solution (both of them purchased from Sigma Aldrich) until the complete dissolution by heating and stirring, following the procedure described by Sharp[9]. Besides, for the $\delta^{34}S$ isotopic analysis, granular tungsten oxide was also used (Elementar, Tungsten (VI) Oxide Fine

Powder Art. No. 11.02-0017). For the samples pretreatment, HCl (Sigma Aldrich, 37%), Eschka reagent 38-42% ($2MgO{\cdot}Na_2CO_3$, Sigma Aldrich, USA) and 10% $BaCl_2$ solution done in the laboratory by the addition of 10 g of $BaCl_2$ (Sigma Aldrich, 99.95%) to 100 mL of MiliQ water were used.

3.2.3 The muffle used for the thermal ageing experiments

For the thermal ageing experiments described in Chapter 11, a Hobersal HD Series muffle was used. The thermal impact and the exposure time for each fragment was the same, trying to simulate faithfully the real impact of the pyroclastic flow into the wall painting.

3.3 Molecular handheld/portable spectroscopic instrumentation

3.3.1 Portable Raman spectrometers

For the molecular in situ analyses of the inorganic and lake pigments (Chapter 4), for the SERS measurements (Chapter 7) and for the characterization of the tesserae of the Pompeian mosaics considered in this PhD Thesis (Chapter 8), two portable Raman spectrometers have been used.

On the one hand, a portable innoRam^{TM} Raman spectrometer ($B_{\&}WTEK_{INC.}$, Newark, USA) provided with a CleanLaze® technology 785 nm excitation laser (< 300 mW laser output power) has been used (see Fig. 3.3). The instrument implements a controller of the laser power (a scale from 0 to 100% of the total power of the laser).

To prevent from thermal decompositions of the pigments, the laser power was carefully controlled. It also includes a two dimensional charge coupled device (CCD) to detect the dispersed Raman signal, which is Thermoelectric Cooled (TC) to -20 ºC to maximize the dynamic range by reducing dark current. A back-thinned CCD is used to obtain 90% quantum efficiency via collection of incoming photons at wavelengths that would not pass through a front illuminated CCD. A spectral resolution (FWHM) of 3.4 cm^{-1}, measured at 912 nm, can be achieved with a double pass transmission optic. The spectra were acquired in the 65-2500 cm^{-1} spectral range.

On the other hand, a portable innoRam^{TM} BWS445-532S ($B_{\&}WTEK_{INC}$, Newark, USA) spectrometer has been also used. In this case, the wavelength of the excitation laser implemented is of 532 nm (45 mW laser output power) and the Raman signals were also collected by a CCD detector refrigerated by Peltier effect. The spectral range of the Raman instrument is 65-3750 cm^{-1} with an average spectral resolution of 5 cm^{-1}, measured at 609 nm. With both spectrometers, in general terms, the spectra were acquired for 1-15 seconds and 5-30 accumulations in order to improve the signal-to-noise ratio. Both Raman spectrometers are provided with a probe connected to an optic fibre (1.5 m length).

To reduce the lateral resolution of analysis, and to conduct in situ microscopic analysis of the pigments, the probes were coupled to a BAC151B portable video-microscope ($B_{\&}WTEK_{INC.}$, Newark, USA), focusing the areas under study. For the microscopic study a 20x (8.8 mm working distance and 105 μm laser beam spot size) and 50x (3.68 mm working distance and 42 μm laser beam spot size) objective lens were used.

Fig 3.3. The innoRam portable Raman spectrometer with the used video-microscope.

The positioning of the portable video-microscope is controlled by a micrometric stage and thanks to the dual laser wavelength optic port system it can be coupled to both probes connected to the spectrometers implementing the 785 and 532 nm laser wavelengths respectively.

The spectral acquisition and data treatment has been performed using the BWSpec™ v.4.0215 ($B_{\&}WTEK_{INC.}$, Newark, USA) and OMNIC 7.2 (Thermo Fisher Scientific, Massachusetts, USA) softwares respectively. The interpretation of all the Raman results was performed by comparing the acquired Raman spectra with Raman spectra of pure standard compounds collected in the e-VISNICH dispersive Raman database[10]. Additionally, free Raman databases (e.g., RRUFF[11]) were also considered for the assignation of Raman bands.

3.3.2 Handheld Diffuse Reflectance Infrared Fourier Transform (DRIFT) spectrometer

The infrared in situ measurements of the mosaic tesserae (Chapter 8) have been acquired using a 4100 Exoscan handheld DRIFT spectrometer from A2 Technologies (nowadays Agilent Technologies, California, USA). In this case, the device implements a Diffuse Reflectance sampling interface (DRIFT), which allows placing it in direct contact with the surface under study. The Michelson interferometer implemented has a maximum resolution of 4 cm^{-1} and a maximum spectral range of 400–4000 cm^{-1}. The system has a ZnSe beam splitter and a temperature stabilized DTGS detector. The background was acquired with a diffuse gold reference cap and the spectra were acquired under 32 accumulations. DRIFT spectra were acquired and saved in a PDA using the A_2 Technologies MicroLab Mobile Software (see Fig. 3.4). The spectra treatment has been performed exporting them to the OMNIC 7.2 software (Thermo Fisher Scientific, Massachusetts, USA).

Fig 3.4. 4100 Exoscan handheld DRIFT spectrometer.

3.3.3 Field reflectance Visible–Near Infrared–Short Wave Infrared (VNIR–SWIR) spectroradiometer

The reflectance measurements presented in the Chapter 11 were acquired using an ASD High Resolution FieldSpec4 spectroradiometer (Analytical Spectral Devices Inc., Boulder, USA). The instrument is equipped with bare optic fibre for remote mode operations (see Fig. 3.5). A halogen lamp (ASD Illuminator) was used as a light source placed at 30 cm of distance from the sample under study. The angle between the sample and the detector fibre was 45°. The fibre has an aperture angle of 25° and was placed to a minimum distance from the sample in order to minimize the surface covered by the fibre. The system works in 350-2500 nm wavelength range. This device uses three detectors for different spectroscopic ranges: a silicon photo-diode array for VNIR (350-1000 nm), a InGaAs photo-diode for SWIR1 (1001-1800 nm) and a InGaAs photo-diode for SWIR (1801-2500 nm). The spectral resolution is 3 and 8 nm in the VNIR and SWIR regions respectively. Sensor optimization and calibration was set with a Spectralon® white reference standard scanned once before each sample was measured. Each spectrum is the result of the average of 10 scans. Spectra were collected with the RS3 software (ASD Inc.), and analyzed with the ViewSpecPro software (ASD Inc.).

Fig 3.5. ASD High Resolution FieldSpec4 spectroradiometer.

3.4 Elemental handheld/portable spectroscopic instrumentation

3.4.1 Handheld energy dispersive X–ray fluorescence spectrometers (HH–EDXRF)

For the in situ elemental characterization of the pigments under study and the mosaic tesserae, two different HH-EDXRF spectrometers have been used.

The X-MET 5100 (Oxford Instruments, UK) HH-EDXRF spectrometer (see Fig. 3.6) has been used to characterize the elemental composition of powdered pigments (Chapter 4 and 6), mosaic tesserae (Chapter 8) and the polychromy of wall paintings (Chapter 10). This instrument is equipped with a Rh tube working at a maximum voltage of 45 kV. The size of the emitted X-ray beam is 9 mm. The analyzer includes a silicon drift detector (SDD) of high resolution that is able to provide an energetic resolution of 150 eV (FWHM of the Mn Kα line at -20 ˚C) and a PDA to control the spectrometer and also to save the spectral and quantitative information.

To determine possible contributions from the set up of the instrument (e.g., detector) and possible contaminations coming from the XRF analyzer window, 20 repetitive spectra of an instrumental blank (a PTFE block) were acquired before each measurement batch.

To determine the presence of the heaviest elements (Z > Ti), the spectra were acquired during 100 seconds (real time) and the voltage and current of the X-ray tube were set at 40 kV and 15 μA respectively. Additionally, to reduce the background of the spectrum for the energy region of heavy elements (energies higher than 7 keV) and to improve then the limit of detection of trace elements, a 500 μm Al filter was occasionally used.

To improve the detection of the lighter elements (Z < 22), additional measurements were performed without the Al filter and at lower voltage (13 kV) and higher current (40 μA). The test time in this case was 35 seconds for each measurement.

Fig 3.6. The X-MET 5100 handheld EDXRF spectrometer measuring a Pompeian wall painting.

The software implements the M-Quant quantification software package based on the use of Fundamental Parameters quantification methods. However, the quantification methods implemented in the device are not related with inorganic or lake pigments, thus in this PhD Thesis, the net counts of K_α lines of the detected elements in the spectrum have been normalized, depending on the case, against the most appropriate line to extract conclusions. The specific normalization of the elemental data is explained in each Chapter.

For the direct analysis of the lake pigments in the MANN, an Innov-X Alpha Series HH-EDXRF spectrometer has been used. This instrument employs a miniature, low power X-ray tube as a source for sample excitation. Transmission Ag-anode tube operates at up to 40 kV with a maximum current of 50 μA.

A high performance Si PiN thermo electronically cooled diode detector with energy resolution ≤230 eV was used to measure the characteristic X-rays from the constituent elements of the pink and purple lake pigments. The Innov-X Alpha Serie has been driven by HP IPAQ pocketPC using SoilMode software including light element analyses (LEAP) from phosphorus (light elements with atomic number higher than 15). The analyses were performed directly introducing the sampling interface in the original bowls containing the lake pigments. To prevent the contamination of the sampling interface, a Mylar film was placed on the top of the lake pigments surface. Ten repetitive measurements have been performed with the HH-EDXRF spectrometer.

3.4.2 Laser induced breakdown spectrometer (LIBS)

Additional elemental studies of the pictorial layer of the mosaic tesserae (Chapter 8) and from yellow and red colored wall paintings (Chapter 10) have been performed using the EasyLIBS IVEA (model Easy 2C) LIBS spectrometer (see Fig. 3.7).

This instrument employs a pulsed Nd:YAG laser, with the possibility of operating in a dual pulse mode, emitting at a wavelength of 1064 nm. The laser energy per pulse on the sample is higher than 25 mJ with a repetition rate of 1 Hz and 4–5 ns duration of laser pulse. Measurements were performed with the double pulse mode. An optimized delay time of 50 μs to the laser pulse and a gate width of 5 ms were employed. Considering that LIBS measurements produces the ablation of a very thin layer of material, in the case of mosaic tesserae analysis about 30 pulses were performed consecutively at the same point of interest to evaluate the stratigraphic evolution of the elements (mainly Fe and Ca) that compose the analyzed matrix.

The Easy 2C model consists of an optic probe that allows focusing the laser connected to a computer and to three spectrometers, covering ultraviolet (UV, 196–419 nm), visible (VIS, 420–579 nm) and near infrared (NIR, 580–1000 nm) spectral ranges. The software used for automatic acquisition, control, visualization and processing of the spectra was the AnaLIBS version 6.3. The analyses were performed directly placing the sampling interface on the surface of the tesserae. Taking into account the signal-to-noise ratio of the collected LIBS spectra, only peaks whose intensity has been greater than a threshold of 0.5σ of the total spectrum (under 150–200 counts) were considered for line determination.

Fig 3.7. EasyLIBS (model Easy 2C) handheld spectrometer from IVEA, measuring a mosaic from Pompeii.

3.5 Analytical techniques to determine the molecular composition of the pigments in the laboratory

3.5.1 Raman micro–spectroscopy

Raw inorganic (Chapter 5) and lake pigments (Chapter 6), efflorescences on wall paintings (Chapter 9) and wall painting fragments (Chapter 11) have been characterized in this PhD Thesis through the use of micro-Raman spectroscopy. The confocal Raman micro-spectrometer inVia (Renishaw, Gloucestershire, UK) has been used (see Fig. 3.8). The spectrometer is coupled to a DMLM Leica microscope (Bradford, UK). For the visualization and first focusing, 5× PLAN (0.12 aperture) objective and 20× N PLAN (0.40 aperture) lens have been used. The spectra have been acquired using 50× PLAN (0.75 aperture and lateral resolution of 2 μm) long range objective. The microscope implements a Prior Scientific motorized XYZ positioning stage with a joystick and is equipped with a micro-camera to facilitate the search of the area of interest on the sample. Moreover, this instrument is installed on an antivibratory table inside a temperature controlled room.

For the Raman analyses, both 532 nm (nominal laser power 50 mW) and 785 nm (nominal laser power 350 mW) excitation lasers were used, selecting the most appropriate one depending on the nature of the sample to be analyzed. The lasers were set at low power (not more than 1 mW at the sample) to avoid thermal decomposition of the samples under study. In specific cases, this laser power was increased avoiding in all the cases the thermal decomposition of the sample. The spectrometer has been calibrated daily by using the 520.5 cm^{-1} Raman band of a silicon chip. Data acquisition was carried out using the Wire 4.2 software package (Renishaw). In general, for the single point analysis, spectra were acquired between 60 and 1800 cm^{-1} spectral region with a resolution of 1 cm^{-1} during 5-60 s and several scans (between 1 and 15) were accumulated for each spectrum to improve the signal-to-noise ratio.

Fig 3.8. The Renishaw InVia confocal micro-spectrometer.

Thanks to the developments in spectroscopic detector technologies combined with multispectral image-processing strategies, the simultaneous recording of spectral and spatial information is nowadays possible. Thanks to this, Raman chemical imaging analyses can be carried out, which show the distribution of molecular compounds within a spatial location of any kind of sample. In this sense, Raman imaging was applied in Chapter 11. For that, the High Resolution (HR) StreamLine option, which is able to generate chemical images preventing from laser induced sample damage, was used. As in the case of single point measurements, in the imaging analyses the lasers have been set at low power (not more than 1 mW at the sample) to avoid thermal decomposition. Thanks to the implementation of the motorized stage, the sample is moved under the lens, to be the line raster across the area of interest. As the line moves across the sample, data are swept synchronized across the CCD detector and read out continuously.

In this PhD Thesis, the Raman images were acquired using the 20x objective since with 50x significant defocusing has been observed, which difficult mapping analysis. For that, Raman spectra were recorded in 0.5 s and 1 accumulation in the 100-1350 cm^{-1} spectral range, with a step size of 20 μm. In the data collected from each map, a cosmic ray removal treatment has been performed followed by a baseline correction. Finally, the spectra have been filtered based on the signal-to-ratio of the main Raman band of each molecular phase to represent the chemical image in the selected mapped area. The Raman quantitative analysis was performed by means of the Direct Classical Least Squares (DCLS) algorithm, implemented in the Wire 4.2 software, which is based on the comparison of each spectrum acquired in the map with the spectrum of pure standards acquired in the same conditions. The scaling factor is automatically selected to fit as best as possible with the spectra of the Raman map.

3.5.2 Infrared spectroscopy (IR)

The infrared spectra of the lake pigments under study (Chapter 6) have been acquired using a Jasco 6300 FTIR spectrophotometer (see Fig. 3.9 left). The equipment implements a Michelson interferometer offering a maximum resolution of 0.07 cm^{-1} and a Ge/KBr beam splitter with a DLATGS detector with Peltier temperature control. The IR measurements have been performed in transmission (FTIR) and in Attenuated Total Reflectance (ATR) mode (see Fig. 3.9 right).

To acquire the spectra in FTIR mode, pressed pellets were prepared using KBr. For FTIR measurements 32 scans per spectrum were accumulated at a resolution of 4 cm^{-1} in the mid-infrared spectral range (4000-400 cm^{-1}). The ATR spectra were collected directly pressing the pigments on the ZnSe crystal from the MIRacle™ Single Reflection ATR unit (PIKE Technologies, Fichburg, USA, see Fig. 3.2 right) inserted in the spectrophotometer.

The spectra were also collected in the mid-infrared region (750-4000 cm^{-1}) recording 32 scans per spectrum at a spectral resolution of 4 cm^{-1}.

Fig 3.9. The Jasco 6300 infrared spectrometer (left) and ATR module integrated in it (right).

3.5.3 X–ray diffraction (XRD)

Apart from the molecular characterization of the pigments using Raman spectroscopy, the mineralogy of the inorganic pigments (Chapter 5) and lake pigments (Chapter 6) was determined using X-ray diffraction. For that, a PANalytical Xpert PRO powder diffractometer (see Fig. 3.10) equipped with a copper tube ($\lambda Cu_{K\alpha mean}$ = 1.5418 Å, $\lambda Cu_{K\alpha 1}$ = 1.54060 Å, $\lambda Cu_{K\alpha 2}$ = 1.54439 Å), vertical goniometer (Bragg–Brentano geometry), programmable divergence aperture, automatic interchange of samples, secondary graphite monochromator, and PixCel detector, was used. The operating conditions for the Cu tube were 40 kV and 40 mA, with an angular range (2θ) scanned between 5 and 70°. The treatment of the diffractograms and the identification of the mineral phases present have been carried out using the specific X'pert HighScore (PANalytical) software in combination with the specific Powder Diffraction File (PDF2) database (International Centre for Diffraction Data – ICDD, Pennsylvania, USA).

Fig. 3.10. PANalytical Xpert PRO powder diffractometer.

3.6 Analytical techniques to determine the elemental composition of the pigments in the laboratory

3.6.1 Scanning electron microscope couple to energy dispersive X-ray fluorescence spectrometry (SEM-EDS)

SEM-EDS has been used to characterize the elemental composition of the lake pigments considered in Chapter 6. Moreover, this technique was used to determine the grain size of the yellow ochre pigment applied on Pompeian painting fragments, the distribution of this pigment in this kind of polychrome and the elemental composition of selected microscopic areas of the polychrome in the mentioned wall painting fragments (see Chapter 11). For that, a JEOL JSM-7000-F (JEOL, Tokyo, Japan) SEM-EDS (Oxford instruments INCA, Energy 350, Oxfordshire, UK) was used. To improve the conductivity of

the samples for the image acquisition, they were previously metalized by depositing ≈20 mm of a carbon layer. SEM images were acquired under high vacuum employing an acceleration voltage of 20-30 kV and 6-13 mm working distance. The elemental analysis was carried out using 8.5 mm working distance, a 35^{o} take-off angle and an acceleration voltage of 20 kV. An integration time of 50 s was employed to improve the signal-to-noise ratio of EDS spectra. The spectral data treatment was carried out using the INCA software (Oxford Instruments, Abingdon, Oxfordshire, UK).

3.6.2 Energy dispersive X–ray fluorescence spectrometry (EDXRF)

The elemental analysis was conducted using the M4 TORNADO (Bruker Nano GmbH, Berlin, Germany) EDXRF spectrometer (see Fig. 3.11). This instrument allows acquiring measures at 1 mm and down to 25 μm of lateral resolutions thanks to its dual configuration. The 25 μm spatial resolution is achieved by using poly-capillary lens, while the one of 1 mm is achieved through the use of a mechanical collimator. In this PhD Thesis both lateral resolution were used depending the aim of the analysis. The used Rh X-ray tube operates up to 50 kV and at a maximum current of 600 μA, in the case of 25 μm lateral resolution, and up to 700 μA when 1 mm lateral resolution is used. In general terms, the conditions considered were 50 kV and 600/700 μA depending on the desired analysis. The detection of the fluorescence radiation was performed by an XFlash® silicon drift detector with 30 mm^2 sensitive area and energy resolution of 145 eV for Mn-Kα. To improve the detection of light elements (Z < Ti), the measurements were conducted under vacuum (20 mbar) without the use of filters. To achieve the vacuum, the diaphragm pump MV 10 N VARIO-B was used. In general, the live time used for each measurement was of 300 seconds in order to improve the detection of minor and trace elements.

For the focusing of the area under study, two video-microscopes integrated in the spectrometers were used, one of them to explore the sample under low magnification areas (1 cm^2), and the other one to perform the final focusing (1 mm^2).

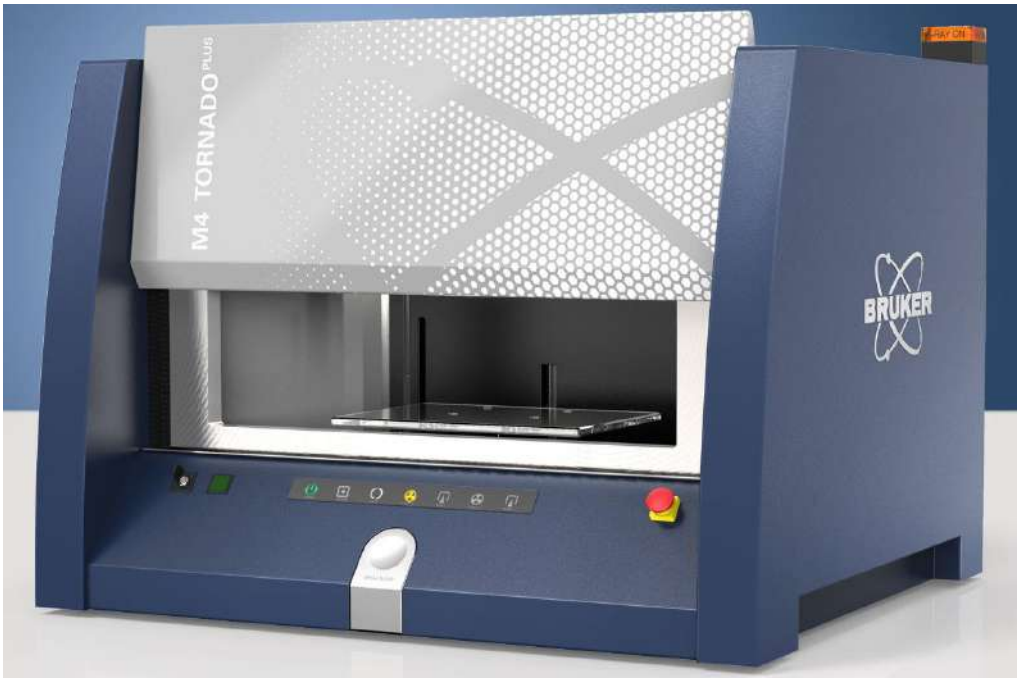

Fig 3.11. M4 Tornado EDXRF spectrometer.

Apart from simple point measurements, the instrument offers also the option of Hypermaps (distributions of the detected elements) acquisition. Concretely, the wall paintings fragments subjected to thermal ageing (Chapter 11) were subjected to XRF imaging study. The conditions for the XRF images acquisition were 5 ms, 5 scans and a step size of 20 μm. To construct the elemental images a previous deconvolution of the signals in the sum spectrum representing the whole mapped area were conducted. After that, the distribution map of each element was represented as a function of the intensity of each detected element K_α line, except for Pb, using in this case the L_β line (12.6 keV). The spectra acquisition and treatment was performed using the M4 TORNADO software.

3.6.3 Inductively coupled plasma–mass spectrometry (ICP–MS)

For the quantification of the major, minor and trace elements present in the pink lake pigments under study, an acid extraction was conducted before the analysis by ICP-MS (see Chapter 6). Considering the few amount of sample available, an isolated extraction of each lake pigment was carried out. For that purpose, 10 milligrams of each lake pigment were digested with 10 mL of 10% HCl and was heated up to 60°C under continuous stirring. The resultant acid extracts were used both for the analysis of the major, minor and trace elements by ICP-MS (Chapter 6) and for the liquid-liquid extraction of the organic colorant present in the lake pigments (Chapter 7). For this last organic extraction, hexane and ethyl acetate were used as potential candidates. Once the dye was extracted into the organic solvent, it was evaporated under a N_2 stream and re-dissolved with methanol (HPLC grade, Scharlab, Spain). Thereby, the posterior addition of the Ag-NP colloid will lead into a miscible mixture of the organic dye and Ag-NPs.

For the quantification of the elements and the determination of the lead isotopic ratio of the pink lake pigments (Chapter 6), a NexION 300 ICP-MS (Perkin Elmer, Massachusetts, USA) was used. This instrument includes a OneNeb nebulizer (Agilent), a cyclonic mix chamber and nickel cones. The calibration standards were prepared gravimetrically in an analytical balance (Mettler-Toledo XS205 model, Columbus, OH, USA) of ± 0.00001 g precision from commercial solutions of 1000 µg/mL supplied by Alfa Aesar (Specpure®, Plasma Standar solution, Germany). The used argon (Ar) was supplied by Praxair (99.999%, Madrid, Spain). Plasma conditions, argon flow of the nebulizer, torch position and the voltages of the lenses of the instrument were optimized before each measurement aspiring a standard solution of 1 ng/mL of Mg, Rh, In, Ba, Pb and U. The gas flow of the nebulizer was optimized obtaining a relation between sensitivity and low level of oxides (lower than 2.5% for CeO/Ce relation).

The quantified elements and their respective isotopes were ^{7}Li, ^{23}Na, ^{24}Mg, ^{27}Al, ^{28}Si, ^{39}K, ^{44}Ca, ^{47}Ti, ^{51}V, ^{52}Cr, ^{55}Mn, ^{56}Fe, ^{59}Co, ^{60}Ni, ^{63}Cu, ^{66}Zn, ^{75}As, ^{88}Sr, ^{107}Ag, ^{111}Cd, ^{120}Sn, ^{121}Sb, ^{137}Ba, ^{184}W, ^{202}Hg, ^{205}Tl and ^{208}Pb. On the other hand, Ni, Be, Sc, Ge, In, Re and Bi were used as internal standards and collision with He was used in order to eliminate possible polyatomic interferences. A blank was also measured in order to detect possible contaminations in the process. The metal analysis presents a detection and quantification limit of few ng/g.

3.6.4 Thermal Ionization Mass Spectrometry (TIMS)

To obtain accurate isotopic compositions of the yellow and red ochre pigments, TIMS measurements were performed (Chapter 5). For that, the sample treatment previous to the purification of the Pb contained in the red and yellow ochres consisted in the sequential digestion proposed by Dold *et al.*[12] TIMS analysis was conducted using the NEPTUNE Multicollector Inductively Coupled Plasma coupled to Mass Spectrometer (MC-ICP-MS) (Thermo Fisher Scientific, Massachusetts, EEUU) using a PFA micronebulizer with nominal suction of 100 $\mu L \cdot min^{-1}$ (Elemental Scientific, Nebraska, EEUU) and an Electrospray Ionization (ESI) Apex IR dewatering system. The baseline (electronic + chemical) of the samples was subtracted based on the measurement of a blank during 60 s. The measurement of the samples was performed in 105 cycles with an integration time of 8 s per cycle. The instrumental mass fractionation was corrected internally with the addition to each sample of a specific amount of the NBS-997 thallium isotope reference material, and using a ^{205}Tl / ^{203}Tl ratio of 2.3889.[13] The reliability and reproducibility of the method was verified by sporadic measurements of the NBS981 certified reference material alternated with measurements of the samples, both under the same conditions.

3.6.5 Stable isotopes analysis through isotope ratio mass spectrometry coupled to an elemental analyzer (EA–IRMS)

For the C and O isotopic analysis, around 2-3 mg of pulverized sample were used, while for the S isotopic analysis, 2-5 g were required to obtain enough mass of $BaSO_4$ precipitate.

For the sulfur isotopic analysis, the sulfates present in the 2-5 g of sample were dissolved using around 10 mL of HCl (pH around 2). Once most of the sample was dissolved, 90 mL of Milli-Q water was added. The solution was boiled during 1 hour under stirring, and after cooling down, filtered with a glass fiber filter (Whatman GF/F). Finally, 5 mL of 10% $BaCl_2$ were added to the filtrate in order to obtain the $BaSO_4$ precipitate. To favor the coarser precipitation, the solution was kept in a sand bath at 50°C for 24h.

The total sulfur extraction of the volcanic strata samples was performed using the Eschka´s reagent, which is able to oxidize the entire present S to SO_4^{-2}. For the extraction, a proportion of sample:Eschka of 1:4 was mixed and subjected to 800°C during 4 h. The dissolution of sulfates was performed by means of hot MilliQ water. The solution was filtered and acidified with HCl to pH around 2. The precipitation of the sulfates as $BaSO_4$ was conducted by addition of 5 ml of the 10% $BaCl_2$ solution.

For all the type of samples, the solution with the $BaSO_4$ precipitate was filtered and the obtained precipitate was dried in the oven. 0.2-0.6 mg of this $BaSO_4$ were used for the $\delta^{34}S$ analysis.

For the carbon and oxygen stable isotope analysis 2-3 mg powdered sampl were placed in a septum vial (Exetainer® 3ml flat bottom vial, Labco, U.K). The air was removed from vials by flushing them during 200 s with He (50 ml/s). Then, about 100 µl of 100% H_3PO_4

was added and the mixture was kept at 60°C during 24 h,[14] in order to react with the calcite of the mortar producing CO_2 (g) which was analyzed in the IsoPrime 100 isotope ratio mass spectrometer with Multiflow Bio equilibrator.

Results are reported in the standard delta notation ($\delta^{18}O$) as per mil difference to the Vienna PeeDee Belemnite (‰ vs. VPDB) standard. In the case of carbon, results are reported in the standard delta notation ($\delta^{13}C$) as per mil difference to the Vienna Pee Dee Belemnite (‰ vs. VPDB) standard. For both, $\delta^{18}O$ and $\delta^{13}C$, reproducibility as determined through replicate measurements was generally better than ± 0.5‰.

For sulfur isotope measurements, 0.2-0.6 mg of the obtained $BaSO_4$ were homogenously mixed with tungsten oxide and packed in tin capsules. An IsoPrime 100 isotope ratio mass spectrometer with elemental analyzer (PyroCube) was used for the isotope analysis. Results are reported in the standard delta notation ($\delta^{34}S$) as per mil difference to the Vienna Canyon Diablo Troilite (‰ vs. VCDT) standard. Reproducibility as determined through replicate measurements was generally better than ± 0.3‰.

3.7 Synthesis of Ag–NPs and verification of their usefulness for the SERS analysis

The synthesis of the Ag-NPs was carried out following the Lee-Meisel[15] method. Briefly, this method consists on the reduction of the silver present in a $AgNO_3$ solution by the addition of trisodium citrate dihydrate as reducing agent. For that, 50 mL of a 1mM $AgNO_3$ solution was heated in a two-neck glass flask with permanent stirring until boiling under reflux. To this solution, 1 mL of 1% trisodium citrate was rapidly added. During the process, the solution was mixed vigorously and it was refluxed for 60 min, until the color becomes turbid gray. Then, the mixture was cooled to room temperature with stirring.

To determine the morphology, aggregation, and size of the synthesized Ag-NPs and also to observe if the dye extract obtained from the previous acid extraction of the whole lake pigment is adsorbed on the surface of the Ag-NPs, Transmission Electron Microscopy (TEM) was used. For that purpose a Philips SuperTwin CM200 TEM instrument operated at 200 kV and equipped with an LaB_6 filament was used. The samples for TEM were prepared via deposition of around 2 µL of the synthesized colloid or colloid + organic extract mixture on carbon-coated copper grids (300 mesh) followed by drying under IR light. To determine the absorbance maximum of the synthesized silver colloid and obtain the UV-visible spectra of the organic extracts from the pink/purple lake pigments and standards, a V-670 double-beam UV-visible-near IR (NIR) spectrophotometer from JASCO, which uses a single monochromator design covering a wavelength range from 190 to 2700 nm, was used. The monochromator features dual gratings (automatically exchanged): 1200 grooves per millimeter for the UV-visible region and 300 grooves per millimeter for the NIR region. A photomultiplier tube detector is used for the UV-Visible region and a Peltier-cooled PbS detector is used for the NIR region. Both the gratings and the detector are automatically exchanged within the user selectable 800-to 900-nm range.

3.8 Data treatment by chemometrics

In some studies of this PhD Thesis, chemometric tools (multivariate statistics) were applied to treat the obtained results (raw data or normalized depending on the case) aiming to extract additional information than the simple analytical data. For this purpose, The Unscrambler® 9.7 software[16] was used to perform mainly Principal Component Analysis (PCA). This chemometric tool has been used in all the Chapters included in the Results section except in Chapter 6 and 7. Concretely, PCA allowed differentiating groups of samples or creating useful prediction models, providing useful information for the further interpretations performed in this PhD Thesis.

3.9 REFERENCES

1. Madariaga, J. M. Analytical chemistry in the field of cultural heritage. *Anal. Methods* **7**, 4848–4876 (2015).

2. Kong, K. *et al.* Raman spectroscopy for medical diagnostics—From in-vitro biofluid assays to in-vivo cancer detection. *Adv. Drug Deliv. Rev.* **89**, 121-134 (2015).

3. Kuhar, N., *et al.* Challenges in application of Raman spectroscopy to biology and materials. *RSC Adv.* **8**, 25888–25908 (2018).

4. Doty, K. C. *et al.* Raman spectroscopy for forensic purposes: recent applications for serology and gunshot residue analysis. *TrAC Trends Anal. Chem.* **103**, 215–222 (2018).

5. Leona, M. Raman Spectroscopy in Conservation. *Encycl. Archaeol. Sci.* 1–4 (2018).

6. Edwards, H. G. *et al.* Raman spectroscopy in art and archaeology. (London, The Royal Society, 2016).

7. Bersani, D., *et al.* Methodological evolutions of Raman spectroscopy in art and archaeology. *Anal. Methods* **8**, 8395–8409 (2016).

8. Casadio, F. *et al.* Analytical Chemistry for Cultural Heritage (New York, Springer, 2017).

9. Sharp, Z. 2007. Stable isotope geochemistry. 1st ed., Pearson Prentice Hall, New Jersey, 344 pp., ISBN-13: 978-0-13-009139-0.

10. Castro, K. *et al.* FTIR Spectra Database of Inorganic Art Materials. *Anal. Chem*. **75**, 214A-221A (2003).

11. Downs, R. T. The RRUFF Project: an integrated study of the chemistry, crystallography, Raman and infrared spectroscopy of minerals. *Proceedings of the 19th General Meeting of the International Mineralogical Association in Kobe, Japan,* (2006).

12. Dold, B. Speciation of the most soluble phases in a sequential extraction procedure adapted for geochemical studies of copper sulfide mine waste. *J. Geochem. Explor.* **80**, 55–68 (2003).

13. Thirlwall, M. F. Multicollector ICP-MS analysis of Pb isotopes using a ^{207}Pb-^{204}Pb double spike demonstrates up to 400 ppm/amu systematic errors in Tl-normalization. *Chem. Geol.* **184**, 255–279 (2002).

14. McCrea, J. M. On the isotopic chemistry of carbonates and a paleotemperature scale. *J. Chem. Phys.* **18**, 849-857 (1950).

15. Lee, P. C. *et al.* Adsorption and surface-enhanced Raman of dyes on silver and gold sols. *J. Phys. Chem.* **86**, 3391–3395 (1982).

16. Camo, A. S. A. The Unscrambler software v 9.7. *Camo ASA Oslo* (2007).

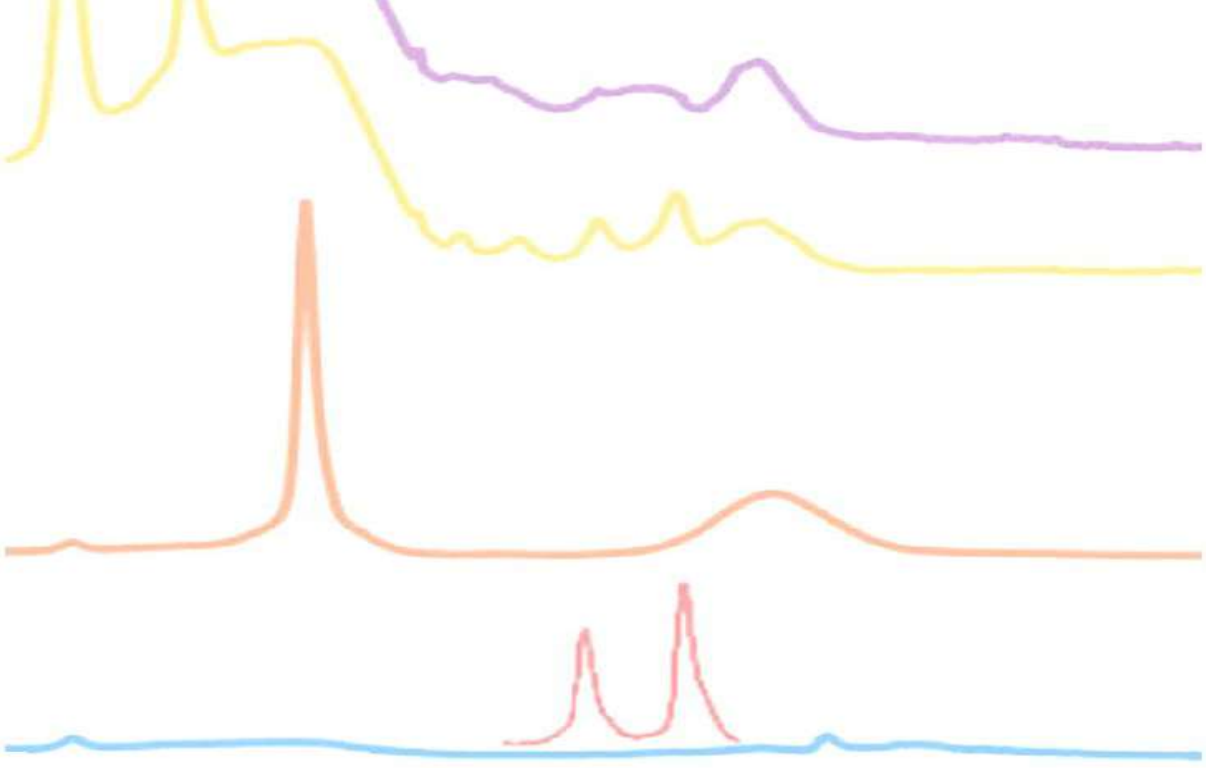

RESULTS AND DISCUSION

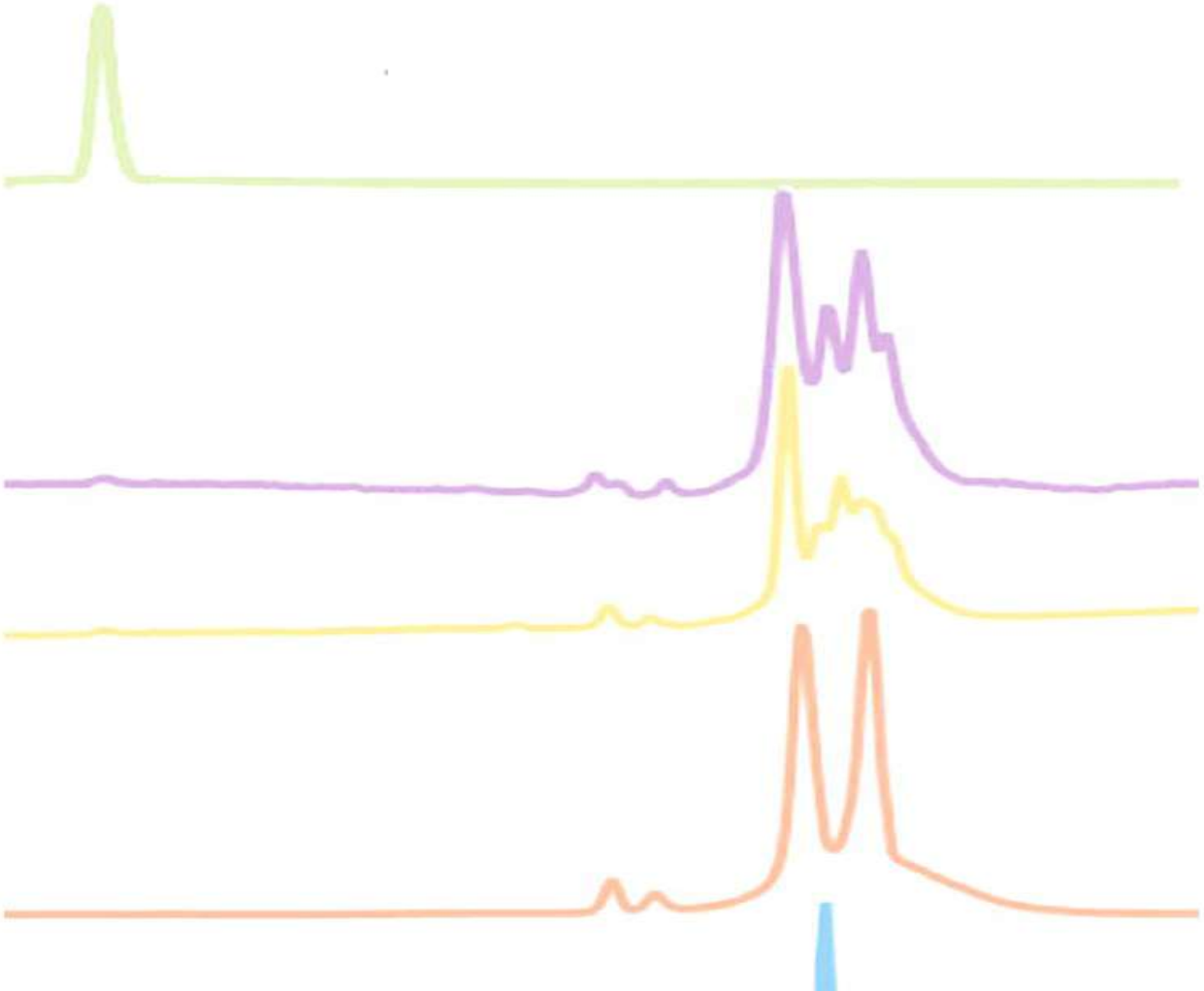

OVERVIEW OF THE THESIS

This PhD Thesis is articulated in two different parts. The first one (Chapters 4 to 7) deals with the characterization of the powdered pigments (red, yellow, blue, green, pink and white) recovered in their original bowls or containers from the archaeological site of Pompeii and preserved since then in the storehouse of the Applied Research Laboratory of the Archaeological Park of Pompeii and in the Naples National Archaeological Museum (MANN).

In Chapter 4, an in situ study of mainly inorganic pigments is presented, as an example of the usefulness of portable/handheld instruments to determine the elemental and molecular composition of these materials, and by extension the composition of the color palette used by the Roman artists from the ancient Pompeii. Thanks to the sampling permission given by the MANN, a deeper characterization of some specific pigments (red, yellow and pink) has been conducted in the laboratory to extract additional information about their inorganic composition, the probable local origin of some pigments and to track the provenance of red ochre/hematite pigments from the collection of the MANN (Chapter 5). In the Chapter 6, a specific multianalytical methodology has been applied in the laboratory to determine the nature of the inorganic binder (mordant) used to create different Pompeian pink and purple lake pigments from the MANN. To finish with the characterization of these lake pigments, in the Chapter 7 a Surface Enhanced Raman Spectroscopy-based methodology has been developed to determine the nature of the colorants used to dye the mordant of the Pompeian pink and purple lake pigments. Considering their high value, the lowest sample amount needed to extract reliable conclusion has been optimized.

The second part comprises Chapters 8 to 11. In the Chapter 8, the colors used to create Pompeian mosaics have been investigated. In this Chapter, an in situ study has been carried out to determine the nature of both, the pigments applied on mosaic tesserae and the materials used to create those tesserae, also useful to provide color decorations to the mosaics by themselves.

Once identified the colors used in Pompeii and considering that the wall paintings of this Roman city show a pronounced loss of polychromy, a study of the binder (calcite) that joins the pigments grains into the wall has been conducted. This information is presented in Chapter 9. Through the C and O isotopic analysis, the possible transformation of the calcite from the *intonaco* (external part) of the wall paintings has been assessed to obtain experimental evidences about the binder degradation and its subsequent reduction of binding action. Moreover, the possible source that promotes the transformation of this calcite into sulfates has been also approached through the S isotopic analysis.

The Chapters 10 and 11 are focused on the study of Pompeian yellow ochre pigment into red color transformation promoted by the thermal impact that took place in the 79 AD eruption due to the different pyroclastic density currents emitted by Mount Vesuvius. In this sense, a discrimination model based on in situ measurements using a handheld XRF spectrometer and a subsequent data treatment through Principal Component Analysis (PCA) has been created to differentiate the original hematite red pigments from the nowadays visible red areas coming from the transformation of yellow ochre. To finish with the study of this transformation, two additional models were created, using molecular spectroscopic techniques such as Raman imaging and reflectance spectroscopy, to determine the temperature that impacted specific transformed areas on the walls and the yellow ochre degree of transformation as a function of the impacted temperature. To simulate the 79 AD thermal impact and to create some of the mentioned models, original Pompeian wall painting fragments including yellow ochre were considered in this PhD Thesis.

PART 1

IN SITU AND LABORATORY METHODOLOGIES TO CHARACTERIZE INORGANIC AND LAKE PIGMENT POWDERS FROM POMPEII

PART 1. IN SITU AND LABORATORY METHODOLOGIES TO CHARACTERIZE INORGANIC AND LAKE PIGMENT POWDERS FROM POMPEII

The magnificent wall paintings of Pompeii were created by ancient artists with different colored materials that were used as pigments. Fortunately, as mentioned before, during the excavations carried out in the 19th and 20th centuries these pigments powders contained in pottery bowls were recovered and nowadays they are preserved in the storage room of the Applied Research Laboratory of Pompeii and both in the exhibition and storehouse of the MANN. It is well known that in the earthquakes that preceded the eruption of the 79 AD (e.g., earthquake of the 62 AD) some of the wall paintings from the ancient Pompeii collapsed. Therefore, it is more than likely that during the 79 AD eruption, the Pompeian artists were executing restoration works in the paintings. The preservation of these raw pigments provides an incomparable opportunity to the scientists to extract information about the original materials used to create or manufacture the colors of Pompeii and also to investigate their provenance.

In fact, these materials were complex mixtures of mineralogical phases and compounds coming from diverse sources. Obviously, the most important compound present in the pigments is the one responsible to give its characteristic color. However, additional non-colored compounds present in the material are also of great interest since they can provide information about the genesis, the source and contamination events that may have taken place during the thousands of years that they have been buried.

Apart from that, the study of the elemental composition can suggest the source of the material under study. In this sense, there are certain mineral ores with specific geochemical markers that make them unique in the world. Thus, the provenance of the material under study could be established according to the presence of these trace elements. In addition to that, unexpected high levels of elements present in a pigment can suggest a contamination during the burial period. The identification of specific elements could give clues about possible sources of contamination in the area and leaching events.

Therefore, it is important to perform a comprehensive chemical and mineralogical characterization of the pigments in order to obtain as much information as possible regarding the original composition and possible contaminations in these archaeological records. To perform this characterization, whenever is possible, in order to preserve their integrity after their analysis, non-invasive analytical techniques should be selected.

In this part of the PhD Thesis, the results related with the chemical characterization of different colored pigment powders conserved in their original pottery bowls, and recovered from the burial of the archaeological excavations of Pompeii are presented. For that, as mentioned in the experimental part of this PhD Thesis, two different pigment collections were considered: The pigment collection from the Naples National Archaeological Museum (MANN), and the one preserved in the Applied Research Laboratory from Pompeii (ARLP).

4. IN SITU CHARACTERIZATION OF INORGANIC AND LAKE PIGMENTS FROM POMPEII

4.1 Introduction

The wall paintings and raw pigments discovered in their original bowls in the Archaeological Park of Pompeii are of extraordinary importance for the identification of the used materials and the painting techniques employed by the ancient Roman artists. For this reason, the chemical analysis of the pigment powders or applied in wall paintings is an important challenge for analytical chemists that work in the archaeological and conservation science fields. Indeed, the information extracted about the composition of these pigments could be useful not only for scientist but also for archaeologists, restorers or historians, among others.

The first chemical analyses of Pompeian pictorial materials date back to the early 19th century. In 1809, seven pigments of different colors found in a shop at Pompeii were

analyzed by Chaptal[1]. Few years later, in 1815, Davy presented the analyses of different pigments from Pompeii recovered from the baths of Titus in a broken vase of earthenware[2]. After these analyses there are not published investigations about Pompeian pigments until 1967, when Augusti analyzed the pigments from the frescoes and bowls that were frequently found in the excavations of Pompeii[3]. Recent works carried out in the 21st century[4–8] have contributed to acquire knowledge about Pompeian pigments giving continuity to the works started by Chaptal, Davy and Augusti.

In 2007 red, yellow and pink colored powders contained in pots recovered in the Forum of Pompeii were analyzed[4]. The analyses performed in the laboratory by FTIR, XRD and SEM-EDS allowed identifying hematite (α-Fe_2O_3), goethite (α-FeOOH), natrojarosite ($NaFe(SO_4)_2(OH)_6$) and purpurissum. In addition to that, the work performed in 2009 by Aliatis *et al.*[5] using benchtop micro-Raman, FTIR and SEM-EDS showed that green pigments from Pompeii were composed by malachite ($Cu_2CO_3(OH)_2$) and green earths, together with mixtures of Egyptian Blue (cuprorivaite, $CaCuSi_4O_{10}$) and yellow ochre. In 2010 also Aliatis *et al.*[6] analyzed powdered pigments found in bowls in the archaeological site of Pompeii. The results obtained in that work gave a great insight of the materials used as pigments in Pompeii, since the composition of various colored pigments was reported. In this sense, apart from the widely used pigments (hematite or goethite), additional ones such as cinnabar (α-HgS), huntite ($CaMg_3(CO3)_4$) and lazurite ($Na_3Ca(Si_3Al_3)O_{12}S$), among many others, were identified as red, white and blue pigments respectively. In that work, pigment powders were extracted and the characterization of their composition was performed in the laboratory by means of Raman microscopy, FTIR, XRD and SEM-EDS analytical techniques.

On the other hand, the work performed by Giachi *et al.*[7] was focused on white, black, grey, blue, yellow, red, pink-violet, and green colored powders. The analyses performed with optical microscopy (OM), SEM-EDS, XRD, and FTIR techniques demonstrated that the colored pigments were both of natural (e.g., ochre, jarosite, celadonite) and artificial

(cuprorivaite) origin. Finally, in the work by Canevali *et al*.[8] nine black powders found in different types of bronze vessels were analyzed. For that, a laboratory multi-analytical approach was adopted, which involved the use of SEM-EDS, FTIR, Raman, XRD, electron paramagnetic resonance spectroscopy, thermogravimetric analysis, gas chromatography coupled with mass spectrometry (GC/MS), and pyrolysis GC/MS. These analyses revealed that these black powders were carbon-based inks.

Those works, which were performed around 10 years ago, identified the chemical composition of many colored pigments recovered from the burial of Pompeii. However, all the analyses in those works were carried out in the laboratory after extracting a pigment sample. Nowadays, due to the changes in the management of the Archaeological Park and with the aim of preserving all these ancient records not only in a good conservation state, but also without losing the material, sampling is restricted and in most of the cases forbidden. For this reason, in this scenario, the laboratory methodologies that were applied 10 years ago cannot be applied anymore. Even so, nowadays thanks to the technological development those analytical techniques used in the laboratory can be applied in situ for the same purpose. Therefore, the use of portable instruments turns mandatory to perform the analysis in situ without extracting sample.

In addition to the analysis of powder pigments, the interest of analyzing the pigments applied in the wall paintings[9–15] has been increased especially during the last decade. For this purpose, portable spectrometers based on spectroscopic techniques such as Raman, DRIFT or handheld XRF have been used. Most of the pigments identified in these works were of inorganic nature, including among them malachite, cinnabar, red and yellow ochres, etc[9–15]. However, lake pigments, composed by an inorganic substrate and an organic colorant, were also used to create the wall paintings[14].

Nowadays, the largest collection of pigments recovered from the burial of Pompeii can be found at two different places. On the one hand, the Applied Research Laboratory of Pompeii has a wide collection of recovered powdered pigments. Thanks to the collaboration agreement between the Archaeological Park of Pompeii (ARLP) and our university (UPV/EHU), mentioning specifically to IBeA research group, some pigments were put to our disposal to be analyzed in situ at the laboratory of the archaeological site of Pompeii. In this sense, the selection of pigments was carried out taking into account the interest of the Archaeological Park to know the composition of certain colors. Due to this limitation, the analytical techniques that were used to obtain in situ as most information as possible were of non-invasive character in order to recover the sample in the same state after its measurement. For this purpose, portable/handheld spectrometers based on spectroscopic techniques were selected.

On the other hand, the Naples National Archaeological Museum (MANN) also stores a large number of bowls containing different colored pigments. Thanks to the demonstrated interest of the MANN it was also possible to carry out in situ measurements of the selected pigments of interest. In this case, it was possible to extract little amount of sample from specific pigments of this collection.

In this chapter an in situ multianalytical methodology based on spectroscopic techniques was applied with the aim of verifying if portable/handheld spectrometers can offer reliable results of the chemical composition of the pigments recovered from the burial. For the molecular characterization, two portable Raman spectrometers with 532 and 785 nm excitation lasers were used, while the elemental characterization was carried out using a handheld XRF spectrometer.

4.2 Samples

Pompeian inorganic pigments of different colors conserved in their original pottery bowls (except one pigment which was contained in a shell) were considered in this study (see Fig. 4.1 and Table 4.1). Due to the special interest of the direction of the ARLP to know the chemical composition of green, pink and red samples, and as mentioned before, since sampling was not allowed, an in situ characterization of those pigments was performed in the ARLP. In the case of the pigments belonging to the MANN, the molecular and elemental analyses were carried out in situ in the store room of the museum.

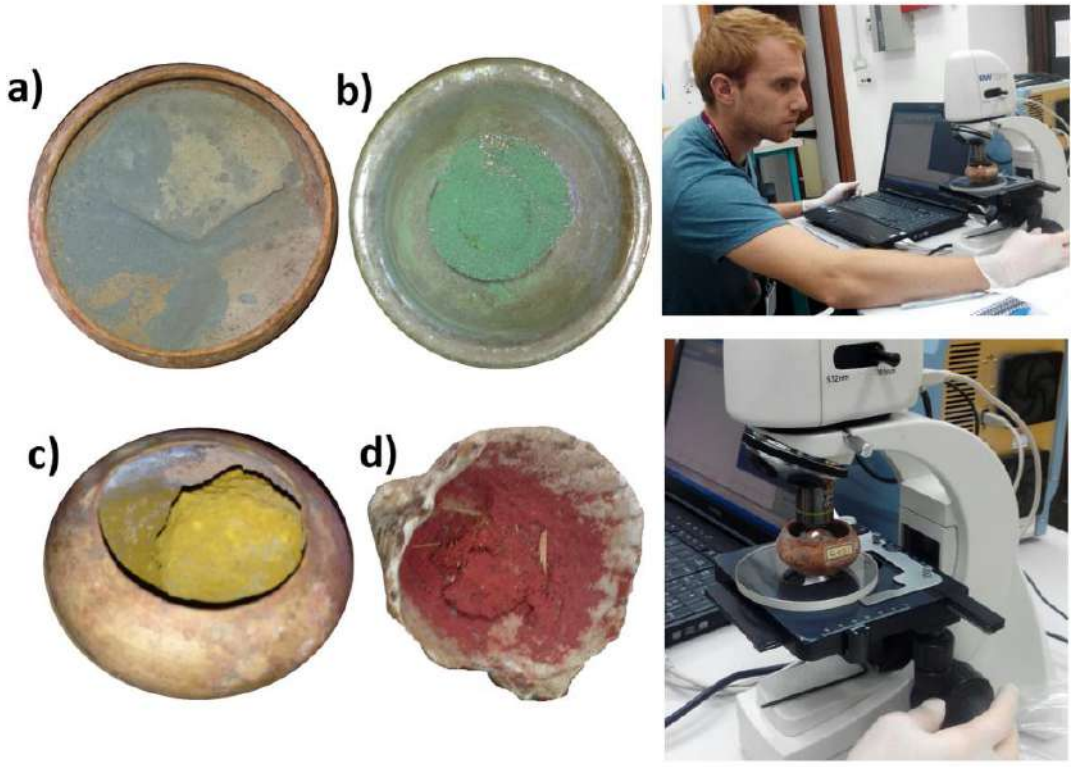

Fig. 4.1. Some of the studied pigments (left) in their original bowls and in a shell: a) 117333 blue b) 11699 green c) 117366 yellow and d) 64628 red; A moment of the process of measuring the pigments directly by Raman spectroscopy in the ARLP (right).

Table 4.1. Samples under study (reference number underlined for those samples belonging to MANN).

COLOR	NUMBER OF SAMPLES	REFERENCE NUMBERS
Green	2	11699, 41505
Pink	6	117323, 117342, 117345, 117365, 18103, 18107
Blue	7	1806, 9535, 9649, 12011, 48562, 117333, 117338
White	1	117368
Yellow	2	117274, 117359
Red	2	64628, 112251

Most of the pigments were conserved in their original bowls (see Fig. 4.1). However, as shown in Fig 4.1D, red pigment 64628 was conserved in a shell. According to the laboratory technicians of the ARLP, the shell was the container for the pigments powders used by the artists at the moment when they were painting the frescoes. Thus, it is supposed that this particular pigment was ready or being used in the moment of the eruption in year 79 AD. Indeed, some works can be found in the literature dealing with red and purple powders contained in shells[17,18] with painting or cosmetic purposes.

For the Raman analyses, microscopic measurements were carried out coupling the probe to a portable video-microscope (x20 and x50). When the size of the bowl allowed putting it under microscope, direct measurements were conducted as it is shown in Fig 4.1 right. In the rest of the cases, some pigments powders were extracted and placed in a slide for the Raman measurements; after that, the pigments grains were returned to its original bowl. For the XRF measurements and to prevent the sampling interface from contaminations, a mylar film was placed on the sampling interface of the instrument fixed in a laboratory support. After that, the sampling area of the interface was covered with the necessary pigment mass. Once again, after the analysis, the pigment grains were returned to their respective containers.

4.3 Green pigments

The understanding of the origin and the way of obtaining green color, both directly from green pigments or by mixing blue and yellow materials is of great interest from the chemical and archaeological point of view. Indeed, as a previous works pointed out[19], Roman artists had a wide knowledge of green pigments, including malachite, verdigris and green earths in their palette. Pliny[20] already mentioned malachite among rare and expensive pictorial materials, and called it *chrysocolla*, the name now used for hydrated copper silicate. Malachite ores were located in Cyprus, Macedonia, Spain, and Armenia (*armenium* was the most precious pigment)[20,21]. Other works[3,5,6], also detected malachite in powdered pigments from Pompeii.

On the other hand, green earths were used as a cheap alternative to malachite. Green earths can contain the glauconite ($(K, Na)(Fe, Al, Mg)_2(Si, Al)_4O_{10}(OH)_2$) and/or celadonite ($KMgFeSi_4O_{10}(OH)_2$) minerals, which mineralogical phases are difficult to differentiate. Therefore, the pigment is simply called green earth. Both minerals would have been available for Romans at that time in form of rocks. Apart from malachite and green earths, Pliny also mentions the use of verdigris and other pigments derived from the corrosion of copper in an acidic environment[20].

In this PhD Thesis, two green pigments were analyzed in situ in order to determine the material used to manufacture them: one green pigment belonging to the collection of MANN (number 11699) and another one from the collection of ARLP (number 41505). For the molecular characterization of these green pigments, the 532 nm excitation laser was selected since better Raman results were systematically obtained using this excitation wavelength. For both green colored powders, malachite, (characteristic Raman bands at 155, 179, 221, 269, 352, 433, 534, 719, 1088, 1367 and 1494 cm^{-1}, see Fig. 4.2), was systematically identified.

This green mineral ($Cu_2CO_3(OH)_2$) was usually crushed in order to obtain a fine powder to be used as pigment[5]. Apart from this green mineral, quartz (α-SiO_2) was also identified punctually by means of Raman spectroscopy.

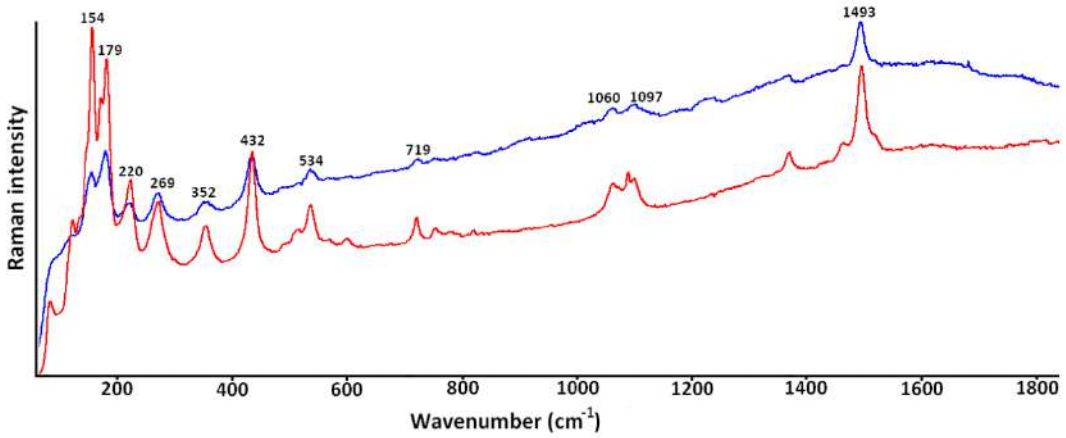

Fig. 4.2 Raman spectra of 11699 green sample from MANN (blue) and malachite standard (red).

To complement molecular results, both green samples were also analyzed by means of HH-EDXRF, obtaining repetitive spectra in which Cu was the major element, together with Ca and Si (see Fig. 4.3). Silicon probably comes from various silicates that compose the bulk pigment (e.g., quartz, already identified by Raman spectroscopy).

Apart from these elements, the unexpected high signal of Pb must be remarked. In this sense, as shown in Fig. 4.3, the L_α line at 10.5 keV, and L_β at 11.5 keV of Pb could be detected in the obtained spectra. Moreover, according to the semi-quantification its concentration is higher than 1000 μg/m. Therefore, the presence of this metal cannot be considered a trace in the pigment. Considering that these pigments were buried for hundreds of years, possible contaminations of leachable metals may took place during the burial.

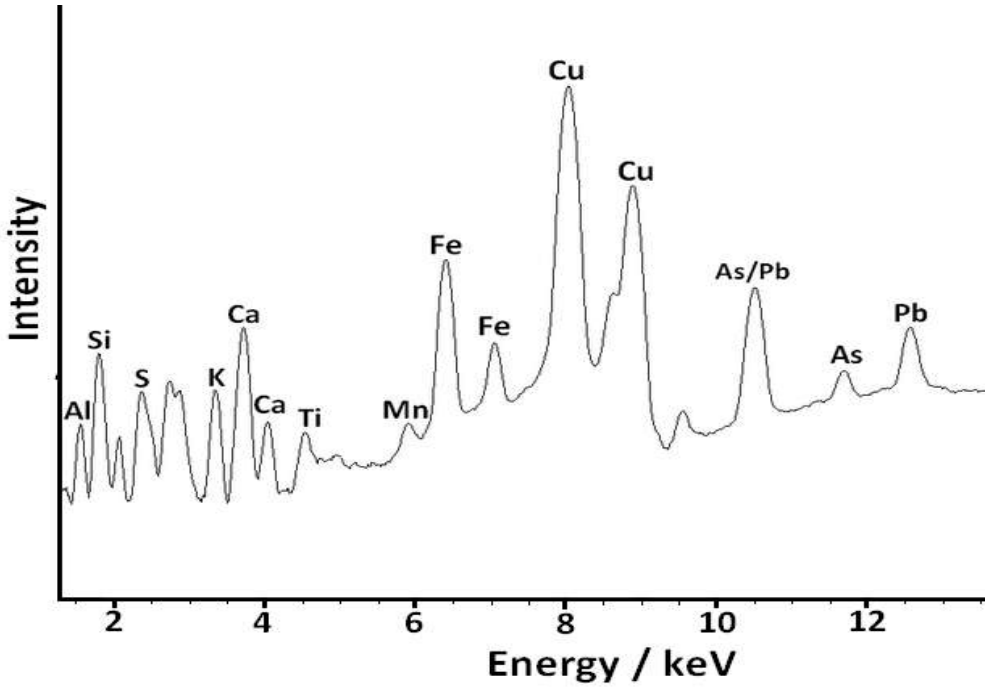

Fig. 4.3. HH-EDXRF spectrum of 11699 green sample from MANN.

4.4. Pink pigments

In this PhD Thesis, 6 pink pigments were analyzed, 4 from the MANN and 2 from the ARLP. In situ molecular analyses performed by portable Raman spectroscopy did not offer useful information about the molecular composition. In fact, the obtained spectra were either saturated using a very low laser power or showed high fluorescence, avoiding the detection of bands related to the compounds present in the pigment. Fig. 4.4 shows some of the obtained representative spectra, in which it was impossible to detect any Raman band. Once obtained these spectral results in the first screening, it was sexpected that the color of these pink pigments was probably achieved by dyeing an inorganic matrix with an organic colorant such as madder lake or Tyrian purple, both used in Roman times in Pompeii[16], leading to the so-called lake pigments.

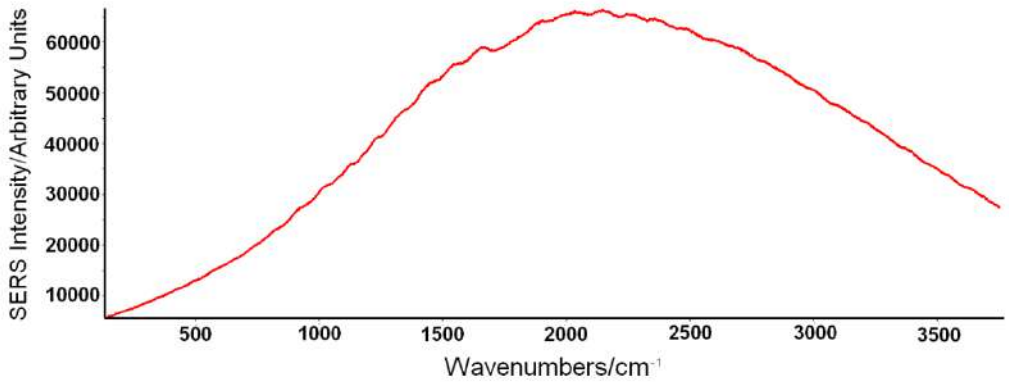

Fig. 4.4. Representative Raman spectrum of 18103 pink lake pigment from ARLP.

Since the molecular analyses performed in the samples from ARLP and MANN did not offer useful information, it was requested a sample extraction to the direction of ARLP. Unfortunately, as commented before, sampling was forbidden in this pigment collection. On the contrary, MANN gave us the possibility of sampling, and hopefully in this case, due to the available amount of mass of 117323, 117342 and 117365 some powders were collected and conserved in glass vials to perform further analyses in the laboratory (see Chapter 6 and 7).

Although the molecular characterization was unsuccessful, it was decided to continue performing the elemental analysis of these pink samples to study their major, minor and traces elements. After acquiring in situ the XRF spectra, and for a better interpretation of the results, with the obtained elemental information of the 6 pink lake pigments (from MANN and ARLP) Principal Component Analysis (PCA) was performed using the counts normalized against Ag line coming from the source. Thereby, similarities and differences according to the acquired signals of minor and trace elements between pigments could be detected. The data set consisted of a matrix which includes 18 analyses (6 pigments x 3 replicates) and the counts normalized against Compton line of 10 elements (Al, Si, P, K, Ca, Ti, V, Cr, Mn, Fe, Ni, Cu, Rb, Sr, Zn,As and Pb) as variables.

The PCA model with two principal components, explaining the 76% of the total variance, was chosen as the most appropriate one (see Fig. 4.5).

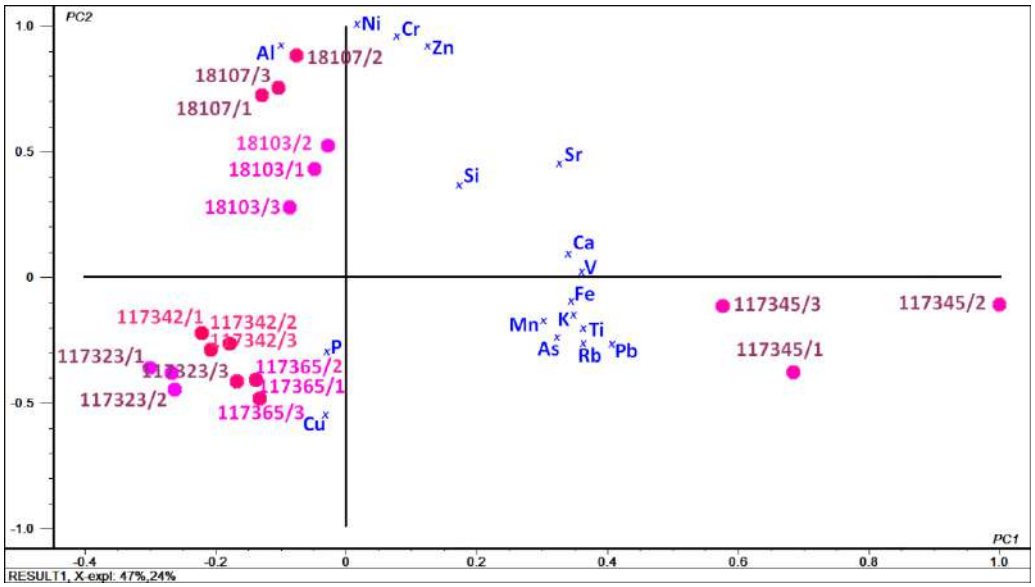

Fig 4.5. Bi-plot (scores and loadings) of pink lake pigments samples 117323, 117342, 117345, 1173565, 18103 and 1807 using the obtained elemental composition by means of HH-EDXRF.

In the bi-plot a clear difference can be observed among the analyzed pigments, since 3 different groups of samples were differentiated. In particular, PC2 divides the samples deposited in the ARLP (positive values) from those belonging to MANN (negative values) according probably to the high content of Al, Ni, Cr and Zn of the samples from ARLP. However, samples from MANN show higher levels in P and Cu. These groupings between samples from different collections could be related to different procedures of manufacturing these potential lake pigments. In fact, it is more than likely that for the manufacture of the 18103 and 18107 pigments, clays rich in Al with traces of Ni, Cr and Zn were used, while the clays used to manufacture the remaining pigments had not that high Al content. Instead of it, Cu is a characteristic element present in those pigments.

In this sense, it has been reported in the literature[2] that since Roman times, copper salts (in form of oxides or sulfates) were added to the inorganic mordant from lake pigments to obtain the desired final hue of the lake pigment. This variation in the original tonality takes place when the added copper (Cu^{2+}) forms a complex with the organic molecule from the colorant used to dye the inorganic mordant.

Apart from those two different groups of pigments, the pink pigment 117345 is placed in the positive part of PC1, far from the other two groups. This pigment showed significant higher signal of Pb than the other pigments. In fact, this particular pigment seems to be contaminated by an external source of Pb, as in the case of the previously analyzed green samples, and due to this higher Pb signal it is probably differentiated in the obtained PCA. This issue will be confirmed in the Chapter 6 of this PhD Thesis.

4.5 Blue pigments

For the blue color, ancient Pompeian artists relied on the same materials as the Egyptians: azurite, Egyptian Blue and lazurite or lapislazuli. Azurite, $Cu_3(CO3)_2(OH)_2$, was a greenish blue pigment whose name came from the Persian word "*lazhward*" meaning blue. On the other hand, Egyptian Blue ($CaCuSiO_4$) was a dark blue pigment used throughout antiquity for the use on a range of mediums such as, wood[22], plasters[23], papyrus[24], etc. Apart from them, lazurite, an alumino-silicate mineral containing sulfate ions, sulfur and chlorine ($(Na,Ca)_8(AlSiO_4)_6(SO_4,S,Cl)_2$) was also used as blue pigment, as it has been already demonstrated[6]. This mineral is found in the well-known precious lapislazuli, already used in the Roman empire from the 1st century as Pliny[20] and Vitruvius[21] described.

In this PhD Thesis seven blue different pigments belonging to both MANN and ARLP collections were considered. Specifically, samples with reference number 1806, 9535, 9649, 12011 and 48562 from ARLP and 117333 and 117338 from MANN were analyzed in situ. For the analysis of blue pigments, the 532 nm excitation laser was used. The obtained spectra were the same for all analyzed samples, showing systematically the same Raman bands. In this sense, Raman spectroscopic results pointed out the same molecular composition of all blue studied samples. As shown in Fig. 4.6, these blue samples corresponded to Egyptian Blue (137, 199, 359, 378, 430, 475, 572 and 1086 cm^{-1} Raman bands).

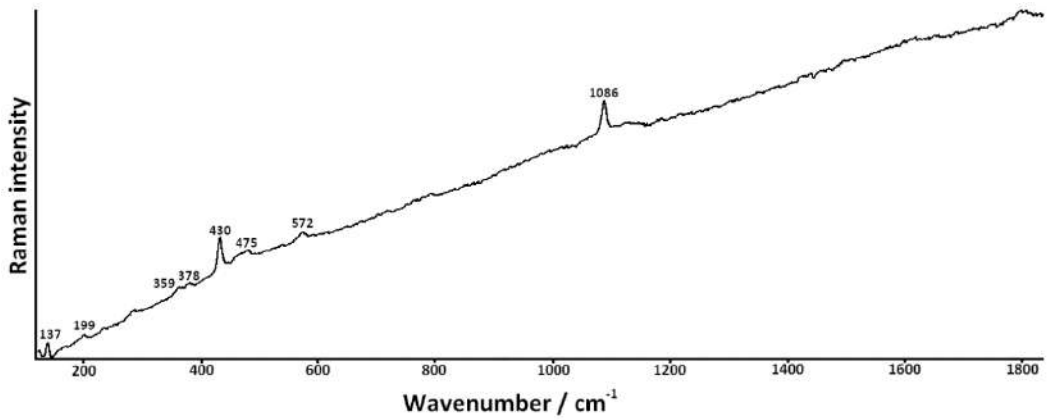

Fig. 4.6. Repetitive Raman spectrum of all the blue samples under study.

Egyptian Blue could be obtained by a natural way from cuprorivaite mineral (found in the Vesuvius lavas in low contents) or through chemical reactions described already by Vitruvius in first century BD[21,25]. This reaction consisted in mixing copper compounds with calcareous sand and a flux (e.g. soda, natron or plant ash). Due to both, the low natural content of cuprorivaite in the Vesuvian area and the knowledge of preparing this material through chemical reactions in the Roman period, it is expected that these blue pigments were not naturally obtained but they were manufactured chemically by the ancient artists.

The elemental in situ analyses by XRF showed that Ca, Cu and Si were the elements with highest signal in all the samples (see Fig. 4.7) confirming the previous obtained molecular results.

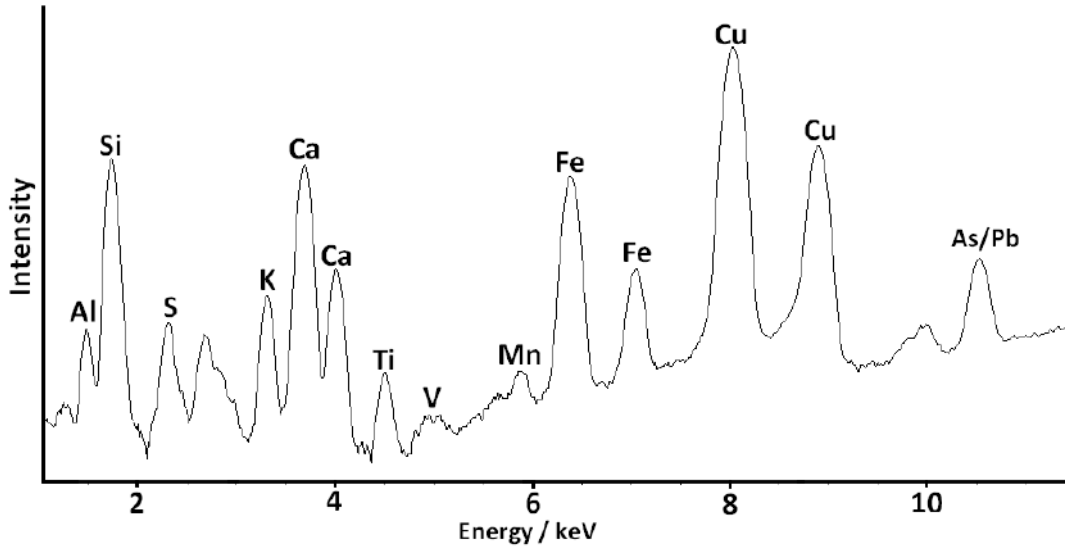

Fig. 4.7. Repetitive HH-EDXRF spectrum of the analyzed 117338 blue pigment.

Moreover, since the number of blue samples was high, it was decided to study the variability of the in situ detected elements between samples. For that, the counts of each detected element normalized against the signal of Cu, one of the main elements of Egyptian Blue pigment, were used. Copper was selected because its content should only be related to the composition of the pigment, while the content of Ca and Si could be also related to additional carbonates and silicates present in the pigment powders.

With the obtained dataset of counts normalized against Cu consisting of 17 measurements and 17 variables (detected elements), a PCA was conducted (see Fig. 4.8) to assess the variability of the elemental composition among different blue pigments.

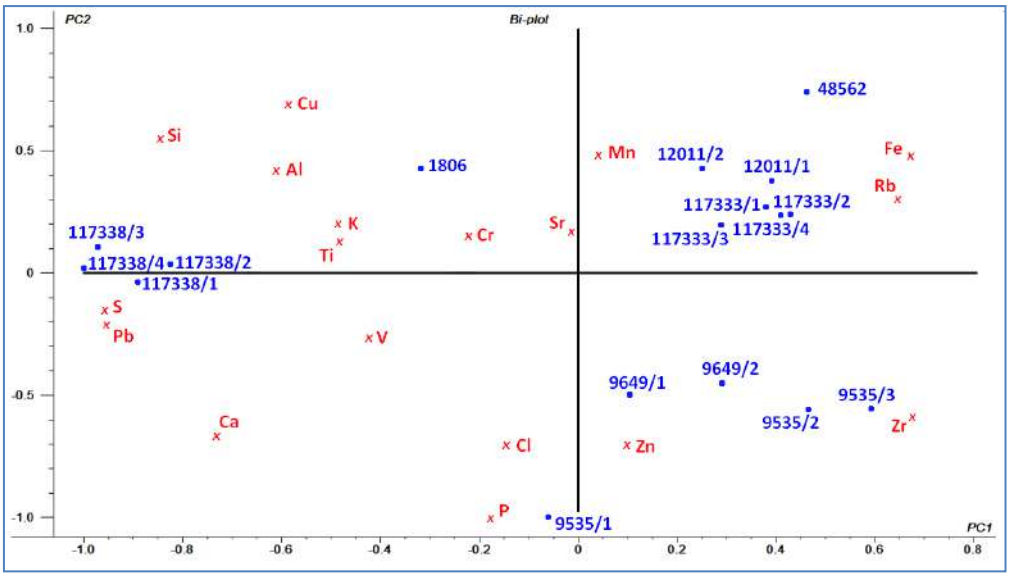

Fig 4.8. Bi-plot (scores and loadings) of blue pigment samples using the elemental composition obtained by means of HH-EDXRF.

As it can be observed, the variability depending on the elemental composition is high among the samples, leading to clear different groupings of samples. The causes of these differences in the trace elemental composition of the final blue pigments might be related to the different source of the used raw materials (copper compounds, limestone, sand, etc.) to manufacture each pigment by chemical reaction. In fact, there existed more than one recipe to synthesize the final Egyptian Blue pigment. For example, a recent work published in the literature[26] prepared this pigment inspired by the uncovered zinc-bearing Egyptian Blue found on the early medieval mural paintings of Santa Maria Church at Castelseprio (Lombardy Region, Italy). In addition to this, a previous work[27] demonstrated that the experimental conditions (e.g., temperature, composition of the initial mixture) of the chemical reaction to obtain Egyptian Blue can influence the final mineralogy, and therefore, the elemental composition, of the obtained material. For example, the presence of calcite could be indicative of an incomplete synthesis[28]. This could be the case of 9535 blue pigment since it showed significantly more Ca signal comparing to the other analyzed pigments, which show similar levels. Similarly to Ca, 9535 pigment is the

one which showed the highest signal of P, K and Fe, while for the other blue pigments the signal of these elements are similar. Apart from those elements, 9535 pigment showed high levels of Ti, Mn, and Sr although for these elements the pigment 117333 is the one which shows the highest levels.

Apart from the differences in the minor/trace composition of the raw materials used to manufacture the Egyptian Blue pigments, other hypothesis to explain this variability in the trace elements content could be the incorporation of specific metals present in the soils and volcanic deposits of the burial. Considering that the blue pigments were recovered from different location in the burial, different contaminations of metals could have produced for each sample, which led to nowadays different elemental compositions. For example, 9535 and 117338 blue pigments showed the highest levels of Pb, pointing out to the possible contamination of this metal as in the case of green pigments. In this case, according to the semi-quantitative data, the concentration of Pb of both blue pigments was also higher than 1000 μg/g.

4.6 White pigment

Pliny[20] and Vitruvius[21] listed many white pigments used by ancient artists during the Roman period. Some of them were earths, while other came from minerals. The minerals that were reported by these classical authors, which have been found in different works, are chalk, limestone (in a number of forms such as dolomite, aragonite and diatomite) and shells, all mostly calcium carbonate ($CaCO_3$), found all over the Roman world. These have been used as pigments, extenders to lighten a colored pigment and as substrates for making lake pigments. In addition, gypsum ($CaSO_4 \cdot 2H_2O$) and bone white ($Ca_3(PO_4)_2$) should be also mentioned as white pigments. Besides, another addition to the classical color palette was lead white ($(PbCO_3)_2 \cdot Pb(OH)_2$.

Due to the lack of availability of white pigments among the studied pictorial collections, in this PhD Thesis only one sample was analyzed. According to the acquired Raman spectra (see Fig. 4.9), the white pigment under study resulted to be a mixture of dolomite ($CaMg(CO_3)_2$; Raman bands at 1098, 723, 299 and 176 cm^{-1}) with a minor contribution of calcite ($CaCO_3$; Raman band at 1086 cm^{-1}).

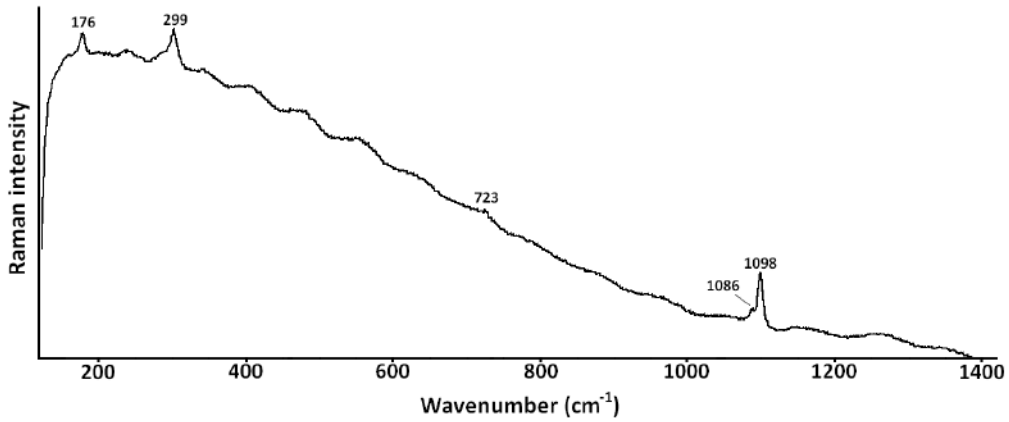

Fig. 4.9. Raman spectrum of the analyzed white sample

According to the molecular results, the main elements present in the sample to be detected by XRF are Mg and Ca. However, due to the high limit of detection of Mg in the in situ XRF measurements performed with the handheld spectrometer, Mg was not detected (see Fig. 4.10).

In this case, the intensity of the Pb lines is lower than in the rest of the cases, pointing out to its possible presence as a trace metal in the original composition of the pigment. According to the semi-quantitative information, the concentration is lower than 1000 μg/g.

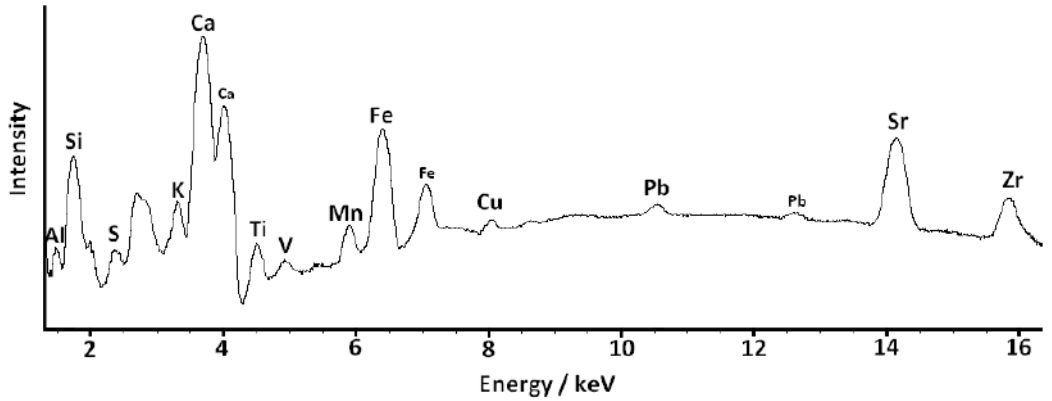

Fig. 4.10. HH-EDXRF spectrum of the analyzed white sample.

4.7 Yellow pigments

Yellow color was often used in wall paintings in Ancient Roman villas and towns such as Pompeii. Indeed, yellow was one of the main colors used in the Pompeian mural paintings. To obtain yellow pigments different materials were used. Yellow, according to Pliny[20] and Vitruvius[21], was derived either from yellow ochre (goethite, α-FeOOH) or from the mineral orpiment (As_2S_3). In 1967, Augusti[3] claimed to find orpiment at Pompeii, but his results were not conclusive. Another yellow pigment was massicot (PbO) also identified by Augusti and more recently at a Roman Villa in France[29].

In this case it was possible to have the access to two different yellow pigments from the MANN collection (117274 and 117359). The microscopic observations carried out under the 50x lens connected to the portable video-microscope of the Raman spectrometers allowed to observe that these samples were composed mainly by yellow grains, but also by some blue and green grains in samples 117274 and 117359 respectively (see Fig. 4.11).

Because of this heterogeneity, yellow, blue and green grains were analyzed separately in situ by micro-Raman spectroscopy. Unfortunately, due to the spot size of the HH-EDXRF spectrometer (9 mm diameter), the selective elemental analysis of the different colored grains was not possible to be performed. Thus, the XRF spectra of the bulk mixture were obtained.

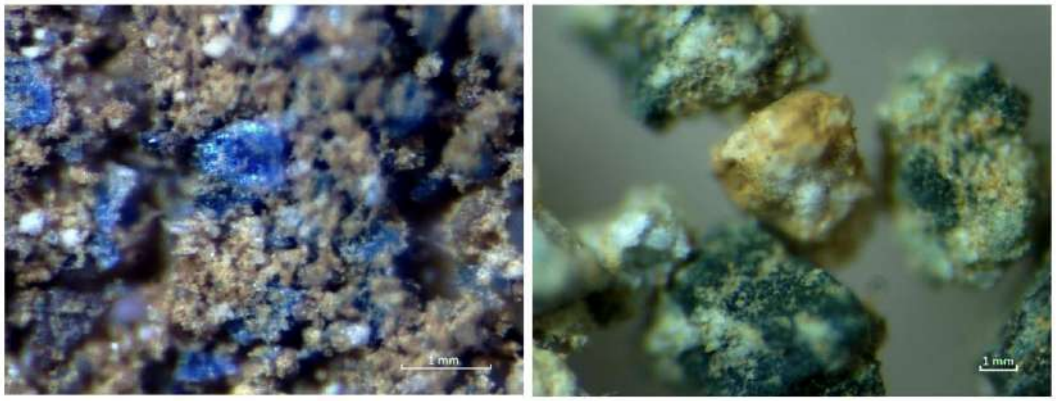

Fig. 4.11. Microscopic observation (x50) of 117274 (left) and 117359 (right) yellow pigments.

With the aim to reduce the fluorescence, the Raman measurements on the yellow grains were conducted using the 785 nm excitation laser. On the contrary, and due to the better spectral results achieved, the Raman analysis of the blue and green grains was obtained by means of the use of 532 nm excitation laser.

In Fig. 4.12 (left) a representative spectrum obtained for the yellow grains in both yellow pigments can be observed. In it, the typical bands of goethite (α-FeOOH), the main component of the yellow ochre, at 246, 300, 387, and 533 cm^{-1} were observed.

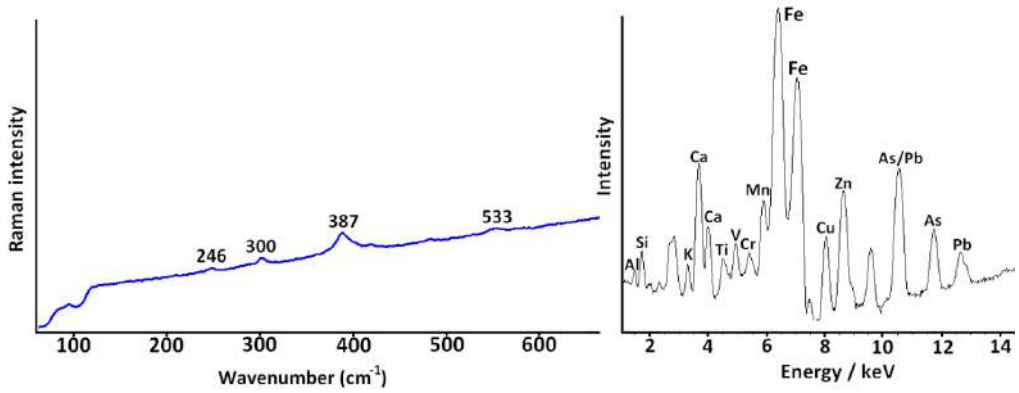

Fig. 4.12. Representative Raman spectrum of the yellow grains (left) and HH-EDXRF spectrum of the bulk sample (right) of 117359 pigment.

The Raman spectra obtained from the blue and green grains in both yellow pigments suggested the presence of Egyptian Blue and malachite respectively, already identified previously as the main colored compounds present in the analyzed blue and green pigments. In this sense, two hypotheses can be mentioned to explain the presence of these blue and green pigments on the yellow ones. On the one hand, an intentionally mixture of little amounts of Egyptian Blue or malachite with yellow ochre by the artist to achieve a different hue; on the other hand, a possible contamination of the yellow pigment due to the use of a non-properly cleaned bowl previously used to apply blue and green pigments.

In situ XRF measurements of sample 117359 (Fig. 4.12 right) showed the presence of Fe as the major element related with the presence of goethite in yellow grains. Moreover, as shown in the XRF spectrum, intense bands related to other elements such as Ca and Pb were also detected. In the case of Pb, the detected intense bands (L_α at 10.5 and L_β at 12.5) could point out once again the possibility of the contamination of Pb during the burial of the Pompeian pigments.

4.8 Red pigments

Regarding red color, two materials dominated the composition of red pigments: red ochre and cinnabar. On the one hand, red ochre was obtained from iron rich soils, composed mainly by hematite mineral together with additional compounds such as silicates and clay minerals (e.g., kaolinite, illite, quartz)[30]. Due to its availability and abundance, it was one of the cheapest and most used pigments in Ancient Roman period.

On the other hand, cinnabar was a mineral which was crushed and the obtained fine powder was used as brilliant red pigment. In this sense, the most highly prized red pigment of the time, ten times more expensive than red ochre, was cinnabar. It appeared in the Mediterranean area about 1500 BD and it was probably mined in central or southern Europe, such as Almadén (Spain), Idria (Slovenia), Monte Amiata (Italy), Moschellandsberg (Germany) and/or Genepy (France)[31]. In the Roman period the mercury sulfide red pigment was obtained from natural sources, probably from the ores of the mentioned locations, while the synthetic route was discovered hundreds of years later. The use of cinnabar at that time was an indicator of richness because it was scarce and difficult to process, increasing in this way the price of this shiny red pigment[32]. Consequently, cinnabar has been identified in Pompeian luxurious houses, whose owners belonged to the high class of that period.

In this PhD Thesis, two different red pigments were analyzed in situ. On the one hand, a brownish-red pigment conserved in an original bowl in the MANN (sample 112251), and on the other hand, a brilliant red powder conserved in a shell deposited in the ARLP (sample 64628) shown in Fig. 4.1D. Considering the different red hues it was more than likely that both red pigments had different molecular composition. In fact, the Raman spectrum acquired in situ in the ARLP, using the 532 nm laser for the brilliant red pigment sample with reference number 64628, was cinnabar as shown in Fig. 4.13, where the typical Raman bands centered at 253, 284 and 343 cm^{-1} are clearly seen.

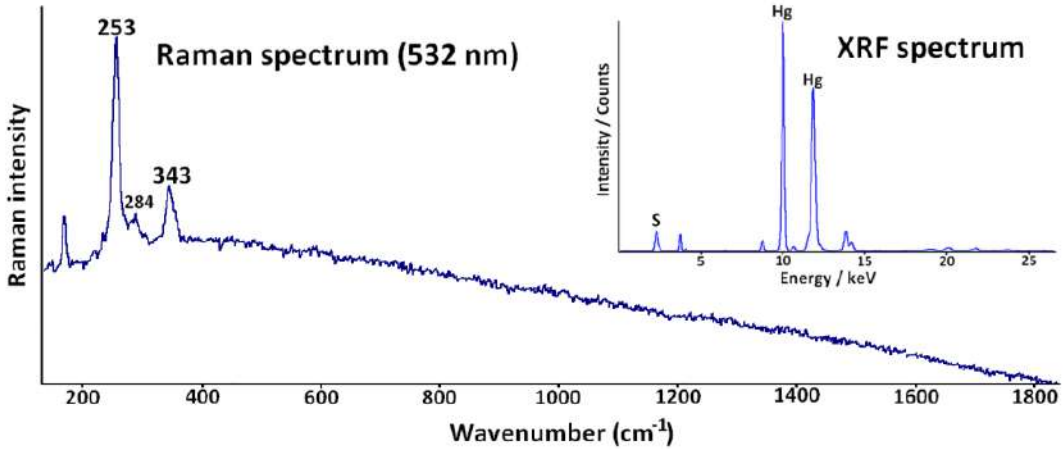

Fig. 4.13. Raman and HH-EDXRF spectra of brilliant red 64628 pigment from ARLP.

Apart from the molecular characterization, elemental analysis was also performed by means of HH-EDXRF to complement and confirm the obtained molecular results. The acquired XRF spectrum of this red pigment confirmed the previous Raman results since the main elements present in the sample were S and Hg (see Fig. 4.13). Apart from these elements, K, Ca, Ti, Cr, Fe, Ni Cu and As were also present in minor/trace levels in the different measurements performed. The mean semi-quantitative values offered by the portable spectrometer of three measurements (three portions of sample placed in the sampling interface) are shown in Table 4.2.

Table 4.2. Semi-quantitative values (% weight) of the different elements detected in 64628 red pigment.

S	4.5 ± 0.8
K	0.078 ± 0.005
Ca	3.6 ± 0.6
Ti	0.030 ± 0.007
Cr	0.0051 ± 0.0006
Fe	0.38 ± 0.06
Ni	0.025 ± 0.001
Cu	0.110 ± 0.008
As	0.102 ±0.003
Zr	0.006 ± 0.005
Hg	91.1 ± 0.3

In this case, Pb was not detected in the analysis of this red pigment suggesting that it has been not influenced by Pb contamination. In addition, this information about the minor/trace composition, together with Pb, S and Hg isotope ratio analysis could be useful in order to identify the provenance of the mineral used to manufacture the final pigment. In fact, there is a work in the literature that analyzed the Pb isotopic ratios of the cinnabar present in Pompeian wall paintings[33].

On the other hand, the in situ Raman spectra of the red pigment 112251 acquired in MANN showed the typical bands of hematite centered at 224, 243, 291, 404 and 608 cm^{-1} (see Fig.4. 14).

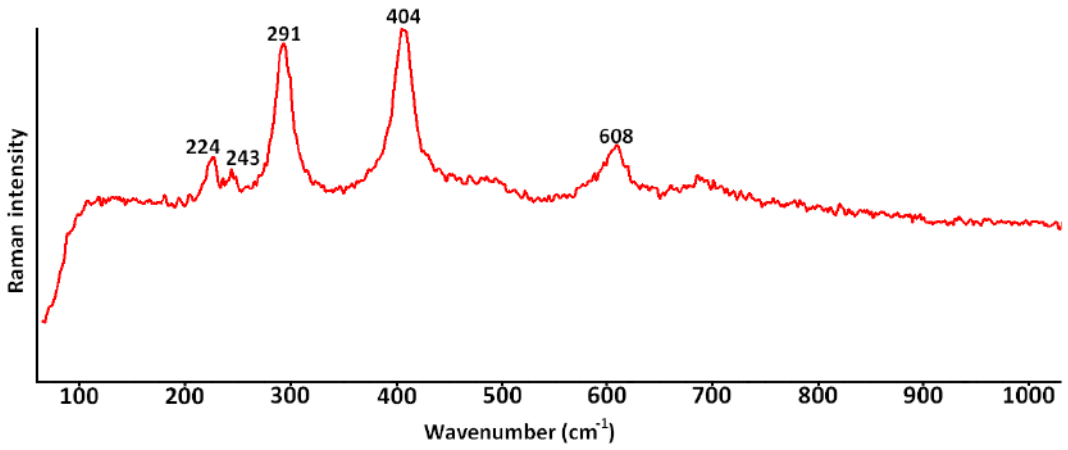

Fig. 4.14. Representative Raman spectrum of the brownish-red 112251 pigment from MANN.

In this case, the 785 nm excitation laser was used to avoid fluorescence effect that usually 532 nm laser promotes in ochre samples due to the clays or alumino-silicates presence in this type of pigments. Apart from the identified hematite, in some punctual measurements quartz (α-SiO_2) was also found as minor compound in sample 112251.

This red ochre pigment was also analyzed by HH-EDXRF to determine its elemental composition. The major element present in the pigment was Fe. In addition to Fe, other elements such as Al, Si, K, Ti, V, Cu, Zn, Sr and Zr (see Fig. 4.15) were also detected at minor or trace levels. Their presence in the composition of the ochre pigment could point out to the use of local soils. In this sense and according to this hypothesis, Al, Si and K could probably come from feldspars (potassium aluminosilicates) present in the raw soil used to obtain the ochre pigment. On the other hand, other elements could also come from local earths since they are characteristic from the Somma-Vesuvius and surrounding area, especially Sr and Zr[34]. These experimental data could point out to a local provenance. However, these preliminary conclusions regarding the mineral phases and elemental composition will be deeply analyzed and verified in Chapter 5.

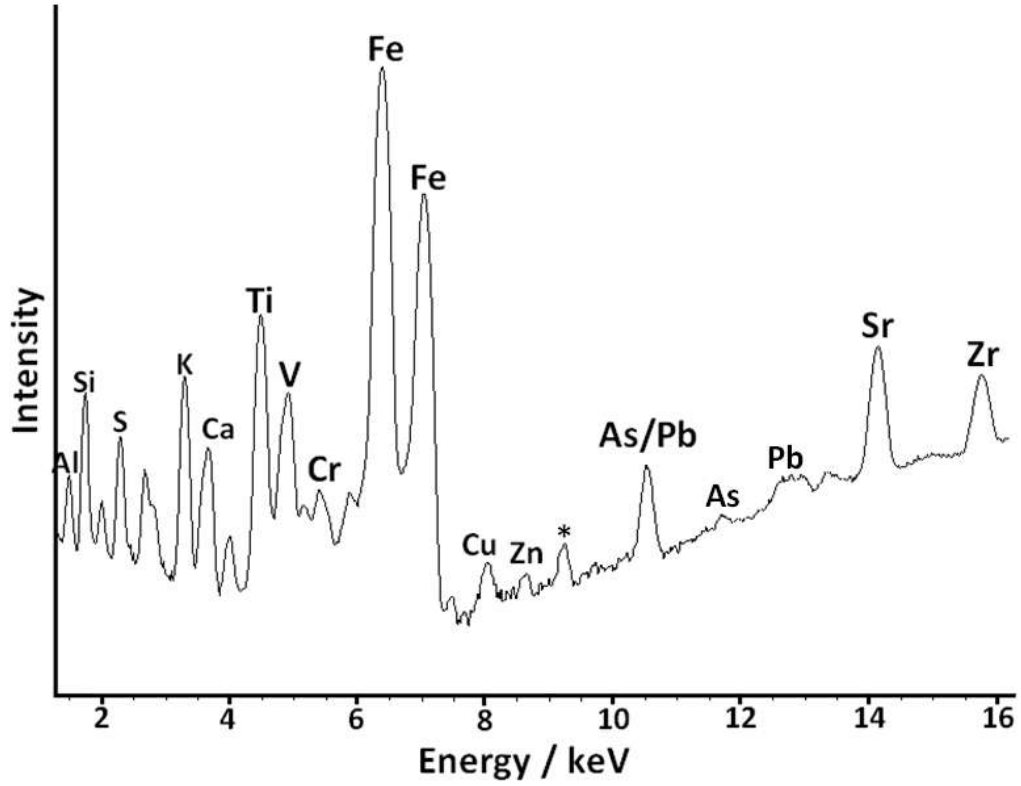

Fig. 4.15. HH-EDXRF spectrum of brownish-red pigment 112251 from MANN.

This red ochre pigment showed a low concentration of Pb, concretely lower than 1000 mg/g suggesting that in this case the possible Pb contamination did not take place as in the previous cases. Finally, a band at 9.2 keV (marked with an asterisk) not related to the pigment appeared in the obtained XRF spectrum.

4.9 Conclusions

The aim of this chapter was to perform an in situ comprehensive characterization of a wide variety of Pompeian pigment powders, with high archaeological value recovered from the burial of the ancient city and nowadays stored at the Naples Archaeological National Museum and at the Applied Research Laboratory of Pompeii. For that, a non-invasive multianalytical approach without consuming sample during the analysis was applied. When the number of pigments of the same color was high enough, a chemometric analysis was performed using the normalized areas of elements against the Compton line in the case of pink and copper line in the case of blue pigments, but never using the semi-quantitative concentration values of elements given by the HH-EDXRF instrument.

The complete set of results obtained in this chapter show the importance that portable/handheld non-invasive techniques have nowadays in the field of cultural heritage objects analysis. In this sense, a complete characterization of the molecular compounds present in the studied samples was achieved in situ, avoiding problems regarding to sampling procedures and losses or contaminations of these unique archaeological records. The results regarding the composition of these pigments were successfully obtained. In this sense, red and yellow ochres, mercury sulfide, malachite, Egyptian Blue, and dolomite were identified in the analyzed pigments.

Apart from that, mixtures of different colored pigments were also identified, probably with the intention of the artists of generating new color hues impossible to achieve without this procedure.

Thanks to the Principal Component Analysis, differences in the elemental composition were identified, probably due to two different possible causes. On the one hand, the different source of the raw minerals (in the case of Egyptian Blue) or clays (in the case of pink pigments) with different elemental composition at minor/trace level. On the other hand, the different area in which the pigments have been buried for thousands of years, which could led to different contaminations of metal presents in soils due to leaching processes, could also influence and change the original elemental composition, as it has been observed systematically with the high presence of Pb. In this sense, the unexpected high presence of this metal in some pigments could come from diverse leaching processes. The source of Pb present in the pigments will be evaluated deeply in Chapter 5.

To conclude, we suggest to use in future field works at least two portable Raman spectrometers, with 785 and 532 nm lasers, having the possibility to couple the Raman probe to a microscope stage, together with a HH-XRF spectrometer. To perform a chemometric analysis on the XRF data, the semi-quantitative values should never been considered; instead, the normalized areas against the most appropriate line in each case are the most adequate values.

4.10 REFERENCES

1. Chaptal, J.A. Notice sur quelques couleurs trouvées à Pompeïa. *Mém. Cl. Sci. Mathématiques Phys. L'Institut Fr. Année* 229–235 (1809).

2. Davy, H. VIII. Some experiments and observations on the colours used in painting by the ancients. *Philos. Trans. R. Soc. Lond.* 97–124 (1815).

3. Augusti, S., I colori Pompeiani (Rome, De Luca, 1967).

4. Cottica, D. & Mazzocchin, G. A. Pots with coloured powders from the Forum of Pompeii. *Proceedings of the conference EMAC '07. 9th European Meeting on Ancient Ceramics. Budapest, Hungary* (2007).

5. Aliatis, I. *et al.* Green pigments of the Pompeian artists' palette. *Spectrochim. Acta. A. Mol. Biomol. Spectrosc.* **73**, 532–538 (2009).

6. Aliatis, I. *et al.* Pigments used in Roman wall paintings in the Vesuvian area. *J. Raman Spectrosc.* **41**, 1537–1542 (2010).

7. Giachi, G., Carolis, E. D. & Pallecchi, P. Raw Materials in Pompeian Paintings: Characterization of Some Colors from the Archaeological Site. *Mater. Manuf. Process.* **24**, 1015–1022 (2009).

8. Canevali, C. *et al.* A multi-analytical approach for the characterization of powders from the Pompeii archaeological site. *Anal. Bioanal. Chem.* **401**, 1801-1814 (2011).

9. Miriello, D. *et al.* Non-destructive multi-analytical approach to study the pigments of wall painting fragments reused in mortars from the archaeological site of Pompeii (Italy). *Minerals* **8**, 134-149 (2018).

10. Germinario, C. *et al.* Multi-analytical and non-invasive characterization of the polychromy of wall paintings at the Domus of Octavius Quartio in Pompeii. *Eur. Phys. J. Plus* **133**, 359-571 (2018).

11. Angelini, I., *et al.* The pigments of the frigidarium in the Sarno Baths, Pompeii: Identification, stratigraphy and weathering. *J. Cult. Herit.* (2019). DOI: 10.1016/j.culher.2019.04.021

12. Rovella, N. *et al.* Tituli Picti in the archaeological site of Pompeii: diagnostic analysis and conservation strategies. *Eur. Phys. J. Plus* **133**, 539-553 (2018).

13. Asscher, Y. *et al.* Combining multispectral images with X-ray fluorescence to quantify the distribution of pigments in the frigidarium of the Sarno Baths, Pompeii. *J. Cult. Herit.* (2019). DOI: 10.1016/j.culher.2019.04.014

14. Madariaga, J. M. *et al.* Portable Raman, DRIFTS, and XRF analysis to diagnose the conservation state of two wall painting panels from Pompeii deposited in the Naples national archaeological museum (Italy). *Appl. Spectrosc.* **70**, 137–146 (2016).

15. Veneranda, M. *et al.* In-situ multianalytical approach to analyze and compare the degradation pathways jeopardizing two murals exposed to different environments (Ariadne House, Pompeii, Italy). *Spectrochim. Acta. A. Mol. Biomol. Spectrosc.* **203**, 201–209 (2018).

16. Clarke, M. *et al.* Pompeii purpurissum pigment problems. *Proceedings of Art'05–8th International Conference on "Non Destructive Investigations and Microanalysis for the Diagnostics and Conservation of the Cultural and Environmental Heritage", Lecce, Italy* (2005).

17. Pérez-Arantegui, J. *et al.* Analysis of the Products Contained in Two Roman Glass Unguentaria from the Colony of Celsa (Spain). *J. Archaeol. Sci.* **23**, 649–655 (1996).

18. Smith, J. C. A Roman chamber tomb on the south-east slopes of Monasteriaki Kephala, Knossos. *Annu. Br. Sch. Athens* **77**, 255–293 (1982).

19. Eastaugh, N. et *al.* Pigment compendium: a dictionary of historical pigments. (London, Routledge, 2007).

20. Murphy, T. M. Pliny the Elder's Natural History: The Empire in the Encyclopedia. (Courier Corporation, 2004).

21. Vitruve *et al*. Vitruvius: Ten Books on Architecture. (Cambridge, Cambridge University Press, 1999).

22. Dodd, L. S. *et al.* The ritual significance of colour: Specialised pigments in a wooden Egyptian funerary statuette from the New Kingdom. *J. Egypt. Archaeol.* **95**, 83–104 (2009).

23. Uda, M. In situ characterization of ancient plaster and pigments on tomb walls in Egypt using energy dispersive X-ray diffraction and fluorescence. *Nucl. Instrum. Methods Phys. Res. Sect. B Beam Interact. Mater. At.* **226**, 75–82 (2004).

24. Olsson, A.M. *et al.* Micro-PIXE analysis of an ancient Egyptian papyrus: Identification of pigments used for the "Book of the Dead". *Nucl. Instrum. Methods Phys. Res. Sect. B Beam Interact. Mater. At.* **181**, 707–714 (2001).

25. Mazzocchin, G. A. *et al.* A short note on Egyptian blue. *J. Cult. Herit.* **5**, 129–133 (2004).

26. Nicola, M. *et al.* Late production of Egyptian blue: synthesis from brass and its characteristics. *Archaeol. Anthropol. Sci.* (2019). DOI:10.1007/s12520-019-00873-w

27. Bianchetti, P. *et al.* Production and characterization of Egyptian blue and Egyptian green frit. *J. Cult. Herit.* **1**, 179–188 (2000).

28. Mazzocchin, G. A. *et al*. Analysis of pigments from Roman wall paintings found in Vicenza. *Talanta* **61**, 565–572 (2003).

29. Dooryhée, E. *et al.* Non-destructive synchrotron X-ray diffraction mapping of a Roman painting. *Appl. Phys. A* **81**, 663–667 (2005).

30. Hradil, D. *et al*. Clay and iron oxide pigments in the history of painting. *Appl. Clay Sci.* **22**, 223–236 (2003).

31. Spangenberg, J. E. *et al*. Sulfur isotope analysis of cinnabar from Roman wall paintings by elemental analysis/isotope ratio mass spectrometry–tracking the origin of archaeological red pigments and their authenticity. *Rapid Commun. Mass Spectrom.* **24**, 2812–2816 (2010).

32. Harris, C. D. Cinnabar: The Symbolic, Seductive, Sublethal Shade of Pompeii. (Massachusetts, Brandeis University, 2015).

33. Mazzocchin, G. A. *et al*. Isotopic analysis of lead present in the cinnabar of Roman wall paintings from the Xth Regio "(Venetia et Histria)" by ICP-MS. *Talanta* **74**, 690–693 (2008).

34. Santacroce, R. *et al.* Age and whole rock–glass compositions of proximal pyroclastics from the major explosive eruptions of Somma-Vesuvius: A review as a tool for distal tephrostratigraphy. *J. Volcanol. Geotherm. Res.* **177**, 1–18 (2008).

5. LABORATORY CHARACTERIZATION OF RED AND YELLOW OCHRE PIGMENTS

5.1 Introduction

Iron-rich earths, mainly in the form of iron oxides, have been used as pigments since the prehistoric period up to now. Some of the characteristics that lend to these iron-rich earths their high usefulness as pigments are their easy preparation and/or its abundance in the nature. For example, the wide presence of iron-rich earths or outcrops of hematite mineral throughout different locations reduces the cost of this kind of pigments comparing with other more exotic or difficult to obtain materials (e.g., red cinnabar, purpurissum…). Red color can be considered one of the most employed ones in Pompeian paintings. Indeed, iron oxide coming from natural red earths (red ochres) together with iron oxyhydroxide, coming also from natural yellow earths (yellow ochres), or from goethite mineral, have been widely identified in Pompeian pigment powders recovered from the burial[1–3] or already applied in paintings[4–9].

Ochre pigments have been widely studied in the literature. A previous work focused on the study of their geological sources and their characteristics[10]. In this sense, clay minerals and iron oxides are intimately related in the process of their natural formation. Unlike other inorganic pigments, ochres have a complex molecular composition. In fact, ochre pigments are natural earths consisting of clayey minerals such as kaolinite and illite, with impurities (gypsum, quartz, magnesium carbonate, or manganese oxide), and of various hydrated forms of iron oxides which give the coloration[11].

In the case of Pompeii, it is supposed that in that period these red and yellow ochre pigments were obtained from local clayey iron rich soils[1]. Due to the location of Pompeii close to Mount Vesuvius it is expected that the local soils present mineral phases of volcanic origin in their composition. Therefore, an exhaustive single point micro-Raman spectroscopic study of the ochre pigments could allow identifying not only the main components responsible to give the red or yellow characteristic color, but also a complex mixture of minor and trace compounds that could suggest the possible local origin of these materials. The precise focusing of microscopic particles of interest could allow detecting mineralogical phases present at minor or trace levels. In this sense, the detection of a certain compound will vary not only depending on the concentration level present on the sample, but also on the Raman scattering offered by it. In fact, compounds with a high Raman scattering would provide strong signals even being present at minor/trace levels.

On the other hand, XRD is a suitable technique for the identification of compounds that have low Raman scattering and are difficult to be detected such as clays. However, amorphous mineral phases cannot be detected by XRD. On the contrary, Raman spectroscopy is capable to detect this type of compounds, being both complementary analytical techniques. In the case of ochre pigments, the use of both analytical techniques is required for a full molecular characterization and to not lose information about not detected compounds but present in the sample.

Apart from the molecular characterization, it is important to determine the elemental composition because it could vary significantly depending on the sample and its origin. Concretely, a previous work[12] established a multivariate statistical model in order to identify provenances of ochre pigments depending on the elemental composition. This work examined the variation in the major, minor and trace element patterns of ochres from different iron oxide sources and the obtained data indicated geochemical trends in the ochre pigments that satisfied the initial provenance postulates. Thus, chemometric analysis can offer information about groupings of samples classified in terms of their elemental composition. Comparing those with the composition of materials that could be the potential source, the provenance can be determined. In addition to this, the work performed by Jercher *et al*[13] also demonstrated that chemometrics applied to the elemental composition could establish at least the geological environment from which the ochre pigments came, and possibly to identify the source quarry. For the latter, as in the previous case, it must be analyzed a large number of samples from different sources to achieve a reliable attribution.

In this chapter, eight ochre pigments (five red and three yellow), recovered from the burial of the archaeological city of Pompeii were analyzed in the laboratory using benchtop instrumentation to identify mineral phases different than the main ones. For that, Raman microscopy was selected. These last minor/trace compounds present in the pigments could provide additional interesting information about the origin of the materials or the procedures used by the ancient artists. Raman experimental evidences will be compared with the results offered by XRD, a traditional technique used to identify mineral phases, in order to check the advantages/disadvantages of each technique among each other. Besides, EDXRF was also applied to perform an elemental characterization, aiming to detect possible similarities or differences between samples and to propose possible identical or different provenances of the analyzed samples according to the minor and trace elements. For that, a statistical study was conducted by means of PCA using the elemental composition.

Finally, to verify the provenance of these pigments lead isotopic ratio analysis was applied by means of Thermal Ionization Mass Spectrometry (TIMS).

5.2 Samples

Taking into account the great variety of red and yellow ochre pigments in the deposit of the MANN, an authorization to sample some of the selected ones was requested.

In this context, we were allowed to sample three yellow ochre (reference numbers 112249, 112257 and 117329) and five red ochre (reference numbers 112251, 112265, 117356, 117357 and 117360) pigments recovered from the burial of Pompeii in their original bowls (see Fig. 5.1). 117356, 117357 and 117360 red ochre pigments were recovered from original clay pottery bowls (with 72, 80 and 94 mm of diameter respectively). 117329 yellow ochre pigment was recovered from a clay pottery bowl with a diameter of 165 mm. Regarding red ochre 112251, it was catalogued as burnt ochre, that is, it was originally a yellow ochre which was burnt obtaining a red colored powders. On the other hand, since 112265 red ochre pigment and yellow ochre pigments 112249 and 112257 were recovered in the first excavations performed in Pompeii during years 1750-1850, no data about them were registered.

The sampling procedure was carried out taking small quantities of powder (around 100-200 mg) from the inner part of each bowl to avoid possible contributions coming from the volcanic materials of the burial. All the samples were preserved in glass containers until their analysis.

Fig. 5.1. The 117356 red ochre and 112257 yellow ochre pigments recovered in their original bowls.

5.3 Molecular characterization of the Pompeian ochres

5.3.1 Major mineral phases in red and yellow ochre pigments under study

The compounds responsible to give the characteristic color to the ochre pigments under study were mainly based on iron oxides, such as goethite (α-FeOOH) in yellow ochre pigments and hematite (α-Fe_2O_3) in the case of red ochres (see Fig. 5.2A-B). Besides, calcite ($CaCO_3$) and quartz (α-SiO_2) were also widely present in them (see Fig. 5.2C-D). All these compounds were identified by both Raman microscopy and X-ray diffraction.

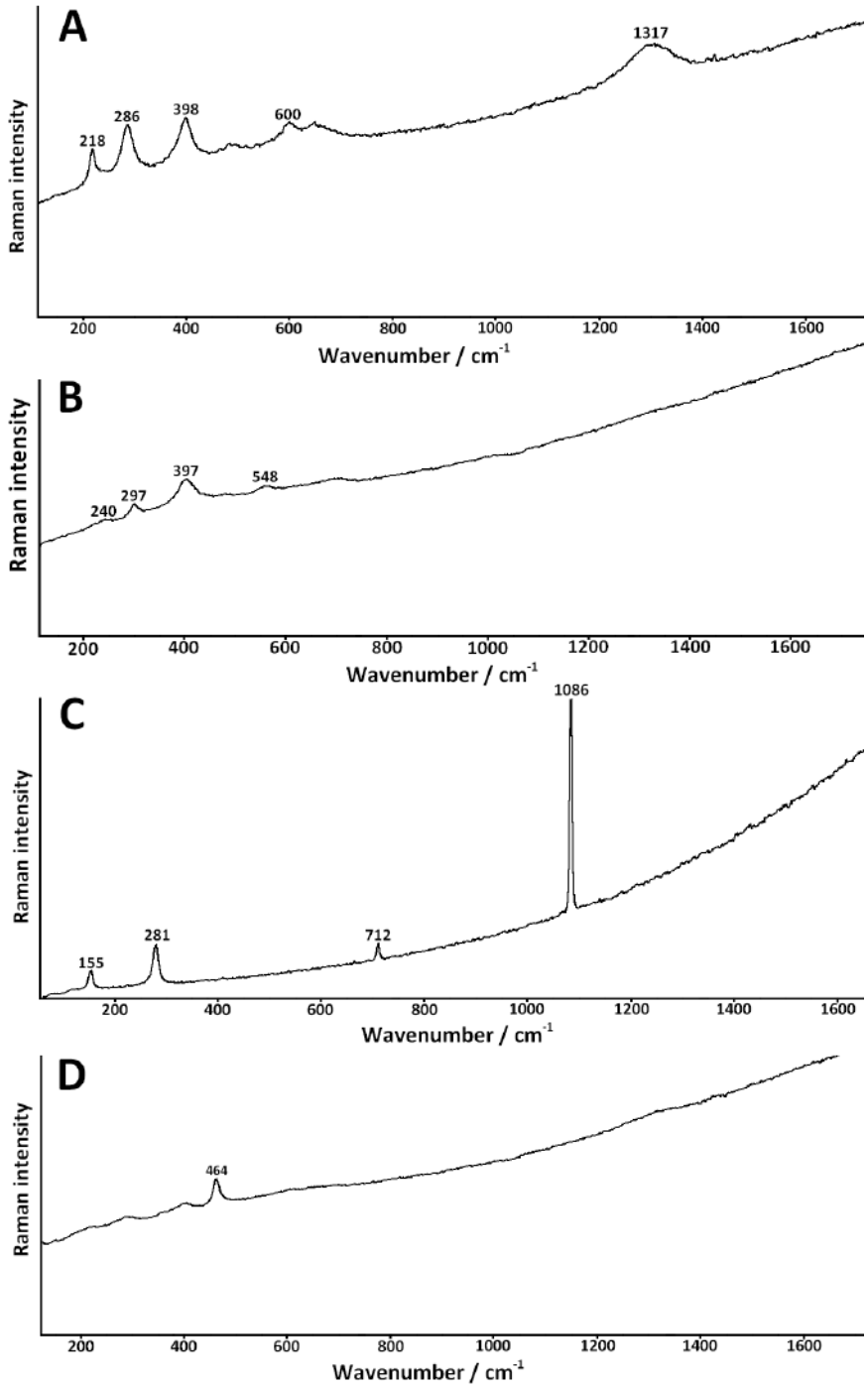

Fig. 5.2. Raman spectra of the detected major compounds a) hematite, b) goethite, c) calcite and d) quartz.

Apart from them, clay minerals such as kaolinite ($Al_2Si_2O_5(OH)_4$) and illite ($((Al,Mg,Fe)_2(Si,Al)_4O_{10}[(OH)_2,(H_2O)]$) were also detected in all the samples except in the 112265 and 117360 red ochre ones. The identification of these clays was only determined by means of XRD, since by Raman spectroscopy these compounds offer a great fluorescence masking any band of interest (see Fig. 5.3).

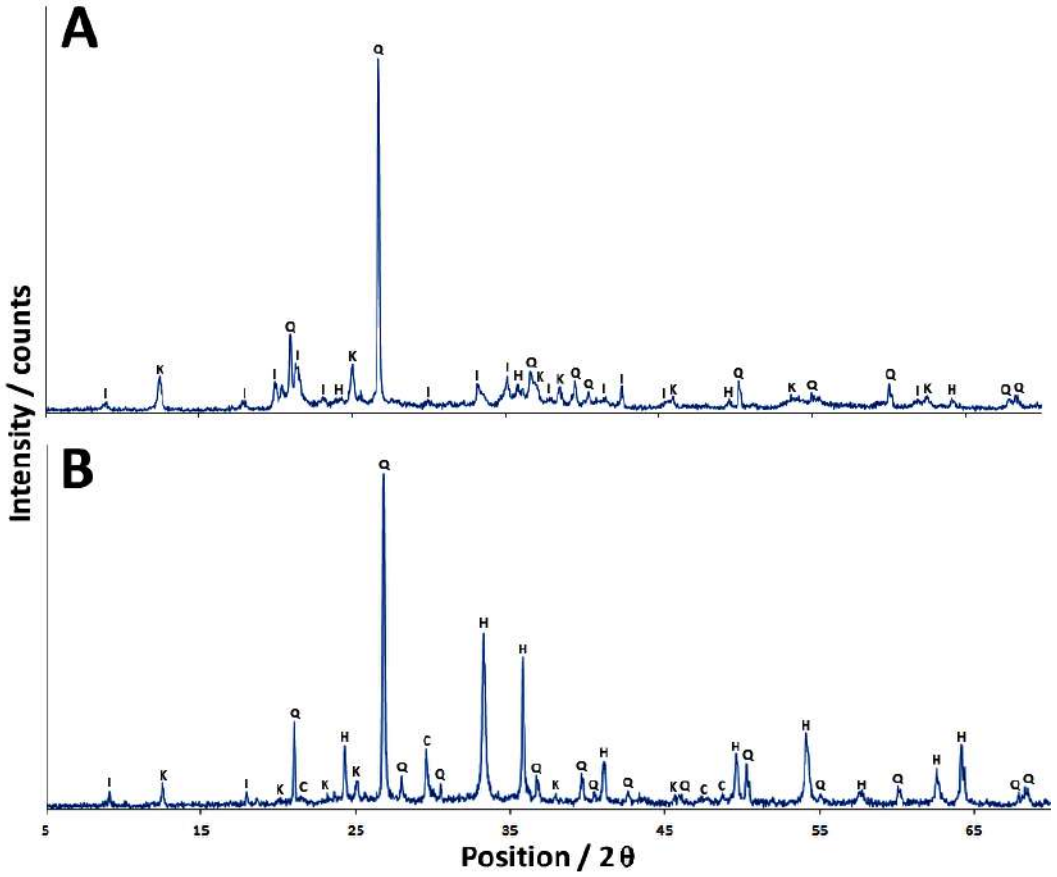

Fig. 5.3. Diffractograms of detected clays in (a) 112249 yellow ochre and (b) 117356 red ochre pigments (C: calcite; H: hematite; I: illite; K: kaolinite; Q: quartz).

The assistance of Raman spectroscopy with other techniques, such as XRD in this case, becomes mandatory to detect the presence of clays. The obtained Raman results regarding minor and traces mineral phases on the ochre pigments were grouped according to the possible origin of the identified compounds. These results were finally compared with the ones obtained by means of XRD.

5.3.2 Minor and trace mineral phases identified by Raman spectroscopy

Raman microscopy allowed identifying the presence of langite in 117357 and 117360 red ochres. As shown in Fig. 5.4, the characteristic Raman bands of langite (436, 502, 602 and 971 cm^{-1}) were clearly identified. Due to the high fluorescence especially from 1200 cm^{-1} up to high wavelengths, the spectra in which langite was detected were recorded between 100-1200 cm^{-1} to avoid the saturation of the detector. This compound was also identified by means of XRD in both samples, suggesting in this way that this mineral is over 1% in weight[14]. Langite is a rare hydrated basic copper sulfate mineral [$Cu_4(SO_4)(OH)_6 \cdot 2H_2O$]. As described in a previous work[15], langite was doubtfully detected as a fumarolic mineral occurring on Mount Vesuvius. Thanks to the identification of this mineral, it can be now affirmed that langite has been detected in the area of Mount Vesuvius, probably generated as fumarolic mineral. As mentioned before, each sample was extracted from the inner areas of the bowls to prevent from possible contaminations coming from the pyroclastic deposits that could have been deposited on the pigments. Moreover, for the Raman microscopic measurements, compacted pigment balls of pigments were broken to perform the measurements in the inner areas. Therefore, considering this strategy we can conclude that the mineral phases of volcanic origin present in the pigment are not related to contamination events. Thus, its presence could suggest that local soils were used to manufacture of these Pompeian ochres.

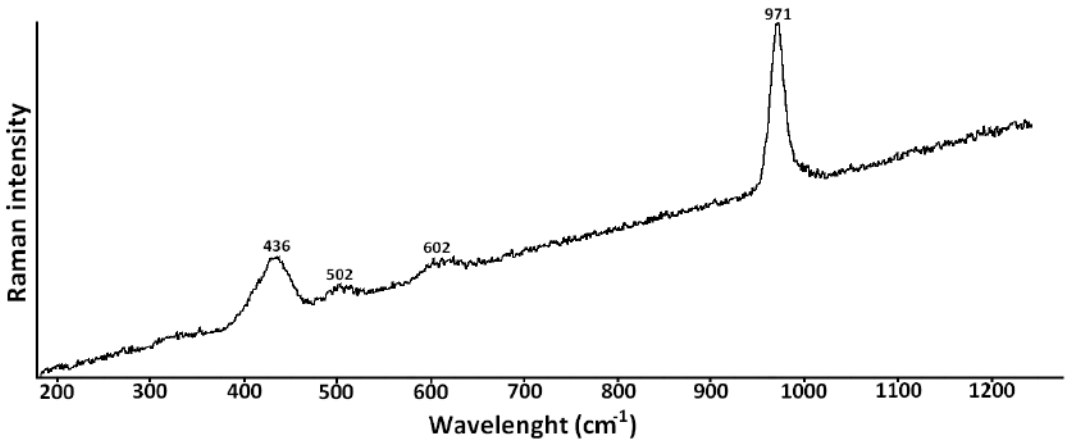

Fig. 5.4. Raman spectrum of langite.

Apart from langite, in all yellow ochre samples, anatase (β-TiO_2) was also found (Raman bands at 145, 198, 396, 514 and 636 cm^{-1}; see Fig. 5.5). This oxide was not detected by XRD in any sample, thus it can be assumed that its presence is very punctual and the concentration is below 1% in weight[14]. Anatase is one of the three possible polymorphs of titanium (IV) oxide, together with rutile (α-TiO_2) and brookite (γ-TiO_2).

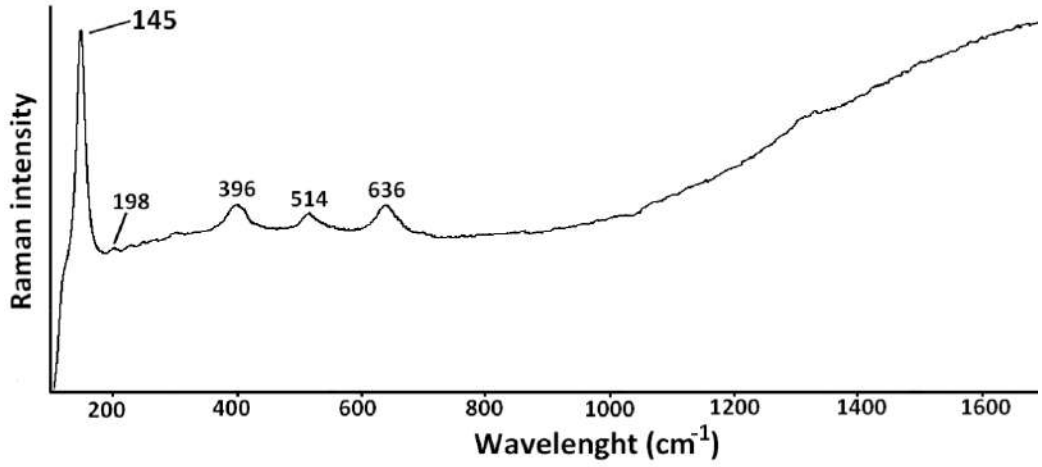

Fig. 5.5. Raman spectrum of anatase.

Anatase is a detrital mineral of titanium oxide that is usually found in sedimentary kaolin deposits and igneous and metamorphic rocks[16]. Thus, anatase could be present in natural earths from Pompeii and surroundings, due to the presence of igneous rocks formed by Mount Vesuvius emissions. Anatase was also found in red ochre sample 112265. Therefore, its presence confirmed once again the possible use of local volcanic soils to manufacture these ochre pigments.

Jarosite, a basic hydrous sulfate of potassium and iron ($KFe_3(OH)_6(SO_4)_2$) was also successfully identified thanks to the detection of its bands at 224, 300, 415, 453, 623, 1008 and 1107 cm^{-1} (see Fig. 5.6).

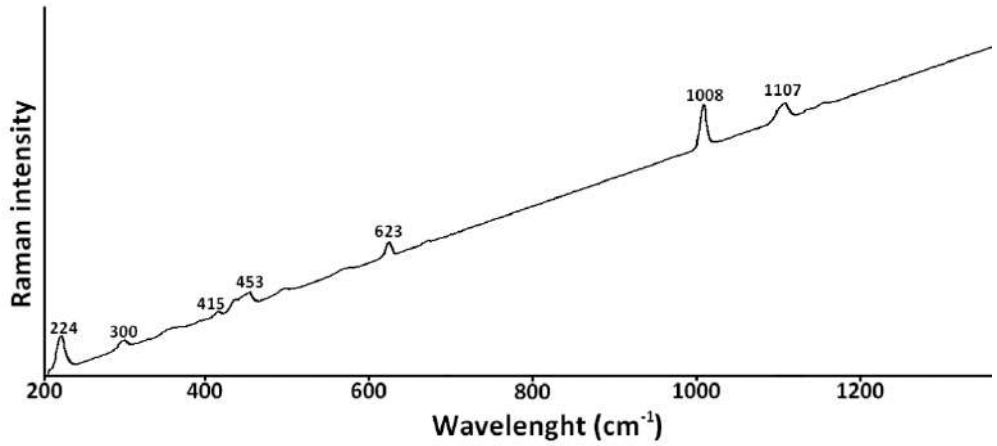

Fig. 5.6. Raman spectrum of jarosite.

This mineral is usually found in localities with higher activity of sulfur, such as volcanic areas. In fact, jarosite has been found in volcanic areas such as Vesuvius[15] and Vulcano Island[17], both in Italy; in the White Island volcano (New Zealand)[18], and in the Kutch district or Kachchh (India)[19]. These examples of occurrence of jarosite in volcanic areas, together with its presence in samples 112265 (red) and 112257 (yellow), pointed out the local origin of these ochres. In the work developed by Giachi *et al.*[2], the presence of this compound was also identified in red and yellow pigments from Pompeii.

In that work and in an additional study mainly based on microscopic observations, jarosite was identified as main coloring component in earth pigments from Pompeii[2,20]. In the red and yellow ochre pigments analyzed in this PhD Thesis, jarosite was detected occasionally and never as the main compound which gives the color to these earth pigments. However, although this mineral is not the main constituent of both ochre pigments, it is not present at trace levels, since in the analyses performed by means of XRD, it was possible also to detect its presence in both pigments.

Apart from that, it is important to remark the presence of atacamite (Raman bands centered at 160 and 513 cm^{-1})[21,22] in yellow ochre sample 112257 as shown on Fig. 5.7. Atacamite is a greenish copper halide mineral ($Cu_2Cl(OH)_3$) , discovered for the first time in Atacama Desert. Moreover, it can occur as a volcanic sublimate from fumarolic deposits and it is associated to the Vesuvius lavas as a previous work demonstrated[15]. Thus, the detection of atacamite in this pigment, once more, points out the use of local soils of volcanic origin. The presence of this compound was not detected by XRD, reinforcing the minor/trace contribution to the total composition of the pigment.

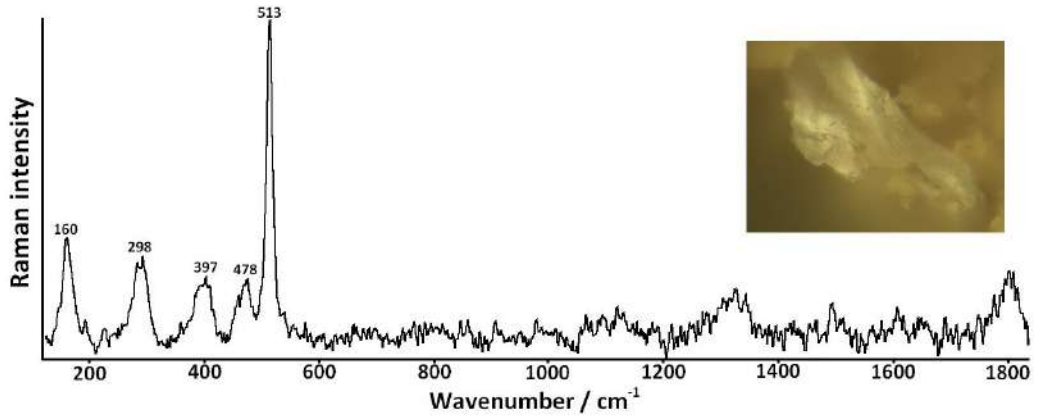

Fig. 5.7. Raman spectrum showing bands of atacamite and goethite.

Apart from the commented bands assigned to atacamite, in the obtained spectrum additional bands at 298, 397, and 478 cm^{-1} (see Fig. 5.7) belonging to goethite, main component of this yellow ochre pigment, were also detected.

5.3.3 Identification of possible contaminations by Raman microscopy

Egyptian Blue ($CaCuSi_4O_{10}$) was identified in yellow ochre sample 112257 and in red ochre samples 112251, 112265, 117357 and 117360 (Raman bands at 120, 135, 163, 195, 228, 378, 430, 462, 568, 788, 989, 1010 and 1083 cm^{-1}, see Fig. 5.8). This inorganic blue pigment was widely used in the Roman Age, but it is not present in the local soils where the ochres were taken. As it has been mentioned in Chapter 4, Egyptian Blue was synthetically manufactured since ancient Egyptian civilizations[23,24].

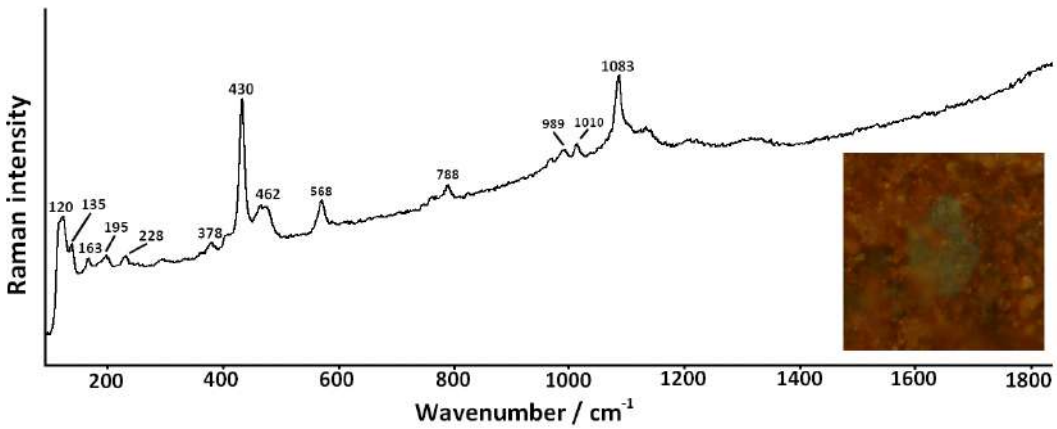

Fig. 5.8. Raman spectrum of Egyptian Blue.

Some works revealed that one type of green color used in the Pompeian wall paintings was achieved mixing Egyptian blue and yellow ochre. Thereby, one hypothesis could be that some grains of this blue pigment were mixed with the red or yellow ochres to obtain

a different final hue. However, the presence of Egyptian Blue is very punctual in these ochre pigments, thus this hypothesis cannot be considered as the most probable one. This evidence is reinforced with the experimental results obtained by means of XRD, since in any of the diffractograms acquired for the samples where Egyptian Blue was identified by means of Raman microscopy, characteristic diffraction peaks of this compound were detected. Therefore, it can be affirmed that its presence in the sample is under the 1% in weight[14].

Considering this, two hypotheses can be suggested to explain the presence of this blue pigment in some of the yellow and red ochres analyzed. On the one hand, its presence can be related with a previous storage of Egyptian Blue pigment in the same bowl where nowadays the yellow and red ochre are preserved. On the other hand, another plausible explanation could be that the artist manipulated both pigments with the same instrument (e.g. paintbrush or spatula) and the ochres were somehow contaminated. Nonetheless, the only sure statement is that the artist who employed the analyzed ochres included also Egyptian Blue in his palette.

Finally, huntite [$Mg_3Ca(CO_3)_4$] was also identified in red ochre sample 117356 (Raman bands at 158, 225, 276 and 1123 cm^{-1}, see Fig. 5.9). It is an unusual white mineral used as pigment in the Roman and Egyptian age[25] which it was already identified as powder pigment in Pompeii in a previous work[1] but, up to now, it was not identified applied in any wall painting. This compound was not detected by XRD, thus it is expected to be present in the sample in a percentage of less than 1%. Due to its low presence (it was just observed punctually) it could be related with a possible contamination.

As commented before, with XRD only the main components of the pigments under study were identified (see Fig. 5.3). In this sense, main components such as hematite, goethite, calcite and quartz, which were detected by XRD, were also identified by Raman microscopy as shown in Fig. 5.2.

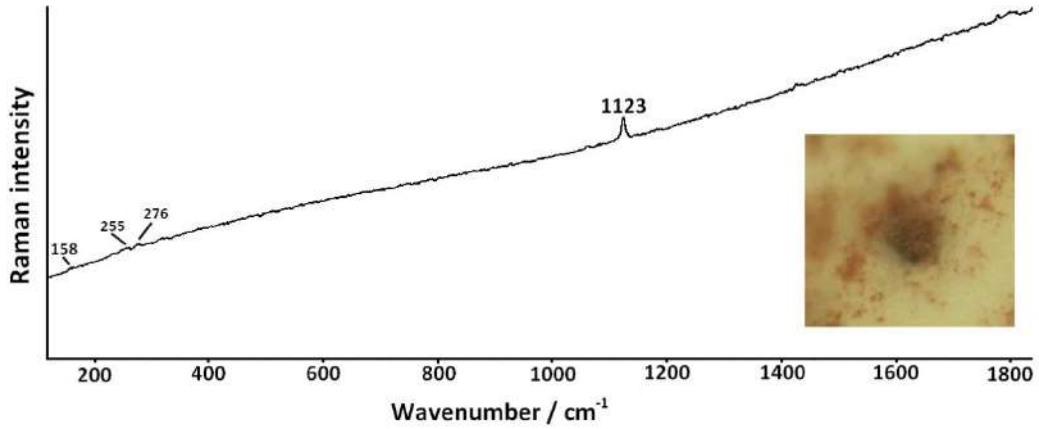

Fig. 5.9. Raman spectrum of huntite.

However, clays present in the samples such as kaolinite and illite were not detected by this last technique due to the high fluorescence observable in the acquired spectra. On the other hand, the discriminative compounds (volcanic origin vs contamination components) which were present at minor or trace level in the ochres under study were only detected by Raman microscopy (except langite and jarosite which were detected by XRD in some samples). Thus, both techniques are really complementary. In Table 5.1, a summary of all the compounds detected by Raman microscopy in the red and yellow ochre pigment samples is presented.

Table 5.1. Identified main components, characteristic mineral phases of volcanic origin, and contamination compounds in the Pompeian ochre pigments under study.

	112251 red	**112265 red**	**117356 red**	**117357 red**	**117360 red**	**112249 yellow**	**112257 yellow**	**117329 yellow**
Main components	Hematite Quartz	Hematite Quartz	Hematite Quartz Calcite Kaolinite Illite	Hematite Quartz Calcite Illite	Hematite Quartz Calcite	Goethite Hematite Quartz Kaolinite Illite	Goethite Quartz Kaolinite Illite	Goethite Quartz Calcite Kaolinite Illite
Mineral phases of volcanic origing	-	Anatase Jarosite	-	Langite	Langite	Anatase	Anatase Atacamite Jarosite	Anatase
Contaminations	Egyptian Blue	Egyptian Blue	Huntite	Egyptian Blue	Egyptian Blue	-	Egyptian Blue	-

5.4 Elemental characterization of red and yellow ochre pigment powders and multivariate analysis

The ochre pigments under study were also measured by means of EDXRF in the laboratory to obtain their elemental composition. For that, six measurements of each pigment were performed. Considering a possible heterogeneity at lateral resolutions of 25 μm, it was decided to make the measurements of the pigment at 1 mm of lateral resolution to obtain representative results. Fig. 5.10 shows representative spectra obtained for each red ochre pigment.

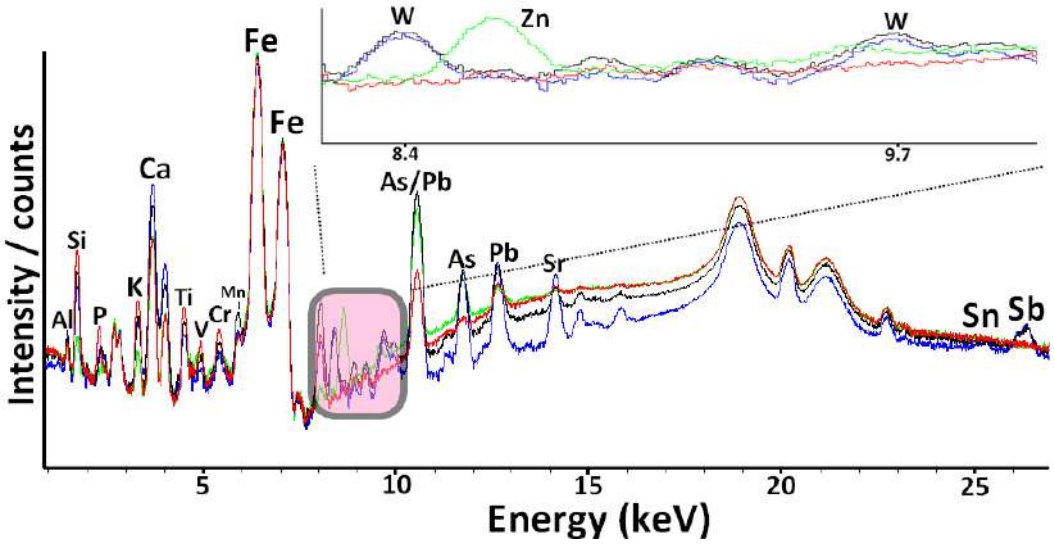

Fig. 5.10. XRF spectra of 112265 (red), 117356 (black), 117357 (blue) and 117360 (green) red ochre pigments.

As it was expected, Fe is the main element present in the pigments because hematite (α-Fe_2O_3) is the main component in the red pigments, and goethite (α-FeOOH) in the case of yellow ochres. In Table 5.2, the detected net counts of each element, normalized against Fe, are shown.

Table 5.2. Net counts normalized against Fe (x100) with the standard deviation.

	112249 yellow	112257 yellow	117329 yellow	112251 red	112265 red	117356 red	117357 red	117360 red
Mg	0.005 ± 0.003	0.004 ± 0.003	0.006 ± 0.002	0.001 ± 0.001	0.003 ± 0.002	0.004 ± 0.001	0.005 ± 0.001	ND
Al	0.37 ± 0.05	0.158 ± 0.006	0.16 ± 0.02	0.079 ± 0.004	0.025 ± 0.002	0.045 ± 0.005	0.046 ± 0.004	0.014 ± 0.001
Si	1.6 ± 0.2	0.82 ± 0.04	1.1 ± 0.3	0.409 ± 0.02	0.67 ± 0.02	0.33 ± 0.03	0.26 ± 0.02	0.037 ± 0.004
Cl	0.006 ± 0.003	0.002 ± 0.002	0.001 ± 0.002	0.005 ± 0.002	0.013 ± 0.003	0.005 ± 0.003	0.004 ± 0.002	0.016 ± 0.004
K	0.85 ±0.09	0.73 ± 0.02	0.50 ± 0.09	0.795 ± 0.07	0.261 ± 0.009	0.128 ± 0.007	0.12 ± 0.02	0.073 ± 0.006
Ca	0.25 ± 0.02	1.3 ± 0.1	2 ± 1	0.275 ± 0.01	1.13 ± 0.09	2.2 ± 0.2	4.7 ± 0.2	1.1 ± 0.4
Ti	1.06 ± 0.08	0.74 ± 0.02	0.6 ± 0.1	1.979 ± 0.05	0.242 ± 0.008	0.14 ± 0.05	0.11 ± 0.02	0.078 ± 0.009
V	0.08 ± 0.01	0.069 ± 0.007	0.07 ± 0.02	0.199 ± 0.02	0.039 ± 0.002	0.023 ± 0.001	0.012 ± 0.004	0.006 ± 0.005
Cr	0.062 ± 0.006	0.035 ± 0.001	0.05 ± 0.01	0.032 ± 0.002	0.12 ± 0.02	0.07 ± 0.01	0.058 ± 0.003	0.030 ± 0.006
Mn	0.35 ± 0.08	0.41 ± 0.03	0.5 ± 0.4	0.012 ± 0.01	0.019 ± 0.004	0.103 ± 0.007	0.050 ± 0.006	0.005 ± 0.007
Co	0.37 ± 0.03	0.39 ± 0.06	0.28 ± 0.01	0.271 ± 0.02	0.27 ± 0.04	0.35 ± 0.04	0.36 ± 0.05	0.27 ± 0.02
Ni	0.015 ± 0.001	0.025 ± 0.002	0.03 ± 0.01	ND	0.003 ± 0.001	ND	ND	ND
Cu	0.15 ± 0.01	0.05 ± 0.01	0.13 ± 0.08	0.033 ± 0.003	0.16 ± 0.03	0.4 ± 0.1	0.12 ± 0.03	0.11 ± 0.07
Zn	0.12 ± 0.02	0.219 ± 0.005	0.22 ± 0.02	0.012 ± 0.003	0.009 ± 0.006	0.001 ± 0.001	0.008 ± 0.003	0.16 ± 0.03
As	1.5 ± 0.2	0.22 ± 0.01	0.17 ±0.02	0.162 ± 0.007	0.46 ± 0.02	4.51 ± 0.08	5.1 ± 0.1	2.9 ± 0.2
Rb	0.19 ± 0.04	0.10 ± 0.01	0.07 ± 0.02	0.065 ± 0.01	0.003 ± 0.002	ND	0.001 ± 0.002	ND
Sr	0.13 ± 0.02	0.45 ± 0.04	0.20 ± 0.04	2.046 ± 0.2	0.13 ± 0.01	0.27 ± 0.01	0.76 ± 0.05	0.07 ± 0.01
Y	0.01 ± 0.01	0.001 ± 0.002	0.007 ± 0.007	0.007 ± 0.004	ND	0.002 ± 0.003	0.005 ± 0.005	ND
Zr	0.17 ± 0.07	0.17 ± 0.01	0.12 ± 0.03	0.901 ± 0.08	0.01 ± 0.01	0.02 ± 0.01	0.01 ± 0.01	0.009 ± 0.002
Sn	0.002 ± 0.002	0.002 ± 0.003	0.001 ± 0.002	0.002 ± 0.004	0.003 ± 0.002	0.005 ± 0.004	0.039 ± 0.008	0.001 ± 0.001
Sb	0.002 ± 0.003	ND	ND	ND	ND	0.17 ± 0.02	0.24 ± 0.04	0.004 ± 0.002
Ba	0.026 ± 0.006	0.05 ± 0.02	0.01 ± 0.02	0.479 ± 0.03	0.018 ± 0.004	0.003 ± 0.003	0.004 ± 0.004	0.10 ± 0.03
W	0.02 ± 0.02	ND	ND	ND	ND	0.31 ± 0.02	0.34 ± 0.02	ND
Pb	0.01 ± 0.02	0.42 ± 0.04	0.56 ± 0.04	0.195 ± 0.01	0.73 ± 0.03	1.72 ± 0.08	2.1 ± 0.1	0.55 ± 0.06

ND: Non detected

5.4.1 Multivariate analysis of the elemental data

To classify the pigment samples according to their elemental composition, the obtained elemental data matrix (Table 5.2) consisting of 48 measurements and 24 variables (detected elements) was subjected to PCA. As shown in Fig. 5.11, four clearly distinguishable groups were obtained.

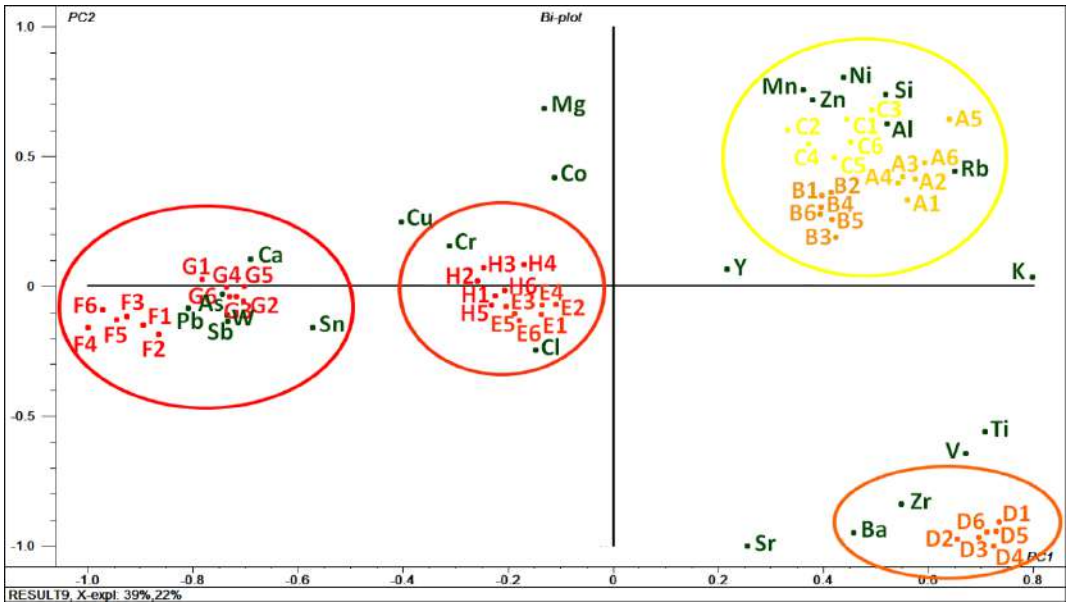

Fig. 5.11. Bi-plot (loadings and scores) obtained in the PCA of the measured red and yellow ochre pigments [A: 112249 (yellow), B: 112257 (yellow), C: 117329 (yellow), D: 112251 (red), E: 112265 (red), F: 117356 (red), G: 117357 (red), H: 117360 (red)].

PC1 classifies the samples according to their color: red ochres in the negative part, except red sample 112251 which is placed with yellow ochres that are in the positive part of the PC1. In fact, s commented in section 5.2, red sample 112251 belongs to a burnt yellow ochre pigment. In this sense, PCA results comes in agreement with the previous observation, since red sample 112251 is grouped with all the yellow samples, because before its burning it was an original yellow pigment. As shown in Fig. 5.11, arsenic is one of the elements that characterize red ochre samples (and it is not present in original yellow ochre samples) in terms of elemental composition.

In the case of red ochre samples two additional groups can be observed. Samples 112265 and 117360 were placed together. On the other hand, 117356 and 117357 red ochres, which are the samples characterized mainly by high levels of W, Sn, As and Sb, are placed at the lowest values of the PC1.

Regarding the elemental composition of yellow ochre pigments, all of them are similar since they are grouped all together with Al, Si, K, Mn, V, Ni, Rb and Zr as characteristic elements of this group. These elements are also characteristic of the volcanic material, concretely from the pyroclastic flow from Somma-Vesuvius eruption episodes[26]. Thus, this composition could suggest that the analyzed yellow ochres were probably taken from local soils.

In the yellow ochre pigments the unusual concentration of W, Sn, As and Sb observed in two red ochre pigments was not detected except for the case of sample 112249 which showed W in its composition in three out of the six performed measurements. The microscopic observations of this particular sample showed that it was composed by yellow and red grains (see Fig. 5.12).

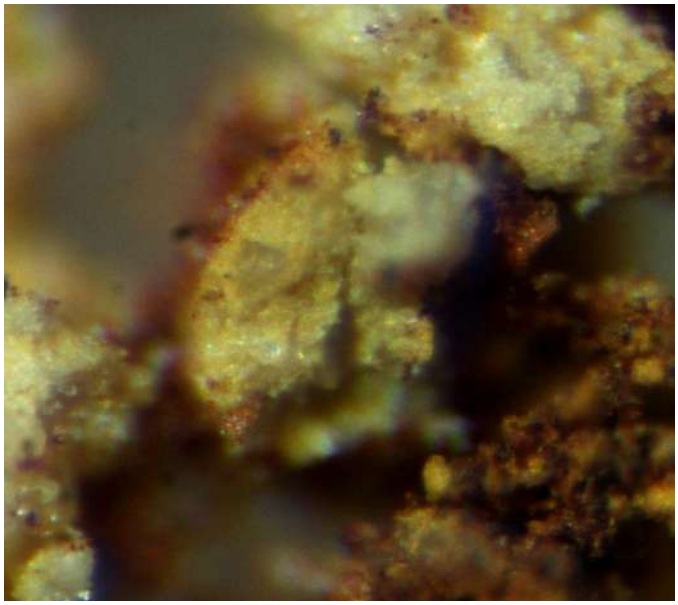

Fig. 5.12. Microscopic image of the 112249 yellow ochre pigment.

Moreover, at the naked eye, this sample was orange-brown colored. Indeed, hematite was detected previously by Raman and XRD spectroscopies (see Table 5.1).

Therefore, the mixture of yellow ochre with red ochre powders it is proven, probably in order to achieve a different hue. The mixture of different pigment types with this purpose has been already observed previously in Pompeian yellow pigments (see Chapter 4). Taking into account the elemental results related with this yellow pigment, the W detected could be associated with yellow and/or red grains. Therefore, it was decided to conduct additional microscopic XRF measurements (down to 25 μm lateral resolution) to obtain the independent elemental composition of the yellow and red grains separately in order to conclude if W presence is only related with the hematite pigment grains. In this sense, the obtained semi-quantitative results showed an average value of 1050 ± 38 $\mu g \cdot g^{-1}$ of W in red grains, while in yellow grains this element was not detected. Therefore, it can be affirmed that the presence of W is related with the red grains (hematite) present in the yellow ochre pigment.

According to the obtained PCA, and taking into account that the different elemental composition could suggest a possible different source of this material, four different origins could be differentiated: two red samples (112265 and 117360) probably have a different origin than the other two red ochres (117356 and 117357) due to the very different elemental composition. Yellow ochre samples, probably manufactured from local soils as commented before, are grouped together showing a different origin from all the red ochres under study. Finally, the red sample 112251, which was already identified as yellow burnt ochre, nowadays red, would have a different origin from the rest ochre pigments.

As commented before, some works demonstrated that PCA of the elemental composition can be used as a tool to identify different sources of ochres[12,13]. However, for that purpose, the material from the potential source of origin is necessary in order to correlate with the pigments under study. Since in this case these materials were not available, the presented PCA results cannot offer conclusive provenance results, but similarities in the elemental composition could suggest a possible common origin. Nevertheless, this fact

must be confirmed with other techniques. Moreover, taking into account that these samples are archaeological pigments that have been buried for thousands of years, possible contaminations by leachable metals present in the soil or volcanic tephra might have modified the original elemental composition of the samples.

As shown in Table 5.2 and in the PCA (Fig. 5.11), it is remarkable the highest value of Cu in pigment 117356; Cr in 112265; Mn in 112249, 112257 and 117329 pigments; and Zn in 112251, 112265, 117356 and 117357 red pigments. Pigments 112251 also showed high levels of Ti, V, Sr, Zr, Ba and Pb. On the contrary, pigments 117360 shows the lowest levels of trace metals. However, the most noteworthy and evident unexpected levels correspond to the red samples 117356 and 117357, which showed the highest levels of As, Pb, W, Sn and Sb.

5.4.2 Tungsten and tin as geochemical markers for provenance tracing

In Table 5.3, the unexpected concentrations of W, Sn, As and Sb in red pigments 117356 and 117357 obtained semi-quantitatively by EDXRF is presented. These elements can be present in the different terrestrial systems (surface soils, rocks, lithosphere, earth crust…) but at much lower concentrations that those detected in the red pigments under study (see Table 5.3).

In the literature, it is reported that the hematite ore from Elba Island (Tuscany, Italy) is considerably enriched in both W and Sn[31]. The presence of both elements makes this iron ore unique in the world[31], because there is not any registered place with these elemental features. Thus, W and Sn could be considered the geochemical markers characteristic of this particular ore.

Table 5.3. Background concentrations of W, Sn, As and Sb in different soils[27–30] and obtained concentrations together with its 95% confidence interval of 117356 and 117357 red ochre pigments in $\mu g \cdot g^{-1}$ units.

Element	Soils	117356 red pigment	117357 red pigment
W	0.1-83	2640 ± 54	2500 ± 79
Sn	2-3	96 ± 34	660 ± 57
As	2-45	19900 ± 128	19500 ± 356
Sb	1-10	4100 ± 200	4800 ± 328

Moreover, iron mined from Elba was extensively traded throughout the Mediterranean region from antiquity to modern times. Both the geographical location of the island, just at the crossroads of the main sea routes of the Western Mediterranean, and the extremely favorable geological setting of the ores (mostly in massive ores at low depth and close to the coast), were key factors in assuring a primary role in the iron industry to Elba Island[31].

Concretely, the 117356 and 117357 red ochre pigments present both elements at high and similar concentrations. Moreover, during the Roman period, concretely from 3 BD to 1 BD, a dramatic increase in the iron exploitation and in the production of ores from Elba Island had been described in previous works[32–34]. Therefore, the presence of W and Sn, and the coincidence in the production dates with the ones of ancient Pompeii could point out to the use of this specific ore to manufacture these two Pompeian pigments. Although the presence of both geochemical markers may be conclusive, considering that these two pigments also show high levels of Pb, coming from a possible contamination, it was decided to perform Pb isotopic analysis to obtain additional clues about the provenance of these two pigments.

5.5 Lead isotopic ratio analysis

To verify the conclusions obtained in the multivariate analysis extracted from the XRF results and to corroborate the possible provenance of red ochre pigments from Elba Island, lead isotopic ratio analysis was performed by means of TIMS. Among all of the naturally occurring lead isotopes, only ^{204}Pb is non radiogenic, whereas ^{206}Pb, ^{207}Pb, and ^{208}Pb are daughter products from the radioactive decay of ^{238}U, ^{235}U, and ^{232}Th, respectively. This fact produces small Pb isotope abundance variations in nature. Furthermore, it is well-known that the isotopic composition of Pb in natural materials is clearly dependent on the ore deposits from which it comes, thus the lead isotopic ratio can provide analytical information about sources of lead contamination[35].

The isotopic ratios obtained by TIMS together with the lead concentration determined semi-quantitatively in each sample by means of EDXRF are shown in Table 5.4. Deviations (2σ) of the obtained isotopic values were below 0.1% for all samples.

Table 5.4. Lead concentrations and lead isotopic ratios of the samples under study. The results are expressed as the average value together with the standard deviation.

SAMPLE	Pb concentration ($\mu g \cdot g^{-1}$)	$^{206}Pb/^{204}Pb$	$^{207}Pb/^{204}Pb$	$^{208}Pb/^{204}Pb$	$^{208}Pb/^{206}Pb$	$^{207}Pb/^{206}Pb$
112251 red	680 ± 60	18.6743	15.6653	38.6375	2.07137	0.85618
112265 red	2850 ± 267	18.4854	15.6363	38.5642	2.08620	0.84587
117356 red	8130 ± 315	18.3476	15.6776	38.5430	2.10071	0.85448
117357 red	8700 ± 583	18.3605	15.6670	38.5254	2.09828	0.85330
117360 red	1700 ± 924	19.2002	15.7244	38.9178	2.02695	0.81897
112249 yell	35 ± 25	18.7824	15.6848	38.7035	2.06063	0.83508
112257 yellow	1000 ± 160	18.4905	15.6721	38.6691	2.09130	0.84758
117329 yellow	1150 ± 185	18.5188	15.6859	38.7520	2.09258	0.84702
Elba Island		18.7492	15.7041	39.0045	2.08033	0.83759

The lead isotopic ratios of 117356 and 117357 red ochre samples, which showed high concentrations of W and Sn, are not in agreement with those referenced for the hematite from Elba Island in the OXALID database[36] (see Table 5.4). As it has pointed out in the previous chapter, during the burial Pb contamination may take place. therefore, this event can modify the Pb isotopic values comparing to the ones in the original pigments.

As far as we know[37], the $^{207}Pb/^{206}Pb$ ratio for the volcanic materials is 0.8242. Moreover, a previous work[38] performed leaching experiments of the in-depth soil from the Campania region, where the ancient city of Pompeii is located, determined in the leaching solutions a mean $^{207}Pb/^{206}Pb$ ratio of 0.8425.

In addition to this, lead pipes were commonly employed in all the area of Bay of Naples, and in particular in the ancient city of Pompeii. In fact, in recent excavations, these kinds of pipes came to light. It is also well referenced[39] that the archeological soil from ancient Roman cities was rich in Pb, reaching concentrations of 1000 μg/g. Probably this high concentration could be explained due to the leaching process from the lead pipes of the ancient Roman city water supply/discharge system. In fact, there are evidences about the collapse of the water system during the events prior to the eruption[40], which promoted a lead contamination that has been recently identified in sediments from the Bay of Naples[41]. In this sense, it is reported[42] that the $^{207}Pb/^{206}Pb$ mean ratio of the lead pipes from Pompeii is 0.845, very similar to that determined in the leaching experiments of in-depth soil from the Bay of Naples in Campania[38], obtaining a mean value of 0.8425. Thus, these almost same values confirm that the Pb present in the soils and sediments from the Bay of Naples comes from the ancient lead water system that supplied water to ancient cities such as Pompeii, Herculaneum, Puteoli, Cumae, or Baiae[41].

In this sense, the isotopic ratios of all the samples except red pigment 117360 match with those from the Pb leached from pipes of the ancient water supply. This is clearly observed in Fig. 5.13, where the $^{206}Pb/^{204}Pb$ and $^{207}Pb/^{204}Pb$ values of the analyzed pigments samples are plotted together with the ones of the Pb contaminated surface and in-depth soils from the Campania region, the one from the ancient Pb pipes from Pompeii and the ones of Elba Island.

As seen in Fig. 5.13, only two pigments, 117360 (red) and 112249 (yellow), are not influenced by the Pb contamination coming from the lead pipes. For this reason, in this case, the Pb isotopic composition cannot be used for provenance identification purposes, because the obtained values are not the original due to the contamination influence. Thereby, the provenance from Elba Island of 117356 and 117357 red pigment could not be confirmed by lead isotopic analysis.

On the other hand, regarding yellow pigment 112249, the obtained values matched better with Pb from the soils instead of the ones associated with ancient pipes. In fact, the concentration of Pb determined by EDXRF was quite low (35 ppm, see Table 5.4) comparing with the other pigments under study. Thus, the contamination of leached Pb coming from the water system of Pompeii in this pigment can be considered negligible. Probably this pigment was located in a place protected from this lead leaching.

Finally, the red pigment 117360 showed quite different Pb isotopic values from the explained possible sources. This pigment probably had an additional kind of Pb contribution that changed slightly its Pb isotopic composition. In fact, its Pb composition is close to one sample belonging to the in-depth soils from Campania (see Fig. 5.13).

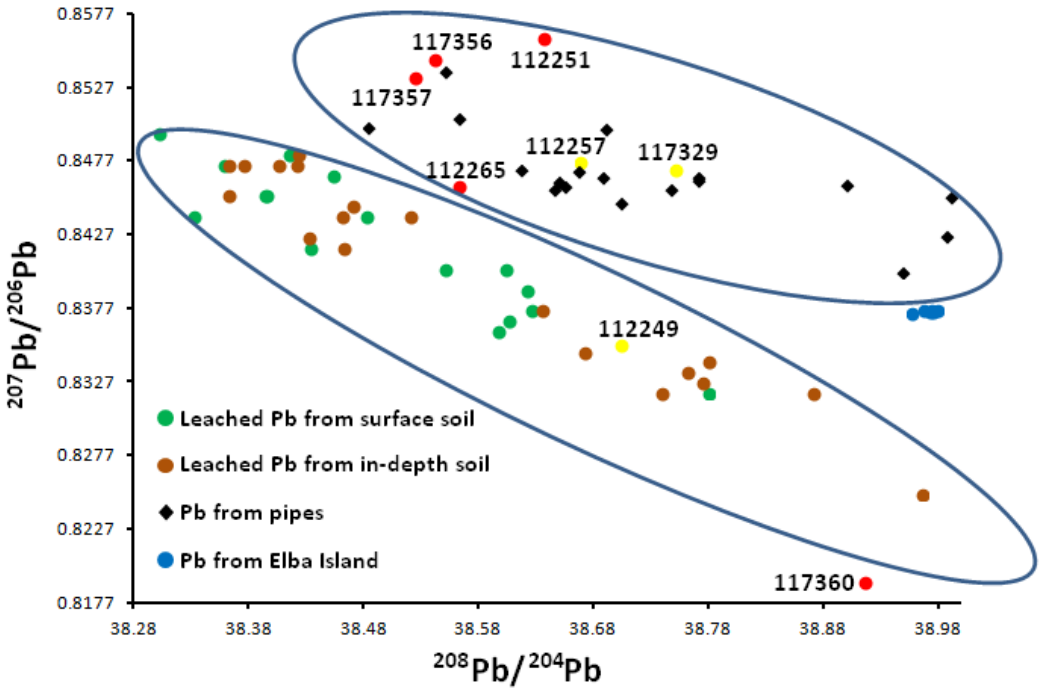

Fig. 5.13. Pb isotopic compositions of red and yellow ochre pigments, Pb leached from the surface and in-depth soils, Pb from the pipes of the ancient water system supply and the Pb from Elba Island.

5.6 Conclusions

The goal of this Chapter was to fully characterize in the laboratory Pompeian yellow and red ochre pigments to detect compounds or elements that could suggest the source of the material used to manufacture these pigments.

Regarding the molecular composition, it was demonstrated that thanks to the use of confocal Raman microscopy, a technique that offers higher sensitivity than XRD due to the focusing on selected particles within microns of spatial resolutions. In this sense, individual grains, particles, or specific regions of a sample can be analyzed. However, some compounds such as clays (kaolinite, illite, etc.), which offer huge fluorescence in the acquired Raman spectra, are difficult to detect by this technique even being at high

concentration in the sample. In contrast, conventional XRD offers information about the mineralogical phases of whole bulk material and does not have this last limitation. Therefore, the application of Raman microscopy must be combined with other technique(s) not to lose information about the molecular composition. In this sense, the molecular methodology proposed in this work was based on Raman microscopy assisted by XRD. It was corroborated that it is a suitable combination for an in-depth identification of mineral phases of interest and could establish a possible local origin due to the presence of characteristic volcanic compounds.

In this case, it was possible to identify characteristic minerals from volcanic origin such as langite, anatase, and atacamite. To the authors' knowledge, this is the first time that these three compounds have been identified experimentally in red and yellow ochre pigments from Pompeii. In addition, the presence of jarosite, a mineral that can be formed under volcanic activity, was also identified. The presence of these compounds suggested the possibility of the local origin of the ochre pigments due to the volcanic material composition.

The impossibility of detecting these minerals of volcanic origin using XRD evidences that sometimes incomplete results can be offered using this technique. Moreover, Raman spectroscopy can also contribute to identify contaminations of pigments (Egyptian Blue and huntite) to the bowl where pigments mixtures were usually prepared. XRD was not able to reveal their presence probably because they are present in the sample in a concentration below 1%. In the case that they would be an intentionally addition by the artist to obtain different color hues, the composition would be much higher. Thus, we can effectively attribute its presence to a contamination problem. Therefore, this information also allows increasing the knowledge about the pictorial practices carried out by the artists in the ancient Pompeii.

The elemental characterization of the red and yellow ochre pigments was used to detect similarities/differences in the composition, useful to extract information regarding their origin. For that, the elemental information (normalized counts) acquired using a benchtop energy dispersive X-ray fluorescence spectrometer was subjected to Principal Component Analysis, classifying the samples in four groups. In this sense, it should be remarked the unexpected high signals of W, Sn and Sb obtained in one group, concretely the one of the red ochre pigments 117356 and 117357. The presence of W and Sn geochemical markers characteristic from Elba Island in both ochre pigments is such significant that proves that the hematite of these pigments was extracted from the iron ores of Elba Island. To confirm this provenance the samples were subjected to Pb isotopic ratio analysis. However, the results demonstrated that all the samples except red 117360 and yellow 112249 ochre pigments were contaminated by the leaching of Pb coming from the pipes of the ancient water system supply. For this reason, the provenance of the Elba Island could not be established by means of Pb isotopic analysis, since the original composition of these recovered pigments has been modified by contaminations from the lead pipes during the burial.

5.7 REFERENCES

1. Aliatis, I. *et al.* Pigments used in Roman wall paintings in the Vesuvian area. *J. Raman Spectrosc.* **41**, 1537–1542 (2010).

2. Giachi, G. *et al.* Raw Materials in Pompeian Paintings: Characterization of Some Colors from the Archaeological Site. *Mater. Manuf. Process.* **24**, 1015–1022 (2009).

3. Cottica, D. *et al*. *Pots with coloured powders from the Forum of Pompeii*. *Proceedings of the conference EMAC '07. 9th European Meeting on Ancient Ceramics. Budapest, Hungary* (2007).

4. Maguregui, M. *et al.* Multianalytical approach to explain the darkening process of hematite pigment in paintings from ancient Pompeii after accelerated weathering experiments. *Anal. Methods* **6**, 372–378 (2014).

5. Maguregui, M. *et al.* Thermodynamic and spectroscopic speciation to explain the blackening process of hematite formed by atmospheric SO_2 impact: the case of Marcus Lucretius House (Pompeii). *Anal. Chem.* **83**, 3319–3326 (2011).

6. Asscher, Y. *et al.* Combining multispectral images with X-ray fluorescence to quantify the distribution of pigments in the frigidarium of the Sarno Baths, Pompeii. *J. Cult. Herit.* (2019). DOI: 10.1016/j.culher.2019.04.014

7. Germinario, C. *et al.* Multi-analytical and non-invasive characterization of the polychromy of wall paintings at the Domus of Octavius Quartio in Pompeii. *Eur. Phys. J. Plus* **133**, 359-371 (2018).

8. Miriello, D. *et al.* Non-destructive multi-analytical approach to study the pigments of wall painting fragments reused in mortars from the archaeological site of Pompeii (Italy). *Minerals* **8**, 134-149 (2018).

9. Angelini, I. *et al.* The pigments of the frigidarium in the Sarno Baths, Pompeii: Identification, stratigraphy and weathering. *J. Cult. Herit.* (2019). DOI: 10.1016/j.culher.2019.04.021

10. Hradil, D. *et al.* Clay and iron oxide pigments in the history of painting. *Appl. Clay Sci.* **22**, 223–236 (2003).

11. Darchuk, L. *et al.* Composition of prehistoric rock-painting pigments from Egypt (Gilf Kébir area). *Spectrochim. Acta. A. Mol. Biomol. Spectrosc.* **83**, 34–38 (2011).

12. Popelka-Filcoff, R. S. *et al.* Trace element characterization of ochre from geological sources. *J. Radioanal. Nucl. Chem.* **272**, 17–27 (2007).

13. Jercher, M. *et al.* Rietveld X-ray diffraction and X-ray fluorescence analysis of Australian aboriginal ochres. *Archaeometry* **40**, 383–401 (1998).

14. Williams, T. J. A needle in the X-ray haystack: detection limits in powder X-ray diffraction of geologic materials. in *GSA Denver Annual Meeting* (2007).

15. Cruciani, G. *et al.* First Italian occurrence of cumengéite from Vesuvius: crystal-structure refinement and revision of the chemical formula. *Mineral. Mag.* **69**, 1037-1045 (2005).

16. Verhoogen, J. Distribution of titanium between silicates and oxides in igneous rocks. *Am. J. Sci.* **260**, 211–220 (1962).

17. Fulignati, P. *et al.* Formation of rock coatings induced by the acid fumarole plume of the passively degassing volcano of La Fossa (Vulcano Island, Italy). *J. Volcanol. Geotherm. Res.* **115**, 397–410 (2002).

18. Johnston, J. H. Jarosite and akaganéite from White Island volcano, New Zealand: an X-ray and Mössbauer study. *Geochim. Cosmochim. Acta* **41**, 539–544 (1977).

19. Bhattacharya, S. *et al.* Jarosite occurrence in the Deccan Volcanic Province of Kachchh, western India: Spectroscopic studies on a Martian analog locality. *J. Geophys. Res. Planets* **121**, 402–431 (2016).

20. Eastaugh, N. *et al.* Pigment compendium: a dictionary of historical pigments. (London, Routledge, 2007).

21. Tomasini, E. P. *et al.* Atacamite as a natural pigment in a South American colonial polychrome sculpture from the late XVI century. *J. Raman Spectrosc.* **44**, 637–642 (2013).

22. Frost, R. L. *et al.* Raman spectroscopy of the basic copper chloride minerals atacamite and paratacamite: implications for the study of copper, brass and bronze objects of archaeological significance. *J. Raman Spectrosc.* **33**, 801–806 (2002).

23. Jaksch, H. *et al.* Egyptian blue—cuprorivaite a window to ancient Egyptian technology. *Naturwissenschaften* **70**, 525–535 (1983).

24. Mazzocchin, G. A. *et al.* A short note on Egyptian blue. *J. Cult. Herit.* **5**, 129–133 (2004).

25. Riederer, J. Recently identified Egyptian pigments. *Archaeometry* **16**, 102–109 (1974).

26. Santacroce, R. *et al.* Age and whole rock–glass compositions of proximal pyroclastics from the major explosive eruptions of Somma-Vesuvius: A review as a tool for distal tephrostratigraphy. *J. Volcanol. Geotherm. Res.* **177**, 1–18 (2008).

27. Koutsospyros, A. *et al.* A review of tungsten: from environmental obscurity to scrutiny. *J. Hazard. Mater.* **136**, 1–19 (2006).

28. O'Neil, M. J. The Merck Index-An Encyclopedia of Chemicals, Drugs, and Biologicals. (Cambridge, RSC publishing, 2013).

29. Venteris, E. R. *et al.* Modeling spatial patterns in soil arsenic to estimate natural baseline concentrations. *J. Environ. Qual.* **43**, 936–946 (2014).

30. Filella, M. *et al.* Antimony in the environment: a review focused on natural waters: I. Occurrence. *Earth-Sci. Rev.* **57**, 125–176 (2002).

31. Benvenuti, M. *et al.* The tungsten and tin signature of iron ores from Elba Island (Italy): a tool for provenance studies of iron production in the Mediterranean region. *Archaeometry* **55**, 479–506 (2013).

32. Chiarantini, L. *et al.* Iron production in the Etruscan site of Populonia: new data. *Proceedings of the 2nd International Conference Archaeometallurgy in Europe, Grado, Italy* (2009).

33. Chiarantini, L. *et al.* Copper production at Baratti (Populonia, southern Tuscany) in the early Etruscan period (9th–8th centuries BC). *J. Archaeol. Sci.* **36**, 1626–1636 (2009).

34. Firmati, M. *et al.* L'impianto metallurgico tardorepubblicano di San Bennato all'Isola d'Elba. *AGWGH Atti Della Scuola Spec. Archeol. Univ. Pisa* **3**, 306–312 (2006).

35. Encinar, J. R. *et al.* A comparison between quadrupole, double focusing and multicollector ICP-MS instruments Part I. Evaluation of total combined uncertainty for lead isotope ratio measurements. *J. Anal. At. Spectrom.* **16**, 315–321 (2001).

36. Stos-Gale, Z. A. *et al.* Metal provenancing using isotopes and the Oxford archaeological lead isotope database (OXALID). *Archaeol. Anthropol. Sci.* **1**, 195–213 (2009).

37. Fulignati, P. *et al.* First insights on the metallogenic signature of magmatic fluids exsolved from the active magma chamber of Vesuvius (AD 79 "Pompei" eruption). *J. Volcanol. Geotherm. Res.* **200**, 223–233 (2011).

38. Bove, M. A. *et al.* Geochemical and isotopic study of soils and waters from an Italian contaminated site: Agro Aversano (Campania). *J. Geochem. Explor.* **109**, 38–50 (2011).

39. Scudder, S. J. *et al.* Soil science and archaeology. *Adv. Agron.* **57**, 2-76 (1996)

40. Duncan Keenan-Jones. Somma-Vesuvian Ground Movements and the Water Supply of Pompeii and the Bay of Naples. *Am. J. Archaeol.* **119**, 191-215 (2015).

41. Delile, H. *et al.* A lead isotope perspective on urban development in ancient Naples. *Proc. Natl. Acad. Sci.* **113**, 6148–6153 (2016).

42. Boni, M. *et al.* Lead isotopic evidence for a mixed provenance for Roman water pipes from Pompeii. *Archaeometry* **42**, 201–208 (2000).

6. CHEMICAL–MINERALOGICAL CHARACTERIZATION OF THE INORGANIC MORDANT USED TO MANUFACTURE POMPEIAN PINK LAKE PIGMENTS

6.1 Introduction

The application of an appropriate analytical methodology could offer key information not only to determine the nature of the materials used, but also about recipes or procedures used to create the colors. This knowledge could also assist the identification of trading routes of pigments[1–4]. In the previous chapters, different kind of inorganic pigments have been studied. These kinds of pigments are the most abundant ones in Pompeii. In some cases, the ancient Pompeian artists used the pink color to decorate specific details from a mural painting. Sometimes, this color was achieved mixing red and white inorganic pigments. However, this color can also be obtained using a pink lake pigment. Lake pigments are made by precipitating an organic dye upon a usually insoluble mordant or binder, which is an inorganic material such as a silicate or an aluminate[5]. In ancient times,

chalk, white clays, and crushed bones were used as mordants[5]. In the last case, for the manufacture of the lake pigments, Romans used to take the clays directly from the earth and dye them with an organic colorant (e.g., madder lake, Tyrian Purple, etc.) to obtain the desired color, as Pliny already described[6]. Apart from pink lake pigments, during the Roman period, purple shades were also obtained using this kind of pigments. These lake pigments were used in wall paintings, textiles, cosmetics, and ceramics, among others[7,8]. In the literature, many are the works dealing with the study of inorganic powder pigments used in the ancient wall paintings from the archeological site of Pompeii[9–14]. Nevertheless, few works can be found about the characterization of pink or purple lake pigments used in its ancient paintings[10,15]. Considering their high historical and artistic value, and due to this kind of pigments are not very usual, the application of non-invasive analytical methods is a necessity. However, in order to obtain a full characterization destructives techniques must be used in some cases.

In this chapter, an analytical methodology based on the combined use of elemental and molecular techniques was applied to perform an unequivocal characterization of the inorganic mordant used to manufacture Pompeian pink and purple lake pigments. For the elemental characterization, an in situ preliminary screening of the pigments in the MANN was conducted using a HH-EDXRF spectrometer. Further analyses in the laboratory were carried out by means of a benchtop EDXRF spectrometer and a SEM-EDS instrument. To determine the concentration of major, minor, and trace elements of the mordant in these lake pigments, ICP-MS analysis, preceded by an acid extraction of the powder lake pigments, was carried out. Apart from the concentrations, lead isotope ratio analysis of the samples was also conducted. Apart from that, X-ray diffraction (XRD) and Fourier Transform Infrared spectroscopy (FT-IR) in the Attenuated Total Reflectance (ATR) mode were also used in order to characterize the molecular composition of the inorganic mordant.

6.2 Samples and sampling strategy

For the characterization of the inorganic mordant, two pink lake pigments (reference numbers 117323 and 117342) and one purple lake pigment (reference number 117365), from the MANN collection were considered (see Fig. 6.1). For the in situ measurements, a mylar film was put on the pigments of each bowl and after that the HH-EDXRF sampling interface was placed on it for the spectral acquisition. After in situ measurements, some powders (around 100-200 mg depending on the sample) of each lake pigment were extracted to perform further analyses in the laboratory. To guarantee the representativeness of the samples, pigment powders were collected taking small quantities from the upper, middle, and lower parts of each bowl. All the samples were preserved in glass containers until their analysis.

Fig. 6.1 Lake pigments under study in their original bowls a) pink 117323 b) pink 117342 and c) purple 117365.

6.3 In situ HH–EDXRF analysis

In situ measurements of 117323 and 117342 pink lake pigments showed almost the same spectral information. In Fig. 6.2, a representative spectrum obtained from both lake pigments is shown, in which the same elements were identified except Zn that only was detected in pigment 117323.

Moreover, the relative intensities are not similar for both pigments, suggesting some differences in the mordant of these two pink lake pigments. Unfortunately, it was not possible to acquire in situ HH-EDXRF measurements of the 117365 purple lake pigment since this pigment was found in the inventory of the MANN after the in situ measurements session. The pigment sample was kindly provided later by the museum for its analysis in the laboratory.

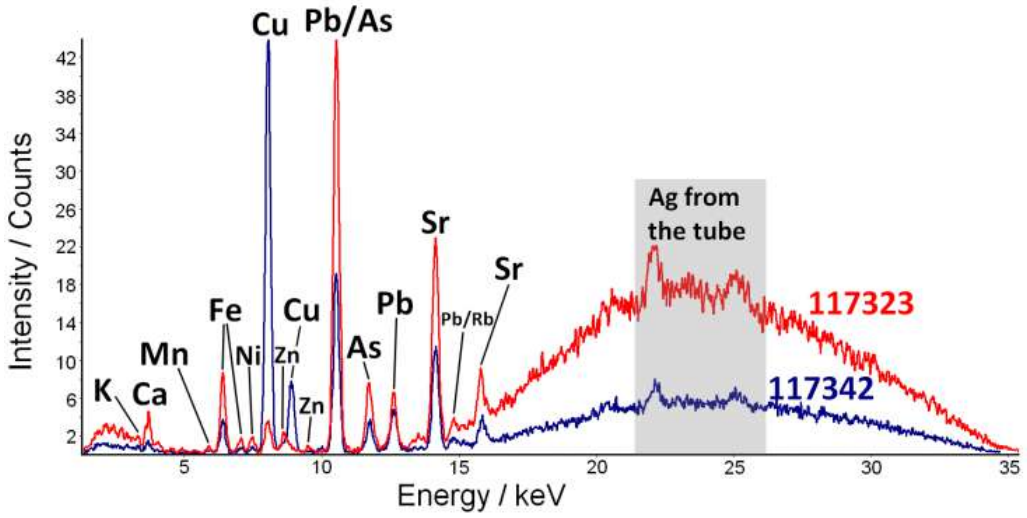

Fig. 6.2. XRF spectra of Pompeian pink lake pigments 117323 (in red) and 117342 (in blue) obtained by using the HH-EDXRF spectrometer at the MANN.

As shown in Fig. 6.2, the 117342 lake pigment provided a more intense signal of Cu than sample 117323. However, to determine possible differences between both mordants, the spectral information was carefully evaluated. To avoid possible matrix effects in the comparison of both mordants results that could led to erroneous interpretations, the obtained net counts of all the detected elements on each pink lake pigment were normalized against the Ag line coming from the source tube of the spectrometer (see Table 6.1).

Table 6.1. Normalized counts of each detected element on the Pompeian pink lake pigments 117323 and 117342.

Elements	117323	117342
K	0.05 ± 0.01	0.050 ± 0.009
Ca	0.23 ± 0.09	0.16 ± 0.05
Mn	0.041 ± 0.008	0.039 ± 0.007
Fe	0.6 ± 0.1	0.52 ± 0.09
Ni	0.13 ± 0.04	0.07 ± 0.01
Cu	0.3 ± 0.1	7.0 ± 1.0
Zn	0.14 ± 0.03	Non-detected
As	0.7 ± 0.1	0.6 ± 0.1
Pb	0.6 ± 0.1	0.8 ± 0.1
Sr	2.5 ± 0.3	2.1 ± 0.2
Rb	0.15 ± 0.05	0.2 ± 0.1

Taking into account the data shown in Table 6.1, it must be noted that the normalized counts of K, Ca, Mn, Fe, Ni, As, Pb, Sr, and Rb are quite similar for both lake pigments. However, the normalized counts for Cu are significantly higher in the pink lake pigment 117342, than in 117323, suggesting a considerably higher concentration of this element in this sample. On the contrary, Zn and Ni normalized counts are higher in the 117323 pigment. Nevertheless, these observations will be confirmed by further non-invasive (qualitative) and destructive (quantitative) analyses in the laboratory.

6.4 Microscopic observations of the lake pigments in the laboratory

Prior to the elemental and molecular analysis of the lake pigments, microscopic observations were conducted to observe the aesthetic appearance and morphology of the pigment grains. In Fig. 6.3, different microphotographs of the studied pigments are shown.

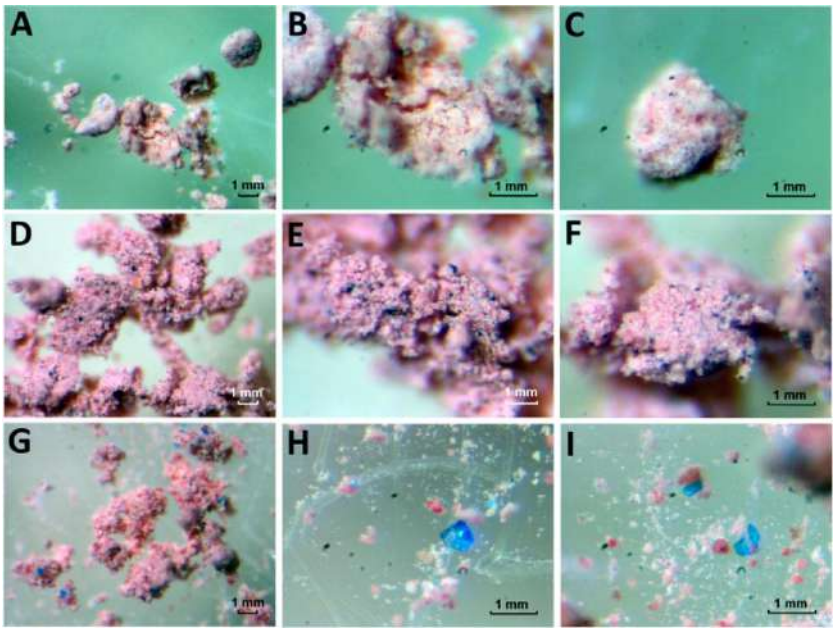

Fig 6.3. Microphotographs of the Pompeian pink lake pigment 117323 (A-C), 117342 (D-F) and the purple lake pigment 117365 (G-I).

The microscopic appearance of the two pink lake pigments is very similar. On the contrary, the purple lake pigment 117365 is made up of a mixture of pink and blue pigment grains (see Fig. 6.3 G–I). Therefore, a selective measurement of the two colored grains should be performed in the laboratory to determine their nature separately.

6.5 Laboratory non–invasive X–ray–based analytical techniques for the elemental characterization of the pink lake pigments

To confirm the elemental results obtained in situ, additional laboratory EDXRF analyses were performed. In this case, to obtain representative results, the measurements were performed at 1 mm lateral resolution achieved by a mechanical collimator.

In this case and considering that the benchtop EDXRF spectrometer incorporates a Rh-tube, the registered Compton (incoherent) scattering was used to avoid the matrix effect during the comparison of the results obtained for the lake pigments under study. The obtained results (counts normalized against Compton line) are shown in Table 6.2. Mn and Sr counts normalized against Compton are quite similar for both pink lake pigments, while Ca, Fe, Ni, and As normalized net counts are higher in sample 117323.

Table 6.2. Normalized counts for each element detected in Pompeian pink lake pigments 117323 and 117342, and the purple lake pigment 117365. (LOD: Limit of detection).

Elements	117323	117342	117365
Al	0.13 ± 0.01	0.162 ± 0.003	0.106 ± 0.002
Si	0.17 ± 0.01	0.21 ± 0.01	0.31 ± 0.01
P	0.0031 ± 0.0004	0.05 ± 0.07	ND
K	0.088 ± 0.003	0.06 ± 0.01	0.076 ± 0.003
Ca	0.82 ± 0.06	0.42 ± 0.04	0.58 ± 0.03
Ti	0.013 ± 0.003	0.007 ± 0.002	0.009 ± 0.001
Cr	0.002 ± 0.001	ND	0.002 ± 0.001
Mn	0.008 ± 0.004	0.006 ± 0.001	0.0225 ± 0.0002
Fe	0.40 ± 0.06	0.25 ± 0.02	0.51 ± 0.03
Ni	0.007 ± 0.001	0.003 ± 0.002	ND
Cu	0.05 ± 0.01	4.3 ± 2.1	10.6 ± 1.2
Zn	0.018 ± 0.003	ND	0.015 ± 0.004
As	0.45 ± 0.02	0.18 ± 0.04	0.11 ± 0.02
Pb	0.25 ± 0.03	1.6 ± 0.1	0.030 ± 0.006
Sr	0.066 ± 0.004	0.05 ± 0.01	0.021 ± 0.002

Comparing the normalized net counts of all the elements in the lake pigments, and taking into account the HH-EDXRF results acquired in the MANN, the values obtained in the laboratory shown in Table 6.2 confirm the conclusions extracted in situ, since most of the detected elements show similar normalized counts. Moreover, Ni and Zn (which again have not been detected in 117342 pigment) present higher normalized counts in pigment 17323, and Cu is present at higher levels in 117342, as they were detected in the in situ analyses. However, the highest normalized net counts value for Cu were recorded in the purple lake pigment 117365, which could suggest that the blue grains composing the

purple lake pigment could be related with the use of Egyptian Blue ($CaCuSi_4O_{10}$). Besides, the Fe value is higher in the purple lake pigment 117365 and the Pb one is considerably higher in the pink lake pigment 117342.

Unlike in the in situ measurements, in this case it was possible to identify additional heavy elements, such as Ti and Cr. Their normalized net counts values are more or less similar in all the lake pigments. However, in the pink lake pigment 117342, Cr was not detected due to both its absence or low concentration set under the limit of detection. The obtained similar values suggest that Ti and Cr can be original elements present in the inorganic binders used to create these pigments.

Through the EDXRF analysis in the laboratory, it was possible to obtain semi-quantitative values by means of Fundamental Parameters (FP) based method implemented in the instrument (not selective for lake pigments). The most remarkable results were, as in the case of the green, blue and yellow pigments presented in Chapter 4, the high concentrations of Pb determined in 117323 and 117365 lake pigments, 2495 and 3124 ppm respectively, while the Pb concentration of 117342 pigment was 340 ppm. In this case also the presence of compounds that contain Pb such as lead white - $(PbCO_3)_2{\cdot}Pb(OH)_2$ - were not detected. Thus, as in the case of the ochre pigments, the origin of this lead was also investigated.

Among elements with an atomic number lower than 13, Al, Si, and P were also detected. The presence of Al and Si could suggest that the inorganic binder used to manufacture this three Pompeian lake pigments could be an aluminosilicate. The ratio of normalized net counts of Si vs Al is coincident in the two pink lake pigments (Si/Al = 1.3) and it is higher for the purple lake pigment (Si/Al = 2.9).

In order to confirm a possible heterogeneity in the composition of the lake pigments at a microscopic scale and to identify the presence of lighter elements non-detectable by

EDXRF, SEM-EDS analyses were conducted. Taking into account that the EDS spectrometer performs elemental analyses at a microscopic scale, selective measurements were conducted on the blue and pink grains of the 117365 purple lake pigment. In Fig. 6.4, the average net areas of each element obtained from 10 repetitive measurements performed on each lake pigment are presented. The high standard deviations obtained are due to the heterogeneity at the microscopic level.

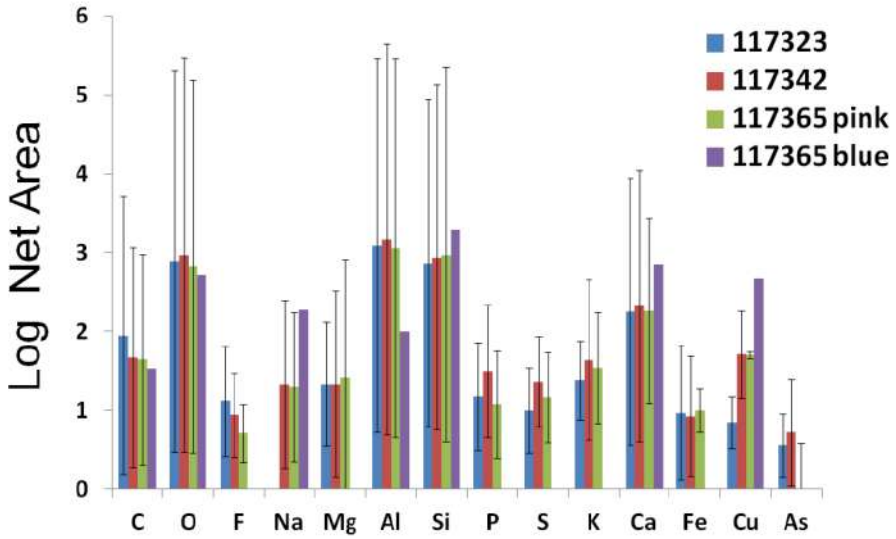

Fig. 6.4. Bar chart representing the net areas and standard deviations of each element detected on the Pompeian lake pigments by means of EDS.

As it can be observed, additional elements with an atomic number lower or equal than 12, such as C, O, F, Na, and Mg were detected with the EDS spectrometer. Taking into account that the ancient Roman town of Pompeii is located very close to the Bay of Naples and, therefore, near the sea, the presence of F, Na, and Mg could be attributed to the influence of the marine aerosol[16–19], since sea salt aerosol usually contains these elements. Moreover, in a work presented recently[20] it was determined that the pyroclastic deposits present in Pompeii are also rich in Na, F and Cl. Therefore, apart from the marine aerosol, an additional influence of the pyroclastic deposits covering the pigments or a possible volcanic origin of the used inorganic mordant cannot be discarded.

It is also remarkable that with the EDS measurements it was possible to detect the presence of S in all of the lake pigments, whereas Cl was only detected in some isolated replicate measurements of the pink lake pigment 117323. This observation comes to conclude that the influence of marine aerosol in this pigment is limited. The presence of S in the pigments could also be due to the influence of volcanic material deposition on the bowls containing the raw lake pigments. Cl was not detected in the laboratory by the EDXRF measurements due to the higher LOD related with the interference of the Rh L-lines from the anode of the X-ray tube in the Cl K-lines. In addition, the presence of Cl in the in situ EDXRF measurement was not possible to assess since the used spectrometer did not offer the possibility of changing the measuring conditions (voltage, current, etc.) in order to facilitate the detection of light elements such as Cl.

On the contrary, EDS analysis did not allow the detection of some heavier elements such as Pb, Ti, Cr, Mn, Ni, Zn, and Sr which, in contrast, were easily detected by means of EDXRF measurements. It is especially remarkable that, although Pb is widely present in the lake pigments, EDS was not able to detect its presence. In a previous work reported in the literature[12], EDS was not able either to detect the presence of heavier elements (including Pb) in Pompeian purple lake pigments. This observation led to conclude that EDXRF spectrometry is a better choice to propose the analysis of heavy metals in pigments.

As far as the purple lake pigment 117365 is concerned, the isolated EDS measurement of the blue crystals revealed a completely different composition showing the presence of C, O, Na, Al, Si, Ca, and Cu. The normalized areas of C, O, and Al K-lines are lower than in the pink lake pigments measurements. On the contrary, the ones of Si, Ca, and Cu K-lines are considerably higher in blue grains of 117365 than in the pink lake pigments. This result supports the hypothesis of the presence of the Egyptian Blue pigment and also the higher Si/Al ratio determined by laboratory EDXRF spectrometry.

6.6 Major, minor, and trace elements quantification by ICP–MS and Pb isotope ratio analysis

To obtain accurate quantitative values by EDXRF spectrometry an appropriate empirical calibration or FP-based method should be developed. Taking also into account that it was not possible to obtain representative standards to construct a calibration, the quantification of the elements present in the lake pigments was performed by ICP-MS. Prior to this analysis the samples were dried in an oven until constant weight and manually homogenized using an agate mortar to ensure the representativeness of the quantitative results. After that, an acid extraction of the three pigments was conducted. Considering the small amount of sample available, an isolated extraction of each lake pigment was carried out using 10 mg, mixing them with 10 mL of 10% HCl. This mixture was heated up to 60°C under continuous stirring and the resultant acid extracts were filtered, diluted and analyzed by the ICP-MS[7]. These acid extracts will allow not only to quantify the elements present in the pigments, but also to perform the lead isotope ratio analysis, necessary to determine the origin of this metal in the lake pigments. As shown in Table 6.3, Al, Si, and Ca are the major elements in the inorganic matrix from the lake pigments, as it was observed with the previously used non-invasive techniques.

The ICP-MS results agree with those obtained with both, the in situ and the laboratory EDXRF measurements, since K, Ca, Fe, Ni, Zn, and As concentrations are higher in the pink lake pigment 117323 than in the 117342. Moreover, the concentration of Fe quantified by ICP-MS agrees with the tendency observed by EDXRF (both in situ and laboratory) and EDS analyses, since it is higher in the pink lake pigment 117323 than in the purple lake pigment 117365. However, the net areas of K, Ca, and As were higher in the pink lake pigment 117342 than in the 117323. This observation suggests that special care must be taken to extract definitive and comparative conclusions using only the spectral information coming from EDS measurements.

Table 6.3. Concentration of major (% weight), minor, and trace elements (μg/g) on the inorganic binder of each lake pigment and %RSD (relative standard deviation) (n=3) obtained by means of ICP-MS.

Major elements (%weight)				
Elements	**117323**	**117342**	**117365**	**% RSD**
Al	14.0	16.9	5.6	5
Si	7.4	2.2	1.8	7
Ca	39.8	2.3	6.5	17
Na	5.0	0.4	1.2	6
Minor and trace elements (μg/g)				
Elements	**117323**	**117342**	**117365**	**% RSD**
Mg	16358	9193	2038	6
K	14172	5153	4000	6
Fe	7970	1556	2771	3
Zn	2528	304	854	10
As	1948	1411	97	11
Cu	1228	12937	7736	18
Pb	987	2083	1466	2
Sr	874	357	196	3
Mn	401	399	227	6
V	369	78	64	5
Ba	312	152	54	1
Ti	270	76	123	8
Cr	150	34	42	3
Hg	129	52	27	3
Ni	112	43	19	4
Sn	58	6	42	4
Li	34	4	5	1
Co	13	12	4	5
W	10	8	3	4
Ag	9	2	3	1
Cd	8	1	1	10
Sb	3	37	3	2
Tl	0.05	0.1	0.04	10

The concentration of metals such as Ba, Na, Mg, Li, Mo, Ag, Sn, Hg, Ti, Co, Cd, V, and Cr detected by means of ICP-MS, which were under the limit of quantification of the EDXRF and EDS techniques, is higher in the pink lake pigment 117323 than in the 117342 one. It is also confirmed by all the used techniques that among the pink lake pigments, the

sample 117342 presents the highest concentration of Cu and Pb. Regarding Cu, the pink lake pigment 117342 presents the highest concentration, followed by the purple lake pigment 117365. This seems to be apparently in contradiction to what it has been observed by means of EDXRF and EDS analyses. However, as the blue pigment grains (probably Egyptian Blue, $CaCuSi_4O_{10}$) of 117365 purple lake pigment cannot be dissolved using the applied acid extraction procedure, its contribution in the acid extracts was little or non-existent. The noticeable concentration of Cu in the pink lake pigments could be related to an intentional addition of this element. It is well referenced that since Roman times, copper salts (in form of oxides or sulfates) were added to the inorganic binder of lake pigments to obtain the desired final hue[21]. This variation in the original tonality takes place when the added copper (Cu^{2+}) forms a complex with the organic molecules (e.g., alizarin and purpurin when madder root dye is used) of the colorant used to dye the inorganic binder[22].

Thanks to ICP-MS, concentrations of Pb close to or higher than 1000 $\mu g \cdot g^{-1}$ were determined. This value cannot be attributed to a natural background of a clay or soil, which are the most plausible components used as an inorganic binder in these lake pigments. Thus, it could be assumed that the Pb present in these lake pigments could have an anthropogenic origin. To confirm this hypothesis, a Pb isotope ratio analysis was conducted. As it has been commented in the previous chapter, as far as we know, the $^{207}Pb/^{206}Pb$ ratio for the volcanic materials[23] is 0.8242; the one coming from the leaching of the in-depth soil from the Campania region[24] is 0.8425; and the one of the lead pipes from Pompeii[25] is 0.845.

On the other hand, this value is also very close or even the same to those determined for the Pompeian lake pigments under study: 0.8453 for 117323 and 117365, and 0.8382 for 117342 pink lake pigment. Therefore, the collapse of the water system promoted for decades or centuries an extraordinary Pb input in the soils from the Vesuvian area[26]. Taking into account that these pigments were in their bowls buried under the soil and the

Pb isotopic ratios match, it can be confirmed that the pink lake pigments under study, as the previously analyzed red and yellow ochres, were contaminated by the leaching of Pb coming from lead pipes.

6.7 Molecular analysis of the lake pigments in the laboratory

To determine the molecular composition of the inorganic matrix of the Pompeian pink and purple lake pigments, micro-Raman measurements were performed directly on all the samples using two portable spectrometers coupled to a microscope with a micro-camera that allows focusing the different grains. The first attempt at studying the lake pigments failed because of the strong fluorescence that occurred during the acquisition, especially when analyzing the pink lake pigments with the 532 nm laser. However, Raman measurements using this laser performed in isolated blue crystals present in the purple lake pigment 117365 allowed to obtain the typical bands of Egyptian Blue, at 200, 230, 358, 377, 431, 462, 571, 597, 762, 789, 992, 1012, and 1085 cm^{-1} (see Fig. 6.5). These Raman results were consistent with the previously obtained elemental results.

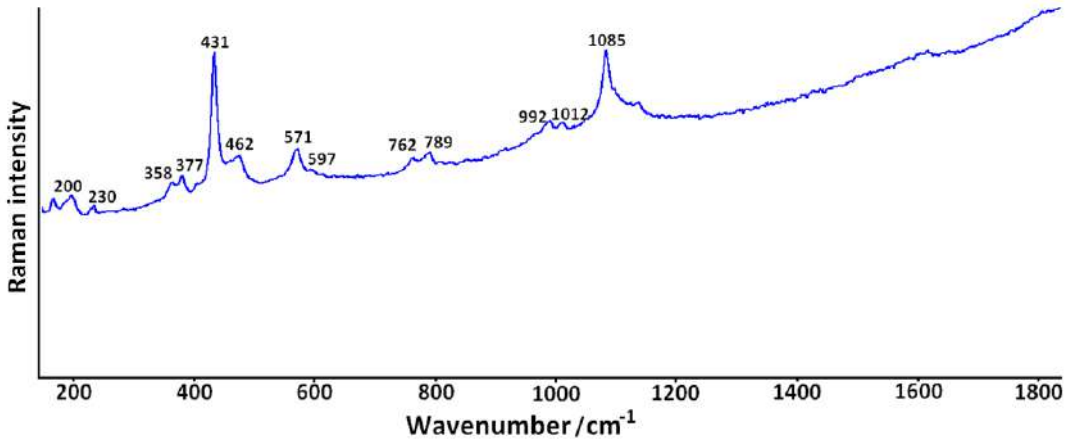

Fig. 6.5. Raman spectrum of blue grains present in sample 117365, attributed to Egyptian Blue pigment.

Since Raman spectroscopy did not give definitive information of the pink pigment grains due to the fluorescence, XRD measurements were also performed to identify the molecular composition of the mordant. The obtained diffractograms showed the typical pattern of an amorphous matrix (see Fig. 6.6). In the pink lake pigment 117323, the possible presence of kaolinite ($Al_2Si_2O_5(OH)_4$) was observed. On the other hand, in the purple lake pigment 117365 quartz and Egyptian Blue (cuprorivaite) were clearly detected (see Fig. 6.6C), confirming the Raman and elemental results.

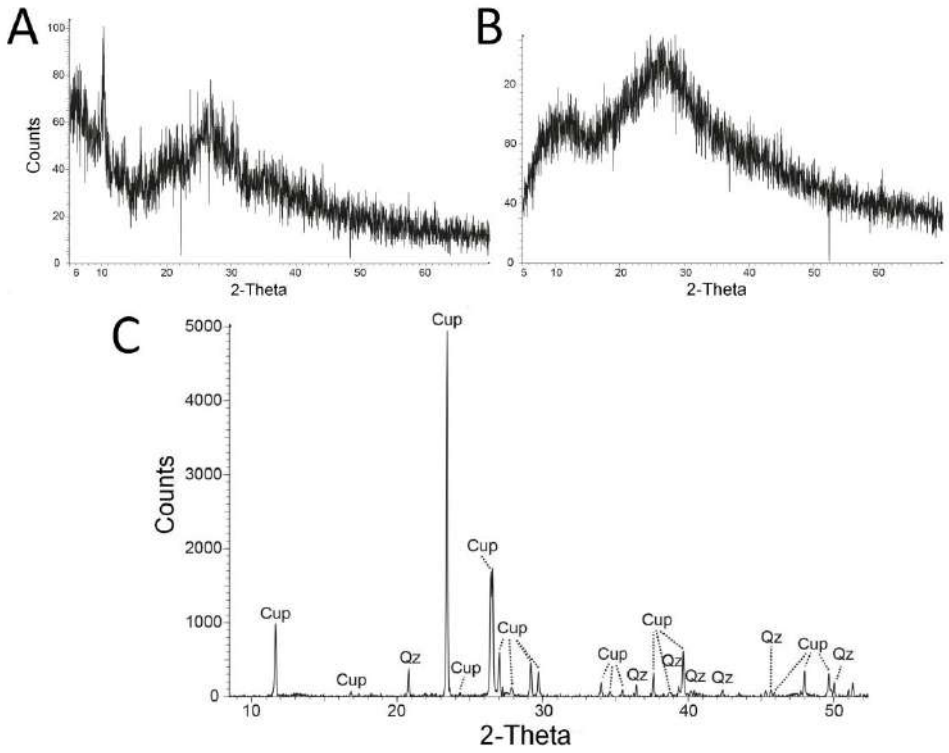

Fig. 6.6. Diffractograms of a) 117323, b) 117342 and c) 117365 pink lake pigments. (Cup: cuprorivaite; Qz: quartz).

To complete the molecular characterization of the inorganic matrix of the lake pigments under study, additional infrared analyses were also performed in the Attenuated Total Reflectance (ATR) mode. Fig. 6.7A shows a representative and repetitive infrared spectrum obtained in all the lake pigments. The infrared bands of the spectrum from the

pink lake pigments can be related with poorly crystalline aluminosilicate clays. This kind of mineral matrix usually provides a high fluorescence when analyzed with Raman spectroscopy. The broad band around 3360 cm^{-1} can be assigned to the stretching vibrations of hydroxyl groups and adsorbed H_2O. The bands of medium intensity (1633, 1576, and 1427 cm^{-1}) can be related to the H−O−H deformation vibrations of adsorbed H_2O. Particularly, the band centered at 1633 cm^{-1} could be associated with O−H deformation vibration of water in silicate clays[27]. The strong band at 998 cm^{-1} can be related with the Si−O−Si stretching vibrations.

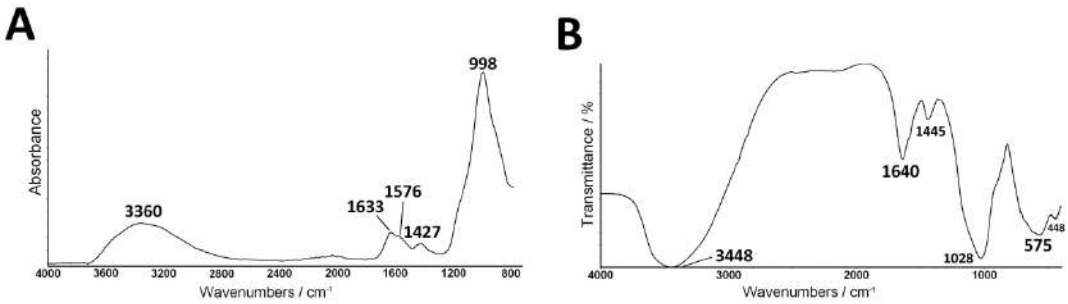

Fig. 6.7. A) ATR representative spectrum and B) FT-IR spectrum of the lake pigments under study.

Considering that with the ATR measurements information can be lost in the 750−400 cm^{-1} spectral range, additional analyses in FT-IR transmission mode of the lake pigments prepared as pellets were conducted (see Fig. 6.7B). The FT-IR spectrum obtained for both pink lake pigments is very similar to the one obtained using the ATR mode, although in the FT-IR spectrum additional infrared bands at 575 and 448 cm^{-1} can be observed. These bands are also related with amorphous to poorly crystalline aluminosilicate clay mineraloids. Indeed, the detected bands between 4000 and 750 cm^{-1} and the two additional bands at lower wavenumber can be related with allophane ($Al_2O_3{\cdot}(SiO_2)_{1.3-2}{\cdot}(2.5-3)H_2O$) or imogolite ($Al_2SiO_3(OH)_4$)[28]. Both clays can occur in soils formed from volcanic ash and they can be rapidly originated by weathering or hydrothermal alteration of volcanic materials under neutral to slightly acidic conditions.

Taking into account that the Pompeian soil has a clear volcanic origin, geological deposits of allophane and/or imogolite would have been potentially available to be used by the artists in this region. Thus, the hypothesis of a local origin for the inorganic binder used to elaborate the lake pigments must be considered.

The infrared bands at 575 and 1028 cm^{-1} in the FT-IR spectrum (998 cm^{-1} in ATR spectrum) can be used as markers to distinguish among these two mineral phases. Imogolite generally has sharper bands than those from allophane, and it also has characteristic doublets[29] of the bands around 575 and 1000 cm^{-1}. All the infrared spectra acquired in both pink lake pigments have broad bands without splitting; therefore, it can be suggested that the main amorphous to poorly crystalline aluminosilicate clay is the allophane.

The obtained FTIR spectrum for the 117365 purple lake pigment was slightly different with respect to the pink ones, especially in the spectral region of 1000–400 cm^{-1} (see Fig. 6.8). The results confirm the presence of Egyptian Blue, already identified by XRD and micro-Raman spectroscopy.

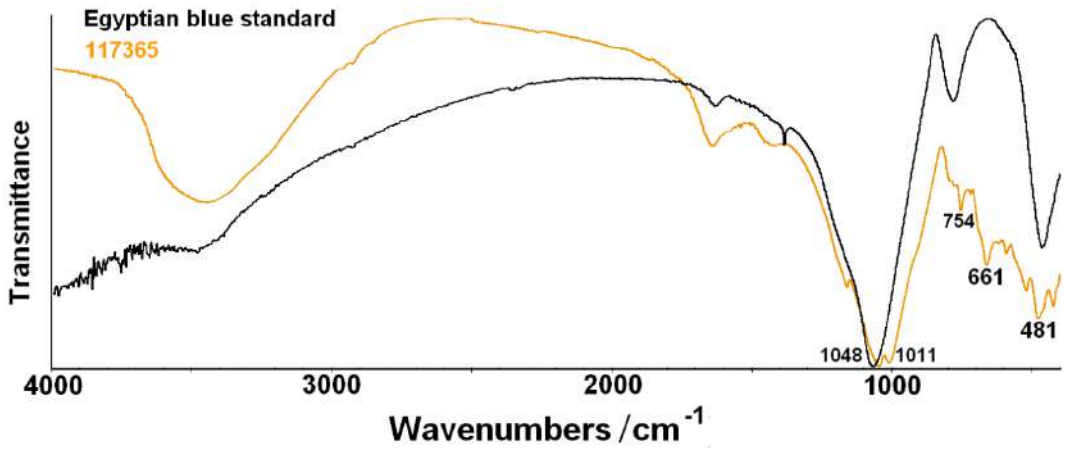

Fig. 6.8. FT-IR spectra of Egyptian Blue standard (black) and 117365 purple lake pigment (orange).

Apart from Egyptian Blue, in the FTIR spectrum of the purple lake pigment (see Fig. 6.8), infrared bands related with clays were also present (1011, 754, and 661 cm^{-1} bands). In this case it was not possible to identify the presence of the infrared band at 575 cm^{-1}, thus it was not possible to exactly determine the composition of the clay used as inorganic binder. Instead, infrared bands related with deformation vibrations of Al−O−Si bonds (754 and 661 cm^{-1}, among others), stretching of Al-O bond (593 cm^{-1})[30] and 520 cm^{-1} assigned to Si–O–Al (octahedral Al) bending vibrations[31] were identified, which only allowed to confirm that the inorganic fraction composing the lake pigment is indeed an aluminosilicate clay.

6.8 Conclusions

A multianalytical approach mainly based on the use of non-invasive spectroscopic techniques, but also on the additional use of a destructive technique such as ICP-MS, has been successfully applied to characterize the inorganic mordant used to manufacture two Pompeian pink (117323 and 117342) and one purple (117365) lake pigments recovered from the excavation of the archeological site of Pompeii and preserved in the Naples National Archaeological Museum (Italy).

The combination of elemental and molecular spectroscopic techniques has proved to be crucial for the proper characterization of the inorganic materials used to elaborate these lake pigments. It has been demonstrated that the results obtained from the handheld EDXRF spectrometer are comparable to those obtained with the benchtop EDXRF configuration. This issue could be of great importance when the possibility of extracting microsamples of archeological remains is not allowed.

SEM-EDS proved to be very useful for the determination of elements with an atomic number lower or equal than 12 such as F, Na, and Mg, although it failed on the detection of heavier elements such as Pb. In this sense, the supplementary use of laboratory EDXRF and ICP-MS elemental techniques, which offer a lower limit of detection for heavier elements, was very helpful.

The employment of the 785 nm laser for the micro-Raman analyses proved to be completely useless when analyzing both types of pigment due to the high fluorescence that masked the bands of any mineral present in the samples. Luckily, thanks to the use of the 532 nm laser, it was possible to distinguish some Raman bands related to Egyptian Blue in blue colored grains composing the purple lake pigment.

XRD and infrared spectroscopy in the ATR mode were very helpful to characterize the mineralogical phase composing the inorganic binder, although it is worth mentioning that the additional analyses in FT-IR mode allowed not only to identify the presence of allophone, but also to confirm the presence of Egyptian Blue in the purple lake pigment.

Regarding the chemical-mineralogical characterization of the inorganic binder used to manufacture the Pompeian pink and purple lake pigments, considering the obtained experimental evidences, it was possible to affirm that an amorphous to poorly crystalline aluminosilicate clay mineraloid was employed.

The presence of F, Na, and Mg could be attributed to the influence of the marine aerosol, although it could also be originated from the volcanic nature of the inorganic binder used in the elaboration of the lake pigments or be part of the sediments covering the raw lake pigments bowls.

It is also noteworthy the unexpected significant presence of Pb in the three lake pigments. The concentration of this element, clearly exceeding the proportions of the trace level, is likely to be related with an anthropogenic origin rather than to a natural

one. After the isotopic ratio analysis of this element, it has been confirmed that the presence of this metal in the pigments can be related to the leaching of the Pompeian ancient lead pipes, contaminating in this way the local soil, whose clays were used to manufacture the lake pigments. This hypothesis is supported by the fact that some amorphous to poorly crystalline aluminosilicates from volcanic soils have a great capacity to absorb metals such as Cu, Zn, Ni, Cd, and Pb[32]. In this sense, taking into account that the bowls containing the three lake pigments under study were buried during more or less 2000 years, the continuous leaching of Pb to the surrounding soils could also contribute to increase this metal concentration in the pigments. As it has been explained before, this is not an isolated casuistry, since the Pb identified in the Pompeian red and yellow ochre pigments can be related also to the leaching of the Pb coming from the pipes of the ancient water system of Pompeii. In the pink lake pigments, the high concentration of Cu can be associated with an intentionally addition of copper salts by manufacturers or with the absorption of this metal by local soil rich in allophane/imogolite.

6.9 REFERENCES

1. d'Errico, F. *et al.* Early evidence of San material culture represented by organic artifacts from Border Cave, South Africa. *Proc. Natl. Acad. Sci.* **109**, 13214–13219 (2012).

2. Dik, J. *et al.* Early production recipes for lead antimonate yellow in Italian art. *Archaeometry* **47**, 593–607 (2005).

3. Sandalinas, C. *et al.* Experimental confirmation by Raman spectroscopy of a Pb-Sn-Sb triple oxide yellow pigment in sixteenth-century Italian pottery. *J. Raman Spectrosc.* **37**, 1146–1153 (2006).

4. Kirby, J. *et al.* The technology of red lake pigment manufacture: study of the dyestuff substrate. *Natl. Gallery Tech. Bull.* **26**, 71–87 (2005).

5. Forbes, R. J. Studies in Ancient Technology Vol V. (Leiden, Brill Archive, 1956).

6. Murphy, T. M. Pliny the Elder's Natural History: The Empire in the Encyclopedia. (Massachusetts, Courier Corporation, 2004).

7. Bruni, S. *et al.* Surface-enhanced Raman spectroscopy (SERS) on silver colloids for the identification of ancient textile dyes: Tyrian purple and madder. *J. Raman Spectrosc.* **41**, 175–180 (2010).

8. Aceto, M. *et al.* Non-invasive investigation on a VI century purple codex from Brescia, Italy. *Spectrochim. Acta. A. Mol. Biomol. Spectrosc.* **117**, 34–41 (2014).

9. Canevali, C. *et al.* A multi-analytical approach for the characterization of powders from the Pompeii archaeological site. *Anal. Bioanal. Chem.* **401**, 1801-1814 (2011).

10. Augusti, S. I Colori Pompeiani (Rome, De Luca, 1967).

11. Aliatis, I. *et al.* Green pigments of the Pompeian artists' palette. *Spectrochim. Acta. A. Mol. Biomol. Spectrosc.* **73**, 532–538 (2009).

12. Aliatis, I. *et al.* Pigments used in Roman wall paintings in the Vesuvian area. *J. Raman Spectrosc.* **41**, 1537–1542 (2010).

13. Cottica, D. *et al.* Pots with coloured powders from the Forum of Pompeii. *Proceedings of the conference EMAC '07. 9th European Meeting on Ancient Ceramics. Budapest, Hungary* (2007).

14. Giachi, G. *et al.* Raw Materials in Pompeian Paintings: Characterization of Some Colors from the Archaeological Site. *Mater. Manuf. Process.* **24**, 1015–1022 (2009).

15. Clarke, M. et al. Pompeii purpurissum pigment problems. *Proceedings of Art'05–8th International Conference on "Non Destructive Investigations and Microanalysis for the Diagnostics and Conservation of the Cultural and Environmental Heritage", Lecce, Italy* (2005).

16. Morillas, H., et al. Characterisation and diagnosis of the conservation state of cementitious materials exposed to the open air in XIX century lighthouses located on the coast of the Basque Country: 'The case of Igueldo lighthouse, San Sebastian, North of Spain'. *J. Raman Spectrosc.* **43**, 1630–1636 (2012).

17. Morillas, H. *et al.* Could marine aerosol contribute to deteriorate building materials from interior areas of lighthouses? An answer from the analytical chemistry point of view. *J. Raman Spectrosc.* **44**, 1700–1710 (2013).

18. Morillas, H., *et al.* Study of particulate matter from primary/secondary marine aerosol and anthropogenic sources collected by a self-made passive sampler for the evaluation of the dry deposition impact on built heritage. *Sci. Total Environ.* **550**, 285–296 (2016).

19. Morillas, H. *et al.* The role of marine aerosol in the formation of (double) sulfate/nitrate salts in plasters. *Microchem. J.* **123**, 148–157 (2015).

20. Pérez-Diez, S. *et al.* Identification of halides in volcanic deposits adhered to Pompeian wall paintings using portable LIBS and evaluation of their leaching to the wall. *TECHNART 2019: the European conference on the use of Analytical methods for Characterization of Works of Art, Bruges, Belgium* (2019).

21. Davy, H. VIII. Some experiments and observations on the colours used in painting by the ancients. *Philos. Trans. R. Soc. Lond.* **105**, 97–124 (1815).

22. Bechtold, T. *et al.* Handbook of natural colorants. (New Jersey, John Wiley & Sons, 2009).

23. Fulignati, P. *et al.* First insights on the metallogenic signature of magmatic fluids exsolved from the active magma chamber of Vesuvius (AD 79 "Pompei" eruption). *J. Volcanol. Geotherm. Res.* **200**, 223–233 (2011).

24. Bove, M. A. *et al.* Geochemical and isotopic study of soils and waters from an Italian contaminated site: Agro Aversano (Campania). *J. Geochem. Explor.* **109**, 38–50 (2011).

25. Boni, M. *et al.* Lead isotopic evidence for a mixed provenance for Roman water pipes from Pompeii. *Archaeometry* **42**, 201–208 (2000).

26. Delile, H. *et al.* A lead isotope perspective on urban development in ancient Naples. *Proc. Natl. Acad. Sci.* **113**, 6148–6153 (2016).

27. Kitagawa, Y. The infrared absorption band of allophane near 1,650 cm-1. *Soil Sci. Plant Nutr.* **20**, 195–196 (1974).

28. Parfitt, R. L. *et al.* Comparison of an oxalate-extraction methon and an infrared spectroscopic method for determining allophane in soll clays. *Soil Sci. Plant Nutr.* **28**, 183–190 (1982).

29. Gustafsson, J. P. *et al.* Allophane and imogolite in Swedish soils. (Stockholm, Royal Institute of Technology, 1998).

30. Senthilkumar, S. *et al.* Synthesis, Characterization and Electrical properties of Nano Metal and Metal-oxide Doped with Conducting Polymer Composites by in-Situ Chemical Polymerization. *MOJ Poly. Sci.* **1**, 31-35 (2017).

31. Madejova, J. FTIR techniques in clay mineral studies. *Vib. Spectrosc.* **31**, 1–10 (2003).

32. Parelho, C. *et al.* Linking trace metals and agricultural land use in volcanic soils—A multivariate approach. *Sci. Total Environ.* **496**, 241–247 (2014).

7. OPTIMIZATION OF A SERS–BASED METHODOLOGY TO IDENTIFY THE ORGANIC COLORANTS USED IN POMPEIAN PINK AND PURPLE LAKE PIGMENTS

7.1 Introduction

The use of pigments or dyes to give color to artworks, textiles or cosmetics is well known since the prehistory[1]. A large amount of colors were used for this purpose: red, pink, blue, yellow, etc[1]. The term dye is applied to any substance used for tinting and most of them are of organic origin. The first used dyes were juice of fruits and berries, extracts of crushed flowers or roots of small plants[2].

In this sense, and as it has been described in Chapter 6, the direct Raman analysis of pink and purple lake pigments did not offer conclusive information about the dye (organic colorant) responsible to give the pinkish color. The identified clayey mordant promoted a great fluorescence, and this matrix effect could easily mask the Raman bands of the

organic dyes present in the pigments[3]. In addition to the latter, organic dyes in lake pigments are present in very low concentrations. Therefore, their Raman bands, obtained after a direct Raman measurement, would be very weak, like it was found observed with the 785 nm excitation laser, or even completely masked by the fluorescence phenomenon, like the one found when applying the 532 nm excitation wavelength.

Different variations to Raman spectroscopy could avoid fluorescence phenomenon or improve the detection of weak Raman bands. For the first case, Shifted Excitation Raman Difference Spectroscopy (SERDS) can be mentioned. In a previous work[4] madder lake was identified by means of a methodology based on this technique. Apart from that, Surface Enhanced Raman Spectroscopy (SERS) is a technique that extends the detection limits of direct Raman spectroscopy to dilute samples and trace analysis, with enhancement factors up to 10^{15} over traditional Raman techniques[5]. This SERS enhancement is produced due to the presence of a rough surface of metal nanoparticles, which provides complex electromagnetic modes. The higher enhancements are produced in the cavities between metal nanoparticles of this rough surface[6]. This is a very complex physical process which involves resonance of localized surface plasmons. In essence, due to the nature of metals, the atoms can be considered as positive charged points inside a “soup” of electrons. When these mobile electrons are perturbed of their equilibrium position and vibrate with a certain frequency, plasmons are produced. To promote this phenomenon, the particle must be smaller than the wavelength of the incident light[7]. The electric field of the incident light induces an electric dipole in the particle displacing the dislocated mobile electrons far away from the metal particle, generating a negative charge in this part of the particle, and thus the dipole. As these electrons are displacing, plasmons are formed[8]. Surface plasmons are surface electromagnetic waves that are propagated in a direction parallel to the metal interface (see Fig. 7.1). Since the wave is on the boundary of the metal and the external medium (air or water for example), these oscillations are very sensitive to any change of this boundary, such as the adsorption of molecules to the metal surface[9].

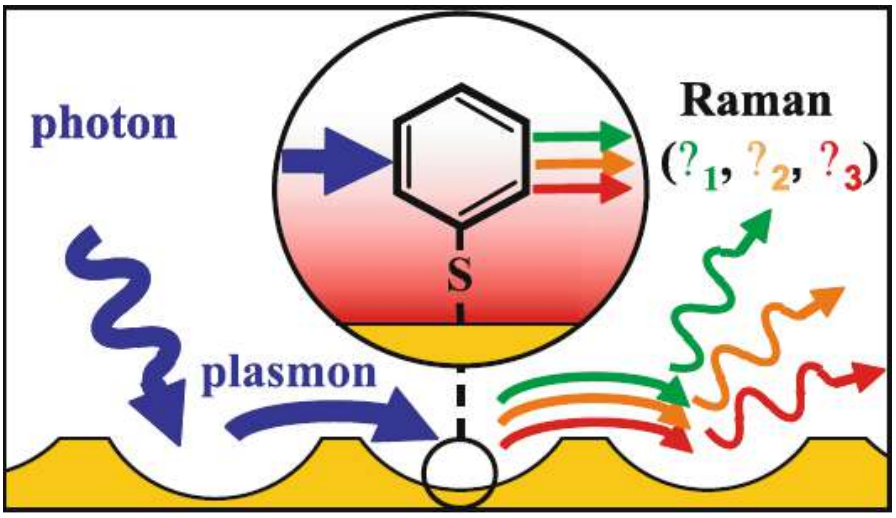

Fig. 7.1. General scheme of the SERS process[10].

When SERS is used, the non-invasive feature of the direct Raman analysis unfortunately disappears since metallic nanoparticles are added to the material or sample under study. Another alternative can be to deposit the sample in a metallic surface made up of nanoparticles.

SERS has been used with very good results in the analysis of lake pigments[11–14]. For this reason, SERS was selected for the characterization of the dye or dyes used to give pink color to the Pompeian lake pigments under study.

The most common nanoparticles used for SERS analysis are silver nanoparticles (Ag-NP). The synthesis of Ag-NPs can be performed by following different recipes that lead to a colloid solution of nanoparticles. In this sense, the most usual methods of synthesis are the so-called Lee-Meisel[15] and Creighton[16], which both consist in the reduction of silver nitrate ($AgNO_3$) using trisodium citrate dihydratate ($Na_3C_6H_5O_7{\cdot}2H_2O$) and sodium borohydride ($NaBH_4$) as reducing agents respectively. Apart from the traditional recipes, Leona *et al.*[17] obtained excellent results by reducing silver sulfate with glucose in the presence of sodium citrate using a high power microwave digestion system. As observed

in that work, the use of microwave radiation can alleviate heat transfer and reagents mixing problems, as the solution is heated at a fast rate without temperature gradients.

In addition to the synthesis of colloids, Ag-NPs can also be synthesized by a photoreduction induced by laser irradiation on a water/solid interface where the aqueous phase contains the Ag^+ cation and the solid surface is of hydrophilic nature (glass and cellulose). The so-prepared Ag-NP demonstrated a high SERS effectiveness in the detection of dispersed adsorbates such as the case of the anthraquinonic dye alizarin[18].

Once the Ag-NP colloid is prepared, some drops of it can be added directly to the sample (fiber, lake pigment…). If the fluorescence given by the mordant still does not allow the identification of the colorant, a sample treatment must be done in order to isolate the organic dye from the inorganic matrix. Sample treatments described in the literature[19,20] for later SERS analysis consist on acid hydrolysis of the lake pigment for the mordant dissolution. In the case of lake pigments, the organic dye can form a chelate with the metal ion of the mordant, forming a very stable complex. Thus, colored lakes formed by the metal ions and the dye molecules resist extraction using water and organic solvents. An acid extraction could be able to replace the metal ion for hydrogen ions, releasing in that way the metal ion from the complex. Single dye molecules should then be free to go into solution[21]. Once the dye is free, an organic extraction using an adequate solvent should be performed to isolate the organic molecule from the inorganic liquid phase. Finally a very small volume of the organic extract with the organic dye is usually evaporated using N_2 stream and the organic residue is re-dissolved in methanol[19,20]. This acid hydrolysis has been applied in textile fibers with the purpose of identifying the organic colorant, concretely Tyrian purple and madder lake[20].

In addition to the acid hydrolysis, it is possible to use HF vapors in a closed chamber to perform a non-extractive hydrolysis of the organic colorant. This method involves a dry reaction capable of breaking down the dye – mordant complex without removing the dye

from the fiber or pigment sample, followed by direct treatment of the sample with Ag colloid. This procedure has been successfully applied in the identification of the dye present in textile fibers from the Department of Textile Conservation at the Metropolitan Museum of Art[22].

Although the reported sample treatments work properly to isolate the organic dye from the mordant, there are no references to both, the sample mass used and the minimum or optimum amount to perform the complete procedure and to achieve the appropriate characterization of the dyes by means of SERS. In the field of archaeological pigments analysis, this is a very important parameter to study and optimize since these types of samples have a high value due to their low availability. Therefore, it is of great interest to develop analytical methodologies that employ the lowest consumption of sample.

Another important parameter to be optimized is the organic solvent used for the extraction. Hexane is well referenced that extracts organic dyes such as anthraquinonic molecules[19,20], but there are not studies that compare the effectiveness of different organic solvents. Due to the very low concentration of organic dyes in solution, it is very important to use the most appropriate solvent in order to obtain an effective organic extraction and not lose analyte in the procedure. Apart from that, the volume of the solvent used for the extraction is another important factor to optimize. Moreover, conditions of analysis (e.g. wavelength of the excitation laser) are also very important to achieve the best spectral results.

In this chapter the optimization of different parameters related with the sample treatment and measurement conditions of the previously mentioned Pompeian pink and purple lake pigments is presented with the aim of identifying the organic colorant responsible to give the pink shade to the mentioned lake pigments. Thereby, the parameters that led to the best spectral results using SERS must be established. For that purpose, Ag-NPs can be synthesized and characterized by Transmission Electron

Microscopy (TEM), and Raman and UV-Visible spectroscopies. Different sample masses, organic solvents and volumes must be tested in order to identify the best and optimum parameters for the sample treatment. Besides, analysis conditions (composition of the microscopic slide used for the deposition of the extract with Ag-NPs and wavelength of the excitation laser) must also be compared with the purpose to assess which parameters offer the best quality SERS spectra. Finally, the SERS results could be confirmed by UV-Visible spectroscopy.

All the SERS analyses carried out in this PhD Thesis were performed with portable Raman spectrometers. In this sense, the usefulness of portable spectrometers can also be assessed as a cheaper alternative to the benchtop confocal Raman microscopes, usually employed in published SERS determinations of dyes.

7.2 Samples and reagents

The pink and purple lake pigments analyzed in this chapter are those that were analyzed in Chapter 6, that is, 117323 and 117342 pink lake pigments and 117365 purple lake pigment from the MANN. The acid extracts coming from the sample prepared in Chapter 6, containing the organic colorant, were used in this case.

7.3 Evaluation of the synthesized silver nanoparticles (Ag–NPs) suitability for the SERS analysis and selection of the best analytical conditions

The synthesis of the Ag-NPs was performed using trisodium citrate dihydrate as reducing agent following the recipe proposed by Lee-Meisel[15]. The synthesized silver colloid was characterized by UV-Visible spectroscopy in the wavelength range from 200 to 750 nm (see Fig. 7.2), obtaining the maximum of absorbance at 414 nm. As some authors point out, the wavelength of the absorbance maximum in the UV-Visible range of silver colloids is usually set around 390-420 nm[23], thus the synthesized colloid fits with this condition.

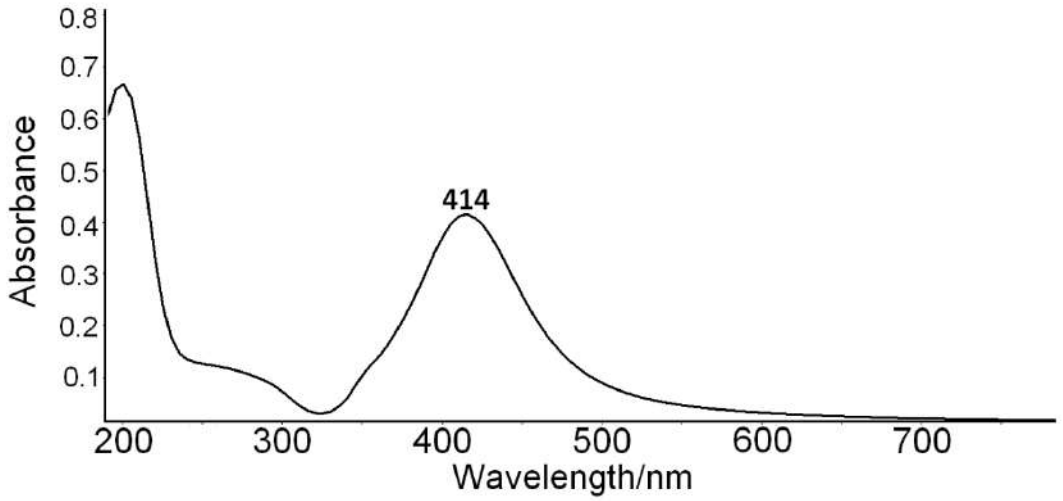

Fig. 7.2. UV-Vis spectrum of the synthesized Ag nanoparticles.

To confirm the preliminary observation obtained using the UV-Visible measurement about the size and distribution of the synthesized NPs, different evaporated drops of the colloid were observed under the transmission electron microscope (TEM). In Fig. 7.3 the Ag-NPs coming from the synthesized Lee-Meisel colloid can be observed.

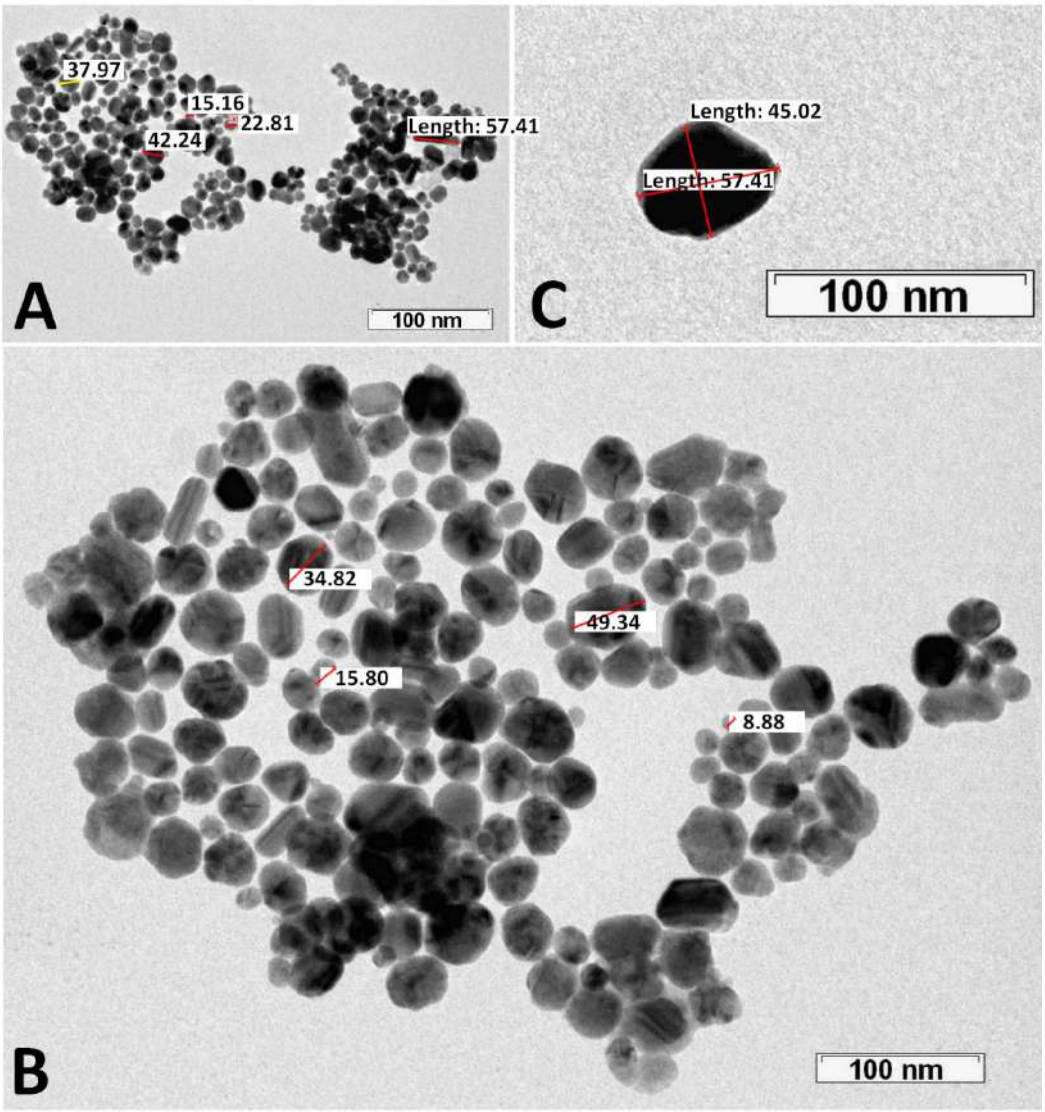

Fig. 7.3. TEM images of the synthesized Ag-NP with their respective diameter in nm.

The shape of most of the synthesized Ag-NPs was spherical and their diameters range from 8 to 60 nm. The diameter of most of the NPs was set between 20-50 nm (Fig. 7.3B). According to different authors, the typical size of the Ag-NPs synthesized following the Lee-Meisel method is around 3-50 nm,[24] and some authors point out that the optimal size of Ag-NPs for SERS is around 50 nm,[25] therefore, the Ag-NPs synthesized in this work fulfill

these requirements. The acquired TEM images show that the aggregation of the synthesized Ag-NPs ensures the active spots for their use in the SERS measurements. Therefore, it was decided not to mix the silver colloid with inorganic salts (KNO_3, NaCl, KCl, etc.) in order to promote their aggregation[26].

Apart from UV-Vis spectra, the Raman spectral feature of the Ag-NPs was also evaluated. In this case, and also to acquire the SERS spectra of the lake pigments, quartz slides instead of more common glass slides were selected, because quartz offers a lower Raman background than the common glass (Fig. 7.4).

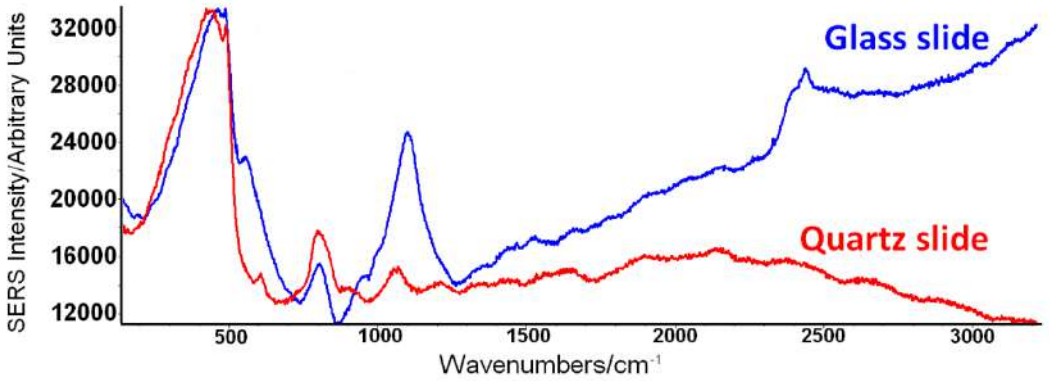

Fig. 7.4. Raman spectra of the quartz and glass slides.

The Raman spectra of the Ag-NPs acquired using the 532 nm excitation wavelength of the colloid shows the typical bands of Ag-NPs at 148 and 237 cm^{-1} and its overtone at 2950 cm^{-1} (Fig. 7.5). Moreover, the use of 532 nm laser to promote the Raman scattering provides a lower background and higher signals than using the 785 nm laser as shown in Fig. 7.5. This observation could suggest that the SERS spectral feature of the dyes on the lake pigments could be improved using the 532 nm laser.

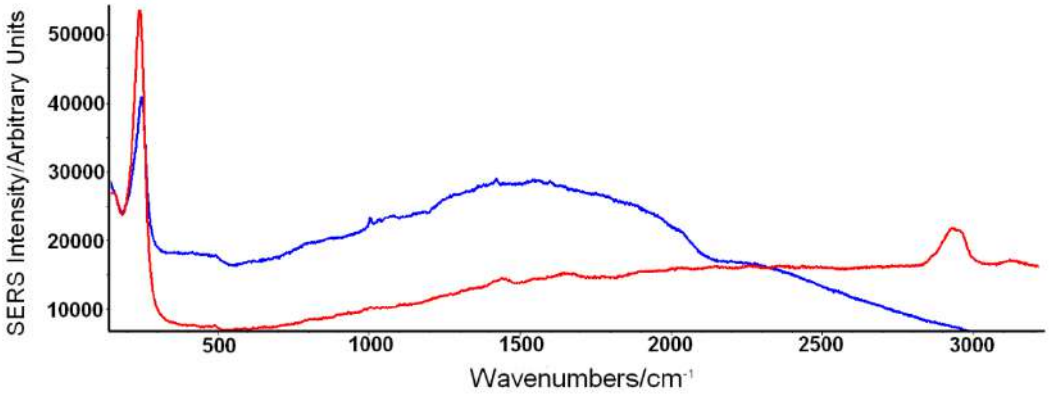

Fig. 7.5. Raman spectra of synthesized Ag-NP acquired using 532 nm (red) and 785 nm (blue) lasers.

7.4. Sample treatment optimization

Prior to perform the extraction of the dye in the lake pigments and the subsequent SERS analysis, it was decided to test if the Raman spectra of the lake pigments under study can be improved by mixing the Ag-NPs and few micrograms of the lake pigments. In this case, the acquired SERS spectra were quite similar to the direct Raman spectra of the lake pigment powder (Fig.7.6), being impossible to detect any Raman signal.

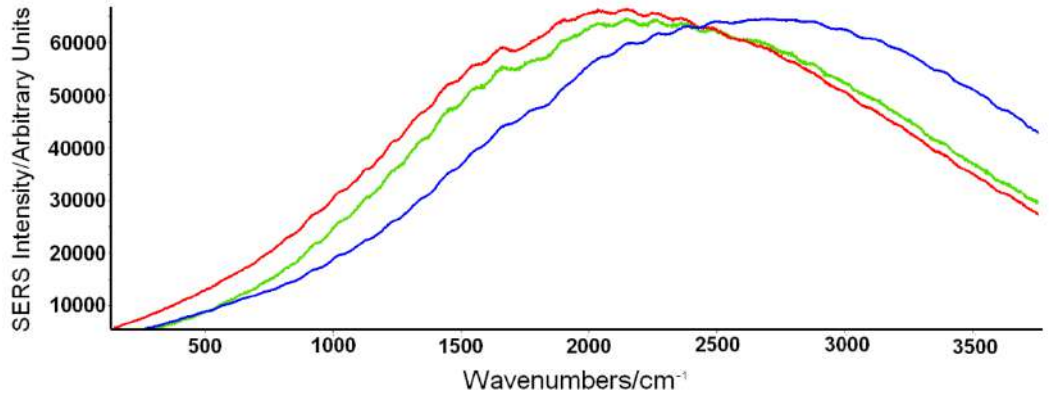

Fig. 7.6. SERS spectra of 117323 (red) 117342 (blue) and 117365 (green) pink and purple lake pigments mixed with Ag-NPs obtained using 532 nm laser.

Considering that it was not possible to detect SERS bands (see Fig. 7.6), it was decided to perform the extraction of the organic colorant using the mentioned acid extracts of the lake pigments. For that, the effectiveness of different organic solvents, the mass required to obtain an assignable spectrum and the selection of the best appropriate laser excitation wavelength were optimized to obtain the best SERS results.

In any case, after the liquid extraction, the solution was evaporated and the organic colorant residue was re-dissolved in 100 μl of methanol-Ag-NP colloid solution (70:30)[19,20]. A drop of this solution containing the Ag-NP and the extracted dye was placed in a quartz slide. This drop was evaporated using an infrared lamp. Finally, the residue of the dye and Ag-NP was observed under a portable video-microscope coupled to the portable Raman spectrometer (see the microscopic appearance of the aggregate Ag-NPs under the 50x objective lens in the Fig. 7.7A).

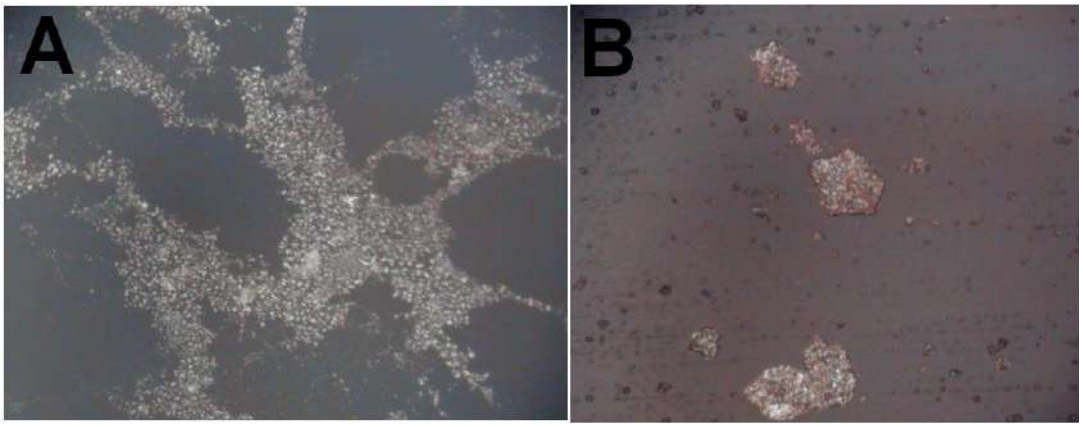

Fig. 7.7. a) Ag-NP and b) Ag-NP + organic colorant adsorbed into it after the sample pretreatment, observed under 50x lens.

To achieve the desired SERS effect, the molecules from the organic dye have to be adsorbed on the metallic surface of the Ag-NPs. As can be seen in Fig. 7.7 B, in some areas of the Ag-NPs pinkish particles can be observed. To ensure that organic molecules are adsorbed in the Ag-NPs metallic surface, additional observations under the TEM were

conducted. In the Fig. 7.8A-D, several micro-photographs showing the adsorption of the organic extract on the Ag-NPs can be observed. These microscopic observations suggest that thanks to this sample preparation, the desired SERS effect will be achieved.

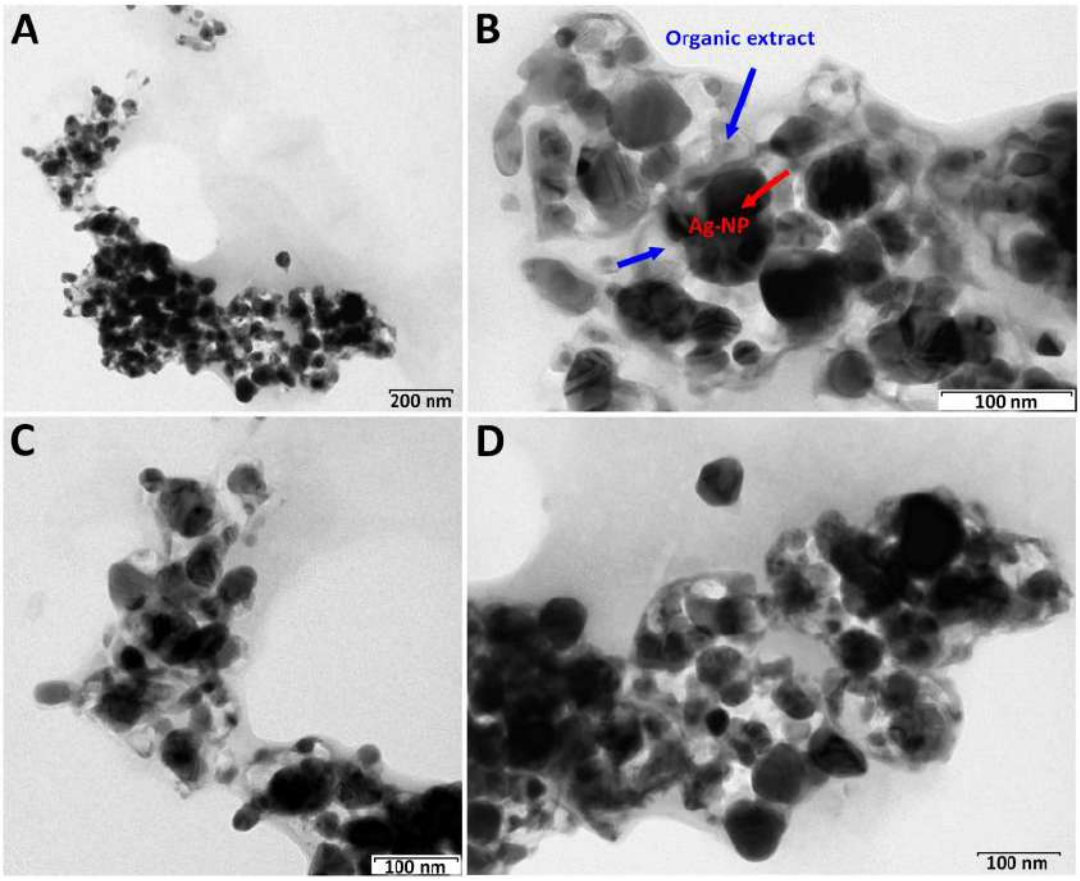

Fig. 7.8. Different magnifications of aggregated Ag-NPs under the TEM showing the organic extract adsorbed on the metallic surface.

7.4.1 Study of the effectiveness of the organic solvents

According to previous works[19,20], ethyl acetate and hexane were tested as potential organic solvents for the extraction of the dye after the acid hydrolysis of the pigments. For that purpose, 5 mg of the sample 117342 were dissolved with the acid (10 mL of 10%) and extracted using 2 mL of each solvent. The final color that the dye gives to the organic solution was compared. At first sight, the extract obtained using ethyl acetate has a more intense color than the one of hexane (see Fig.7.9). This could suggest that ethyl acetate is able to extract more effectively the organic dye. Moreover, as shown in Fig. 7.9 the UV-Vis spectra of both extracts showed that using ethyl acetate more intense bands are achieved than using hexane.

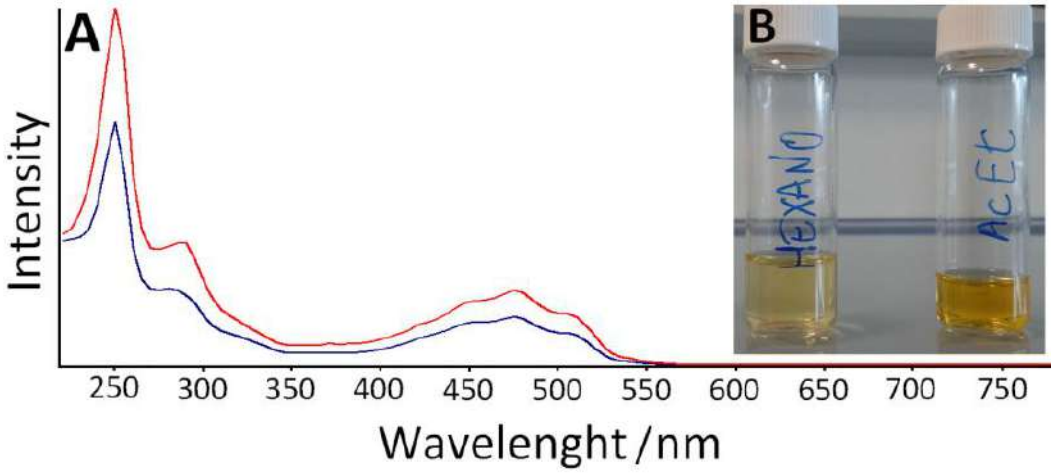

Fig. 7.9. UV-Vis spectra of the organic colorant extracted with ethyl acetate (red) and hexane (blue).

Therefore, taking into account that ethyl acetate extracted more efficiently the dye than hexane, it should be expected that it could have some functional groups that give a slight

polarity to the molecule (e.g. carbonyl and hydroxyl groups in anthraquinonic dyes or amines, ketone and bromines in the case of Tyrian purple).

Moreover, the SERS spectra obtained from both extracts were compared (see Fig. 7.10) and as it can be observed, a spectrum with higher intensity of the peaks was obtained by using ethyl acetate as solvent. The spectra shown in Fig. 7.10 are representative of more than 20 repetitive SERS measurements.

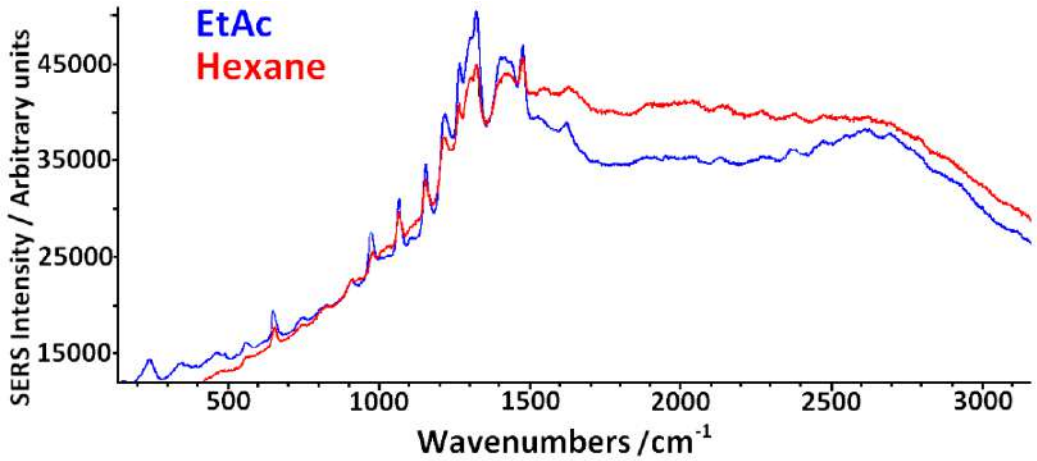

Fig 7.10. SERS spectra of the organic dye extracted with ethyl acetate (blue) and hexane (red) with 532 nm laser.

SERS results, together with the UV-Vis measurements and the visual observations of the color, suggest the better effectiveness of the ethyl acetate to extract the organic molecules coming from the colorant.

7.4.2. Optimization of the volume of the organic solvent

Once ethyl acetate was selected as the best organic solvent to extract the dye, the volume to be used in the extraction was optimized. For that, 5 mg of the pink lake pigment sample 117342 were extracted after the hydrolysis with the acid using different volumes of the selected solvent: two consecutive extractions of 2 mL each (2 mL x 2), two consecutive extractions of 1 mL each (1 mL x 2) and two consecutive extractions of 0.5 mL each (0.5 mL x 2). The SERS spectra (more than 20 repetitive measurements) obtained from each extract were compared (see Fig. 7.11).

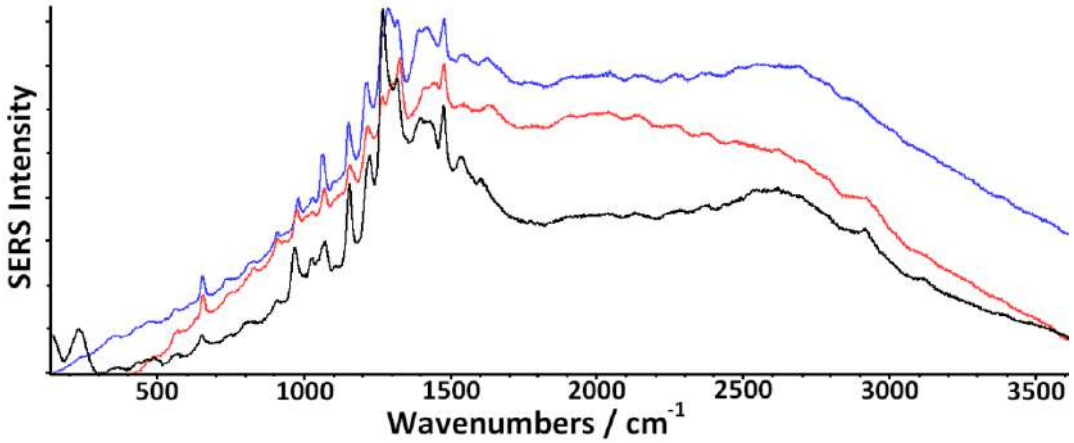

Fig. 7.11. SERS spectra obtained from different volumes of organic solvent with the extracted dye (black: 0.5 mL x 2; blue: 1 mL x 2; red: 2 mL x 2).

As shown in Fig. 7.11, all the spectra are quite similar, but the one belonging to the 0.5mL x 2 extract showed more intense peaks. Since the extracted dye is similar in all the cases, the most concentrate extract will be the one with the lowest extractant volume. Thus, after taking 100 μL of each extract, the remaining residue with highest concentration is the one obtained from the 0.5mL x 2 extract. Therefore, the peaks of its SERS spectrum are more intense, increasing the quality of the spectrum.

7.4.3. Optimization of the mass

The acid hydrolysis was performed using different amounts of mass of the lake pigments to identify the lowest amount of lake pigment which gives reliable SERS spectra. For that purpose, all the procedure was performed using different amounts of masses, using ethyl acetate as organic solvent and performing two sequential extractions of 0.5mL (0.5mL x 2). The Fig. 7.12 shows the final SERS spectra obtained with the 532 nm excitation laser of the pink lake pigment 117342 using 0.4, 1.7, 5, 10 and 57 mg of the mentioned sample. Each spectrum shown in the Fig. 7.12 is the representative of 20 repetitive measurements. For the rest of the lake pigments, it was not possible to perform the mass optimization due to the little amount of sample available. Thus, for those samples the optimized amount determined for 117342 lake pigment was used.

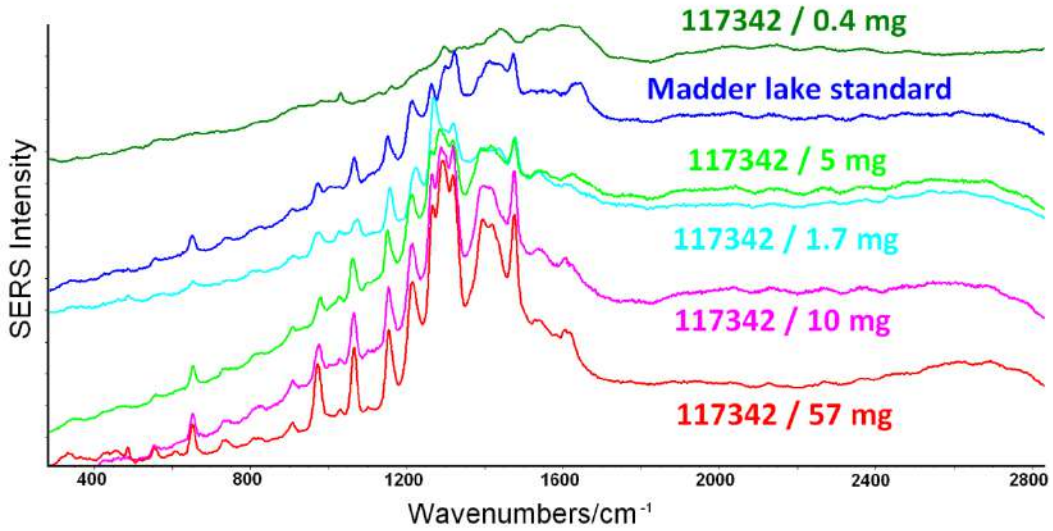

Fig. 7.12. SERS spectra of pink lake pigment 117342 organic extract, using different amounts of the pigment and SERS spectrum of madder lake standard extract using the 532 nm excitation laser.

A mass of around 5 mg could be the optimum one, since useful SERS spectra to assign the nature of the dye used in the lake pigment can be obtained using as lowest amount of

sample. With 10 and 57 mg, the consumption of sample is too high and the obtained spectra were just slightly improved, thus a greater mass of sample is unwarranted. In extreme cases in which the sample amount is very limited, with an amount of 1.7 mg, a good quality SERS spectrum for the identification of the colorant can also be obtained. Thus, thanks to this optimized sample treatment, just a very little amount of mass is necessary for the identification of the organic colorant in a lake pigment.

7.4.4. Selection of the laser excitation wavelength

Finally, it was systematically observed that the obtained SERS spectra using 532 nm excitation laser were always better than the ones obtained using 785 nm laser (see comparative spectra for 117356 lake pigment in Fig. 7.13) for all the lake pigments, confirming the experimental results obtained for the silver colloid by using UV-Visible technique.

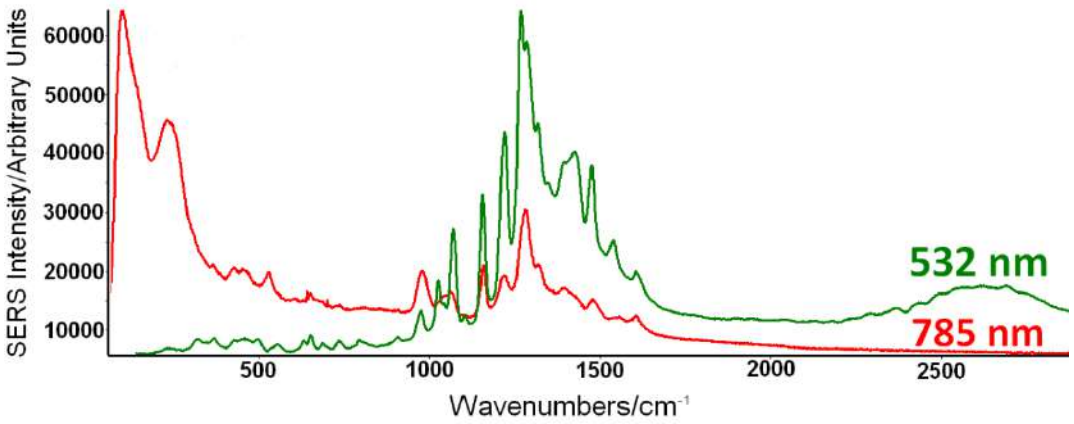

Fig. 7.13. SERS spectra of 117365 purple lake pigment obtained with 532 nm laser (green) and 785 nm laser (red).

Taking into account all the optimized parameters and conditions studied in the previous sections, the procedure to achieve appropriate results is summarized in Fig. 7.14.

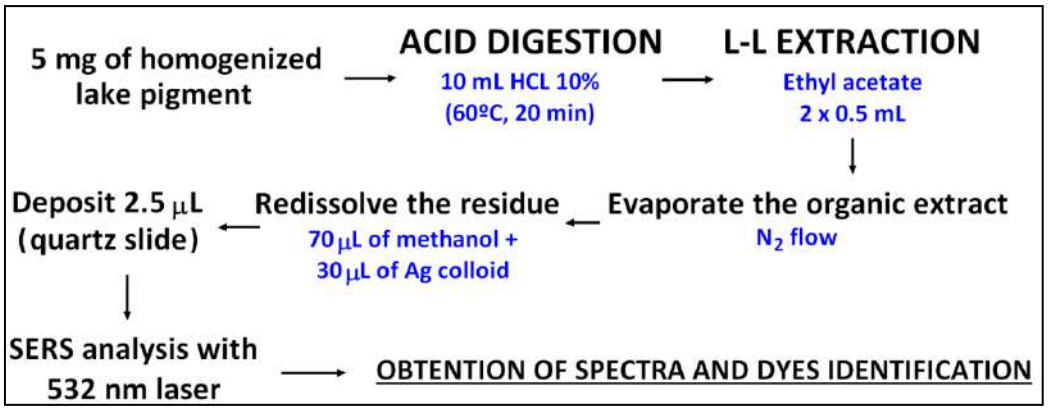

Fig. 7.14. Overview of the whole procedure, including all the optimized parameters (L-L: Liquid-liquid).

7.5 SERS characterization of standards and Pompeian pink and purple lake pigments

The SERS spectra obtained for pink lake pigment 117342 showed bands related to madder lake (see Fig. 7.12) pointing out the use of this kind of lake for its manufacture. Madder lakes can be produced by extracting dyes from the roots of some *Rubiaceae* plants, which include various hydroxyanthraquinones in their composition. The most abundant dyes in madder lakes are alizarin and purpurin (1,2-dihydroxyanthraquinone and 1,2,4-trihydroxyanthraquinone respectively), the main molecules responsible of giving the characteristic red to purple color. Depending on several factors, the alizarin and purpurin content in the root extract can vary. The two main species found in Mediterranean basin are *Rubia Peregrina*, the wild species, and *Rubia Tinctorum*, the cultivated one. In the wild species, the purpurin content is much higher than the alizarin content, which is very low (or absent in some cases), while the cultivated specie (*Rubia Tinctorum*) shows similar contents of both, alizarin and purpurin[27]. Madder has been cultivated as a dyestuff since antiquity in central Asia and Egypt, where it was grown since 1500 BC. Madder dyed fabrics were also found in the tomb of the Pharaoh Tutankhamun and in ancient Corinth[28] and its use was also referenced in cosmetics from the ancient Roman period[29,30].

117365 purple lake pigment was composed by pink and blue grains, giving in this way the final purple color as has been described previously. With the conducted acid digestion (5 mg) blue grains were not dissolved, therefore the obtained SERS spectrum correspond to the organic colorant responsible to give color to the pink pigment grains. In this case, also the SERS spectra obtained with 532 nm laser (Fig. 7.15) was the same to the madder lake standard one.

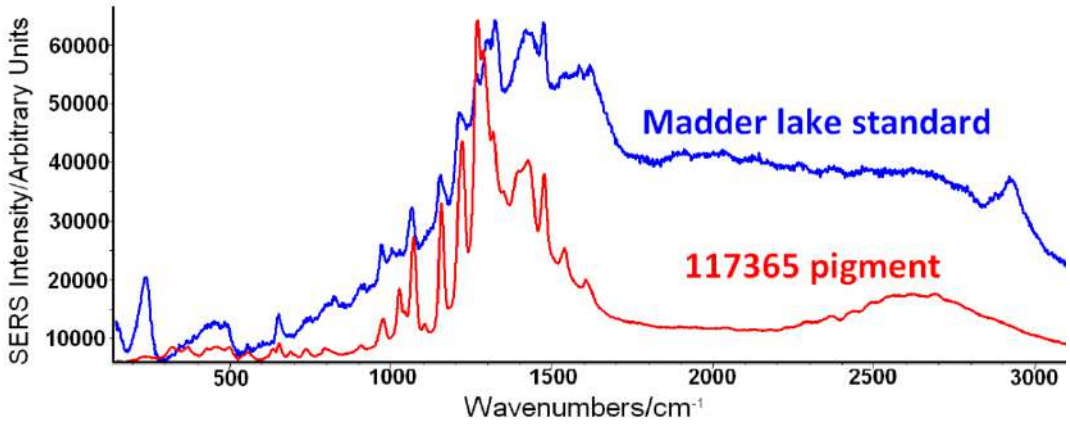

Fig. 7.15. SERS spectra of 117365 purple lake (red) and madder lake standard (blue).

As has been described in the previous chapter, the purple color of this lake pigment was obtained mixing the pink-dyed (madder lake according to the present results) aluminosilicate clay with Egyptian Blue pigment.

In the case of the 117323 pink lake pigment, the obtained SERS spectra was not exactly the same as the one of madder lake standard, thus it was decided to compare the SERS spectra from the organic colorant of the pigment with alizarin and purpurin standards (see Fig. 7.16). Although the available mass of this lake pigment was quite low (1.4 mg), the obtained SERS spectrum was good enough to identify bands that match with the ones of purpurin standard.

The obtained spectrum matches better with the purpurin standard spectrum, which suggests a higher content of purpurin than alizarin. This observation points to the use of madder lake, possibly extracted from *Rubia Peregrina* specie roots, which has more purpurin content in its composition as commented before[27].

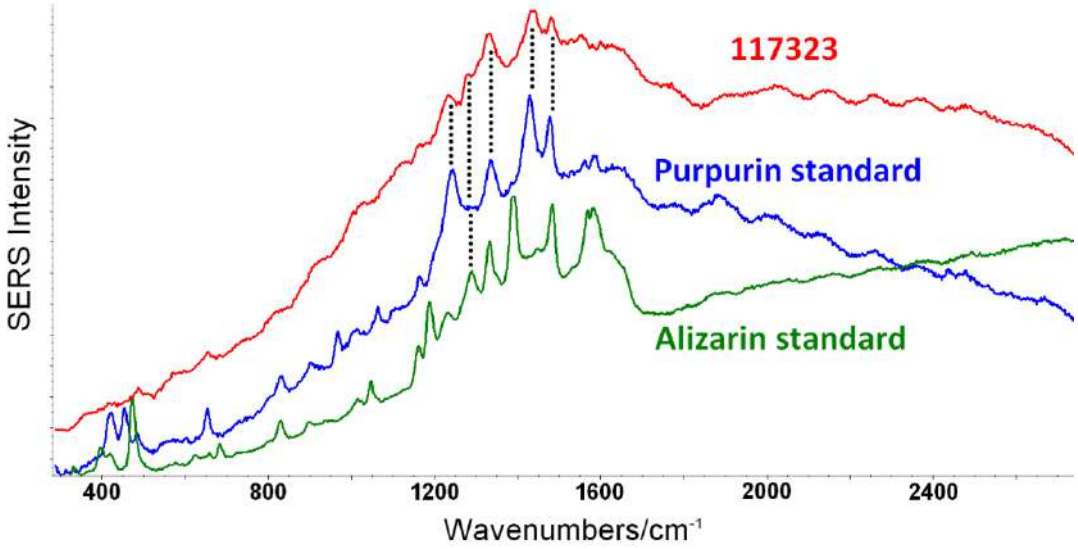

Fig. 7.16. SERS spectra of 117323 pink lake (red), purpurin standard (blue) and alizarin standard (green).

This 117323 sample has been previously analyzed by other authors using HPLC-DAD and HPLC-MS techniques, obtaining results that were not in agreement with each other[31]. With HPLC-DAD alizarin and purpurin were detected while with HPLC-MS indigotin and brominated indigoid compounds were found. Therefore, the first methodology pointed out to the use of madder lake and the second one to the use of Tyrian Purple. With this optimized sample pretreatment and the subsequent SERS analyses anthraquinonic colorant, mainly purpurin, was identified. Thus, our results agree with the ones previously published by Clarke *et al.*[31] obtained using HPLC-DAD. Table 7.1 shows a summary of the

dyes/molecules identified on each lake pigment together with their corresponding main SERS bands.

Table 7.1. Analyzed pink and purple lake pigment samples and the identified dyes with their respective main SERS bands.

Sample	Identified dye/molecule	Identified SERS bands (cm^{-1})
117323 pink	Purpurin, alizarin	Purpurin: 1262 (w), 1320 (s), 1420 (s), 1469 (m) Alizarin: 1290 (m)
117342 pink	Madder lake	650 (w), 906 (w), 969 (w), 1065 (m), 1152 (s), 1217 (s), 1265 (s), 1321 (s), 1474 (s)
117365 purple	Madder lake	650 (w), 973 (w), 1152 (s), 1217 (s), 1265 (s), 1474 (s)

To confirm the obtained SERS results, UV-Visible measurements of the organic extracts coming from the three lake pigments were performed. Considering that pink/purple lake pigments and standards do not absorb in the NIR spectral region, the spectra is shown in the UV-Visible spectral range. The obtained UV-Visible spectra (Fig. 7.17) of the lake pigments under study match perfectly with the UV-Vis spectrum of madder lake, confirming in this way the previous results.

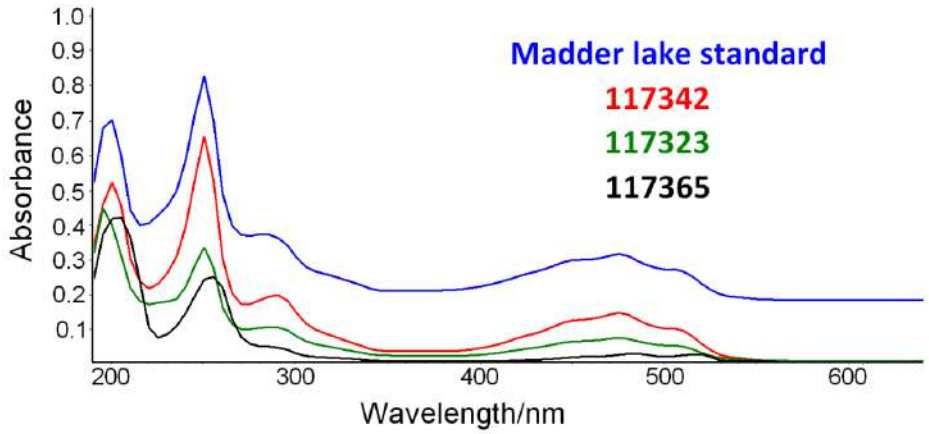

Fig. 7.17. UV-Vis spectra of 117342 (red), 117323 (green), 117365 (black) lake pigments together with madder lake standard (blue).

7.6 Conclusions

In this chapter an optimization of several parameters (mass of pigment, organic solvent nature and its volume) related with the sample treatment necessary to achieve good quality SERS spectra useful to determine the nature of the organic colorants used in ancient pink and purple lake pigments is proposed.

The optimization of the parameters studied in this chapter was applied to Pompeian pink and purple lake pigments and interesting information for future analyses was obtained. Five mg of sample was set as the optimum one to obtain good quality SERS results. However, it was proven that with only 1.7 mg acceptable results can be obtained. Apart from that, ethyl acetate showed the highest effectiveness for the extraction of the dye, probably because its slight polarity. However, this effectiveness will depend on the polarity of the molecule to be identified.

Regarding the best conditions for the SERS analysis, an excitation laser of 532 nm offers the best quality results, probably because of the closeness to the colloid absorbance maximum with respect to the laser wavelength. Finally, it is strongly recommended to use quartz slide instead the more common glass slide, because it provides lower background in the fingerprint area of organic molecules related with dyes.

Concerning the organic colorant present in the lake pigments under study, alizarin and purpurin anthraquinonic molecules coming from madder lake were identified as the main dyes responsible to give the final color. In samples 117342 and 117365 the content of alizarin and purpurin was similar, while in sample 117323 purpurin was the main colorant, pointing out the possible use of the wild *Rubia* plant.

Finally, the purple shade of the 117365 pigment seems to be the result of the mixture of madder lake and Egyptian Blue.

7.7 REFERENCES

1. Barnett, J. R. et al. Colour and art: A brief history of pigments. Opt. Laser Technol. **38**, 445-453 (2006).

2. Forbes, R. J. Studies in Ancient Technology Vol V. (Leiden, Brill Archive, 1956).

3. Casadio, F. *et al.* Identification of organic colorants in fibers, paints, and glazes by surface enhanced Raman spectroscopy. *Acc. Chem. Res.* **43**, 782–791 (2010).

4. Osticioli, I. *et al.* Fluorescence and Raman spectra on painting materials: reconstruction of spectra with mathematical methods. *J. Raman Spectrosc.* **37**, 974–980 (2006).

5. Nie, S. *et al.* Probing single molecules and single nanoparticles by surface-enhanced Raman scattering. *Science* **275**, 1102–1106 (1997).

6. Stefan A. Maier, S. A. Plasmonic field enhancement and SERS in the effective mode volume picture. Opt. Express **14**, 1957-1964 (2006).

7. Moskovits, M. Surface-enhanced Raman spectroscopy: a brief retrospective. *J. Raman Spectrosc.* **36**, 485-496 (2005).

8. Cruz, D. A. *et al.* Nanopartículas metálicas y plasmones de superficie: Una relación profunda. *Av. Cienc. Ing.* **3**, 67-78 (2012).

9. Zeng, S. *et al.* Nanomaterials enhanced surface plasmon resonance for biological and chemical sensing applications. *Chem. Soc. Rev.* **43**, 3426-3452 (2014).

10. Baumberg, J. J. *et al.* Angle-resolved surface-enhanced Raman scattering on metallic nanostructured plasmonic crystals. *Nano Lett*. **5**, 2262-2267 (2005).

11. Mayhew, H. E. et al. Surface-enhanced Raman spectroscopy studies of yellow organic dyestuffs and lake pigments in oil paint. Analyst **138**, 4493–4499 (2013).

12. Pozzi, F. et al. A systematic analysis of red lake pigments in French Impressionist and Post-Impressionist paintings by surface-enhanced Raman spectroscopy (SERS). *J. Raman Spectrosc.* **45**, 1119–1126 (2014).

13. Whitney, A. V. *et al.* An innovative surface-enhanced Raman spectroscopy (SERS) method for the identification of six historical red lakes and dyestuffs. *J. Raman Spectrosc.* **37**, 993–1002 (2006).

14. Roh, J. Y. *et al.* Identifying pigment mixtures in art using SERS: a treatment flowchart approach. *Anal. Chem.* **88**, 2028–2032 (2016).

15. Lee, P. C. *et al.* Adsorption and surface-enhanced Raman of dyes on silver and gold sols. *J. Phys. Chem.* **86**, 3391–3395 (1982).

16. Creighton, J. A. *et al.* Plasma resonance enhancement of Raman scattering by pyridine adsorbed on silver or gold sol particles of size comparable to the excitation wavelength. *J. Chem. Soc. Faraday Trans. 2 Mol. Chem. Phys.* **75**, 790–798 (1979).

17. Leona, M. Microanalysis of organic pigments and glazes in polychrome works of art by surface-enhanced resonance Raman scattering. *Proc. Natl. Acad. Sci.* **106**, 14757–14762 (2009).

18. Cañamares, M. V. *et al.* Ag Nanoparticles Prepared by Laser Photoreduction as Substrates for in Situ Surface-Enhanced Raman Scattering Analysis of Dyes. *Langmuir* **23**, 5210–5215 (2007).

19. Bruni, S. *et al.* Historical organic dyes: a surface-enhanced Raman scattering (SERS) spectral database on Ag Lee–Meisel colloids aggregated by NaClO4. *J. Raman Spectrosc.* **42**, 1267–1281 (2011).

20. Bruni, S. *et al.* Surface-enhanced Raman spectroscopy (SERS) on silver colloids for the identification of ancient textile dyes: Tyrian purple and madder. *J. Raman Spectrosc.* **41**, 175–180 (2010).

21. Tiedemann, E. J. *et al.* Fiber-safe extraction of red mordant dyes from hair fibers. *J. Am. Inst. Conserv.* **34**, 195–206 (1995).

22. Leona, M. *et al.* Application of surface-enhanced Raman scattering techniques to the ultrasensitive identification of natural dyes in works of art. *J. Raman Spectrosc.* **37**, 981–992 (2006).

23. Panáček, A. *et al.* Silver colloid nanoparticles: synthesis, characterization, and their antibacterial activity. *J. Phys. Chem. B* **110**, 16248–16253 (2006).

24. Lombardi, J. R. *et al.* Development of advanced Raman spectroscopy methods and databases for the evaluation of trace evidence and the examination of questioned documents (phase I). (New York, Report 2006-DN-BX-K034 of the US Department of Justice, 2009).

25. Stamplecoskie, K. G. *et al.* Optimal size of silver nanoparticles for surface-enhanced Raman spectroscopy. *J. Phys. Chem. C* **115**, 1403–1409 (2011).

26. Cañamares, M. V. *et al.* Comparative study of the morphology, aggregation, adherence to glass, and surface-enhanced Raman scattering activity of silver nanoparticles prepared by chemical reduction of Ag+ using citrate and hydroxylamine. *Langmuir* **21**, 8546–8553 (2005).

27. Cuoco, G. *et al.* Characterization of madder and garancine in historic French red materials by liquid chromatography-photodiode array detection. *J. Cult. Herit.* **12**, 98–104 (2011).

28. Eastaugh, N. *et al.* Pigment compendium: a dictionary of historical pigments. (London, Routledge, 2007).

29. Pérez-Arantegui, J. *et al.* Colorants and oils in Roman make-ups–an eye witness account. *TrAC Trends Anal. Chem.* **28**, 1019–1028 (2009).

30. Van Elslande, E. *et al.* Micro-Raman spectroscopy (MRS) and surface-enhanced Raman scattering (SERS) on organic colourants in archaeological pigments. *J. Raman Spectrosc.* **39**, 1001–1006 (2008).

31. Clarke, M. *et al.* Pompeii purpurissum pigment problems. *Proceedings of Art'05–8th International Conference on "Non Destructive Investigations and Microanalysis for the Diagnostics and Conservation of the Cultural and Environmental Heritage", Lecce, Italy* (2005).

PART 2

THE COLORS USED IN MOSAICS, TRANSFORMATION OF THE BINDER IN FRESCOES AND MODELLING OF THE YELLOW OCHRE PIGMENT TRANSFORMATION

PART 2. THE COLORS USED IN MOSAICS, TRANSFORMATION OF THE BINDER IN FRESCOES AND MODELLING OF THE YELLOW OCHRE PIGMENT TRANSFORMATION

Since all the majestic *domus* of Pompeii came to light after the organized excavations, different deterioration processes have been detected in their wall paintings after years of exposure to the modern atmosphere. The reproduction of the rooms of some houses through watercolors after the first excavations around 200 years ago and later photographic registers in the 19th century showed that, excluding the physical damages caused by the eruption, the conservation state of the wall paintings from the ancient Pompeii was acceptable before their exposure to the contemporary atmosphere. In Fig. 1, different pictures from a panel of a mural painting of the House of Gilded Cupids in Pompeii are shown. As it can be observed, at the moment of its excavation (photo taken in 1904) the decorations were perfectly visible. However, nowadays (see the photo taken in 2015) the decorations are almost imperceptible. This graphical comparison through years illustrates the evident loss of the polychromy of the painting.

Fig 1. Wall painting from the House of Gilded Cupids, showing the progressive loss of polychromy through years.

One of the main responsibles of polychromy loss in wall paintings could be the crystallization of soluble salts. Pigment grains in fresco painting are binded by the calcium carbonate of the last mortar layer applied to the wall (the *intonaco*). If calcium carbonate suffers a sulfation process, the new calcium sulfate formed is more soluble than the original calcium carbonate. If the mural painting suffers the impact of rainwater, this newly formed sulfate can be dissolved, promoting the de-cohesion of the pigment grains. Moreover, the crystallization of salts in the pores of the mortar, can also promote de detachment of the external layer in the wall painting, that is, the *intonaco*/*intonachino* were the pigments are fixed.

Apart from the crystallization of salts, there are many other pathologies that have a negative influence on the conservation state of Pompeian wall paintings, most of them caused by diverse environmental stressors. In fact, this numerous processes of degradations are usually activated in the post-excavation phase and they are the responsible of the different degradations that have taken place in the last decades. The stressors that affect the conservation state of Pompeian wall paintings can be divided in natural and anthropogenic. Among the natural ones, biocolonizations[1], infiltration of waters rich in different ions (salts) by capillarity[2] or the impact of rainwater/wind[3] can be

mentioned. In addition to these, the 79 AD volcanic eruption can be also considered a natural stress source. This event promoted a thermal impact, a dramatic increase of acid aerosols (SO_2, H_2S, HCl, HF…) in the atmosphere and the deposition of pyroclastic materials on the surface of the paintings[4].

As it has been explained in the introduction of this PhD Thesis (see Chapter 1), apart from all the processes that promote the loss of pigment grains in the mural paintings, some of the pigments (e.g., hematite and cinnabar) used in the polychromy of the Pompeian wall paintings can also suffer color transformations. Probably, the most evident transformation of pigments in Pompeii is the yellow ochre transformation into red (see Fig. 2). The color transformation into red that suffered yellow ochre (FeOOH) in Pompeii almost 2000 years ago was caused by the impact of materials at high temperatures emitted during the 79 AD pyroclastic density current events. Nowadays, there are 246 walls perceived as red and 57 as yellow. However, the number of walls decorated in red color could have been lower before the Vesuvius eruption in the year 79 AD[5].

When yellow ochre, mainly composed by goethite (α-FeOOH), is exposed to high enough temperatures (at around 250°C) a dehydration reaction occurs, leading to the formation of the anhydrous red hematite (α-Fe_2O_3).[6-8] It is known that this temperature was easily reached during the emissions of pyroclastic density currents in the 79 AD eruption[8]. Moreover, depending on the temperature impact, this transformation may be incomplete, that is, yellow and red ochres (orange colors) could coexist in the same area because the temperature was not high enough to dehydrate the entire goethite area.

Fig 2. Wall painting from Pompeii showing the transformation of yellow ochre into red in its middle-upper part.

The transformation of goethite into red color (hematite, Fe_2O_3) begins at temperatures ranging 230 and 280°C.[9] At this temperature, the dehydration process of the goethite takes place. The estimated temperature of the pyroclastic flow emitted by Mount Vesuvius is set at around 180–400°C, even if the main part of the emissions reached temperatures between 240–340°C in Pompeii[10,11]. Thus, the dehydration of the yellow goethite into red hematite in Pompeii was plausible at the moment of the impact.

Currently, in some areas of wall paintings from the Archaeological Park of Pompeii it is quite difficult to differentiate, at first sight, between original red areas and those obtained from transformation of the yellow pigment. For this reason, discrimination models based on elemental and/or molecular analysis could allow to differentiate both kinds of areas. In this sense, a recent work[12] attempted to discriminate original ochre

pigments from yellow ochres transformed into red in real Pompeian wall painting fragments. For that, the size of the hematite crystals obtained by XRD analysis and Rietveld refinements were used. However, the number and the nature of the samples together with the performed interpretation of the results were not conclusive enough to obtain a reliable discrimination model[12]. Moreover, with the proposed methodology, the wall painting samples were destroyed. For this reason, further non-invasive and more conclusive methodologies should be developed.

In this second part of the PhD thesis, the colors used to create Pompeian mosaics have been studies using an in situ strategy (Chapter 8). Additionally, the possible transformation of the calcite acting as the binder of the pigments in the pictorial layer, but also in the rest of the mortars stratigraphy of Pompeian wall paintings, has been also investigated in the laboratory (Chapter 9). Moreover, the sources potentially responsible of the transformation will be also explored. Continuing with the transformations in the pictorial layers of Pompeian wall paintings, different models based on the use of elemental and molecular results, and useful to discriminate the original red ochre pigment from the one obtained from the thermal transformation of the yellow ochre, have been also created under the framework of this PhD Thesis (Chapter 10 and 11). The added value of some of the models that will be presented below is the capacity of predicting the temperature at which a specific transformation took place in the 79 AD.

REFERENCES

1. Veneranda, M. *et al.* Biodeterioration of Pompeian mural paintings: fungal colonization favoured by the presence of volcanic material residues. *Environ. Sci. Pollut. Res*. **24**, 19599-19608 (2017).

2. Prieto-Taboada, N. *et al.* Study of the soluble salts formation in a recently restored house of Pompeii by in-situ Raman spectroscopy. Scientific reports, **8**, 1613-1620 (2018).

3. Traversetti, L., *et al.* Wind-driven rain as a bioclimatic factor affecting the biological colonization at the archaeological site of Pompeii, Italy. *Int. Biodeter. Biodegr*. **134**, 31-38 (2018).

4. Luongo, G. *et al.* Impact of the AD 79 explosive eruption on Pompeii, I. Relations amongst the depositional mechanisms of the pyroclastic products, the framework of the buildings and the associated destructive events. *J. Volcanol. Geotherm. Res*. **126**, 201-223 (2003).

5. https://www.theguardian.com/science/2011/sep/22/pompeii-red-yellow (Last accessed November 2019).

6. de Faria, D. L. A. *et al.* Heated goethite and natural hematite: can Raman spectroscopy be used to differentiate them? *Vib. Spectrosc.* **45**, 117–121 (2007).

7. Ruan, H. D. *et al.* Infrared spectroscopy of goethite dehydroxylation: III. FT-IR microscopy of in situ study of the thermal transformation of goethite to hematite. *Spectrochim. Acta. A. Mol. Biomol. Spectrosc.* **58**, 967–981 (2002).

8. Pomies, M. P. *et al.* TEM observations of goethite dehydration: application to archaeological samples. *J. Eur. Ceram. Soc.* **19**, 1605–1614 (1999).

9. Prasad, P. S. R. et al. In situ FTIR study on the dehydration of natural goethite. *J. Asian Earth Sci.* **27**, 503-511 (2006).

10. Gurioli, L. *et al.* Complex changes in eruption dynamics during the 79 AD eruption of Vesuvius. *Bull. Volcanol*. **67**, 144-159 (2005).

11. Zanella, E. *et al.* Temperatures of the pyroclastic density currents deposits emplaced in the last 22 kyr at Somma–Vesuvius (Italy). *Geol. Soc. London*. **396**, 13-33 (2015).

12. Angelini, I. *et al.* The pigments of the frigidarium in the Sarno Baths, Pompeii: Identification, stratigraphy and weathering. *J. Cult. Herit.* (2019). DOI: 10.1016/j.culher.2019.04.021

8. MATERIALS USED TO OBTAIN THE COLORS IN POMPEIAN MOSAIC TESSERAE

8.1 Introduction

When the Romans conquered the region of Greece during the second century BC, mosaics were already common in the Greek world[1]. Thereby, the art of the mosaics easily passed to the Roman culture giving way to an artistic-industrial genre. It was spread in such a way that there were almost not houses or Roman villas without mosaics[2]. The Roman mosaics are easy to discover for archaeologists and so far their number is very high, but they present a great difficulty of conservation.

In this sense, in the surroundings of Pompeii, specifically in the Bay of Naples area, a great number of mosaics have been discovered since this area is rich in archaeological sites. Apart from Pompeii, probably the most famous archaeological cities of the area are Herculaneum and Stabiae. Normally, Roman mosaics were created on the floor. However, good examples of wall mosaics can be found in the region of Campania, for example the

Neptune and Salacia wall mosaic in the house 22 from Herculaneum. Many of these mosaics located in the Bay of Naples have been analyzed in the laboratory with the purpose of identifying the materials used for their manufacture or to determine the provenance of the materials used[2-5].

The archaeological excavations carried out in Pompeii allowed the recovery of mosaics in excellent state of conservation, but the numerous processes of degradations that are usually activated in the post-excavation phase require the application of periodic maintenance treatments. Considering that these deterioration mechanisms are usually associated with weathering phenomena, the ideal place to store the mosaics is in museums where temperature, humidity, etc., are under control.

A mosaic is a pictorial work elaborated with a set of tesserae joined by the action of lime[5] or other binders to form geometric or figurative decorative compositions. A tessera is an individual piece of cubic form, made of calcareous rocks, glass or ceramic material[6]. The ancient artists used to arrange them into representational designs and geometric patterns. The tesserae used in Ancient Rome were made of calcareous rocks obtained from local sources (natural stone), with additions of crushed brick, tile and pottery creating colored shades of, predominantly, black, red, white, blue and yellow[7]. Polychrome patterns were the most common ones; however monochrome examples are also known[8].

Analyzing individual tesserae to know the composition of the used materials and the compounds responsible to give the characteristic color to each piece is an interesting challenge from the chemical and archaeological point of view. In the specific case of Pompeii, nowadays very serious degradation problems can be identified (e.g., biodeterioration processes, salts crystallizations, etc.). For this reason, many houses of the archaeological site need an analytical study which could allow the conservators to guide towards the approach of effective and long-lasting rehabilitation interventions.

But despite this need, nowadays it is not possible to collect samples for laboratory analyses purposes. Therefore, the use of portable analytical instrumentation is essential to perform non-destructive in situ analysis. In this sense, Raman spectroscopy has been applied in the last years for the molecular characterization of Roman mosaics[6,9-11]. Previous works showed that Raman spectroscopy not only can be used to characterize the base material, but also to identify colorants and opacifiers present within the matrix mosaic tesserae[12]. Apart from those, mosaics from other locations around the world such as Lisbon (Portugal)[13], Guangxi (China)[14], Daphni (Greece)[15] or Ifriqiya (Tunisia)[16] have been characterized by means of Raman spectroscopy. This variety of works evidences the usefulness, powerfulness and robustness of Raman spectroscopy in order to characterize mosaic tesserae, since calcareous, glassy or mineral-based compounds can be detected by this technique. For this reason, in this work Raman spectroscopy was selected as main analytical technique to identify the used base material and the applied pictorial layer of different colored tesserae.

Apart from Raman spectroscopy, infrared spectroscopy in Diffuse Reflectance mode (DRIFT) can be also used as supporting technique. The use of DRIFT to complement the results obtained by means of Raman spectroscopy could permit a complete identification of the compounds present in the mosaic. In the literature there are not works dealing with the use of portable infrared spectrometers applied in situ for the characterization of mosaics. Instead of diffuse reflectance, a spectroradiometer covering the visible, the near infrared, and the short wave infrared (350-2500 nm) has been used in a previous work[17].

Regarding the elemental analysis, X-ray fluorescence spectrometry (XRF) could be one of the best options due to its non-destructive feature and the reliable qualitative and/or semi-quantitative information that can be obtained. In this sense, XRF has been already applied in the analysis of colored tesserae of mosaics to establish the compositional major and minor elements. Some works[5,6] were developed in the laboratory with extracted samples prepared as cross sections applying Scanning Electron Microscopy

coupled with Energy Dispersive X-ray fluorescence (SEM-EDS), XRF and X-ray diffraction, obtaining interesting results regarding the composition of white and black materials used to manufacture the mosaics tesserae. In this sense, limestone for the white tesserae and tephritic lava for the black tesserae were identified[6]. On the other hand, other research works[18-20] used portable non-invasive techniques to characterize in-situ the materials used in the decoration objects. Concretely in these latter works some tesserae from a mosaic located in the Domus of Octavius Quartio (Pompeii) were analyzed with portable instrumentation obtaining interesting results. This spectroscopic data can be treated with statistical tools, such as Principal Component Analysis (PCA), in order to extract more information. PCA with the elemental data (XRF or LIBS) have been applied in archaeological analysis, particularly in trace analysis of ochre pigments[21,22]. In this PhD Thesis, this strategy was considered of interest for the analysis of the elemental composition of the tesserae under study.

Pompeian mosaics have not been deeply analyzed from a chemical point of view in literature. In fact, there is only few works dealing with them[6,19,20], in which the chemical composition of some tesserae from Pompeian mosaics was analyzed. Therefore, the available information about the materials used to manufacture the tesserae that were used to create the final Pompeian mosaic in literature is scarce. Moreover, to manufacture colored tesserae it is supposed that pigments were used. To confirm this, both the substrate matrix and the pictorial layer of the tesserae should be analyzed. These identifications could help to understand more about the custom procedures and materials used to manufacture Pompeian mosaics.

In this PhD Thesis, two mosaics exposed to the open air and suffering the indirect impact of the rainwater located in rooms E and G of the House of Gilded Cupids (Reg VI, Ins 16, 7, 38) were analyzed in situ with non-invasive portable instruments. Raman spectroscopy, supported with DRIFT, was used as the main analytical technique to ascertain the molecular composition of both, the matrix of the used tesserae and the existing pictorial

layers. The elemental analysis was performed by means of HH-EDXRF and p-LIBS. The data matrix obtained after HH-XRF measurements was subjected to multivariate analysis (PCA) to observe similarities/differences between tesserae of different colors, while p-LIBS results were used to estimate the thickness of the applied pictorial layers.

8.2 Mosaic description

The two mosaics considered in this work are located in room E and room G of the House of Gilded Cupids in the Archaeological Park of Pompeii (see Fig. 8.1). This house was first excavated between 1903 and 1905. It is situated on the *Via del Vesuvio*, and it is believed to have been owned by Gnaeus Poppaeus Habitus, a wealthy local figure of that time.

Fig. 8.1. Part of the mosaic under study placed in room E with additional details showing black, red, orange and white tesserae (up) and analyzed mosaic placed in room G (down).

As can be observed in Fig. 8.1, the mosaics present in the House of Gilded Cupids show mainly four different colored tesserae: black, red, orange and white tesserae. Regarding red and orange tesserae, taking the advantage that some of them were spontaneously detached, a visual inspection was performed, observing that they were composed by the application of a pictorial layer in the top of each red and orange tessera. The combination of the four different colored tesserae allowed creating a figurative decoration inside a perimetric geometric design (see Fig. 8.1).

Taking into account that some interventions were performed in the past to preserve the mosaics under study, with the advice of Archaeological Park of Pompeii, not intervened areas were selected in order to perform the analyses in original areas. Before performing the measurements, the tesserae were carefully cleaned using a dry paper tissue to remove all the possible dust and depositions present in the surface of tesserae in order to not affect the obtained analytical results.

8.3 Molecular characterization of the mosaics

The different colors (white, orange, red and black) of the mosaics were analyzed in situ not only to obtain the mineralogical composition but also to understand the compounds used to give the different colors to each tessera. The discussion of the obtained results is grouped according to the color of the analyzed tesserae.

8.3.1. Red and orange tesserae

Raman measurements of the red and orange colored tesserae offered the typical spectrum of hematite as shown in Fig. 8.2 (Fe_2O_3, 227, 291, 411 and 609 cm^{-1} bands[23]) and calcite ($CaCO_3$, 155, 282, 712 and 1086 cm^{-1} bands[23]).

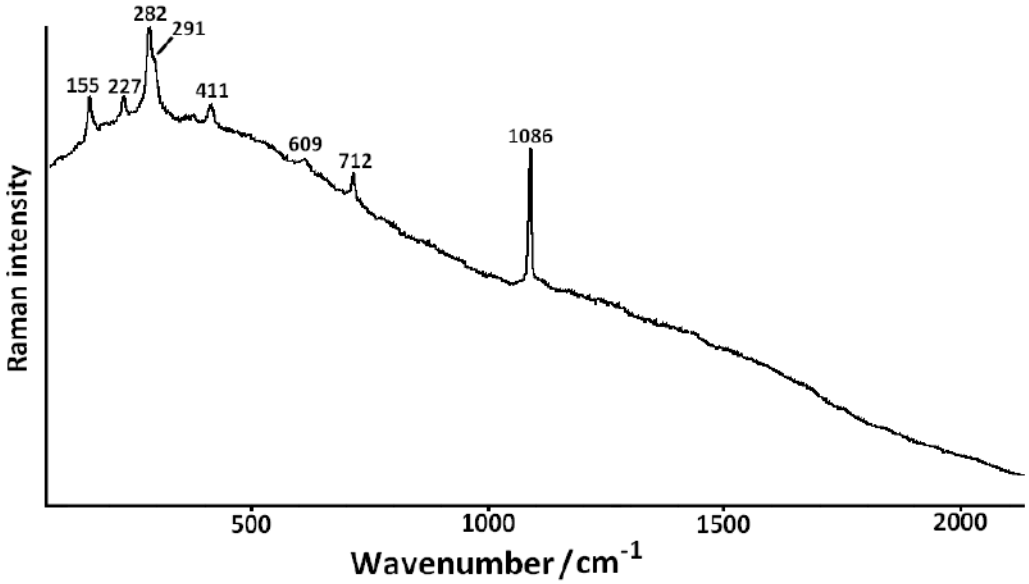

Fig.8.2. Representative Raman spectrum of red and orange colored mosaic tesserae.

The use of hematite in Ancient Roman period is well known and has been widely identified in previous works and in this PhD Thesis. Moreover, its use in Pompeii has been clearly proven in the literature[23-27]. Therefore, Raman results suggest that these reddish colored tesserae were obtained by using hematite red pigment layer applied over a calcite-based tessera. On the other hand, the acquired DRIFT spectra only showed the presence of calcite (see Fig. 8.3).

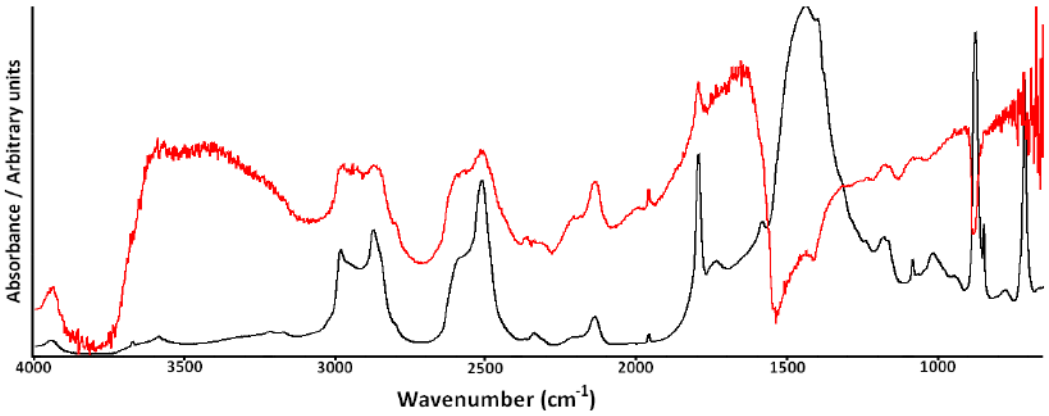

Fig. 8.3. DRIFT spectrum of calcite standard (black) and red tessera (red).

Hematite is difficult to detect by means of DRIFT because the main bands of red iron oxide appear in the 400-500 cm^{-1} spectral region, concretely at 446 and 530 cm^{-1}. In this spectral region the energy falls down in the portable infrared spectrometer, thus it is not possible to detect any band in this wavenumber region. Thereby, it was not possible to detect hematite by means of DRIFT portable spectrometer, but its presence in red and orange pictorial layers was clearly proven by means of Raman spectroscopy.

8.3.2 White tesserae

White mosaics, however, were composed mainly by a calcite-based matrix without the application of any pictorial layer, as shown in the obtained Raman spectrum. In Fig. 8.4 the typical bands of calcite at 282, 712 and 1086 cm^{-1} can be observed[23]. In this case, no more colored compounds apart from calcite were detected pointing out that the molecular composition of these white tesserae consisted only in calcite. As observed in previous works[5,11], in Roman white tesserae the presence of calcite-bearing rock was clearly and frequently identifiable as the mineral constituting the substrate. In this case, pictorial layers were not added to obtain different colored hues.

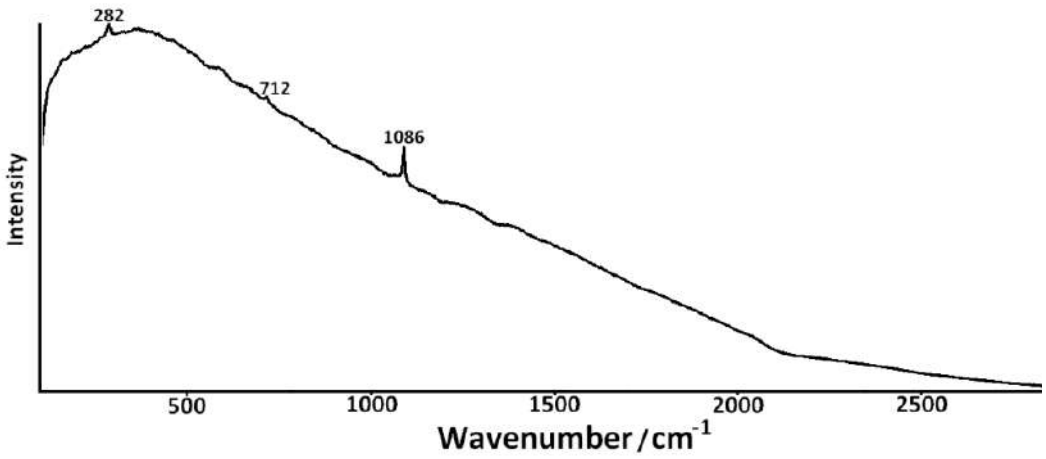

Fig. 8.4. Representative Raman spectrum obtained in white tesserae.

Apart from calcite, gypsum ($CaSO_4 \cdot 2H_2O$) was also punctually identified (415, 1008 and 1136 cm^{-1} Raman bands[23], see Fig. 8.5). Since the tesserae were subjected to a previous cleaning process, this gypsum could belong to a degradation process that is taking place in the calcite matrix of the tesserae with environmental factors such as SO_x gases present in the past and current Pompeian atmosphere. These SO_x gases, when oxidized, form H_2SO_4 aerosols with the rain water that impact mosaics, producing the degradation process of the calcite into gypsum, which it is soluble in water.

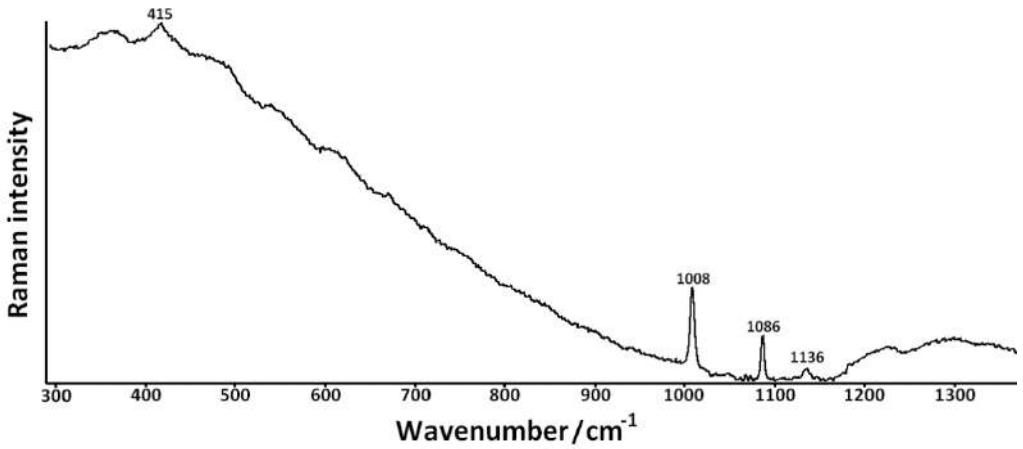

Fig. 8.5. Raman spectrum obtained punctually in white mosaic tesserae.

This is one of the most dangerous degradations due to the fact that it might jeopardize the structure of tesserae, making possible the loss of material due to the water soluble gypsum formation. However, the presence of gypsum was only punctually detected, suggesting that this deterioration process has not affected the integrity of the matrix.

Even so, this degradation must be taken into account and some protection actions should be considered in order to protect the tesserae for their adequate preservation. The data that will be presented in further section regarding the elemental analysis acquired by HH-EDXRF revealed also higher net counts of sulfur in specific areas of the measured white tesserae, reinforcing the molecular evidences about sulfates punctual presence.

DRIFT measurement confirmed Raman results since all the acquired spectra matched with the DRIFT spectrum of calcite standard (see Fig. 8.6). In this case, gypsum was not detected. Considering that the presence of this sulfate is punctual and also that with the DRIFT sampling interface the measured area is higher (2 mm) than the Raman spot size (85 μm), the presence of this sulfate at minor/trace level can be diluted in the calcite matrix measured area giving rise to the non-detection of gypsum.

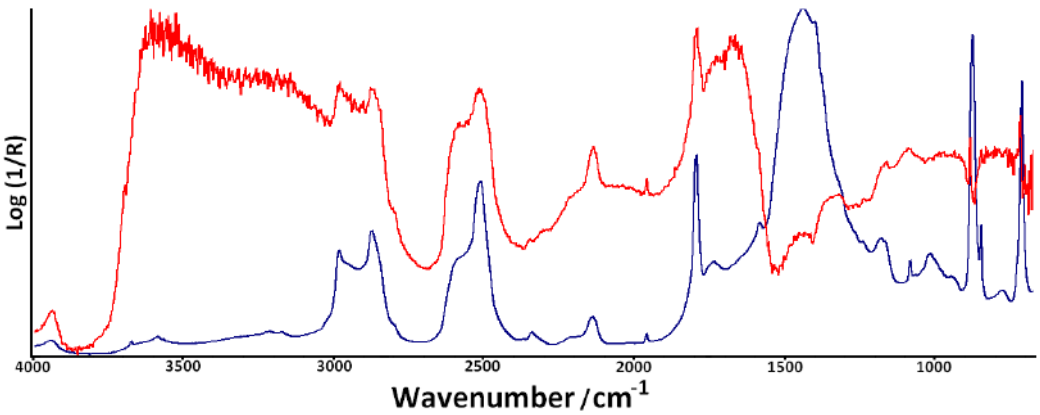

Fig. 8.6. Representative DRIFT spectrum of white mosaic tesserae (red) and calcite standard (blue).

8.3.3 Black tesserae

The acquired Raman spectra of black tesserae showed the typical feature of a silicate-bearing material (see Fig. 8.7), most probably from local black-colored volcanic rocks. In fact, the closeness to Mount Vesuvius completely influences the topography and the geological composition of the soils of Pompeii and surroundings.

The presence of volcanic and igneous rocks creates a dark landscape, because the color of this type of rocks is usually black. In this sense, diopside, which has $CaMgSi_2O_6$ chemical formula, is a very common rock-forming mineral that gives black color to many igneous rocks. Moreover, this clinopyroxene has been recognized in the composition of the Vesuvian lavas and pyroclastic materials[28-30]. As can be observed in Fig. 8.7A, the obtained representative spectra of the black tesserae fit with the diopside standard spectrum, confirming the presence of this compound widely present in the tephritic lava from Mount Vesuvius.

Apart from that, feldspar, with the most intense peaks[31,32] at 481 and 512 cm^{-1} could be also present in the composition of black tesserae, as shown in Fig. 8.7B, in which those commented bands related to feldspar together with others related to diopside can be observed. Feldspars also represent one of the main constituent of Vesuvian rocks, therefore its presence, together with the diopside, points out the local origin of the material used for black tesserae, as a previous work already have demonstrated[5]. In the same figure, bands at 665 and 324 cm^{-1} could also suggest the presence of magnetite (Fe_3O_4).[33]

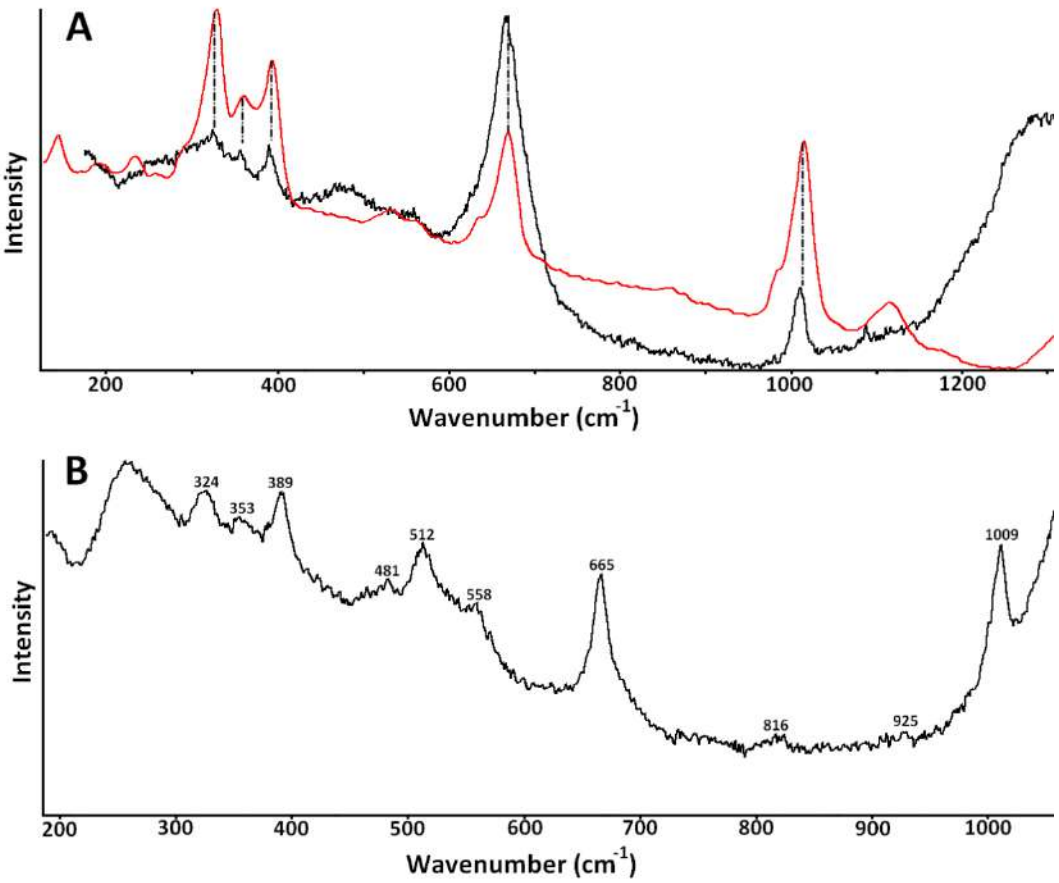

Fig. 8.7. A) Raman spectrum of black colored mosaic tesserae (black) and diopside standard (red) and B) another Raman spectrum of black colored mosaic tesserae.

Apart from the previously identified volcanic compounds, which were extensively detected, in some spots also leucite was detected (see Fig. 8.8). Leucite has also been identified as a ubiquitous component in the area of Mount Vesuvius[34], which once again points out the local origin of the material used for the black tesserae.

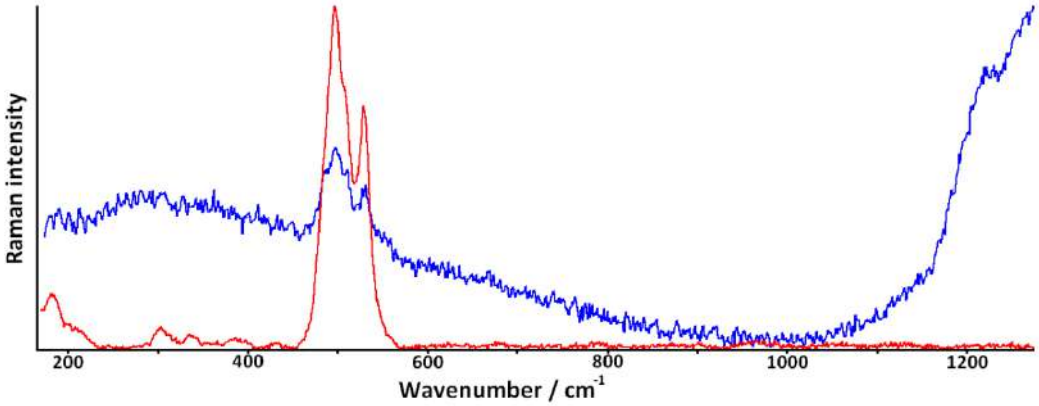

Fig. 8.8. A Raman spectrum acquired in black tesserae (blue) and Raman spectrum leucite standard (red).

8.4 Elemental characterization of the mosaics

As mentioned before an in situ elemental characterization was performed by means of HH-EDXRF to study possible similarities/differences on the elemental composition of the colored mosaics. For that, four to nine measurements in different tesserae of the same color were performed to have a big enough replicate measurements from each type of tesserae. Thanks to that, representative analysis and further chemometric data treatment were performed.

The multivariate analysis was performed by means of PCA using the raw net counts of the detected elements. In previous works[35,36], a normalization of the net counts was applied to correct the obtained intensities against (a) the line of one element that showed constant levels in all the samples or (b) the Compton line. In this work, two datasets were prepared to compare which one offered the best and most realistic results. One of them was composed by the raw net counts and another dataset with the normalized net counts. As the signal of each element showed high variability depending on the color of the analyzed tessera, the normalization process did not offer realistic PCA results and the explained variance was quite low. On the other hand, the PCA obtained with the raw net

counts dataset showed a more real and faithful image of the elemental composition of the mosaic tesserae, with an explained variance of 72% with two principal components. The results shown in Fig. 8.9 were obtained using the raw net counts dataset.

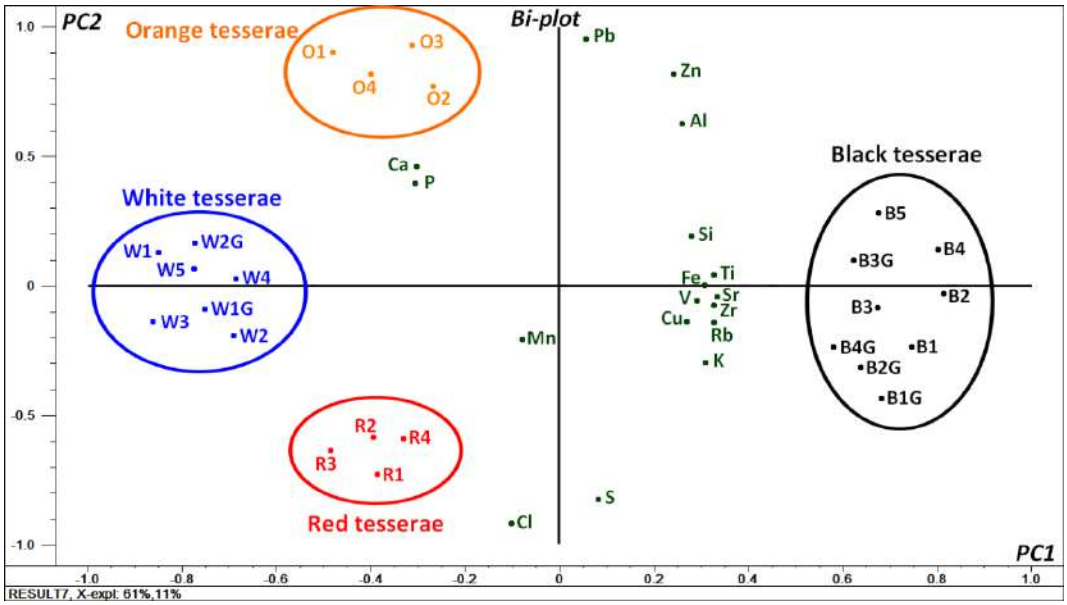

Fig. 8.9. Projection of the scores and loadings (bi-plots) on PC1–PC2 obtained from the PCA with all the HH-EDXRF measurements performed on the white (W), orange (O), red (R), and black (B) mosaic tesserae from the room E, and room G (measurements of this last room marked with a G) of the House of Gilded Cupids.

As shown in Fig. 8.9, PC1 divides white, orange and red mosaic tesserae (placed in the negative part) from those of black color (in the positive part). The obtained PCA showed that black mosaic tesserae are the ones with the highest level in metals such as Al, Si, K, Ti, V, Fe, Cu, Zn, Rb, Sr and Zr. Most of these metals are highly present in rocks of volcanic origin, particularly from the Somma-Vesuvius area[28,37], confirm the previous Raman results and demonstrate that black color was achieved using local minerals emitted by Mount Vesuvius, such as diopside. Moreover, the presence of these elements come in agreement with the main compound identified molecularly by Raman spectroscopy, augite which is an iron alumina-silicate with magnesium (not detectable by means of HH-

EDXRF) and calcium, which in the PCA is placed together with white and orange tesserae because they are composed by a calcite-based matrix.

White colored mosaics presented higher levels of Ca, P and in a minor extent, Mn. The major element was calcium as expected, because white mosaic tesserae were manufactured by a calcite-based matrix, as shown in the results obtained by Raman and DRIFT spectroscopies. Thus, elemental measurements corroborate the previous results. Moreover, unlike black tesserae, white ones do not present any of the previously mentioned elements related with volcanic origin in significantly high levels. Instead of them, white tesserae together with the orange ones, presented the highest level of P and Mn among all the analyzed tesserae. However, the intensity of the K_{α} line of P and Mn was very low in all the cases. The case of Cl in red tesserae was exactly the same as the previous one.

As stated previously, white, orange and red tesserae are placed in the same part of the PC1. This is probably due to the common calcite-based matrix. However, there are significant differences in the PC2 axis. The amount of hematite (Fe mainly) could explain such differences, because (a) the white tesserae did not have iron, and (b) the amount of Fe in the red tesserae is much higher than in the orange ones. To confirm the reasons for such differences between red and orange tesserae, the mean value of Fe/Ca net counts ratio was calculated from these two tesserae (see Fig. 8.10).

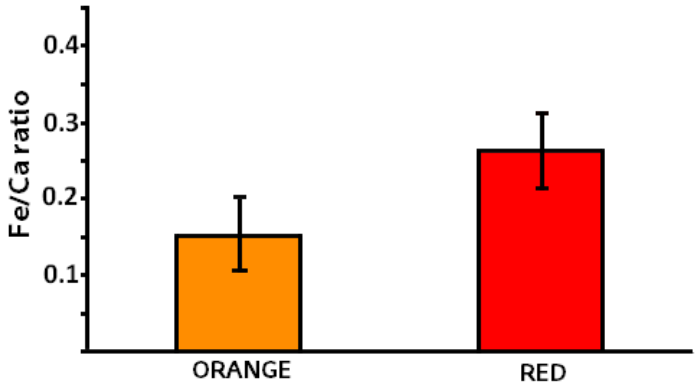

Fig. 8.10. Mean values of Fe/Ca net counts ratio of red and orange colored tesserae.

As shown in the figure, the orange colored samples have a lower level of Fe/Ca. The obtained mean value of Fe/Ca normalized net counts for red tesserae was 0.26 ± 0.04, while for orange ones was 0.15 ± 0.04. Thus, it confirms that orange color was obtained by using less quantity or diluting the hematite within the calcite matrix of the mosaic.

Finally, p-LIBS was used to determine the thickness of the applied pictorial layer in the case of red colored tesserae. For that, a certain red tessera was selected and subsequent pulses were performed in the same point of analysis (depth-profile study). In order to assess the pictorial layer thickness, the levels of Ca and Fe were monitored using their characteristic lines at 393.2 and 374.55 nm respectively. As shown in Fig. 8.11, both Fe and Ca levels are maintained constant in the applied 28 pulses, suggesting that there is no change in the in-depth levels of both elements. This means that no layer change was observed in the subsequent analyses. Therefore, taking into account that in 28 LIBS pulses approximately about 140 μm were penetrated, it points out that the pictorial layer is thicker than this value.

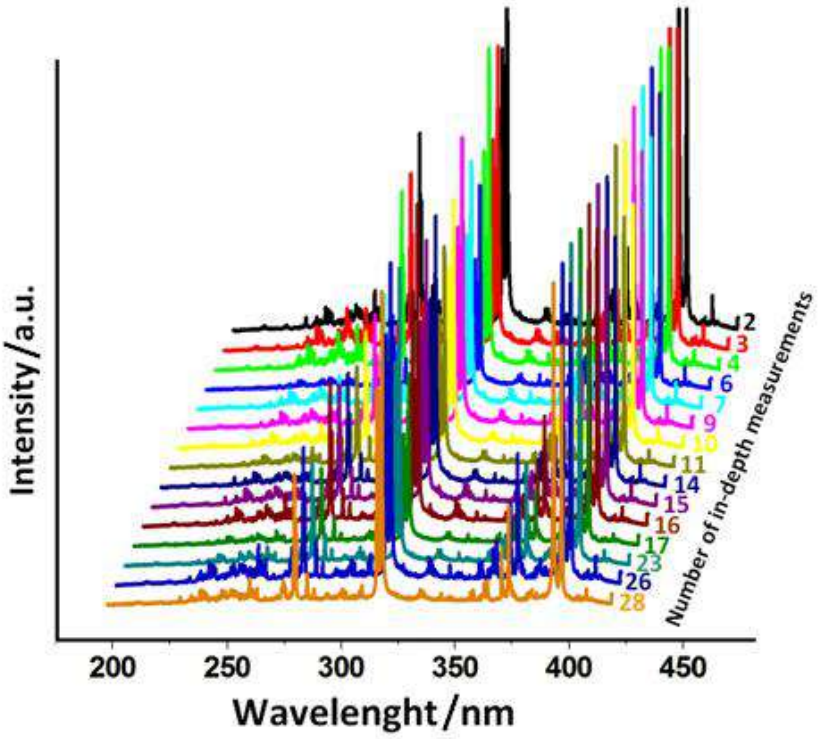

Fig. 8.11. Ca and Fe lines intensity variation after 28 shots obtained by means of LIBS.

8.5 Conclusions

In this part of the PhD Thesis, useful information about the materials used to manufacture colored tesserae of mosaics from the House of Gilded Cupids in Pompeii has been obtained without sampling and only using portable/handheld instruments,. In this sense, to obtain white color tesserae calcite-bearing rocks were used. On the other hand, to achieve the black color, instead a calcite-based matrix, lava pieces from Mount Vesuvius activity containing diopside, feldspar, leucite and magnetite were used. Therefore, it can be affirmed that the artists used the local mineral resources to produce the materials that they needed for their works, as previous works already demonstrated[5].

Reddish and orange hues were obtained by using hematite pictorial layer over the calcite based tessera. Orange color was obtained diluting in a calcite matrix the used hematite pigment. The applied hematite pictorial layer was thicker than 140 μm as showed the in-depth p-LIBS analysis.

Apart from that, the punctual presence of gypsum was identified in some white tesserae. This sulfate is probably present due to a degradation process involving the SO_x gases present in the actual polluted atmosphere, which with the rain water can react with the calcite matrix of the tesserae, producing gypsum. Since gypsum is soluble in water, a loss of the material of the tesserae could be produced, jeopardizing those mosaics which are exposed to the rainfalls. Therefore, extreme care must be taken to preserve this type of ancient artworks.

Regarding the molecular non-invasive techniques used in this work, Raman spectroscopy provided much more results than DRIFT, which only offered information about calcite presence in white tesserae. Thanks to Raman spectroscopy typical volcanic compounds (diopside, leucite, feldspar, and magnetite) were identified in the black tesserae and hematite as colorant agent in red and orange ones. In the case of white tesserae, gypsum was detected by means of Raman spectroscopy but not by DRIFT. Thus, this work demonstrated that in this case Raman spectroscopy is a more appropriate technique than DRIFT – which showed great limitations - since this latter technique was not able to offer signals of compounds that are present in the sample.

8.6 REFERENCES

1. Broome, B. J. Exploring the Greek mosaic: A guide to intercultural communication in Greece. (London, Hachette, 1996).

2. Christensen, A. M. From Palaces to Pompeii: The Architectural and Social Context of Hellenistic Floor Mosaics in the House of the Faun. PhD Thesis, (Florida State University, 2006).

3. Petriaggi, R. *et al.* An experimental conservation treatment on the mosaic floor and perimeter walls of room n. 1 of the so-called "Villa con ingresso a Protiro" in The Underwater Archaeological Park of Baia (Naples). *Archaeol. Marit. Mediterr.* **1**, 109-126 (2004).

4. Ricca, M. *et al.* Mosaic marble tesserae from the underwater archaeological site of Baia (Naples, Italy): determination of the provenance. *Eur. J. Mineral.* **26**, 323-331 (2014).

5. Izzo, F. *et al.* The art of building in the Roman period (89 B.C. - 79 A.D.): Mortars, plasters and mosaic floors from ancient Stabiae (Naples, Italy). *Constr. Build. Mater*. **117**, 129-143 (2016).

6. Ricciardi, P. *et al.* A non-invasive study of Roman Age mosaic glass tesserae by means of Raman spectroscopy. *J Archaeol. Sci*. **36,** 2551-2559 (2009).

7. Witts, P. Mosaics in Roman Britain. (Tempus, 2005).

8. Packard P. A Monochrome Mosaic at Isthmia. *Hesperia*. **49,** 326-346 (1980)

9. Gedzevičiūtė, V. *et al.* Chemical composition and coloring agents of Roman mosaic and millefiori glass, studied by electron microprobe analysis and Raman microspectroscopy. *Archaeol. Anthropol. Sci*. **1,** 15-29 (2009).

10. Galli, S. *et al.* Raman and scanning electron microscopy and energy-dispersive x-ray techniques for the characterization of coloring and opaquening agents in Roman mosaic glass tesserae. *J. Raman Spectrosc*. **35**, 622-627 (2004).

11. Boschetti, C. *et al.* Raman characterization of painted mortar in Republican Roman mosaics. *J. Raman Spectrosc.* **39**, 1085-1090 (2008).

12. Basso, E. *et al.* Characterization of colorants and opacifiers in roman glass mosaic tesserae through spectroscopic and spectrometric techniques. *J. Raman Spectrosc.* **45**, 238-245 (2014).

13. Muralha, V. S. F. *et al.* Baroque glass mosaics from the Capela de São João Baptista (Chapel of Saint John the Baptist, Lisbon): unveiling the glassmaking records. *J. Raman Spectrosc.* **46**, 483-492 (2015).

14. Zhao, H. *et al.* Characterization of microcrystals in some ancient glass beads from china by means of confocal Raman microspectroscopy. *J. Raman Spectrosc.* **44**, 643-649 (2013).

15. Di Martino, D. *et al.* The intriguing case of silicon crystals unveiled in ancient mosaic tesserae. *J. Raman Spectrosc.* **43**, 1824-1827 (2012).

16. Colomban, P. *et al.* Raman identification of materials used for jewellery and mosaics in Ifriqiya. *J. Raman Spectrosc.* **34**, 205-213 (2003).

17. Lysandrou, V. *et al.* Towards a spectral library of Roman to Early Christian Cypriot floor mosaics. *J. Archaeol. Sci. Reports.* **14**, 782-791 (2017).

18. Gill, M. S. *et al.* Material characterization of ceramic tile mosaic from two 17th century Islamic monuments in northern India. *Archaeometry*. **53**, 22-36 (2011).

19. Germinario, C. *et al.* Multi-analytical and non-invasive characterization of the polychromy of wall paintings at the Domus of Octavius Quartio in Pompeii. *Eur. Phys. J. Plus.* **133**, 359-370 (2018).

20. Grifa, C. *et al.* The domus of Octavius Quartio in Pompeii: Damage diagnosis of the masonries and frescoed surfaces. *Int. J. Conserv. Sci.* **7,** 885-900 (2016).

21. Popelka-Filcoff, R. S. *et al.* Trace element characterization of ochre from geological sources. *J. Radioanal. Nucl. Chem.* **272**, 17-27 (2007).

22. Jercher, M. *et al.* Rietveld X-ray diffraction and X-ray fluorescence analysis of Australian aboriginal ochres. *Archaeometry*. **40** ,383-401 (1998).

23. Aliatis, I. *et al.* Pigments used in Roman wall paintings in the Vesuvian area. *J. Raman Spectrosc.* **41**, 1537–1542 (2010).

24. Castriota, M. *et al.* Micro-Raman characterizations of Pompei's mortars. *J. Raman Spectrosc.* **39**, 295–301 (2008).

25. Miriello, D. *et al.* Non-destructive multi-analytical approach to study the pigments of wall painting fragments reused in mortars from the archaeological site of Pompeii (Italy). *Minerals*. **8**, 134-148 (2018).

26. Piovesan, R. *et al.* The Temple of Venus (Pompeii): a study of the pigments and painting techniques. *J. Archaeol. Sci.* **38**, 2633–2643 (2011).

27. Giachi, G. *et al.* Raw materials in Pompeian paintings: characterization of some colors from the archaeological site. *Mater. Manuf. Process.* **24**, 1015–1022 (2009).

28. Santacroce, R. *et al.* Age and whole rock-glass compositions of proximal pyroclastics from the major explosive eruptions of Somma-Vesuvius: a review as a tool for distal tephrostratigraphy. *J Volcanol. Geotherm. Res.* **177**, 1-18 (2008).

29. Cioni, R. *et al.* Thermal and compositional evolution of the shallow magma chambers of Vesuvius: evidence from pyroxene phenocrysts and melt inclusions. *J. Geophys. Res. Solid. Earth.* **103**, 18277–18294 (1998).

30. Morra, V. *et al.* Urban geology: relationships between geological setting and architectural heritage of the Neapolitan area. *J. Virt. Explor.* **36**, 26-85 (2010).

31. Freeman, J. J. *et al.* Characterization of natural feldspars by Raman spectroscopy for future planetary exploration. *Can. Mineral.* **46**, 1477–1500 (2008).

32. Bersani, D. *et al.* Plagioclase composition by Raman spectroscopy. *J. Raman Spectrosc.* **49**, 684–698 (2018).

33. Shebanova, O. N. *et al.* Raman spectroscopic study of magnetite ($FeFe_2O_4$): a new assignment for the vibrational spectrum. *J. Solid State Chem.* **174**, 424–430 (2003).

34. Shea, T. *et al.* Leucite crystals: surviving witnesses of magmatic processes preceding the 79 AD eruption at Vesuvius, Italy. *Earth Planet Sci. Lett.* **281**, 88-98 (2009).

35. Madariaga, J. M. *et al.* Portable Raman, DRIFTS, and XRF analysis to diagnose the conservation state of two wall painting panels from Pompeii deposited in the Naples national archaeological museum (Italy). *Appl. Spectrosc.* **70**, 137–146 (2016).

36. García-Florentino, C. *et al.* A fast in situ non-invasive approach to classify mortars from a construction of high historical value. *Microchem. J.* **133**, 104–113 (2017).

37. Savelli C. The problem of rock assimilation by Somma-Vesuvius magma. *Contrib. Mineral Petrol.* **16**, 328-353 (1967).

9. EVALUATION OF CALCIUM CARBONATE DEGRADATION IN THE WALL PAINTINGS THROUGH STABLE ISOTOPES ANALYSIS

9.1 Introduction

Mortars are artificial mixtures of a binder, water and sand. Most of the mortars used in Ancient Roman period were lime mortars[1], in where the binder used was the lime. Previous studies revealed that in the Pompeian lime mortars, natural pozzolana or cocciopesto fragments were added to the mortars[2,3]. The advantages of pozzolanic additives to the lime mortars are well known since antiquity. In Pompeii volcanic materials were added to create the pozzolanic mortars and brick and pottery fragments as cocciopesto fragments[2,3].

Considering that Pompeian mortars are based on lime, calcium carbonate is widely present in them after their setting. Therefore, the stable isotope analysis mainly of C and O in this type of mortars[4], becomes of great interest for several reasons. On the one

hand, this kind of analysis can offer information about similarities or differences in the isotope composition, which can allow establishing a similar or different technological production of the construction materials or even information about the origin of the materials used[5]. On the other hand, C and O isotope analysis can help to explain possible degradations[5]. Secondary carbonates can be formed once the original carbonates are exposed to the atmosphere[6]. As it has been mentioned at the beginning of this part, the loss of pictorial layer in the wall paintings of Pompeii is nowadays evident. If the calcium carbonate in the *intonachino*/*intonaco*, which acts as the binder of the pigment grains, is transformed into a more soluble compound, the binding ability decrease, jeopardizing in this sense the adhesion of the pigment grains to the *intonaco* of the wall. Nowadays, in the literature, few works can only be found dealing with the stable isotope ratio analysis of calcite-based mortars[5-7]. In some of the mentioned works[5,7], the C and O isotopic composition of the calcite matrix was analyzed to get knowledge about the environmental conditions during calcite formation. For that, Roman, medieval and early modern buildings mortars from Styria (Austria)[5] and Attiki (Greece)[7] were used. CO_2 absorption experiments performed by Kosednar-Liegenstein *et al.*[5] showed that, in an ideal case, the calcite in lime mortar and plasters is isotopically lighter in the external vs. the internal parts of the mortar. This variation was related to the evaporation of water in the mortar, the influence of surrounding CO_2 (e.g., from biogenic origin), recrystallization of calcite during the reaction of lime, etc. However, no references can be found in the literature dealing with the C and O isotopic analysis of the *intonachino*, *intonaco* or *arriccio* in a Roman wall painting stratigraphy.

Apart from C and O stable isotopes, sulfur isotope analysis could be also of interest to extract information about weathering of mortars in wall paintings. Nowadays, it is possible to identify the presence of sulfur in the ancient mortars of Pompeii[8]. In Pompeii, sulfates can be found mainly crystallized as efflorescences, but also as sub-efflorescences inner in the mortar. A previous work pointed out that the salts crystallizations in Pompeian walls can be formed due to the rainwater infiltration among the pores of the

calcite-based walls[8]. In this sense, sulfur isotope analysis can help to conclude the origin of the sulfur[9,10]. Apart from the influence of rainwater, sulfates can be present in the mortar coming from the waters used to create the original mortars, or they can be formed due to the interaction of the calcium carbonate from the mortar with atmospheric SO_x (from the 79 AD eruption or from the current atmosphere). Moreover, new sulfates input can be included also in the mortar coming from infiltration waters rich in sulfates.

During the thousands of years that the ancient city of Pompeii was buried, the walls and wall paintings have been in constant contact with the tephra deposits emitted by Mount Vesuvius (ashes and lapilli mainly). Volcanic ash and lapilli in contact with rainwater and/or groundwater can leach different anions and cations[11-13], sulfates among them. In the case of Pompeii, these ions might migrate to the walls contributing to the formation of new salts crystallizations. However, this hypothesis is not confirmed yet by any author.

Since the excavations conducted in the 19th century, walls and wall paintings of Pompeii have been subjected to different restorations. In the last decades, modern mortars were also incorporated to the walls. These materials might also promote the formation of efflorescences due to the inclusion in the wall of some ions present in their composition such as SO_4^{2-}, K^+, Na^+, etc[14]. These ions can be dissolved and can be mobilized giving rise to the formation of new salts crystallization on the porous structure of the mortars and on their surface[14].

In this chapter, the stable isotopic composition (C, O and S) of different mortars and wall painting fragments from the Archaeological Park of Pompeii, some of them recovered from the burial and others exposed nowadays to the atmosphere since the excavation of the Pompeian house, was determined. Concretely, samples were obtained from two private Pompeian houses: The House of Marcus Lucretius (HML) and The House Ariadne (HA). Two were the main objectives proposed in this case: (i) to identify possible

similarities or differences in the mortars extracted from different areas of each house, and among the two considered houses, according to the stable isotope analysis, (ii) to explain possible degradations in the mortars, such as the formation of secondary carbonates in the mortars, that can suggest a possible transformation process of the calcium carbonate that binds the pigment grains to the wall. For that, carbon ($\delta^{13}C$) and oxygen ($\delta^{18}O$) isotopic ratios were determined not only in the original Pompeian mortars, but also they were investigated in commercial restoration mortars used nowadays to consolidate historical mortars. The second established objective was to evaluate if the volcanic strata covering the Pompeian walls, SO_2 emissions during the volcanic events of the 79 AD, the used modern restoration mortars and/or the atmospheric SO_x of the current atmosphere are the responsible of the sulfate salts crystallizations widely present in the Pompeian walls and wall paintings. To achieve this objective, S isotopic ratio analysis ($\delta^{34}S$) was determined on the mentioned Pompeian mortars, modern restoration mortars and volcanic strata recovered from the Archaeological Park of Pompeii. Moreover, the mentioned stable isotopic values were also determined in efflorescences of recent formation from the HA to determine the possible origin of the salts present in the salts crystallizations formed on the surface of the mural paintings.

9.2 Description of the samples

In this chapter, four groups of samples were considered: Pompeian mortars and wall painting fragments, restoration mortars, efflorescences and volcanic strata (see Table 1).

As it has been mentioned above, mortars and wall painting fragments from two Pompeian houses were considered. On the one hand, fragments recovered in 2007 from the burial of the House of Marcus Lucretius (Reg IX, Ins 3, 5/24), and not exposed to the current atmosphere since their recovery were considered. These fragments were kindly

provided by the *Expeditio Pompeiana Universitatis Helsingiensis* group[15]. This house was firstly excavated between years 1846 and 1847.

On the other hand, additional fragments from the House of Ariadne (Reg VII, Ins 4, 31/51) were also analyzed. This house was excavated during the years 1822, 1832 and 1846. The fragments considered in this work were extracted in 2014 from exposed areas to the atmosphere since the recovery of the house in the 19th century.

To determine the stable isotopic composition of mortars and wall paintings fragments, the different parts of the samples were separated using the Dremel® 3000 (Wisconsin, USA) and connecting various polishing tools. For the mortar samples without decorations, the *intonaco* and *arriccio* layers were separated. If the aggregate was easily separable from the rest of the mortar, it was also considered as a separated sample. In the wall painting fragments, minimally the pictorial layer, *intonaco* and *arriccio* were separated. In some cases, the *arriccio* was also separated as external and internal. Besides, a thin layer on the top of the *intonaco* was also separated and considered as *intonachino*. In specific cases, on the top of the intonaco two thin layers were identified and separated as "i*ntonachino* external" and "*intonachino* internal". In some samples also, two *intonaco-s* were distinguished on the top of the *arriccio* and they were separated as "*external intonaco*" and "*internal intonaco*".

The separated pictorial layer compromises the superficial pigment. In some cases two pigment layers were identified, associated with possible repaints. These layers were labeled as "Pictorial layer, external" and "Pictorial layer, internal". Moreover, since the polychrome in the fragment 44 + 45 was scarce, sample 44 represents the mixture of the pigment layer and *intonaco*. In all the cases when the sample label refers to "external" or "internal" it belongs to the most external and most internal layer in the stratigraphy respectively.

Apart from mortars and wall paintings, additional efflorescence samples extracted from the wall paintings of rooms 17 and 22 from the HA were also considered. These rooms have been restored less than 10 years ago. A sample of the restoration mortar used in the HA was also considered (see sample 54 in Table 9.1). Moreover, Biocalce and GeoLite mortars from Kerakoll® (Castellón, Spain) were also considered for comparison purposes. The Biocalce is a lime mortar which includes natural puzzolanic materials for its use in the restoration of mortars. The GeoLite is a geo-mortar usually employed for the concrete restoration or reparation. This last kind of mortar should not be used for the restoration of wall paintings. However, its sulfur isotopic ratio was evaluated to determine the possible influence of this kind of modern mortars in the formation of new salts crystallizations.

Finally, a stratigraphy of seven tephra deposits or volcanic materials ("Layer 1" or superficial/external to "Layer 7" or the most internal one) recovered from the vicinity of *Porta Marina* in the Archeological Park of Pompeii were also considered.

Fig. 9.1. Description of the samples together with the obtained $\delta^{13}C$, $\delta^{18}O$ and $\delta^{34}S$ compositions.

Sample	Location	Code	Sample description	$\delta^{13}C$	$\delta^{18}O$	$\delta^{34}S$
1	House of Marcus Lucretius (triclinium)	Intonaco	East wall	-12.99 ± 0.19	-18.47 ± 0.13	-
2			North wall	-8.66 ± 0.08	-12.73 ± 0.01	-
3			West wall	-14.94 ± 0.09	-20.43 ± 0.24	-
4			East wall	-14.26 ± 0.06	-17.94 ± 0.18	-
5	House of Marcus Lucretius (north wall of triclinium)	Wall Painting	Pictorial layer	-14.95 ± 0.98	-11.54 ± 0.44	-
6			Intonaco	-9.51 ± 0.09	-9.21 ± 0.13	2.63 ± 0.27
7			Arriccio	-8.95 ± 0.35	-15.19 ± 0.22	2.57 ± 0.05
8	House of Marcus Lucretius (north wall of triclinium)	Wall Painting	Pictorial layer	-11.47 ± 0.16	-10.77 ± 0.55	2.35 ± 0.19
9			Intonaco	-9.58 ± 0.17	-11.08 ± 0.32	2.82 ± 0.18
10			Arriccio	-11.29 ± 0.05	-17.71 ± 0.18	2.8 ± 0.28
11	House of Marcus Lucretius (south wall of the atrium)	Wall Painting	Pictorial layer	-15.85 ± 0.12	-10.4 ± 0.18	-
12			Intonachino	-13.72 ± 0.13	-9.82 ± 0.24	-
13			Intonaco	-12.36 ± 0.03	-8.99 ± 0.19	-
14			Arriccio	-11.85 ± 0.13	-9.4 ± 0.35	12.13 ± 0.02
15	House of Marcus Lucretius (north wall of the atrium)	Wall Painting	Pictorial layer	-12.99 ± 0.06	-14.66 ± 0.05	-
16			Intonachino	-11.33 ± 0.14	-13.90 ± 0.20	-
17			Intonaco	-9.41 ± 0.10	-11.64 ± 0.40	-
18			Arriccio, external	-9.76 ± 0.45	-13.92 ± 0.43	-
19			Arriccio, internal	-10.17 ± 0.28	-13.93 ± 0.24	10.44 ± 0.03
20	House of Marcus Lucretius (room 7, Tablinum)	Wall Painting	Pictorial layer	-13.57 ± 0.08	-8.67 ± 0.10	14.60 ± 0.29
21			Intonachino, external	-13.58 ± 0.10	-8.54 ± 0.16	13.25 ± 0.25
22			Intonachino, internal	-11.84 ± 0.02	-7.25 ± 0.04	-
23			Intonaco, external	-10.72 ± 0.03	-7.11 ± 0.02	11.75 ± 0.20
24			Intonaco, internal	-11.83 ± 0.46	-16.05 ± 1.09	11.27 ± 0.43
25			Arriccio	-13.06 ± 0.21	-16.20 ± 0.05	15.51 ± 0.14
26	House of Marcus Lucretius	Wall	Pictorial layer	-13.72 ± 0.08	-8.83 ± 0.06	-

27	(room 7, Tablinum)	Painting	Intonachino	-12.20 ± 0.05	-7.44 ± 0.10	-
28			Intonaco	-12.73 ± 0.38	-13.13 ± 0.15	13.73 ± 0.29
29			Arriccio, external	-12.78 ± 0.28	-13.16 ± 0.38	14.28 ± 0.08
30			Arriccio, internal	-14.09 ± 0.11	-13.87 ± 0.07	14.19 ± 0.25
31	House of Ariadne (behind room 17)	Wall Painting	Pictorial layer, external	-11.69 ± 0.15	-9.09 ± 0.31	6.41 ± 0.11
32			Pictorial layer, internal	-12.06 ± 0.03	-5.97 ± 0.02	7.07 ± 0.12
33			Intonachino	-11.12 ± 0.05	-6.08 ± 0.04	6.89 ± 0.14
34			Intonaco, external	-10.09 ± 0.06	-5.99 ± 0.13	8.70 ± 0.28
35			Intonaco, internal	-11.28 ± 0.05	-6.70 ± 0.11	10.79 ± 0.20
36	House of Ariadne (room 18)	Wall Painting	Pictorial layer	-13.15 ± 0.06	-11.43 ± 0.25	-
37			Intonaco	-12.03 ± 0.10	-11.20 ± 0.31	-
38			Arriccio	-12.85 ± 0.26	-17.04 ± 0.33	9.28 ± 0.03
39	House of Ariadne (room 28)	Wall Painting	Pictorial layer	-8.92 ± 0.16	-8.15 ± 0.14	2.99 ± 0.17
40			Intonaco	-10.77 ± 0.23	-9.36 ± 0.13	4.26 ± 0.03
41			Arriccio	-11.24 ± 0.16	-15.17 ± 0.26	6.59 ± 0.23
42	House of Ariadne (behind room 31)	Wall Painting	Pictorial layer	-10.69 ± 0.13	-16.17 ± 0.14	4.23 ± 0.43
43			Intonaco	-9.76 ± 1.76	-13.69 ± 1.43	2.11 ± 0.06
44	House of Ariadne (room 31)	Wall Painting	Pictorial layer + Intonaco	-11.67 ± 0.6	-14.22 ± 0.45	-0.49 ± 0.10
45			Arriccio	-10.36 ± 0.06	-7.08 ± 0.09	1.57 ± 0.12
46	House of Ariadne (impluvium)	Mortar	Pozzolanic aggregate	-3.41 ± 0.45	-4.46 ± 0.05	5.47 ± 0.18
47			Arriccio	-1.15 ± 0.22	-5.94 ± 0.19	6.55 ± 0.03
48	House of Ariadne (room 22)	Mortar	Intonaco	-12.11 ± 0.42	-15.60 ± 0.38	6.37 ± 0.07
49			Arriccio	-8.71 ± 0.04	-7.42 ± 0.12	5.27 ± 0.21
50	House of Ariadne (between room 22 and 23)	Mortar	Intonaco	-10.71 ± 0.50	-10.13 ± 0.88	13.57 ± 0.04
51			Arriccio	-5.50 ± 0.09	-6.04 ± 0.14	2.41 ± 0.17
52	House of Ariadne (room 7)	Mortar	Intonaco	-13.1 ± 0.21	-9.19 ± 0.30	7.72 ± 0.06
53			Arriccio	-13.07 ± 0.20	-15.03 ± 0.23	-
54	House of Ariadne (room 17)	R. Mortar	Restoration mortar	-5.04 ± 0.56	-6.54 ± 0.18	-
55		Effl.	Efflorescence	-	-	6.39 ± 0.04
56	House of Ariadne (room 22)	Effl.	Efflorescence	-	-	2.2 ± 0.06

57		Effl.	Efflorescence	-	-	1.9 ± 0.07
58	Commercial mortar	R. Mortar	Geolite mortar	-	-	0.3 ± 0.03
59		R. Mortar	Biocalce mortar	-	-	3.9 ± 0.12
60	Volcanic strata	VS	Layer 1	-	-	5.43 ± 0.21
61			Layer 2	-	-	5.27 ± 0.19
62			Layer 3	-	-	5.47 ± 0.23
63			Layer 4	-	-	5.82 ± 0.12
64			Layer 5	-	-	4.77 ± 0.12
65			Layer 6	-	-	5.41 ± 0.16
66			Layer 7	-	-	4.79 ± 0.15

9.3 Molecular characterization of the efflorescences

The efflorescences considered in this work were analyzed directly by means of Raman microscopy, obtaining the representative spectrum shown in Fig. 9.1. Bands centered at 452, 621, 630, 93, 1084 and 1202 cm^{-1}, can be attributed to aphthitalite ($(K,Na)_3Na(SO_4)_2$).[8] On the other hand, Raman bands at 648, 1100, 1129 and 1152 cm^{-1}, together with main band at 993 cm^{-1} suggested the presence of thenardite (Na_2SO_4).[8]

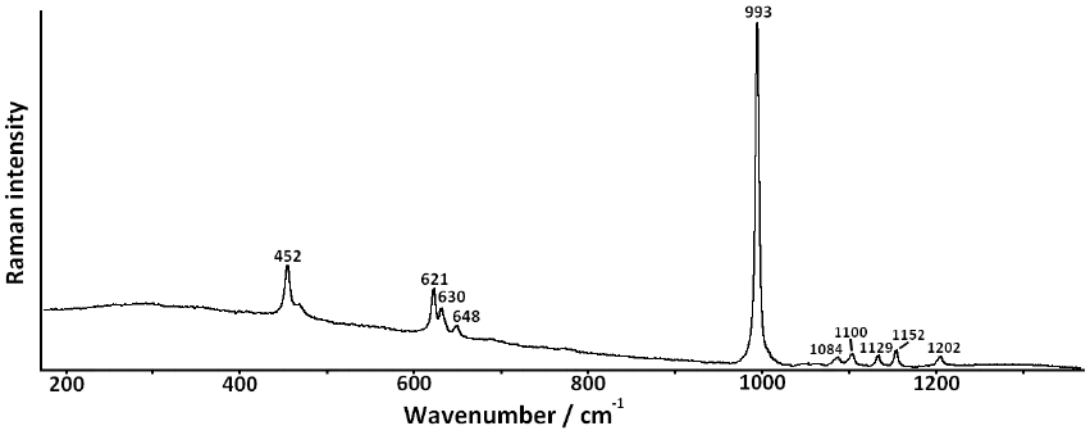

Fig. 9.1. Raman spectrum of the efflorescence present in room 17 showing the presence of aphthitalite and thenardite.

Both sulfate salts were previously determined in the composition of various efflorescences present in the House of Gilded Cupids of Pompeii, also in recently restored areas[8]. Therefore, aphthitalite and thenardite could be considered as common sulfates present in efflorescences of Pompeian houses**.**

9.4 Stable isotope composition analysis

9.4.1 Carbon and oxygen isotopic composition analysis

The analyzed carbonates exhibit a large range of $\delta^{13}C$ and $\delta^{18}O$ values (-20.4 to -7.1 and -17.0 to -1.15 ‰, respectively; see Fig. 9.2). The values of $\delta^{13}C$ and $\delta^{18}O$ obtained from the Pompeian wall painting fragments and mortar samples considered in this study is set within the determined ones in Roman mortars from Europe[5,7].

While the clusters of $\delta^{13}C$ and $\delta^{18}O$ values for the samples of the House of Marcus Lucretius (HML) and the House of Ariadne (HA) are almost overlapped, the average $\delta^{13}C$ and $\delta^{18}O$ values of the samples from the HML were depleted in heavy isotopes compared to the HA by about 2 ‰. In fact, the $\delta^{13}C$ values in the samples from HML were set between -15.9 and -8.7 ‰ (average of -12.1 ± 1.9 ‰, where the ± applies to 1 Standard Deviation) and $\delta^{18}O$ between -20.4 and -7.1 ‰ (average of -12.4 ± 3.6 ‰). In the samples from HA, the $\delta^{13}C$ values were set between -13.15 and -1.15 ‰ (average of -10.0 ± 3.1 ‰) and $\delta^{18}O$ between -17.0 and -4.5 ‰ (average of -9.9 ± 3.9 ‰). As it can be observed in Fig. 9.2, the shift toward less negative values in the samples from the HA is influenced by a group of samples extracted from the mortar used in the *impluvium* of this house (samples 46 and 47, see Table 9.1), mortars from rooms 17 (samples 31 to 35, see Table 9.1) and those from rooms 22/23 (samples 50 and 51, see Table 9.1).

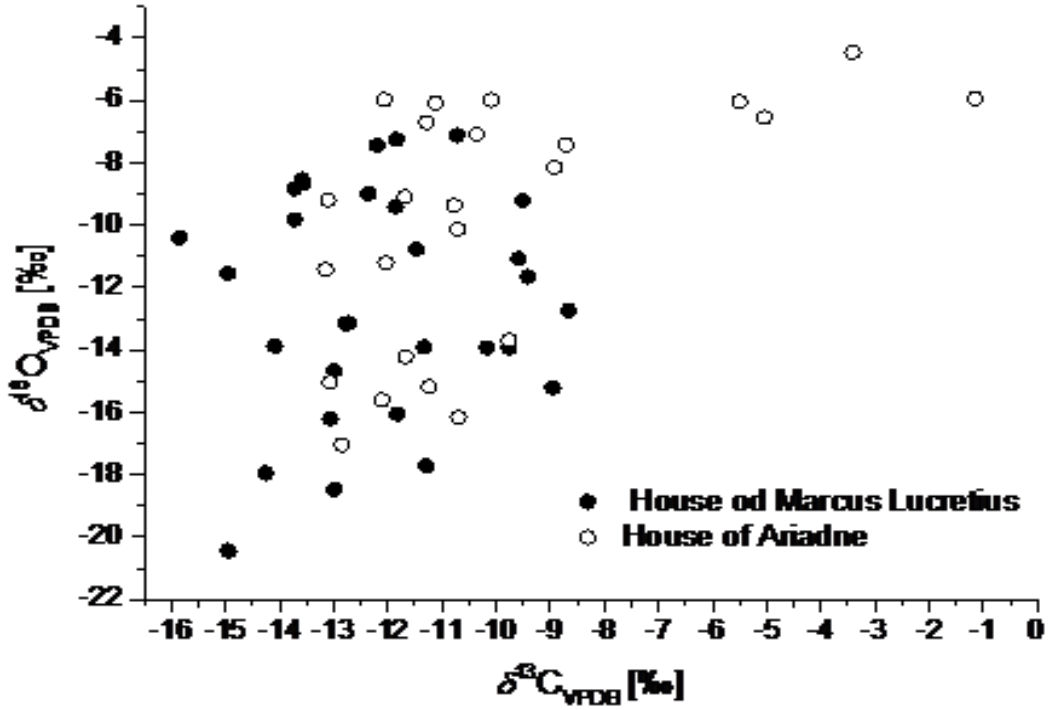

Fig. 9.2. $\delta^{13}C$ and $\delta^{18}O$ values for the mortars and wall painting samples from both houses.

Comparing with the mortars from Styria analyzed in a previous work[5], in this case, more positive $\delta^{18}O$ values were obtained. This could suggest that the water for the setting of the lime mortar was isotopically heavier than the one used in the mortars from Styria. Besides, the possibility that the water may be enriched in ^{18}O because of evaporation should be taken into account because the rainwater in Pompeii is enriched in heavy isotopes compared to the one of Austria due to the continental and latitude effects[16]. Comparison of the weighted average annual $\delta^{18}O$ values of local precipitation in Graz (Styria, Austria) and Fogliano (the closest coastal GNIP station to Pompeii) for the period from 1998 to 2002 showed a difference of 3.1 ‰ (annual average $\delta^{18}O_{VSMOW}$ of -8.37 ‰ in Graz and -5.27 ‰ in Fogliano)[17].

Since to manufacture the ancient mortars under analysis, the used limestone was burnt ($CaCO_3$ --> $CaO + CO_2$) the isotopic C signature of the raw material was lost in that process evaporated as CO_2. Thus, the original C signature that should be present in the mortars is the one coming from two different sources: (i) the bicarbonates present in the water used to react with the CaO ($CaO + H_2O$ --> $Ca(OH)_2$), that may be remained as residue in the formed $(CaOH)_2$; and ii) the CO_2 present in the ancient atmosphere that reacted with $Ca(OH)_2$ to produce the final lime mortar by a carbonation mechanism following the reaction $Ca(OH)_2 + CO_2$ --> $CaCO_3$. Possible traces of the original limestone in the mortars should not be discarded. Leaving aside this low contribution, the obtained results could be probably related to the combination of the C signature of the ancient CO_2 and the bicarbonates present in the water, although this last input surely had a minor contribution comparing to the ancient CO_2**.**

In fact, local limestone in the vicinity of Pompeii, which is suggested as ancient raw materials for burning[18], have $\delta^{13}C$ values around 0-1‰.[18,19] Accordingly, the calcite matrix of the historical lime mortar and plaster are mostly isotopically lighter compared to those of the local natural limestone, which are assumed to have been used for burning and as aggregates. Obviously, the isotope values of the calcite matrix are attributed to the slaking and especially to the setting of the lime mortar and plaster as commented above.

To compare the results from both houses, statistics were applied. The ANOVA with post-hoc Tukey-Kramer HSD calculator showed that both groups of samples (HML and HA) differ significantly from the statistical point of view at $p < 0.05$. Since the difference between the groups of samples is that those from HML were taken during excavation and they were not exposed to the current atmosphere, and those from the HA have been exposed to the recent atmosphere for 180 years, it can be expected that the exposure of fragments from the HA to the modern atmosphere, and concretely to modern CO_2, has influenced the original isotopic $\delta^{13}C$ and $\delta^{18}O$ values of the carbonates. This suggests that

secondary carbonates could have been produced in more extent in the HA due to the exposure to the modern CO_2.

In fact, degradation of mortars results in the formation of secondary carbonate in alkaline water film. This phenomenon occurs after atmospheric CO_2 absorption. Such carbonate incorporates the isotopic composition of oxygen from both sources[5,20], the OH^- from the dissociation of water and from atmospheric CO_2:

$$\delta^{18}O_{calcite} = \frac{1}{3}\,\delta^{18}O_{OH^-} + \frac{2}{3}\,\delta^{18}O_{CO_2} \qquad /1/$$

The O isotope fractionation factor between water and OH^- is 1.035 at 16°C (average annual temperature in Pompeii)[21] and the average $\delta^{18}O_{VPDB}$ of local precipitation is -35 ‰ (converted from the VSMOW scale using the equation $\delta^{18}O_{VSMOW} = 1.03092 \cdot \delta^{18}O_{VPDB} + 30.92$).[22] Using the equation /1/ and considering that the $\delta^{18}O_{VPDB}$ value of atmospheric O_2 is 10 ± 2 ‰,[23] the obtained $\delta^{18}O_{VPB}$ value of precipitates (secondary carbonates formation) is around -17 ‰ (between -18.3 and -15.6 ‰), which matches well with the measured values in this work. In principle, this should be the cut-off value for degradation of mortars (secondary carbonates formation). However, in the literature it is mentioned that due to the non-equilibrium conditions and rapid precipitation of carbonates, both the $\delta^{18}O$ and $\delta^{13}C$ values of secondary carbonates could be lower[5,7,24].

However, in both houses the isotopic C and O compositions show that more or less extended carbonate dissolution/re-precipitation had taken place on the surface of the walls and progressed toward the interior of them, because in most of the cases, both isotopic ratios shift to more positive values while going deeper in the stratigraphy of the wall paintings from the external to the internal layers (see Table 9.1). In this tendency, the *arriccio* layers should be not taken into consideration, since this kind of mortar usually includes a higher proportion of pozzolanic materials as aggregates in the mortar.

Once the walls or wall paintings are exposed to the atmosphere, the water sources that promote the re-crystallization of the calcium carbonate (secondary carbonates formation) could be either rain water or condensed water on the wall surfaces. In the samples from Pompeii, the $\delta^{13}C$ values are higher comparing with other Roman mortars such as the ones from Styria[5,7], which could suggest a possible influence of the exposure to the CO_2 coming from the Mount Vesuvius volcanic emissions.

In this sense, Mount Vesuvius in Pompeii represents from the past a constant source of CO_2 emanations to the atmosphere. However, there is little data on the isotopic composition of volcanic gases. Chiodini *et al.*[25] reported $\delta^{18}O_{VPDB}$ values between -7.5 to -0.5 ‰ for Mount Vesuvius CO_2 emissions. Moreover, for the CO_2 emission of Campi Phlegrei, a volcanic chain from the Campania region, values of -0.9 ‰ and +4 ‰ were reported for $\delta^{13}CV_{PDB}$ and $\delta^{18}O_{VPDB}$ respectively[26]. However, in the literature it is not possible to find any data related to the isotopic composition of atmospheric CO_2 in Pompeii. It is evident that the presence of volcanic CO_2 may shift slightly the $\delta^{18}O$ value of secondary calcium carbonate in Pompeian mortars toward more positive values. This comes in agreement with the mean $\delta^{18}O$ values of the fragments from both houses since the HML average is -12.4 ± 3.6 ‰ and the one from HA average is -9.9 ± 3.9 ‰, which suggest the influence of the CO_2 coming from Mount Vesuvius in the fragments from the HA exposed to modern CO_2 in the last 200 years.

9.4.2 Sulfur isotopic composition analysis

Due to the low content of sulfates in the mortar composition of some samples, in some cases it was not possible to obtain enough $BaSO_4$ precipitate after the sample treatment. Therefore, for some samples the $\delta^{34}S$ is not presented in Table 9.1. The results are reported in ‰ vs VCDT.

Regarding the $\delta^{34}S$ composition of the different volcanic strata, the obtained results were similar to those obtained in a previous work[27] following a different procedure described in the literature[28]. In this sense, as it is shown in Table 9.1, the obtained $\delta^{34}S$ ranged from 4.77 to 5.82‰, whereas results of the previous work showed that Plinian pumices of 79 AD eruption ranged from 5 to 5.3‰, which is consistent with the results obtained in this case.

Two different wall painting fragments from the HML showed $\delta^{34}S$ values between 2.3 and 2.8‰ (see samples 6 to 10 in Table 9.1,). The mortar of these fragments was light grey and easily breakable. Moreover, white accumulations or nodules, associated to calcium carbonate (verification done by Raman spectroscopy) were visually observed in the mortar. These calcium carbonate nodules were not identified in the rest of the mortar samples from the HML. In this case, the rest of the mortars showed a more grey appearance. These last fragments showed a completely different $\delta^{34}S$ composition, ranging from 10 to 15‰ (samples 14 and samples 19 to 30, see Table 9.1). Therefore, two different groups of mortar samples were determined in the HML according to the $\delta^{34}S$ composition (from 2.5‰ to 12-13‰). Taking into account that these fragments were recovered from the burial and thus, they were not exposed or influenced by the current atmosphere, the sulfur present should be related to the original materials used to manufacture the mortars.

Regarding the samples from the HA, the obtained $\delta^{34}S$ compositions ranged from -0.5‰ to 13‰. The values obtained for the *arriccio* were set between 5.3 to 7.7‰ (samples 31, 32 33, 41, 47, 48, 49 and 52; see Table 9.1), similar to the values obtained for the volcanic strata (4.7 to 6.4 ‰). This coincidence could indicate that volcanic materials were used as pozzolanic materials in the aggregate used to manufacture the mortars from the HA.

Three wall painting fragments (samples 31 to 35, 39 to 41 and 44-45; see Table 9.1) showed lighter $\delta^{34}S$ composition in the external areas comparing with the internal ones.

This lighter composition in the surface layer can be associated to: (i) leaching of sulfates present in the volcanic materials in contact with the walls in the burial, (ii) impact of the SO_x gases present in the past and current atmosphere. However, in the literature there are not works dealing with the $\delta^{34}S$ analysis of the SO_x from the current atmosphere.

Inner areas of mortars (*arriccio*) and wall painting fragments from the HA (samples 38, 41, 45, 49 and 51; see Table 9.1) showed different values, ranging from 1.5 to 9‰. There are significant differences in the $\delta^{34}S$ composition of all the analyzed *arriccio* samples. Considering that *arriccio* layers have not been exposed to the atmosphere since there are protected by the rest of the stratigraphy of the wall painting, the possible differences can be related to the original materials used to create the different *arriccio* layers from different areas in the HA. In fact, the fragments under study showed different aggregate particles (in color, shape…) which can led to these differences in the $\delta^{34}S$ composition.

Additionally, three wall painting fragments from the HA (samples 42-43, 48-49 and 50-51, see Table 9.1) showed heavier $\delta^{34}S$ values in the surface layers than in inner ones. Finally, the mortar fragment showing visually the use of pozzolanic aggregate (samples 46 and 47; see Table 9.1) showed values between 5.5 and 6.5‰, which matches with those obtained in the thephra deposit or volcanic materials.

Regarding the analyzed efflorescences, as it has been mentioned above, they belong to salts crystallizations of recent formation since those two rooms of the HA have been restored some years ago. The obtained $\delta^{34}S$ composition ranged from 1.9 to 6.41‰ (see Table 9.1), lower values comparing with the tephra deposits and the rest of the wall painting and mortar samples. In the literature there are not data regarding the $\delta^{34}S$ composition of sulfur containing gas emanations from Mount Vesuvius. However, it is expected that this value could be set quite close to the one of the tephra deposits.

The following additional external source which can contribute to the crystallization of sulfates in the walls and wall paintings of Pompeii can be also mentioned to explain the obtained results: (i) sulfates present in the rainwater, which in some cases can impact directly on the surface of the wall or impact from its back penetrating through the porous matrix, (ii) recently added modern restoration mortars, which incorporate sulfur in their composition and could migrate and react forming new salts in the surface or inside the pores of the mortar.

Unfortunately, due to technical problems, it was not possible to determine the $\delta^{34}S$ in the restoration mortar of the HA. However, it was possible to obtain the value in two different commercial restoration mortars. Their $\delta^{34}S$ composition ranged from 0.3 to 4‰ (see samples 58 and 59 in Table 9.1). It is necessary to remark that the $\delta^{34}S$ values obtained for the efflorescences present in the room 17 and 22 are quite different, being a lower value the one of the room 22 (see Table 9.1). This difference in the $\delta^{34}S$ value of both kind efflorescences could suggest that more than one input that promote the sulfate efflorescence formation are present. In this sense, the restoration mortars showed lower $\delta^{34}S$ values comparing with the ones obtained from the tephra deposits in the volcanic stratigraphy (see Table 9.1). This observation could suggest that a possible leaching of the sulfates present in the volcanic materials could contribute in a higher proportion in the formation of the salts crystallizations from the room 17, while efflorescences from room 22 (1.9-2.2‰ $\delta^{34}S$) could have been originated due to the influence of the modern restoration mortars, since $\delta^{34}S$ values are similar. Unfortunately, the applied restoration mortar could not be analyzed and the comparison is made with other commercial restoration mortars.

Moreover, this variability in the $\delta^{34}S$ values from the efflorescences of both rooms could be associated with the different volcanic materials accumulated in each parts of the Archaeological Park of Pompeii depending on the orientation of considered house/room inside the house.

9.5 Conclusions

In this part of the PhD Thesis, stable isotope analysis (carbon, oxygen and sulfur) of various Pompeian mortars and wall painting fragments, efflorescences and different volcanic strata obtained from the archaeological site from Pompeii has been conducted. The $\delta^{13}C$ and $\delta^{18}O$ results obtained came in agreement with the isotope compositions already identified in Roman mortars in previous works[5,7]. However, some variations in the obtained values were detected, mainly related probably to the volcanic CO_2 emissions. Additionally, the enrichment in heavy isotopes due to the impact of rainwater should be also confirmed in the future. According to the variation of the C and O isotopic values from the external to the internal part of the stratigraphy of the painting fragments (excluding the *arriccio*), a possible calcium carbonate dissolution/re-precipitation on the wall surfaces promoted by rainwater or condensed water had taken place on the surface of the walls and progressed toward the internal parts.

On the other hand, the $\delta^{34}S$ isotopic composition of the analyzed volcanic of tephra strata was established from 4.77 to 5.82‰. In the case of the HA, the obtained $\delta^{34}S$ values in the *arricio* and *intonaco* samples were between 5.3 to 7.7‰, similar to the ones of volcanic strata. This similar composition confirms that volcanic materials were used as pozzolanic materials as the aggregate in the manufacture of mortars from this house. Regarding the HML, two fragments showed $\delta^{34}S$ light values (around 2.5‰), while the remaining fragments offered heavier values (around 12-13‰). This difference could be associated to the specific kind of mortar used in the periods when the specific painting styles were executed. The $\delta^{34}S$ composition of the efflorescences was slightly lighter than the volcanic strata and *intonaco* and *arriccio* samples, and even lighter in one of the samples. The different values obtained in efflorescences formed in different rooms of the same house could suggest the influence of different sources (e.g., modern restoration mortars, leaching of sulfates present in the tephra deposits, etc.) in the formation of the analyzed sulfate crystallizations.

9.6 References

1. Laycock, E. A. *et al.* An investigation to establish the source of the Roman lime mortars used in Wallsend, UK. *Constr. Build. Mater.* **196**, 611-625 (2019).

2. De Luca, R., *et al.* Archaeometric study of mortars from the Garum Shop at Pompeii, Campania, Italy. *Geoarchaeology*, **30**, 330-351 (2015).

3. Miriello, D. *et al.* Characterisation of archaeological mortars from Pompeii (Campania, Italy) and identification of construction phases by compositional data analysis. *J. Archaeol. Sci.* **37**, 2207-2223 (2010).

4. Sharp, Z. Principles of stable isotope geochemistry. (New Jersey, Pearson Education, 2007).

5. Kosednar-Legenstein, B. *et al.* Stable carbon and oxygen isotope investigation in historical lime mortar and plaster–Results from field and experimental study. *J. Appl. Geochem.* **23**, 2425-2437 (2008).

6. Dotsika, E. *et al.* $\delta^{13}C$ and $\delta^{18}O$ Stable Isotope Analysis Applied to Detect Technological Variations and Weathering Processes of Ancient Lime and Hydraulic Mortars. *Geosci. J.* **8**, 339 (2018).

7. Dotsika, E. *et al.* Isotopic analysis for degradation diagnosis of calcite matrix in mortar. *Anal. Biooanal. Chem.* **395**, 2227-2234. (2009).

8. Prieto-Taboada, N., *et al.* Study of the soluble salts formation in a recently restored house of Pompeii by in-situ Raman spectroscopy. *Sci. Rep*. **8**, 1613 (2018).

9. Vallet, J. M. *et al.* Origin of salts in stone monument degradation using sulphur and oxygen isotopes: First results of the Bourges cathedral (France). *J. Geochem. Explor.* **88**, 358-362 (2006).

10. Kloppmann, W. *et al.* Building materials as intrinsic sources of sulphate: A hidden face of salt weathering of historical monuments investigated through multi-isotope tracing (B, O, S). *Sci. Total Environ.* **409**, 1658-1669 (2011).

11. Fiantis, D. *et al.* Leaching experiments in recent tephra deposits from Talang volcano (West Sumatra), Indonesia. Geoderma, **156**, 161-172 (2010).

12. Bosshard-Stadlin, S. A. *et al.* Leaching of lava and tephra from the Oldoinyo Lengai volcano (Tanzania): Remobilization of fluorine and other potentially toxic elements into surface waters of the Gregory Rift. *J. Volcanol. Geotherm. Res.* **332**, 14-25 (2017).

13. Cabré, J. *et al.* Volcanic ash leaching as a means of tracing the environmental impact of the 2011 Grímsvötn eruption, Iceland. *Environ. Sci. Poll. Res.* **23**, 14338-14353. (2016).

14. Maravelaki-Kalaitzaki, P. *et al.* Sorel's cement mortars: Decay susceptibility and effect on Pentelic marble. *Cement Concrete Res.* **29**, 1929-1935 (1999).

15. https://blogs.helsinki.fi/pompeii-project/ (Accessed: 8th October 2019)

16. Dansgaard, W. Stable isotopes in precipitation. *Tellus,* **16** , 436-468 (1964)

17. IAEA/WMO (2019). Global Network of Isotopes in Precipitation. The GNIP Database. Accessible at: http://www.iaea.org/water (Accessed: 8th October 2019)

18. Kastenmeier, P. *et al.* The source of stone building materials from the Pompeii archaeological area and its surroundings. *Period. Mineral*. **79**, 39-58 (2010).

19. Vinci, F. *et al.* Early dolomitization in the Lower Cretaceous shallow-water carbonates of Southern Apennines (Italy): Clues about palaeoclimatic fluctuations in western Thetys. *Sediment. Geol*. **362**, 17-36 (2017).

20. Usdowski, E. *et al.* Oxygen isotope Exchange between carbonic acid, bicarbonate, carbonate and wáter: a re-examination of the data of McCrea (1950) and an expression of the overall partitioning of oxygen isotopes between the carbonate species and water. *Geochim Cosmochim. Acta*, **57**, 3815-3818 (1993).

21. Walters, W.W. *et al.* Theoretical calculation of oxygen equilibrium isotope fractionation factors involving various NO_y molecules, OH, and H_2O and its implications for isotope variations in atmospheric nitrate. *Geochim Cosmochim. Acta,* **191**, 89-101 (2016).

22. Coplen, T.B. New guidelines for the reporting of stable hydrogen, carbon, and oxygen isotope ratio data: *Geochim Cosmochim. Acta,* **60**, 3359-3360 (1996).

23. Eiler, J.M. *et al.* ^{18}O, ^{13}C, ^{16}O in Earth's atmosphere. *Geochim Cosmochim. Acta,* **68**, 4767-4777 (2004).

24. Zavadlav, S. *et al.* C and O stable isotopic signatures of fast-growing dripstones on alkaline substrates: reflection of growth mechanism, carbonate sources and environmental conditions. *Isot. Environ. Healt. S.* **48**, 354-371 (2012).

25. Chiodini, G. *et al.* ^{18}O exchange between steam and carbon dioxide in volcanic and hydrothermal gases: Implication for the sources of water. *Geochim Cosmochim. Acta,* **64**, 2479-2488 (2000).

26. Federico, C. *et al.* CO_2 degassing at La Solfatara volcano (Phlegrean Fields): Process affecting $\delta^{13}C$ and $\delta^{18}O$ of soil CO_2. *Geochim Cosmochim. Acta,* **74**, 3521-3538 (2010).

27. Marini, L. *et al.* Effect of degassing on sulfur contents and δ 34 S values in Somma-Vesuvius magmas. *Bull. Volcanol.* **60**, 187-194 (1998).

28. Sasaki, A. *et al.* Kiba reagent method of sulfur extraction applied to isotopic work. *Bull. Geol. Surv. Jpn.*, **30**, 241-245 (1979).

10. IN SITU EDXRF METHOD TO DIFFERENTIATE ORIGINAL RED OCHRES FROM TRANSFORMED YELLOW OCHRES INTO RED

10.1 Introduction

Spectroscopic techniques for molecular analysis such as Raman and infrared spectroscopy, do not offer conclusive information to discriminate between original red ochre from yellow ochre transformed into red, since both of them offer the same molecular information (α-Fe_2O_3). As it has been mentioned in the introduction of the Part 2 of this manuscript, at this moment, there is not a robust analytical methodology to discriminate the original red from the one obtained from the transformation of the yellow ochre. Moreover, the unique attempts made in this sense involved the extraction of samples[1]. Considering the actual restrictions in the Archaeological Park of Pompeii, a

discrimination methodology based on the use of portable/handheld non-invasive techniques would be convenient to develop.

In this sense, some minor/trace elements present in the original red ochres against the transformed yellow ochre could allow to obtain a possible discrimination. The main analytical techniques to detect such elements that can be used in their portable version are Laser Induced Breakdown spectroscopy (LIBS) and X-ray fluorescence spectrometry (XRF).

LIBS technique cannot be considered a totally non-invasive technique, since during measurements nanograms-micrograms of material are ablated by the action of the laser that impacts the surface under study[2–5]. The result of this process is the formation of a micro-crater[5–7] whose diameter, usually around 100-300 μm, depends on the energy pulse of the laser, the number of pulses and the nature of the ablated material[5]. The information collected by the detector is the emission of the elements excited in the plasma generated during the ablation process, most of them already collected and published in *National Institute of Standards and Technology* (NIST) database[8,9]. In some cases, elements can be recombined in the formed plasma giving rise to molecules that can offer molecular emissions detectable by the spectrometer and useful to detect/quantify the elements present in the surface under study[10–15].

On the contrary, X-ray fluorescence spectrometry can be considered a completely non-invasive technique. As LIBS, XRF is able to detect/quantify the presence of minor/trace elements up to $\mu g \cdot g^{-1}$ units (ppm). If both techniques are compared, the main advantage of LIBS against XRF could be the improvement in the detection of light elements with atomic numbers lower than nine. However, as a previous work pointed out[16], if portable/hand-held LIBS systems are used, the discrimination of the origin of elements such as H, C, N and O would be quite difficult since they could come from the atmospheric composition. Moreover, in both techniques the sensitivity could be limited

by the interferences from other elements, which is more marked in the case of LIBS due to the higher number of emission lines comparing with XRF.

Previous works dealing with the XRF elemental analysis of different ochres[17–19] determined the presence of trace elements with the aim of classifying them depending on the source. Concretely, in the works performed by Popelka-Filcoff *et al.*[17,18] the elemental composition of ochre pigments from Missouri (USA) was analyzed by means of XRF and Neutron Activation Analysis (INAA). Afterwards, the elemental compositions were compared with the ones of near iron ore formation materials that could postulate to be the source of these ochre pigments. In that work, Principal Component Analysis (PCA) was applied to the elemental data matrix, confirming the provenance of the analyzed ochre pigments against the iron ore formation candidates. Thereby, similarities or differences in the minor/trace elemental composition between samples and source materials could give useful information regarding their possible provenance or origin.

Besides, Jercher *et al.*[19] characterized red and yellow ochre samples from Aboriginal deposits in South and Western Australia. The ochres were found to have complex trace elemental signatures. Thus, once again, the geochemistry of the ochres was used to identify their source.

Recently, in this year 2019, Richards *et al*.[20] has demonstrated that elements such as Ti, Zr, Y and Nb are good tracers to achieve a reliable classification of volcanic rocks and for alkaline or sub-alkaline determinations. Besides, many are the works[21–24] dealing with the use of PCA or discriminant analysis based on the elemental data acquired by XRF in the provenance study of volcanic glass and obsidians. Therefore, as demonstrated in the literature, the combination of XRF data with chemometrics is a powerful tool for classification and provenance studies.

LIBS, in less extent than XRF, in combination with chemometrics has been also used with the same purpose[25–27]. In the work developed by Alvey *et al.*[25], statistical signal processing and classification techniques were applied to LIBS spectra acquired on mineral garnet. LIBS spectra of 157 garnets of different composition from 92 locations worldwide were acquired and Partial Least Squares discriminant analysis (PLS-DA) was used to successfully classify the garnet samples based on both their composition and geographic origin. However, in that work the measurements were performed in the laboratory by means of a benchtop LIBS instrumentation instead of using a portable spectrometer.

The work by Colao *et al.*[26] presents the characterization of historical building materials according to the geographic origin of the quarries from which they were mined. Major and trace elements on 48 different specimens were determined using LIBS. The sample set was divided in two different groups: a reference set from 8 different quarries located in Seville province and a second set of specimens of unknown provenance collected in several historical buildings and churches in the city of Seville. Data analysis was performed using PCA and SIMCA. A clear separation among reference sample materials mined from different quarries was observed in the PCA score plots. Moreover, a supervised SIMCA classification was used to assess the provenance of unknown samples.

The study performed by Harmon *et al.*[27] illustrated through four examples (carbonate minerals and rocks, columbite–tantalite mineral pair, garnet and native gold) how portable LIBS analyzers can be used for real-time chemical analysis for provenance determination and natural resource exploration. In this sense, the distinguishing chemical characteristics of the analyzed samples were identified through PCA. PLS-DA was also used to distinguish and classify the materials, with excellent results.

In this chapter, HH-XRF and p-LIBS spectrometers were tested as potential techniques useful to construct discriminative models able to distinguish the original red ochre areas from those formed due to the transformation of original yellow ochre pigment in the wall

paintings of the Archaeological Park of Pompeii. The results obtained with both techniques are compared to decide if both or only one of them will be useful for the construction of the discrimination model of original red pigment against yellow ochre pigment transformed into red.

In order to guarantee the representativeness of the results, two mural paintings from The House of Marcus Lucretius (Reg IX, Ins 3,5,24) and The House of Gilded Cupids (Reg VI, Ins 16, 7, 38) were selected. Both panels show a clear transformation of the yellow ochre pigment and areas of original red and yellow ochre pigments.

To ensure that in the original red, original yellow and transformed yellow (nowadays red) areas no additional mineralogical phases to those related with ochre pigments are present, in situ Raman spectroscopy was used for the molecular screening of the painting areas under study. The elemental data matrix obtained was subjected to multivariate analysis using PCA to construct the discrimination model based on the minor/trace elements present in all the areas under study. To confirm the conclusions extracted from the in situ analyses of the affected wall paintings, additional elemental analyses were conducted in the laboratory using a benchtop EDXRF spectrometer on raw red and yellow ochre pigments from the Naples National Archaeological Museum (MANN). These pigments are the same than those presented in the Chapter 5 of this manuscript.

10.2 Description of the analyzed wall paintings

Two Pompeian wall paintings showing the transformation of the yellow ochre were considered in this work. One located in the House of Marcus Lucretius (Reg IX, Ins 3,5,24), previously described in Chapter 9, and the second one in the House of Gilded Cupids (Reg VI, Ins 16, 7, 38) (see Fig. 10.1). The House of Marcus Lucretius excavated between years

1846 and 1847 preserves nowadays *Fourth Style* wall paintings in a relatively well state of conservation.

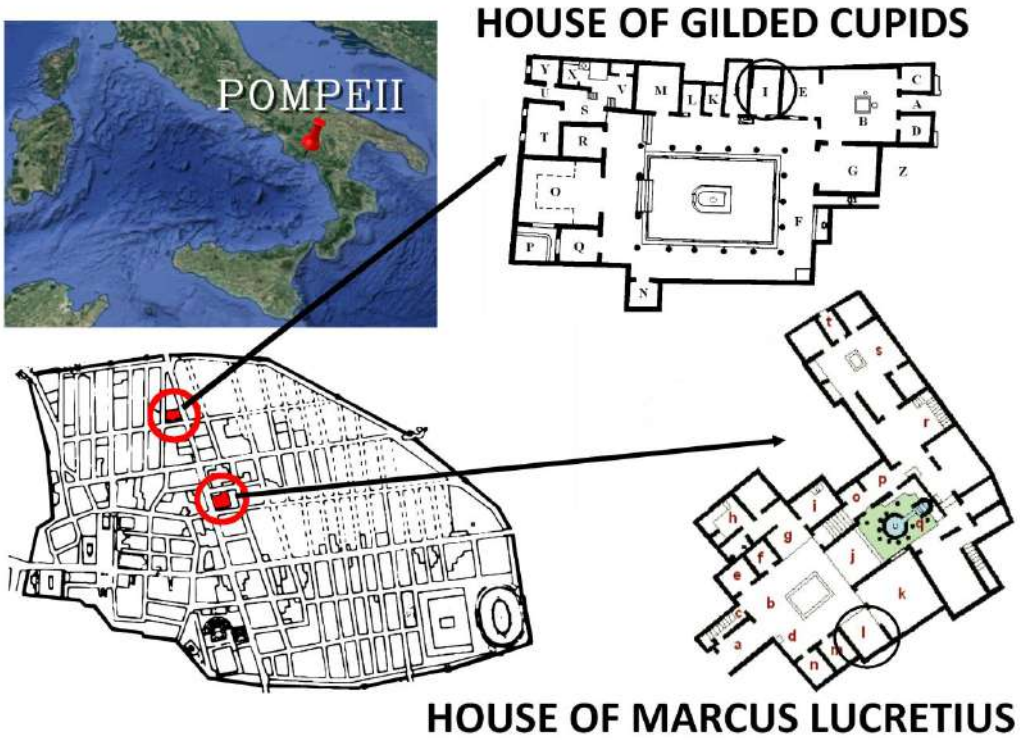

Fig. 10.1. A map of the archaeological site of Pompeii showing the location of the House of Marcus Lucretius and Gilded Cupids together with the respective plans of both houses.

The wall painting of the House of Marcus Lucretius considered in this case is the one presented in the Fig. 10.2. and 10.3 (left). It is located in the west wall of the room L of the house, a typical *cubiculum* of a Roman *domus* (see room "L" in the plan of the house from Fig. 10.1).

In this case, the yellow ochre transformed into red is placed in the upper part of the painting (see Fig. 10.2). The lower (original red) and middle (original yellow) part of the painting in Fig. 10.2 was protected against the pyroclastic flow. This protection was probably achieved by the rubble generated by the collapsed roofs that fell down during

the first event of the eruption[28] Over this lower-middle part of the wall, the pyroclastic flow, which reached the city after the roofs collapse[29], impacted the yellow ochre of the painting, probably causing its transformation into red color (see Fig. 10.2 and 10.3 left).

Fig 10.2. Wall painting from the House of Marcus Lucretius showing the transformation of yellow ochre into red in its upper part.

The second wall painting considered for the yellow ochre transformation study is placed in the House of the Gilded Cupids (see Fig.10.1). This house is characterized by extremely refined mural paintings from the *Third* and *Fourth Styles*. The frame of the door that gives entrance to the room "I" was painted originally in yellow (see Fig 10.3 right). This decorated frame is also placed in a west orientation, like in the case of the selected painting of the House of Marcus Lucretius, and also shows yellow color transformation into red in the middle-upper parts (see Fig. 10.3 right).

Fig. 10.3. Wall paintings on the House of Marcus Lucretius (left) and House of Gilded Cupids (right) showing the in situ analyzed three areas. (OR: Original red; OY: Original yellow; TY: Transformed yellow).

As shown in Fig. 10.3, the distribution of the colors in the wall paintings analyzed in both houses is different. In the House of Marcus Lucretius, the analyzed area showed the presence of original red ochre area at the bottom of the wall, while in the middle-upper part of the same wall an original yellow ochre area reaching up to 4.4 meters is observable (see Fig. 10.3, left). The color distribution in the painting from the House of Gilded Cupid shows two areas, the one of the original yellow color at the bottom, and the transformed yellow ochre in the middle-upper part (see Fig. 10.3, right). Considering that this area do not show original red ochre pigment remains, the original red ochre pigment

from the inner areas of the same room of the House of Gilded Cupids was considered for its in situ XRF and LIBS characterization.

10.3 Raw pigments samples

Three yellow ochre raw pigments (reference numbers 112257, 112265 and 117329) and three red ochre raw pigments (reference numbers 117356, 117357 and 117360) from the MANN were also considered in this chapter (see their description in Chapter 5).

10.4 In situ Raman analyses

The original red areas, the original yellow areas and the ones transformed into red from the mural paintings of both Pompeian houses were analyzed by means of Raman spectroscopy. On each area around 70 measurements were conducted being impossible to identify the presence of additional colored compounds to hematite in original red and transformed yellow areas (Raman bands at 296 and 411 cm^{-1}) and goethite in original yellow areas (Raman bands at 287 and 395 cm^{-1}). Apart from goethite or hematite, only the calcite (main Raman band at 1086 cm^{-1}) used as the binder of the pigment grains, was detected in the different Raman analyses (see Fig. 10.4).

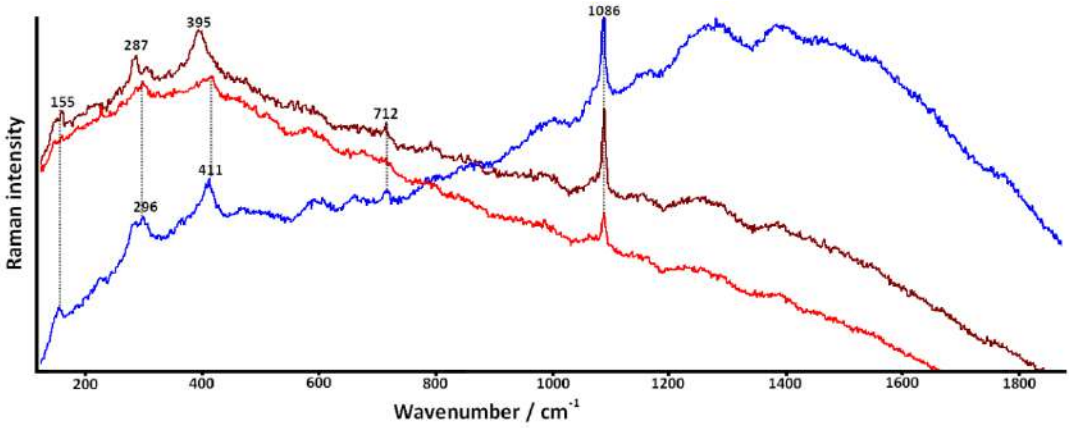

Fig. 10.4. Raman spectra of original yellow (brown), transformed yellow into red (blue), and original red (red).

As can be observed in Fig. 10.4, the Raman spectra obtained in areas of original red and yellow transformed into red are identical. Moreover, the positions of the Raman bands and the relative intensities of both were analyzed and no notable differences that could predict a discrimination of original red from a transformed yellow into red were detected.

10.5 In situ elemental analyses: HH–EDXRF vs. p–LIBS

The performed measurements and their subsequent treatment were carried out as explained in the experimental procedure (Chapter 3). The major elements detected by HH-EDXRF in the three areas under study were Fe and Ca. To discriminate the original red ochre pigment from the yellow ochre transformed into red, minor and trace elements were determined by HH-EDXRF and p-LIBS. In Fig. 10.5, a representative X-ray fluorescence spectrum of each pigment acquired in the House of Gilded Cupids is shown.

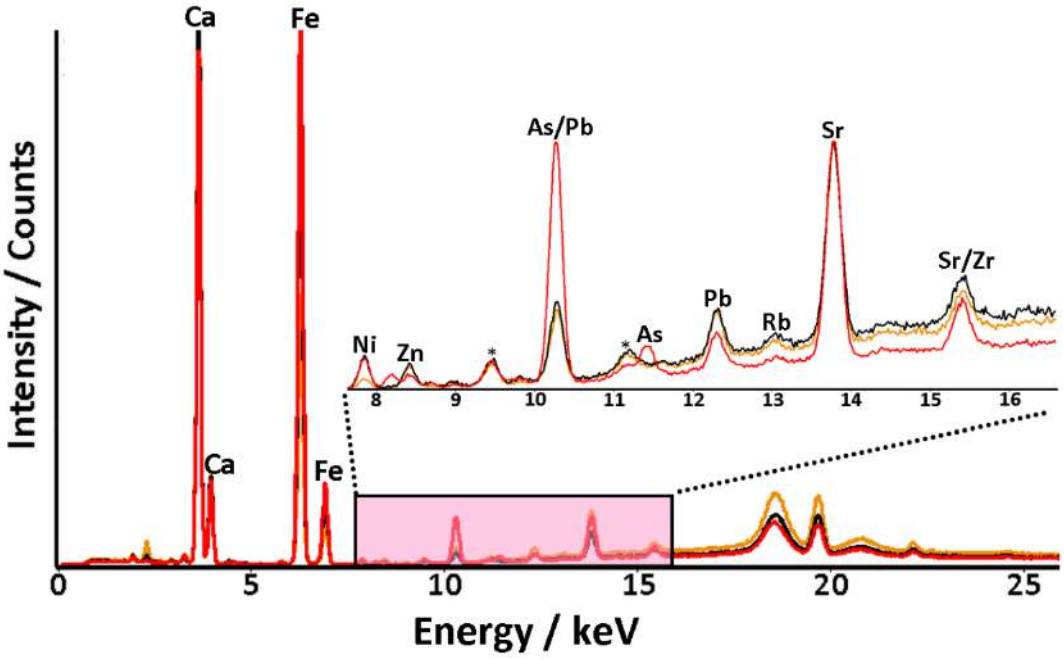

Fig. 10.5. In situ EDXRF spectra of the original red ochre (red) original yellow ochre (orange) and transformed yellow ochre (black). (*: Au bands coming from the setup of the spectrometer).

In this case, the EDXRF counts were normalized against Compton line in order to extract conclusions. The most significant element identified in the in situ XRF measurements was the As in the original red ochre areas, which was not detected in the original and transformed yellow color. The K_α line of As shows an interference with the L_α line of Pb at 10.5 keV. Thus, for the data treatment the K_β line at 11.7 keV for As and L_β line at 12.5 keV were considered. In the spectra obtained in situ, only in the original red ochre areas the K_β line of As was detected, therefore the red ochre presents As in its composition, while in the original and transformed yellow ochres the K_β line was not detected (see Fig. 10.5).

Moreover, as it can be seen in the Fig. 10.5, the line at 10.5 keV of original red ochre areas is more intense. This could suggest that in this case, As contributes significantly in the intensity of this line. To study this contribution, Pb L_α/L_β intensity ratio was calculated based on the results obtained from ten repetitive measurements performed on a pure lead foil using the HH-EDXRF spectrometer. The obtained ratio was 1.35 ± 0.08 (see Fig. 10.6).

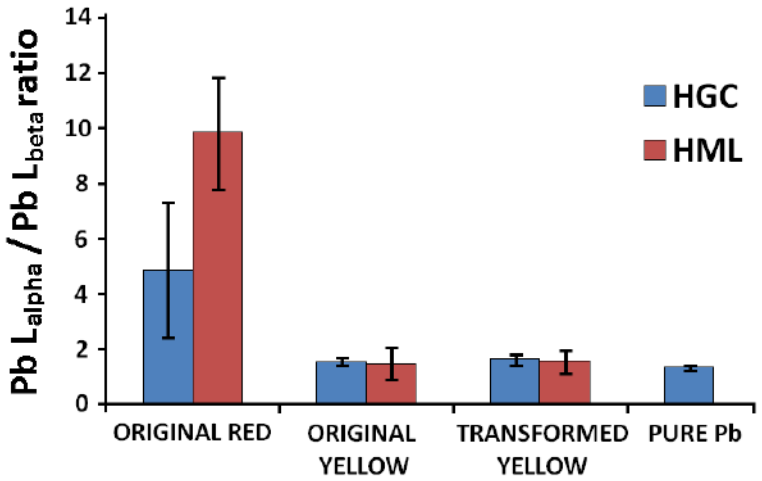

Fig. 10.6. Pb $_{L\alpha}$ / Pb $_{L\beta}$ net area ratios of a pure lead foil and the ones obtained in the different colors from the analyzed wall paintings of the House of Gilded Cupids (HGC, blue) and House of Marcus Lucretius (HML, red).

In the original red ochre the mean ratio was 4.9 ± 2.4 in the House of Gilded Cupids and 9.9 ± 2.0 in the House of Marcus Lucretius (see Fig. 10.6). This shows a quite higher contribution of As at 10.5 keV line because these ratios are much higher than the one of pure lead, suggesting the presence of As in the original red ochre areas. On the contrary, in original yellow color and transformed yellow areas this ratio was set at 1.5 ± 0.6 and 1.6 ± 0.4 respectively in the House of Marcus Lucretius and 1.5 ± 0.1 and 1.6 ± 0.2 in the House of Gilded Cupids (see Fig. 10.5). This shows the non-significant contribution of As at 10.5 keV line in the original yellow and transformed yellow areas, which means absence of this metal or presence under the limit of detection.

To explore the usefulness of p-LIBS in the discrimination of original red ochre and transformed yellow, additional measurements were conducted in both areas. According to the NIST database, the emission lines of As (229, 235, 237, 246 and 249 nm) are placed quite close to some of the emission lines of Fe (see Fig. 10.7).

Moreover, considering that with the used p-LIBS device no additional improvements can be performed, the detection of Fe cannot be considered efficient (see Fig. 10.6). In the Fig. 10.6 B, a zoom of the lower spectral region, in which the As emission lines usually appear, is presented. The line of As concretely at 228.81 nm usually shows the highest intensity. However, Fe presents an emission line close to it, at 229.82 nm. Although this area shows a poor signal-to-noise ratio, a very weak peak at 229.62 nm could be detected in the original red ochre sample (see Fig. 10.6 B), suggesting the presence of Fe and not of As. The obtained results suggests that LIBS technique cannot be considered the most adequate, at least with the used instrument configuration, to detect differences in the minor/trace elements of the three colors (yellow, red and transformed yellow into red). Therefore, HH-EDXRF results were considered to construct the discrimination model.

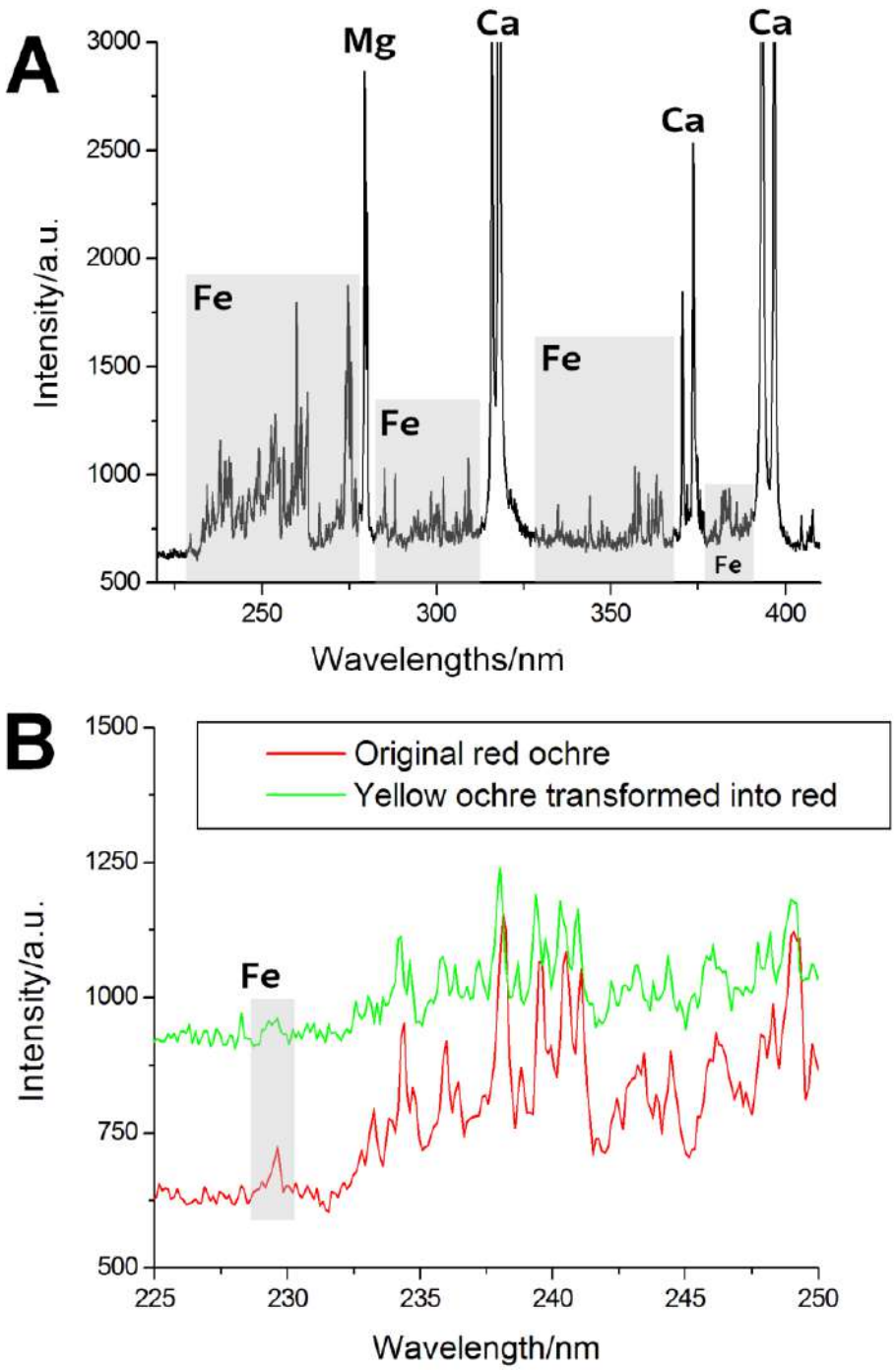

Fig. 10.7. (A) Representative LIBS spectrum obtained in the original red ochre areas (B) comparison of representative spectra acquired in the original red ochre areas and yellow ochre areas transformed into red.

10.6 Discrimination model based on Principal Component Analysis (PCA) of the HH–EDXRF results

To obtain a fast discrimination model, the counts of each element obtained by HH-EDXRF normalized against their respective Compton line were subjected to PCA analysis. The data set of each mural painting from each house was centered and scaled before carrying out the PCA analysis. PCA of the both datasets was carried out using Leverage correction as validation method.

The data set for the House of Marcus Lucretius consisted on a matrix of 30 analyses on wall paintings and the normalized net counts of 13 elements (Al, Si, Ti, Sr, Fe, K, Pb, Mn, Zn, P, Ca, As and Sr) or variables. The PCA model with three Principal Components (PCs) explaining the 77.3% of the variance was chosen as the best one. The obtained results as a superposed representation of the scores and loadings in the space formed by three of the PCs are shown in Fig. 10.8. In the scores of the PCA model of the House of Marcus Lucretius three groups corresponding to the different analyzed colors (original red, original yellow and transformed yellow) are distinguished.

It is important to remark that elements such as S and K are characteristic of the group of samples of original yellow areas (OY) (see Fig. 10.8). In the original yellow area from this painting of the House of Marcus Lucretius, an area with high amount of efflorescences was observable. In previous analyses conducted on these efflorescences using Raman spectroscopy[30], gypsum ($CaSO_4 \cdot 2H_2O$) and niter (KNO_3) were identified, explaining the higher contribution of K and S in the original yellow areas of the wall painting (see Table 10.1). On the contrary, as it is shown in Table 10.1, in the House of Gilded Cupids sulfur and potassium levels in the measured three different colors remain quite constant.

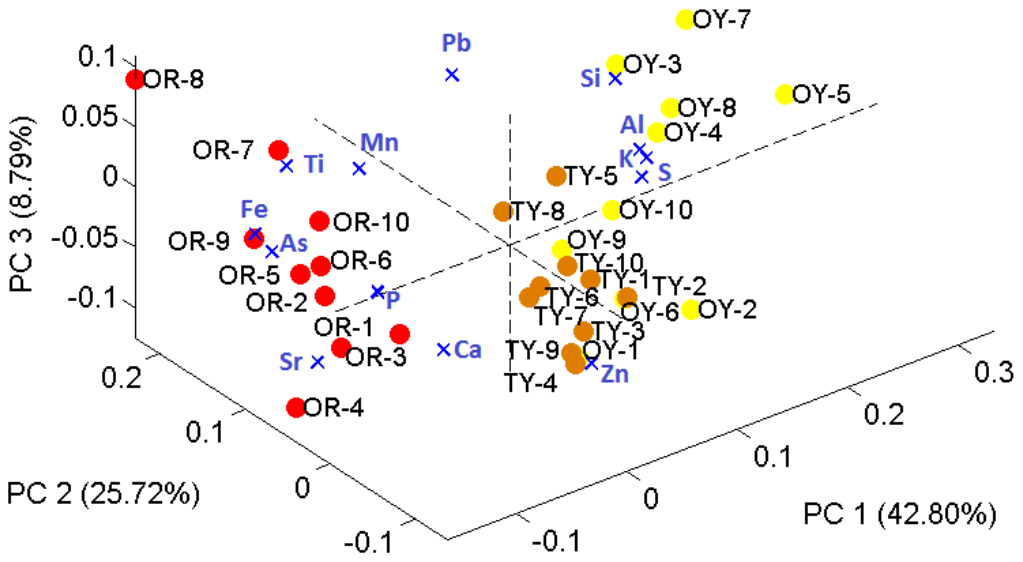

Fig. 10.8. Three-dimensional bi-plot on PC1/PC2/PC3 obtained after Principal Component Analysis with all the EDXRF measurements performed on the original red ochre (OR), original yellow ochre (OY) and transformed yellow ochre (TY) areas from the House of Marcus Lucretius wall painting.

Table 10.1 Normalized net counts of S and K in the original red (OR), original yellow (OY) and transformed yellow (TY) areas of the House of Marcus Lucretius (HML) and the House of Gilded Cupids (HGC).

	Normalized S counts	**Normalized K counts**
OR-HML	0.05 ± 0.02	0.02 ± 0.01
OY-HML	0.5 ± 0.3	0.4 ± 0.3
TY-HML	0.019 ± 0.005	0.02 ± 0.02
OR-HGC	0.07 ± 0.09	0.013 ± 0.006
OY-HGC	0.20 ± 0.07	0.015 ± 0.007
TY-HGC	0.17 ± 0.07	0.016 ± 0.003

The PCA for the spectra taken in the House of Gilded Cupids was carried out with the data of 37 analyses on the wall paintings and the same 13 variables. The model with two principal components explaining the 67.7% of the total variance was selected. In the bi-plot (scores and loadings) of PC1 and PC2 (see Fig. 10.9) a clear grouping of each analyzed color on each painting is observable as in the case of the House of Marcus Lucretius.

However, in this case some of the original red ochre measurements (points OR-1 to OR-4) were placed separated respect to the most of the red ochre measurements, concretely in the negative part of PC2.

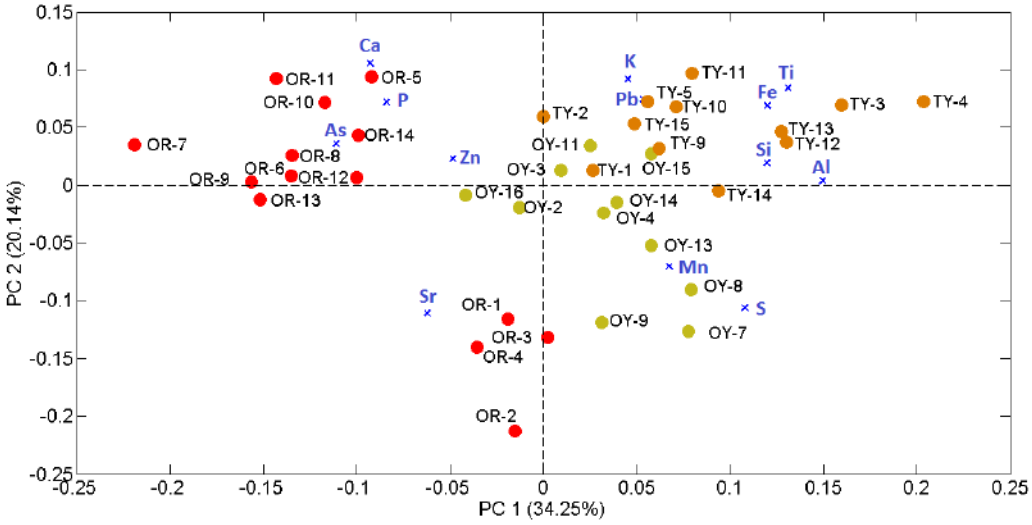

Fig. 10.9. Projection of the bi-plot (scores and loadings) on PC1–PC2 obtained after Principal Component Analysis with all the EDXRF measurements performed on the original red ochre (OR), original yellow ochre (OY) and transformed yellow ochre (TY) areas from the House of Gilded Cupids wall painting.

Indeed, the OR-1, OR-2, OR-3 and OR-4 spectra were acquired in the right wall of the room "I" (see Fig. 10.3, right), while the rest of the measurements were acquired in the front and left wall. The most evident difference between these inner walls was the high S signal that showed the spectra acquired in the right wall (points OR-1 to OR-4) comparing to the rest (see Fig. 10.10), which promoted a differentiation of the original red ochre measurements in two groups in the obtained PCA.

This high signal of S in the right wall of the room may suggest the presence of efflorescences in that wall.

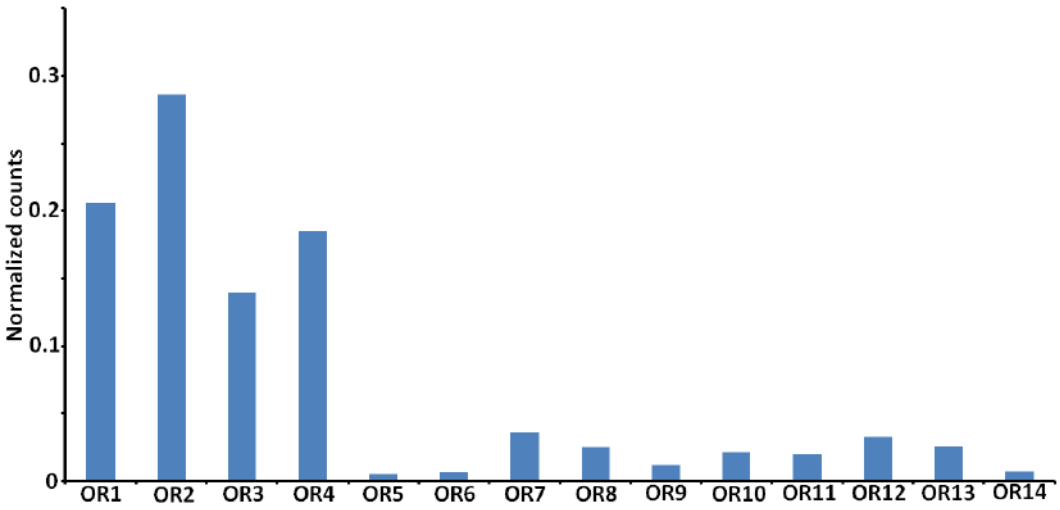

Fig. 10.10. Normalized counts of S in the different analyzed original red areas.

In fact, pictures taken at the same day of the analyses show clearly the widespread presence of efflorescence in the analyzed area, the red square next to the floor, at the right of Fig. 10.11. For this reason, in the PCA shown in Fig. 10.9, the first four HH-EDXRF measurements (OR-1 to OR-4) were separated from the main group of red ochre analyses.

Fig. 10.11. Right wall of room I showing a widespread presence of efflorescences, where OR-1, OR-2, OR-3 and OR-4 measurements with high signal of S were performed.

The elements that determined the groupings of original red color are As and Sr in both houses under study. This could suggest that the red ochre pigment used to paint these areas in ancient times was richer in As and Sr than the yellow ochre. Original yellow and transformed yellow areas present also Sr in its composition, but in a lower proportion, while As was not detected with the HH-EDXRF spectrometer, as mentioned before. In fact, strontium can be related to the calcium carbonate present in the *intonacchino*/*intonaco* of the wall painting due to substitution process of Sr^{2+} for Ca^{2+} in the calcium carbonate lattice[31], therefore it is not the most suitable element to take into account for discrimination purposes.

10.7 EDXRF analysis of the red and yellow ochre raw pigments in the laboratory

To verify the results obtained in situ, yellow and red ochre raw pigments were analyzed in the laboratory using a benchtop EDXRF spectrometer. For that, six different measurements of 300 s were acquired for each raw pigment at 1 mm of lateral resolution. As shown in Fig. 10.12, the spectra acquired on the yellow ochre raw pigments do not show the contribution of As K_β line, while red ochre raw pigments show a clear contribution of this element line in the spectral results.

In this case, the software of the benchtop EDXRF instrument is able to perform a proper deconvolution of the line at 10.5 keV including a contribution of the As K_α line and Pb L_α line. Applying this deconvolution process, the software indicated that As was also present in the yellow ochre raw pigments but in a very low concentration, close to the limit of detection (around 15 μg/g). Considering that the limit of detection of As using the HH-EDXRF device is higher than the one of the benchtop instrument, it is clearly justified the no detection of this element using the hand-held spectrometer.

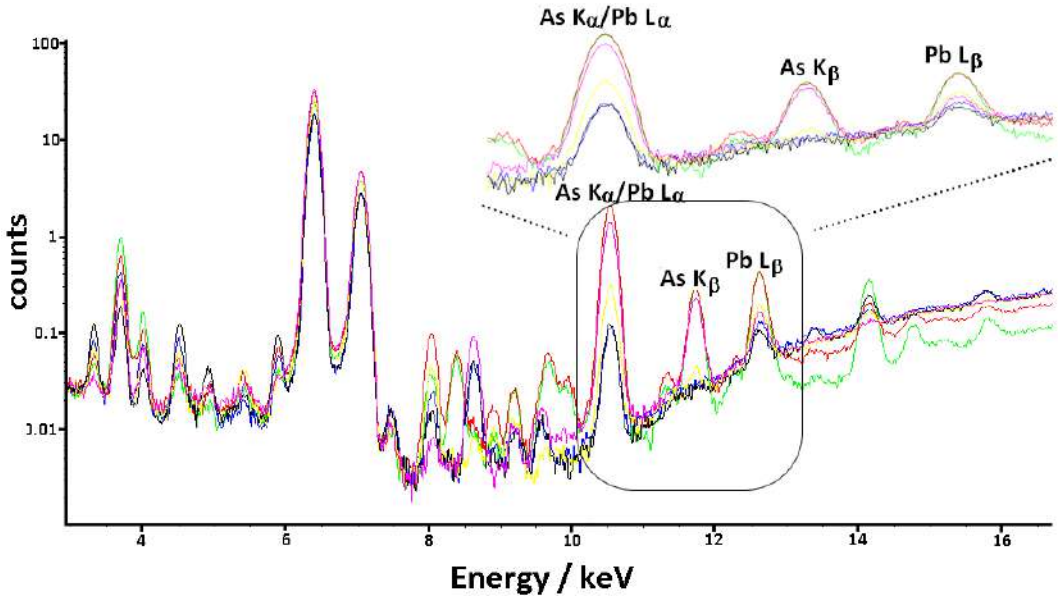

Fig. 10.12. EDXRF spectra of yellow ochre pigment 112257 (black), yellow ochre pigment 112265 (yellow), yellow ochre pigment 117329 (blue), red ochre pigment 117356 (red), red ochre pigment 117357 (green) and red ochre pigment 117360 (pink).

To extract conclusions, the net counts related with As and obtained from the deconvolution of the line at 10.5 keV from all the spectra of red and yellow raw pigments were normalized against the Fe K_α line, which is a constant and major element in the red (α-Fe_2O_3) and yellow ochre (α-FeO(OH)) pigments. In Fig. 10.13 the normalized net counts of each raw pigment are presented showing that As presence in yellow ochre raw pigment can be considered insignificant in comparison with its presence in the red ochre raw pigment. The laboratory results confirm those obtained in situ in the wall paintings from both Pompeian houses, which confirm that As could be the key or tracer element to distinguish an original red ochre from a red colored transformed yellow ochre.

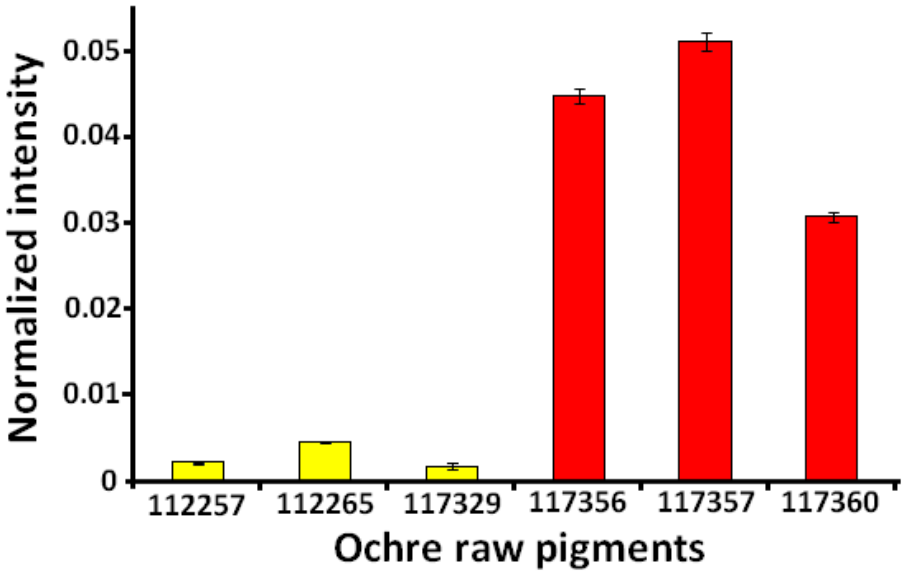

Fig. 10.13. Normalized net counts of As in three yellow ochre and three red ochre raw pigments.

10.8 Conclusions

In this chapter an in situ analytical methodology based mainly on the use of a HH-EDXRF spectrometer was applied to differentiate original red ochre pigments used in Pompeian wall paintings from areas of the wall paintings originally painted using yellow ochre but transformed into red colors due to the pyroclastic flow impact at high temperatures. This impact promoted the transformation of the yellow ochre pigment (α-FeOOH) into red hematite (α-Fe_2O_3), this last impossible to discriminate in situ by Raman spectroscopy from the original red ochre pigment.

An elemental analysis was proposed as a good alternative to construct a quick in situ methodology to discriminate between both areas from an analytical point of view. The obtained EDXRF results showed that As is the tracer element to discriminate between both areas, since it is always present in the original red ochre in higher proportions and it is not present or it is present in very low concentrations in the transformed yellow ochre.

To extract suitable conclusions, the K_β line of As at 11.7 keV, free from interference, was considered for the data treatment of the results obtained in situ by the hand-held EDXRF spectrometer. However, to check if there was a contribution of As in the 10.5 keV line (the interfered one), the Pb L_α/L_β ratio analysis was performed using a pure lead foil, obtaining a value of 1.35. Higher ratio values than this one point out the contribution of As in this line. Thus, apart from the detection of the K_β line at 11.7 keV, this ratio analysis provides of useful information for further conclusions.

The experimental evidences presented also suggest that, at least with the p-LIBS device used in this work, it is not possible to achieve a proper detection of As in presence of Fe at the concentration levels. Therefore, in this case, it can be concluded that p-LIBS against HH-EDXRF is not a proper alternative to perform the discrimination of both areas.

To confirm the EDXRF results extracted in situ, additional analyses of yellow and red ochre raw pigments recovered from the excavations of the archaeological site of Pompeii were carried out with the same technique but using a benchtop instrument. The laboratory results confirmed the ones obtained in situ.

Finally, in the original yellow ochre of the wall painting of the House of Marcus Lucretius high levels of S and K were detected, while some measurements taken from the original red ochre areas in the House of Gilded Cupids showed high levels of S. These levels were due to the abundant efflorescences observed at the moment of the analysis. This observation corroborates the previous conclusions extracted after molecular analyses which indicated the presence of gypsum ($CaSO_4 \cdot 2H_2O$) and niter (KNO_3) in those areas[30].

10.9 REFERENCES

1. Angelini, I. *et al.* The pigments of the frigidarium in the Sarno Baths, Pompeii: Identification, stratigraphy and weathering. *J. Cult. Herit.* (2019). DOI: 10.1016/j.culher.2019.04.021

2. Bekefi, G. Principles of laser plasmas. *N. Y. Wiley-Intersci. 1976 712 P* (1976).

3. Fabbro, R. *et al.* Laser-wavelength dependence of mass-ablation rate and heat-flux inhibition in laser-produced plasmas. *Phys. Rev. A* **26**, 2289-2292 (1982).

4. Goldsack, T. J. *et al.* The variation of mass ablation rate with laser wavelength and target geometry. *Opt. Commun.* **42**, 55–59 (1982).

5. Gondal, M. A. *et al.* The role of various binding materials for trace elemental analysis of powder samples using laser-induced breakdown spectroscopy. *Talanta* **72**, 642–649 (2007).

6. Corsi, M. *et al.* Effect of laser-induced crater depth in laser-induced breakdown spectroscopy emission features. *Appl. Spectrosc.* **59**, 853–860 (2005).

7. Noll, R. Laser-induced breakdown spectroscopy. *Laser-Induced Breakdown Spectroscopy* 7–15 (Springer, 2012).

8. Sansonetti, J. E. *et al.* Handbook of basic atomic spectroscopic data. *J. Phys. Chem. Ref. Data* **34**, 1559–2259 (2005).

9. Suplee, C. Atomic Spectra Database. *NIST* (2009). Available at: https://www.nist.gov/pml/atomic-spectra-database. (Accessed: 7th October 2019)

10. Gaft, M. *et al.* Elemental analysis of halogens using molecular emission by laser-induced breakdown spectroscopy in air. *Spectrochim. Acta Part B At. Spectrosc.* **98**, 39–47 (2014).

11. Alvarez-Llamas, C. *et al.* A novel approach for quantitative LIBS fluorine analysis using CaF emission in calcium-free samples. *J. Anal. At. Spectrom.* **32**, 162–166 (2017).

12. Bhatt, C. R. *et al.* Study of atomic and molecular emission spectra of Sr by laser induced breakdown spectroscopy (LIBS). *Appl. Opt.* **54**, 10264–10271 (2015).

13. Alvarez-Llamas, C. *et al.* Quantification of fluorine traces in solid samples using CaF molecular emission bands in atmospheric air laser-induced breakdown spectroscopy. *Spectrochim. Acta Part B At. Spectrosc.* **123**, 157–162 (2016).

14. Gaft, M. *et al.* Laser-induced breakdown spectroscopy of Br and I molecules with alkali-earth elements. *Spectrochim. Acta Part B At. Spectrosc.* **157**, 47–52 (2019).

15. Vogt, D. S. *et al.* CaCl and CaF emission in LIBS under simulated Martian conditions. *Icarus* **335**, 113393 (2020).

16. Fdez-Ortiz De Vallejuelo, S. *et al.* Portable laser induced breakdown spectrometry to characterize the environmental impact of potentially hazardous elements of suspended particulate matter transported during a storm event in an urban river catchment. *Microchem. J.* **135**, 171–179 (2017).

17. Popelka-Filcoff, R. S. Applications of elemental analysis for archaeometric studies: analytical and statistical methods for understanding geochemical trends in ceramics, ochre and obsidian. (PhD thesis, University of Missouri–Columbia, 2006).

18. Popelka-Filcoff, R. S. *et al.* Trace element characterization of ochre from geological sources. *J. Radioanal. Nucl. Chem.* **272**, 17–27 (2007).

19. Jercher, M. *et al.* Rietveld X-ray diffraction and X-ray fluorescence analysis of Australian aboriginal ochres. *Archaeometry* **40**, 383–401 (1998).

20. Richards, M. J. Realising the potential of portable XRF for the geochemical classification of volcanic rock types. *J. Archaeol. Sci.* **105**, 31–45 (2019).

21. Craig, N. *et al.* Comparison of XRF and PXRF for analysis of archaeological obsidian from southern Peru. *J. Archaeol. Sci.* **34**, 2012–2024 (2007).

22. Galipaud, J. C. *et al.* Long-distance connections in V anuatu: New obsidian characterisations for the M akué site, A ore I sland. *Archaeol. Ocean.* **49**, 110–116 (2014).

23. Jia, P. W. *et al.* Moving sources: A preliminary study of volcanic glass artifact distributions in northeast China using PXRF. *J. Archaeol. Sci.* **37**, 1670–1677 (2010).

24. Sheppard, P., Trichereau, B. & MiLiCiCh, C. Pacific obsidian sourcing by portable XRF. *Archaeol. Ocean.* **45**, 21–30 (2010).

25. Alvey, D. C. *et al.* Laser-induced breakdown spectroscopy-based geochemical fingerprinting for the rapid analysis and discrimination of minerals: the example of garnet. *Appl. Opt.* **49**, C168–C180 (2010).

26. Colao, F. *et al.* Quarry identification of historical building materials by means of laser induced breakdown spectroscopy, X-ray fluorescence and chemometric analysis. *Spectrochim. Acta Part B At. Spectrosc.* **65**, 688–694 (2010).

27. Harmon, R. S. *et al.* Geochemical Fingerprinting by Handheld Laser-Induced Breakdown Spectroscopy. *Geostand. Geoanalytical Res.* **41**, 563–584 (2017).

28. Cioni *et al.* Temperatures of the AD 79 pyroclastic density current deposits (Vesuvius, Italy). *J. Geophys. Res. Solid Earth.* **109**, B02207, (2004).

29. Foss, P. *et al.* The world of Pompeii. (London, Routledge, 2009).

30. Madariaga, J. M. *et al.* In situ analysis with portable Raman and EDXRF spectrometers for the diagnosis of the formation of efflorescence on walls and wall paintings of the Insula IX 3 (Pompeii, Italy). *J. Raman Spectrosc.* **45**, 1059–1067 (2014).

31. Brand, U., Morrison, J. O. & Campbell, I. T. Strontium in sedimentary rocks. *Geochemistry* 600–603 (1998).

11. MOLECULAR SPECTROSCOPIC TECHNIQUES TO CLASSIFY AND QUANTIFY THE THERMAL TRANSFORMATION DEGREE OF YELLOW OCHRE INTO RED

11.1 Introduction

In the previous chapter, totally transformed yellow areas have been considered for the study. However, in wall painting from Pompeii and Herculaneum, yellow ochre areas partially transformed into red are also nowadays visible. This could mean that pyroclastic density currents did not impact those areas at high enough temperatures to dehydrate completely the yellow ochre pigment. Therefore, in these cases, a mixture of yellow ochre and yellow ochre transformed into red can coexist (see Fig. 11.1).

Fig. 11.1. Wall painting from Herculaneum showing original yellow, incomplete transformation (orange areas) and complete transformed yellow into red areas[1].

To verify if these incomplete yellow ochre transformations were promoted due to an insufficient temperature impact, real yellow ochre painting fragments recovered from the burial of Pompeii or Herculaneum can be used as model samples. In this way, the thermal impact that suffered the walls of Pompeii and Herculaneum can be simulated in the laboratory. Considering that the thermal impact was heterogeneous along both archaeological sites, the experiments should be performed at different temperatures simulating the range of temperatures reached in the 79 AD eruption. With these experiments, the temperature at which the yellow ochre transformation starts, the range of temperatures that promote the incomplete transformation, and the temperature at which the transformation is complete can be determined. This set of thermally aged samples can be analyzed by different molecular spectroscopic techniques to obtain analytical evidences about the transformation degree depending on the temperature. The obtained empirical information could allow to construct a model to establish the

temperature impact that suffered each wall during the eruption of 79 AD depending of its position and orientation against Mount Vesuvius, and to indirectly reconstruct the volcanic events that took place through the study of the transformed materials –yellow ochre pigment in this case- from the wall paintings of Pompeii and/or Herculaneum.

As it has been commented previously, the thermal impact that suffered Pompeii during the eruption of Mount Vesuvius in the 79 AD is set between 240-340°C. It is well known that goethite can be dehydrated at temperatures around 225-250°C[2–6]. This temperature was easily achieved during the volcanic events. In the literature there are many works dealing with the study of the dehydration of goethite pigment into hematite within this range of temperatures[2–6]. However, all these studies are not focused in the transformation of real goethite pigment from Pompeii and/or Herculaneum and, there is not experimental data about the quantitative transformation degree depending on the temperature to explain the complete and incomplete dehydration processes that took place in the yellow wall paintings from Pompeii and/or Herculaneum.

For this purpose, and as commented in the previous chapter, molecular techniques such as Raman or infrared spectroscopy did not offer conclusive information to discriminate between original red ochre from yellow ochre transformed into red. Although Raman spectroscopy is not able to discriminate between an original red from the yellow ochre transformation, this technique can be used to determine the relative content of goethite/hematite as a function of the thermal impact. In this case, a quantitative Raman imaging strategy was followed to construct a model based on the transformation degree of yellow ochre as a function of the thermal impact (temperature). In the methodology developed totally quantitative results were obtained using a set of real Pompeian wall painting fragments aged at different temperatures. Apart from Raman spectroscopy, reflectance information in the Visible-Near Infrared-Short Wavelength Infrared (Vis-NIR-SWIR) spectral range can be also obtained. This technique is based on the principle of selective light absorption. The result of this analysis is the extraction of the reflectance

spectrum in which both reflected and scattered light is recorded.[7] Therefore, reflectance spectroscopy (RS) in the visible (400-700 nm) and/or infrared range can be tested as a potential analytical technique to track the color transformation of yellow ochre into red. However, in the literature it cannot be found any work dealing with the capacities of this technique for this purpose. In fact, there are only two works that examined the potential of RS in the VIS-NIR–SWIR spectral region with the purpose of identifying the thermal processes that occur in heated minerals such as goethite[8,9]. In this two works laboratory instrumentation was used. In one of them[8], spectral information about the dehydroxylation of goethite to form hematite was obtained in the VIS-NIR region. Besides, the second work[9] demonstrated that it is possible to determine the temperature and mineralogical changes that a soil experimented before and after its heating, based on their spectral changes in the Vis-NIR–SWIR region.

In this chapter, molecular spectroscopic methodologies are proposed to discriminate, classify and set the transformation degree of Pompeian yellow ochre pigment as a function of the temperature range that impacted the walls of Pompeii in the 79 AD eruption. For that, yellow ochre fragments recovered from the burial of Pompeii were thermally aged simulating the impact of the different pyroclastic density currents that took place in the volcanic events of the 79 AD eruption. The exposed fragments were analyzed using a portable reflectance spectroradiometer in the Vis-NIR-SWIR obtaining the spectra in a fast and non-invasive way. The spectral information was subjected to chemometric treatment (PCA) to create a model useful to discriminate the original red ochre and the one obtained from the transformation of yellow ochre, and also to have available a tool to predict at which temperature was impacted an specific mural painting originally decorated with yellow ochre. This last aim will allow transversely reconstructing the thermal impact induced by the 79 AD eruption.

The second molecular methodology developed is related with the use of quantitative Raman imaging. In this case, and also using the yellow ochre fragments subjected to thermal ageing, the transformation degree of yellow ochre depending on the temperature was determined. To develop this methodology, original yellow ochre fragments were analyzed using micro energy dispersive X-ray fluorescence (μ-EDXRF) spectrometry and micro-Raman spectroscopy. Yellow ochre fragments were mapped using Raman imaging before and after thermal exposition in a specific range of temperatures and the goethite transformation degree depending on the temperature was quantitatively determined using Raman imaging. The quantification procedure was previously validated using synthetic goethite and hematite pigment standards mixed at different percentages and prepared as pressed pellets.

11.2 Samples

Two detached yellow wall painting pieces recovered from the excavations conducted by the *Expeditio Pompeiana Universitatis Helsingiensis* group[10] in the House of Marcus Lucretius (Reg IX, Ins 3, 5-24) from Pompeii were considered for the thermal ageing experiments. These samples did not show goethite transformation evidences and they had not been exposed to the atmosphere since the recovery moment. The first piece was divided in three fragments (A, B and C) and the second one in six fragments (D, E, F, G, H and I) as shown in Fig. 11.2.

Apart from those, two original yellow (OY1 and OY2) and three original red (OR1, OR2 and OR3) fragments were also considered and analyzed for the construction of the reflectance classification model.

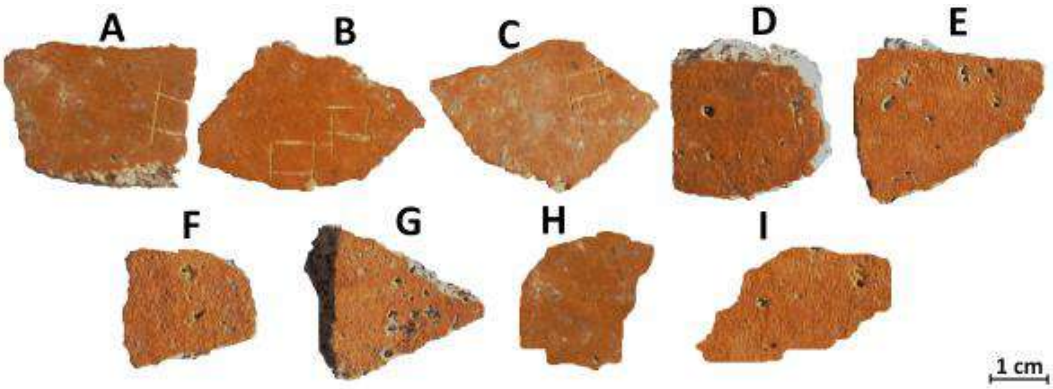

Fig. 11.2. Wall painting fragments recovered from the House of Marcus Lucretius showing goethite pictorial layer.

11.3 Thermal ageing of the yellow ochre fragments

The ageing experiments were designed taking into account the possible range of temperatures at which the pyroclastic flow impacted the wall paintings of Pompeii[11]. Therefore, temperatures from 200˚C to 400˚C were selected. The exposure temperatures were the following ones: 200˚C, 225˚C, 250˚C, 275˚C, 300˚C, 325˚C, 350˚C, 375˚C, and 400˚C. After all the considered thermal ageing experiments notable color changes were observed at the naked eye in the fragments under study (see Fig. 11.3).

As shown in Fig. 11.3, a clear and progressive transformation of goethite into hematite can be observed at the naked eye mainly from 200 to 275˚C. From this last temperature up to 400˚C no changes were visually observed.

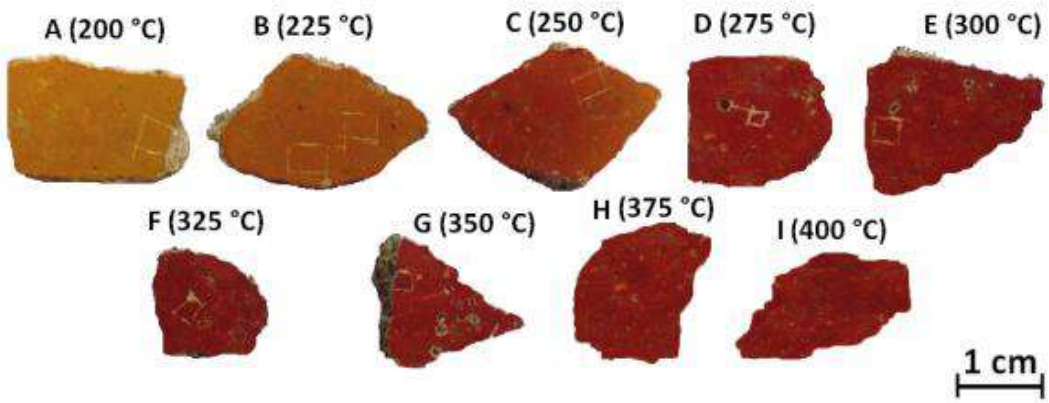

Fig. 11.3. Yellow goethite fragments transformed into red after the different thermal ageing experiments.

11.4 Classification model using reflectance spectroscopy

Although the used spectroradiometer that covers the Vis-NIR-SWIR (350 to 2500 nm) is portable, the reflectance of both original yellow and red ochre fragments and thermally aged fragments was measured in the laboratory. The acquisition of the measurements was performed illuminating the fragments with an external light source consisting of a halogen lamp (ASD Illuminator) placed at 30 cm of distance from the samples. The angle between sample and detector fiber was 45°.

First of all, the reflectance analysis of the not aged yellow samples was performed. The obtained spectra were almost the same. In Fig. 11.4 a representative spectrum of the reflectance of samples OY1 and OY2 are shown.

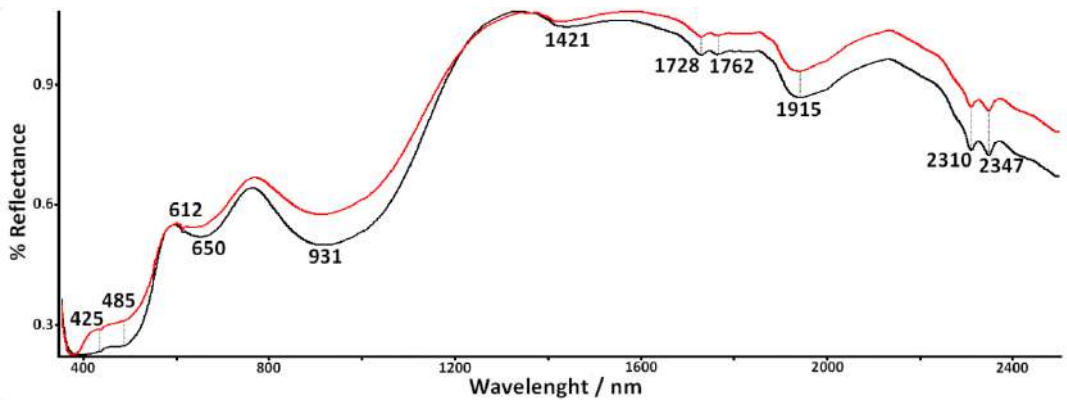

Fig. 11.4. Representative reflectance spectra of OY1 and OY2 fragments.

The bands centered at 425, 485, 673 and 978 nm are typical from goethite as different works pointed out[8,12,13]. In this case, the spectra obtained from the original yellow ochre fragments showed the bands at 425 and 485 nm, while the bands at 673 and 978 nm were slightly shifted to 650 and 931 respectively.

In the case of the original red fragments some spectral differences were detected also in the region from 1400 to 2500 nm (see Fig. 11.5).

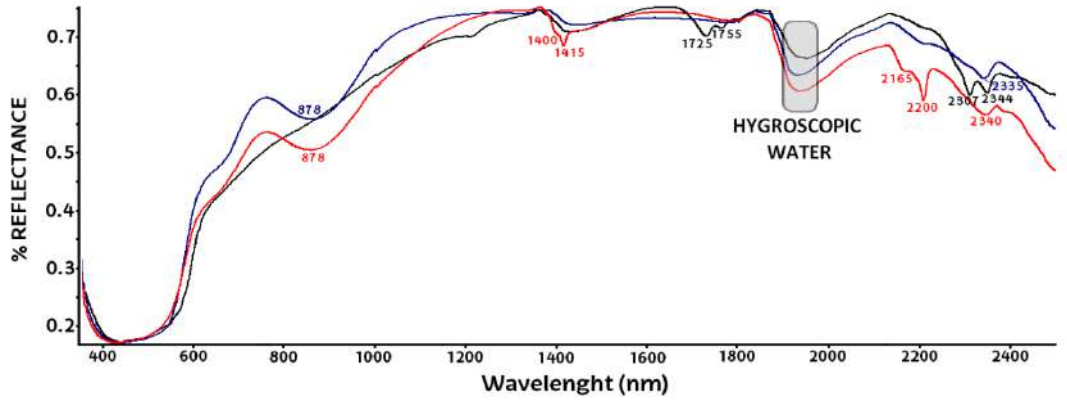

Fig. 11.5. Reflectance spectra of OR1 (black), OR2 (red) and OR3 (blue) fragments.

Apart from the typical band of hematite at 878 nm[8,12,13], additional bands appeared mainly in the obtained spectra of OR1 (black) and OR2 (red) due to the presence of additional compounds in the pictorial layer of the red ochre fragments under study. Indeed, in the OR1 spectrum the band centered at 2307 nm, is characteristic of carbonates and the one around 2340 nm (2344 and 2335 in the case of OR1 and OR3 fragments) is related with calcite[8], which suggests the presence of calcium carbonate, most probably coming from the calcite acting as the binder of the pigments grains. Moreover, the band at 1400 nm and the doublet at 2165 (w) and 2200 (s) nm in the spectrum of OR2 fragment pointed out to the presence of kaolinite[8], which has been already identified in the composition of Pompeian red ochre pigments (see Chapter 5). Apart from kaolinite, in this OR2 fragment the bands related with hygroscopic water at 1415 and 1915 nm were also detected. Therefore, the obtained reflectance spectra suggest that the different original red ochre fragments were composed all of them mainly by a hematite pictorial layer with additional compounds, such as calcite or kaolinite depending on the sample.

On the other hand, the fragments aged at different temperatures showed some slight differences between them (Fig. 11.6). As can be observed, some differences can be appreciated in the reflectance spectra of the fragments aged at 200˚C (green line), 225˚C (blue line), 250˚C (pink line), 375˚C (purple line) and 400˚C (red line). However, fragments aged at 275˚C, 300˚C, 325˚C and 350˚C showed similar reflectance spectra.

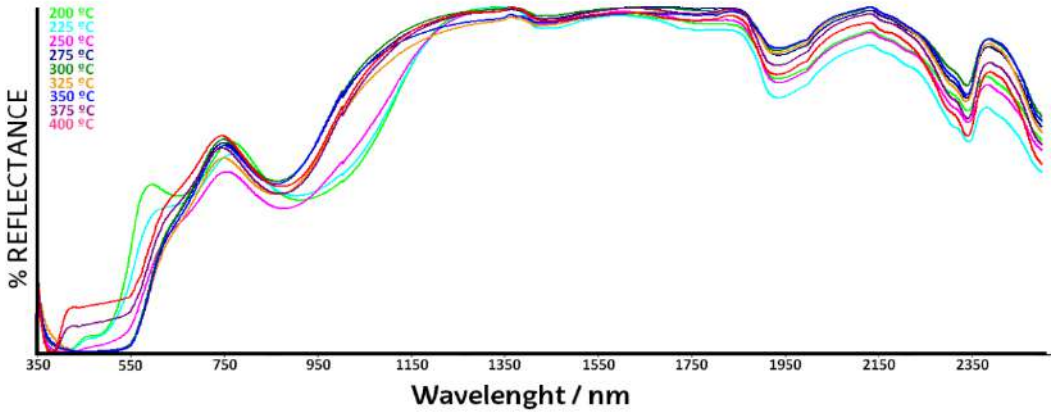

Fig. 11.6. Reflectance spectra of the aged yellow ochre fragments.

Since the identification of differences taking into account only the raw spectra can be a complicate task, and to study in a deeper way the obtained reflectance spectra from a statistical point of view, chemometrics were used. For this purpose, a data matrix consisting on 93 rows (14 samples with an average of 6 replicates of each) and 2151 variables (the entire spectral region from 350 to 2500 nm) was used to perform PCA. Nevertheless, the obtained PCA did not offered any grouping of the different aged fragments. For this reason, the first-derivative of the spectra was calculated. Fig. 11.7 shows the first-derivative of the reflectance spectra of yellow ochre fragments aged at the different temperatures in the Vis-NIR-SWIR spectral range.

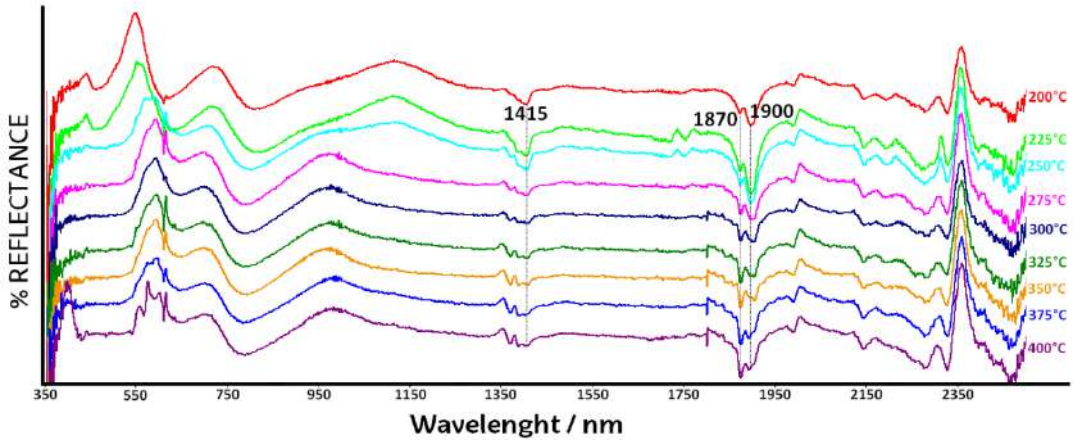

Fig. 11.7. First-derivative of the reflectance spectra of yellow ochre fragments aged at the different temperatures.

As can be observed, the first-derivative spectra show a marked difference related to the bands at 1415 nm (hygroscopic water presence). As shown in Fig. 11.7, this band tends to disappear while the ageing temperature increases. This variation, non-observable in the raw spectra was only revealed using the first-derivative. Apart from that, the doublet that appears in all the spectra at 1870-1900 nm, also shows a clear change depending on the temperature of exposition. At lowest temperatures the band at 1900 nm is more intense than the one at 1870 nm. However, while the ageing temperature increases, the band at 1900 nm decreases in intensity and the band at 1870 nm increases, being more intense from the thermal impact at 325˚C (see Fig. 11.7). Once again, this variation could not be observed in the raw spectra.

With the data matrix including the first-derivative of the spectra, the PCA of the data set was created to assess if different groups according to the thermal exposure can be differentiated. In this case, as significant differences were observed in various spectral ranges, the obtained PCA offered clear groupings. The best classification model was obtained considering the whole spectral range (see Fig. 11.8).

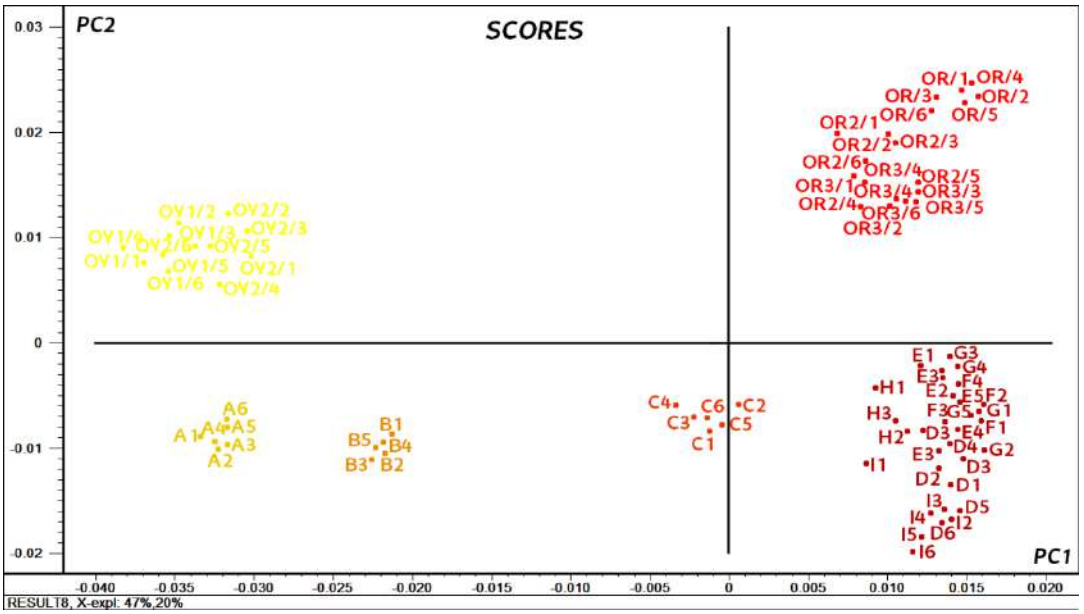

Fig. 11.8. Principal Component Analysis of the obtained multivariate reflectance spectral data (OY1 and OY2: original yellow fragments; OR1, OR2 and OR3: original red fragments; A to I: fragments thermally aged from 200˚C to 400˚C every 25˚C).

According to the scores plot, six groups completely separated were obtained. In this sense, PC1 divided yellow colored samples (OY1, OY2, A and B), which were placed in the negative part, from the red ones (OR1, OR2, OR3, D, E, F, G, H, and I), with positive values. The group of the fragment C (aged at 250˚C) was placed approximately in the center of the axis of PC1, between yellow and red samples pointing out that it probably achieved a transformation of around 50%. This transformation degree will be confirmed later using the quantitative Raman analysis.

The fragments aged from 275˚C to 400˚C (samples D to I) were grouped together suggesting that at 275˚C the transformation is already completed. Moreover, according to the PCA it seems that the transformation began at temperatures of 200˚C, because this group (A) is placed at the same PC1 value, while group B (aged at 225˚C) is shifted to more positive values respect to the non-exposed yellow fragments (OY1 and OY2).

PC2 is able to discriminate between original yellow ochre fragments not exposed to a thermal impact (positive values) from those that were aged at different temperatures (negative part of PC2). Thus, the obtained classification model can also discriminate easily original red from yellow ochre pigments transformed into red color. Moreover, with this model the different transformation degrees of yellow ochre into red can also be differentiated depending on the temperature exposition.

11.5 Transformation degree quantification using Raman imaging analysis

Apart from the Vis-NIR-SWIR reflectance classification model, it would be very interesting to determine the goethite transformation percentage in each aged fragment to complement the obtained classification model. For that, a quantitative methodology based on the use of Raman imaging was developed.

11.5.1 Elemental characterization of the fragments before the thermal ageing by means of μ–EDXRF imaging

μ-EDXRF spectrometry by means of an imaging strategy was applied to observe mainly the distribution of iron in the surface of the fragments (see Fig. 11.9). The elemental maps acquired on each fragments allowed identifying the best areas for the subsequent Raman imaging analysis, since areas showing the highest signal of Fe were selected to monitor properly the transformation. Moreover, those areas showing lines, grooves or marks which favor the elimination of the pictorial layer were avoided to minimize the inclusion of heterogeneities in the areas under study.

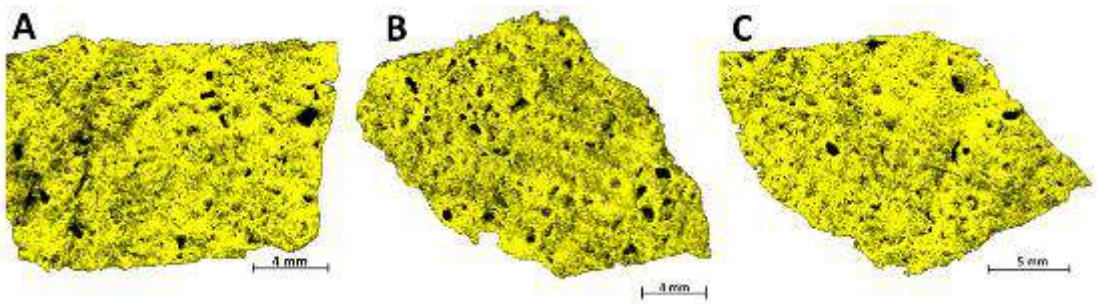

Fig. 11.9. Iron distribution XRF maps (in yellow) in A, B and C fragments.

As shown in Fig. 11.9, as it was expected, Fe is homogeneously distributed in the fragments. However, at the microscopic scale, some areas did not show high Fe signal while some others showed higher intensity. In this way, as the goethite content was higher in those areas, the transformation into hematite could be better monitored. Therefore, those areas were selected and marked as squares (sizes of around 4x4 mm) with a scalpel.

Apart from Fe, other elements such as Na, Mg, Al, Si, P, S, K, Ca, Ti, V, Cr, Mn, Fe, Co, Cu, Zn, As, Sr and Pb were also detected (see Fig. 11.10). In addition to those, a diffraction peak appeared at 10.1 keV (marked with an asterisk in Fig. 11.10E) due to the use of the poly-capillary lens of the instrument.

The obtained XRF map of fragment B (see sum spectrum of the analyzed area in Fig. 11.10E) was representative for all the considered samples, since the same elements were detected in the nine mapped fragments. Thanks to these elemental analyses, some heterogeneities in the fragments under study were observed. In this sense, as shown in Fig. 11.10B the elemental distribution of P showed some hotspots in which this element was distributed in a higher extend. The presence of P could be related with phosphate deposition coming from the soil of the burial in contact with the fragments for thousands of years. In this way, some areas could be enriched in certain elements such as P, Na or K.

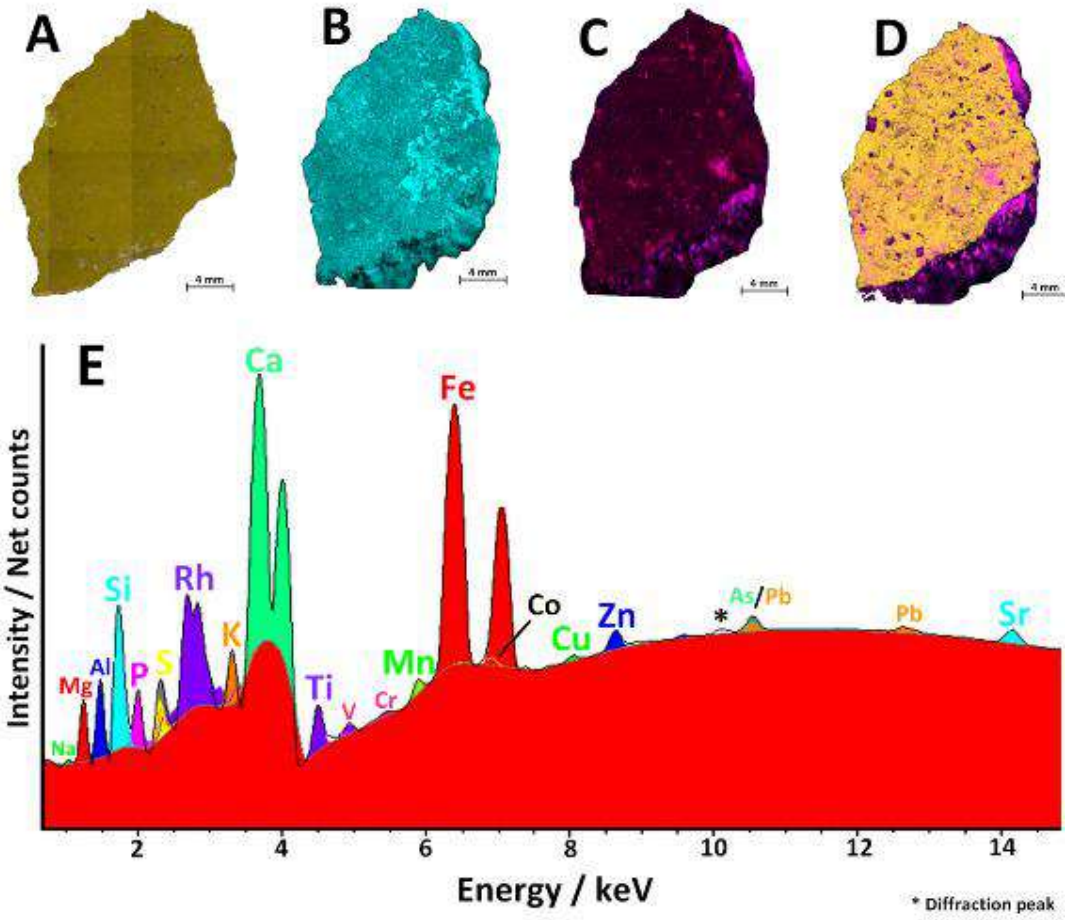

Fig. 11.10. A) Optical image of Fragment B collected as mosaic under the video-camera of the instrument and elemental distribution maps of B) phosphorus (blue), C) potassium + silicon (blue + red = purple), D) iron (yellow), silicon (red) and aluminum (blue) and E) sum XRF spectrum of the analyzed area. * Diffraction peak.

Moreover, as shown in Fig. 11.10C-D, in the fragment specific areas rich in Al, Si and K were also observed. This could be due to the presence of some potassium alumino-silicates like feldspars (e.g. $KAlSi_3O_8$) coming from the burial, which might be stuck to the fragment. Besides, some Si-rich hotspots (Fig. 11.10D) matched with the presence of quartz in the surface of the analyzed fragment. These detected areas with contributions of the soils and volcanic materials from the burial were avoided for the Raman imaging monitoring, in order to prevent from contaminations of the yellow ochre pictorial layer.

11.5.2 Molecular characterization of the fragments before thermal ageing by means of Raman Imaging

To obtain goethite (α-FeOOH) distribution maps before the thermal ageing, Raman image acquisitions were performed in different areas of the fragment, selected according to the previously obtained μ-EDXRF results. The maps were acquired in the 100-1300 cm^{-1} spectral region, the fingerprint area of goethite. To obtain the molecular distribution images, the spectral dataset was represented according to the signal-to-baseline of the main band of goethite centered at 397 cm^{-1}, and the main band of calcite at 1086 cm^{-1} (see Fig. 11.11).

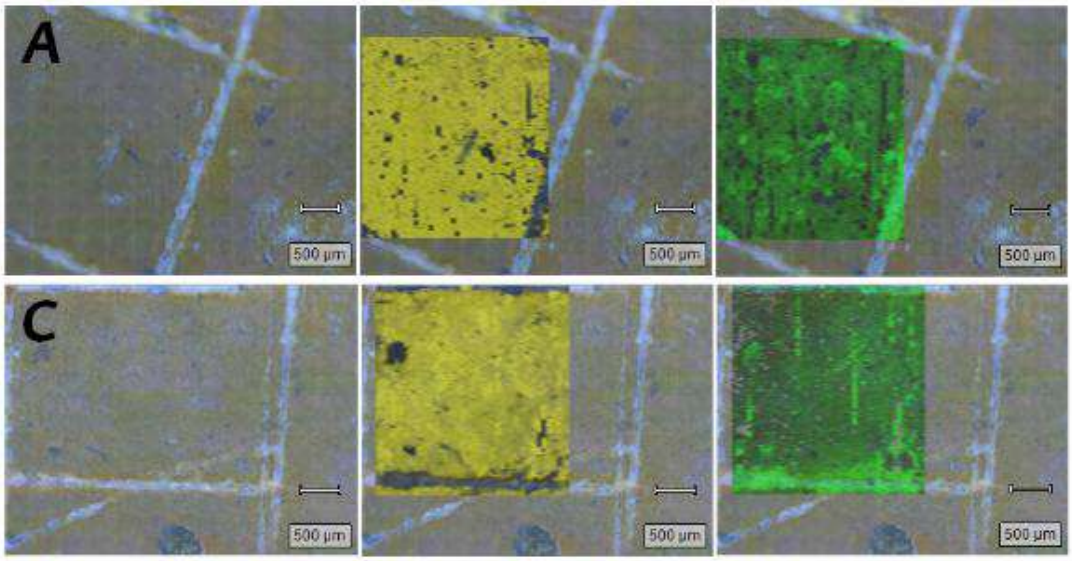

Fig. 11.11. Optical image of the analyzed area (x20, left), distribution maps of goethite (yellow, middle) and calcite (green, right) acquired by Raman microscopy in fragments A and C.

The goethite and calcite distribution images acquired in fragments A and C are shown in Fig. 11.11 as representative images of all the acquired Raman mappings. As it can be seen in this last figure, goethite is homogeneously distributed in the selected areas, except in the lines marked with the scalpel where the goethite pigment was removed.

In these lines the calcite belonging to the render mortar (*intonaco*) was observed. In the yellow pigment area, calcite was also detected in specific points. This calcium carbonate can be related with the calcite acting as the binder of the pigment grains in the *intonacchino*.

In the measured areas hematite (α-Fe_2O_3) was not detected, discarding its presence in the studied pictorial layer. In addition, quartz (α-SiO_2) was also identified in some spots of the surface of the fragments, which came in agreement with the acquired elemental distribution maps showed in Fig. 11.10.

11.5.3 Raman imaging quantification of goethite transformation degree as a function of thermal impact

After the successfully thermal ageing experiments at different temperatures of the different yellow ochre fragments (Fig. 11.3), different areas of the transformed fragments were analyzed by means of Raman microscopy following an imaging strategy. Thanks to this study, the quantitative transformation of goethite into hematite was determined at each exposed temperature. The used conditions were the same in all cases: 0.5 s and 1 accumulation acquired in 100-1350 cm^{-1} spectral region. Spectra were acquired every 20 μm in both directions of the image (step size). After the Raman image was acquired, baseline correction, smoothing and cosmic ray removal were applied to all the set of spectra to avoid problems arising from the background of the spectra, which in this case showed some fluorescence.

The Raman quantitative analysis was performed by means of Direct Classical Least Squares (DCLS) algorithm. It is based on the comparison of each spectrum acquired in the map with the spectrum of goethite and hematite standards acquired in the same conditions. The scaling factor is automatically selected to fit as best as possible with the

spectra of the Raman map. For that, four different images were acquired before and after the thermal exposure in different areas in order to obtain the average value with its 95% confidence interval. To validate the quantitative methodology, synthetic pellets using different amounts of hematite and goethite standards (50/50%, 25/75% and 75/25% w/w, hematite/goethite) were prepared. The accuracy and precision of the quantitative results based on Raman imaging and using different magnification lenses are shown in Table 10.1.

Table 10.1 Quantitative results (average concentration in w/w % together with the 95% confidence interval in weight percentage unit) obtained for the hematite/goethite synthetic standards employing the Raman imaging quantitative method.

Real Hematite/Goethite w/w %	Hematite/Goethite w/w % 50x objective lens	Hematite/Goethite w/w % 20x objective lens	Hematite/Goethite w/w % 5x objective lens
25/75	23.5 ± 2.2 / 76.5 ± 7.3	23.8 ± 0.3 / 76.2 ± 1.0	23.4 ± 0.1 / 76.6 ± 0.4
50/50	48.8 ± 5.2 / 51.2 ± 5.5	49.8 ± 1.1 / 50.2 ± 1.1	48.9 ± 0.8 / 51.1 ± 0.9
75/25	77.8 ± 10.3 / 22.2 ± 2.9	77.3 ± 1.7 / 22.7 ± 0.5	77.1 ± 1.5 /22.9 ± 0.4

Notice that the 95% confidence interval connected to the estimated concentrations using the objective lens of 50x magnification was high (up to 10.3%). This increase of the error using the highest magnification objective lens could be related with the heterogeneity in the surface of the pellets at the lateral resolution achieved with this objective lens (around 20 μm). In Fig. 11.12 a microscopic image acquired using the 50x objective lens is presented to show that the grains of goethite and hematite mixed to prepare this pellets are heterogeneously distributed at the scale of 20 μm.

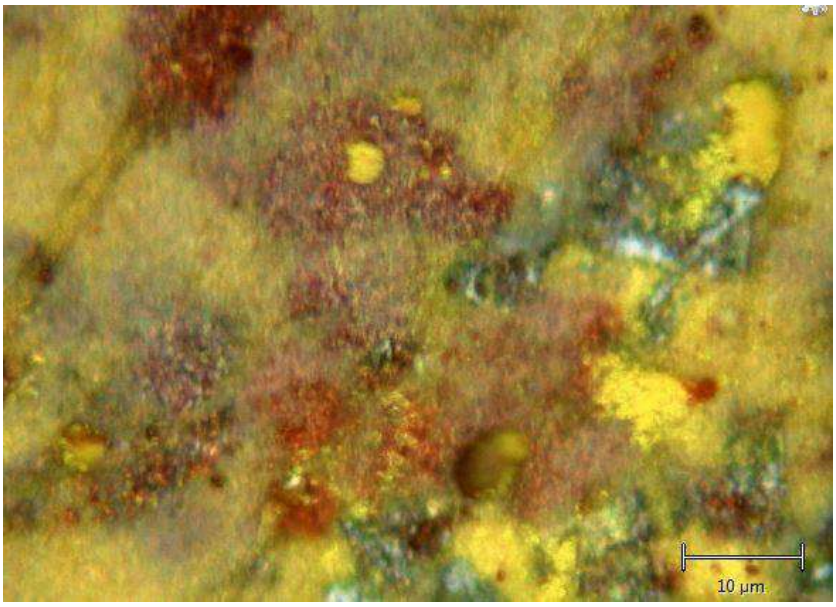

Fig. 11.12. Hematite and goethite heterogeneous distribution in the synthetic pellets observed microscopically with the 50x objective lens.

A homogeneous distribution of the compounds was not achieved since the goethite and hematite used to perform these pellets were mixed manually by grinding both compounds. To achieve a better homogenization of the mixture additional strategies such as sintering process could be applied. However, since in this last procedure heat of pressure is applied, it was totally discarded to prevent any change in the molecular composition of the original yellow ochre.

The mentioned heterogeneity includes a higher variability in the obtained quantitative result and therefore an increase in the associated error. On the contrary, the distribution of both hematite and goethite obtained using the 5x objective lens (120 µm spot size or lateral resolution) can be considered homogeneous, minimizing the uncertainty due to sampling (effective diameter spot), and reducing the error associated to the estimated result (see Table 10.1).

Considering that the heterogeneous distribution of the compounds in the synthetic pellet led to the major contribution of the error comparing with the contribution of the instrumental or methodological error itself, the selection of the objective lens for the monitoring of the thermal transformation degree quantitatively by Raman imaging will be crucial. Before this selection, it will be mandatory to verify the grain size of goethite and hematite in the fragments under study. Unlike the synthetic pellets, the pictorial layer in the fragments seems homogenous observed under the 100x objective lens (see Fig. 11.13).

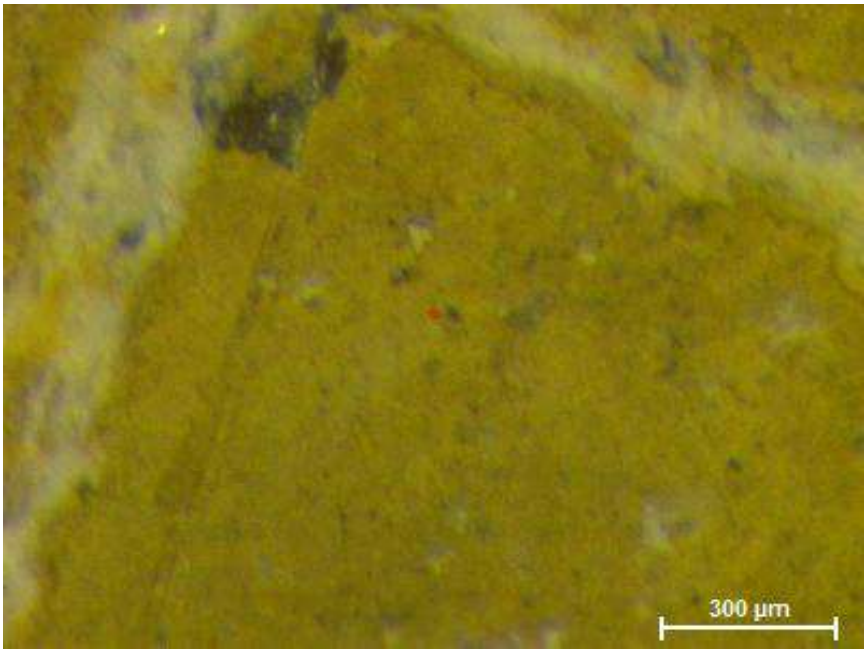

Fig. 11.13. Microscopic image (100x) of the pictorial layer of fragment A, showing the sides of the square marked with the scalpel.

Moreover, in Fig. 11.14 two SEM-EDS images showing the distribution of Fe in two selected fragments are presented. Although those areas free of marks were selected for the study it is necessary to consider that the goethite pigment grains are bounded by calcite ($CaCO_3$) in the pictorial layer (fresco painting). Calcium carbonate is represented as black holes in the EDS maps and Fe coming from goethite as white spots in Fig. 11.14,

right. Considering that the size of calcium carbonate acting as binder of the pigment grains cover areas lower than 20 μm, the pictorial layers in the fragments under study can be considered heterogeneous at lateral resolutions down to the mentioned value. Additionally, the grain size of goethite in the fragments under study was set between 3-10 μm (see Fig. 11.14).

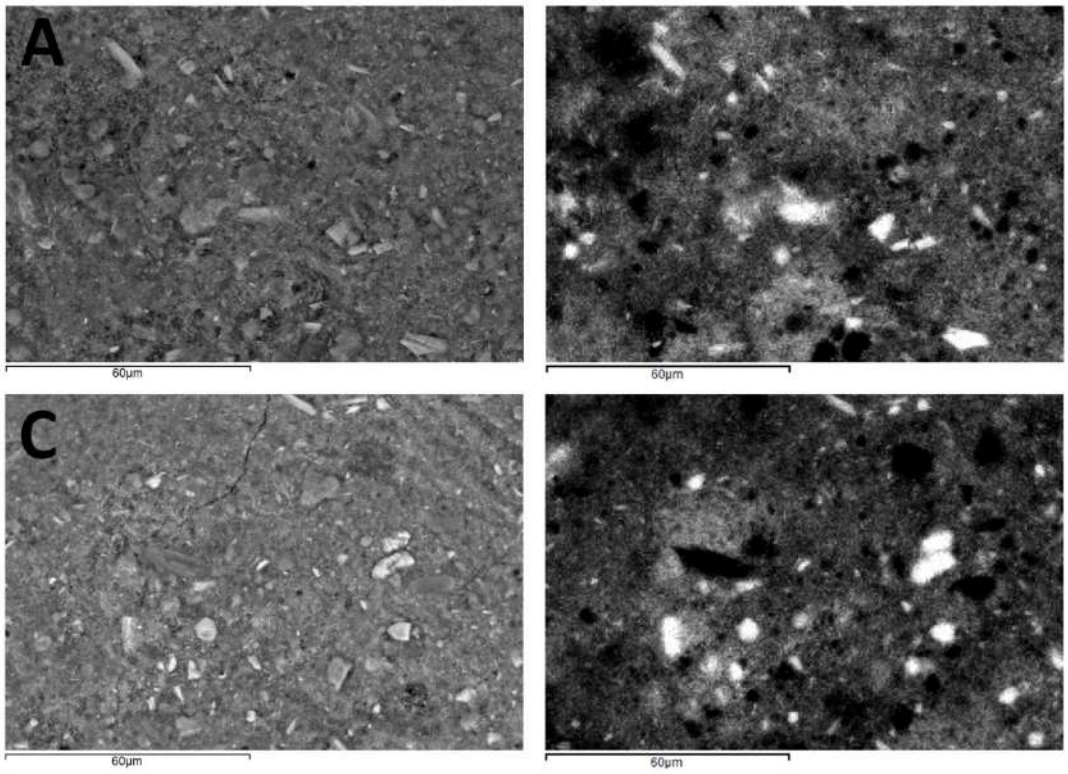

Fig. 11.14 SEM microphotographs of the pictorial layer of fragments A and C (left) and their respective EDS images (right).

Taking this into account, it was decided to use the 50x lens to acquire the Raman maps before and after the thermal impact in all the fragments. In this case, the spot size is around 20 μm (larger than the size of the individual grains of pigment), which ensures to minimize the error associated to the estimated concentration.

The molecular distribution of hematite in the exposed fragments was determined using its main band at 411 cm^{-1}. As shown in Fig. 11.15, quite homogeneous Raman images of hematite were obtained for all fragments, with except of some points inside the measured areas in which there is not pictorial layer, and therefore hematite was not present. For example, the spot in the upper-left side of fragment E where there was not hematite corresponds to a spot in which there was not any color (see Fig. 11.15), and thus, calcite was detected in the Raman image.

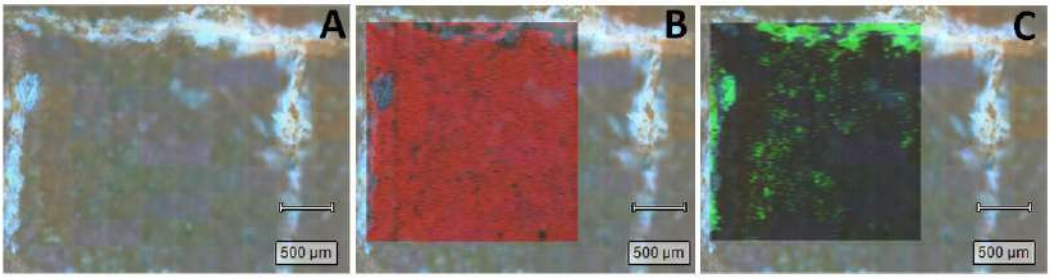

Fig. 11.15 (A) Optical image of the analyzed area (x50, left), (B) hematite distribution map and (C) calcite distribution map in fragment E aged at 300°C.

These areas showing calcite were avoided for the goethite/hematite concentration calculations. In this sense, areas where the presence of calcite was the minimum one, or even negligible, were selected not to distort the quantitative results. Four different frames of 1 mm x 1mm were analyzed and considered for the quantitative calculations. The obtained transformation percentages of goethite into hematite at different temperatures are presented in Fig. 11.16, showing the corresponding uncertainties.

As shown in Fig. 11.16, the transformation of goethite into hematite seems to start at temperatures around 200°C. At this temperature, a very small transformation of goethite into hematite (0.5 ± 0.4%) was observed. To check if the exposure time has some influence in the transformation process, further thermal ageings were conducted at longer exposition times (3, 4, 5, 6 and 7 hours) at 200 °C to observe if a longer time of exposition at this temperature increase the transformation.

In this case, additional transformation was not observed. Therefore, it can be assumed that the key factor to promote the transformation of goethite into hematite is the temperature and not the exposure time during the thermal impact.

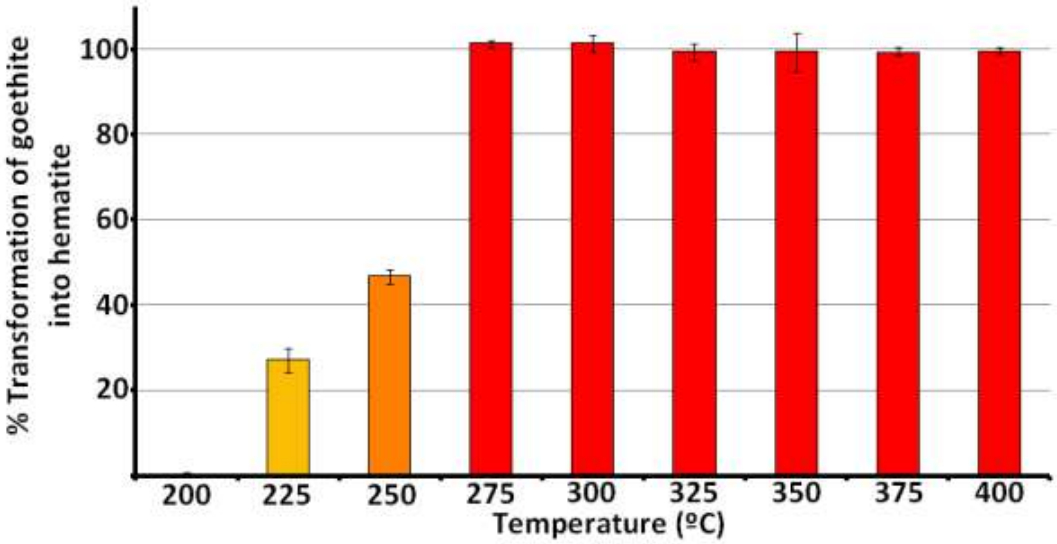

Fig. 11.16 Transformation of goethite into hematite degree (w/w %) at increasing temperatures with the standard deviation of the different measurements.

At the ageing temperature of 225°C some reddish hues were observed at the naked eye (see Fig. 11.3), and a transformation into hematite of 26.9 ± 2.8% was determined by the quantitative Raman imaging methodology (see Fig. 11.16). After the transformation had started in the interval of 200-225°C, the highest increase takes place at temperatures between 225-275°C maintaining stable from 275 up to 400 °C. These results suggest that the thermal transformation is completed at 275°C because from this temperature up to 400°C, the obtained transformation values did not show any significant variation (46.7 ± 1.7% at 250°C; 101.1 ± 1.2% at 275°C; 101.2 ± 1.9% at 300°C; 99.2 ± 1.9% at 325°C; 99.3 ± 4.4% at 350°C; 99.4 ± 0.6% at 375°C; 99.6 ± 0.8% at 400°C). These results come in agreement with the ones obtained in the reflectance model, in which it was previously hypothesized that the fragment aged at 250 °C presented a transformation around 50%.

The fitting of the Raman spectra acquired during the Raman imaging quantitative studies, and therefore those data used to extract the transformation percentages of goethite into hematite in the fragments, was performed using the spectrum of a real Pompeian raw goethite pigment recovered from the burial. The spectrum of hematite used for the fitting was obtained by ageing the used Pompeian goethite pigment at 350 °C and therefore obtaining a hematite as similar as possible as the one present in the pictorial layer of the aged fragments under study.

To confirm to what extent the quantitative results, and therefore the calculated transformation percentages can change using different Raman spectra as standards for the fitting of the Raman spectra in the imaging study, pure goethite and hematite commercial pigment standards were also used for this purpose. The quantitative results obtained using both alternatives were similar for the fragments aged up to 250°C. However, the transformation percentages of the fragments aged from 275°C up to 400°C obtained by using the spectra acquired from the commercial pigments were of around 70%. On the other hand, as shown in Fig. 11.16, by using the real Pompeian goethite pigment, the transformation degree reached the 100%, being a more realistic result.

The high difference in the obtained quantitative transformation degree could be related with the presence of additional molecular phases at minor levels in the pictorial layer of goethite in the Pompeian wall painting fragments. Among these possible compounds, different kind of silicates such as quartz, kaolinite and illite, all of them identified in Pompeian yellow ochre pigments (see Chapter 5), can be mentioned. Considering that the composition of goethite and hematite commercial standards is almost 100% of goethite or hematite, the differences in the predicted quantitative transformation degrees can be related with the different molecular composition between Pompeian ochre pigments and commercial ones.

11.6 Conclusions

The aim of this chapter was to study the transformation of goethite into hematite in wall painting fragments from Pompeii caused by the thermal impact of the pyroclastic flows coming from the 79 AD Mount Vesuvius eruption. This is the first time in which this kind of research has been performed on real Pompeian wall painting fragments instead of using goethite pigment powders or mock ups and, therefore, obtaining the quantitative percentages of transformation depending on the specific temperature exposure.

Some of the proposed methodologies in this chapter are valid to identify, in a very easy way ,the temperatures of the pyroclastic flow that reached Pompeii without the necessity of performing more complex geochemical analyses described in the literature, such as the analysis of a high number of samples (about 200) of lava clasts by thermal remnant magnetization (TRM)[13]. Therefore, thanks to this work, yellow painted walls transformed into red can be used as a witness of the thermal impact of 79 AD Mount Vesuvius eruption, and a map of temperatures depending on the area and the orientation could be constructed.

In this sense, the thermal ageing steps were successfully performed in the yellow fragments under study and the transformation of goethite into hematite was determined both at the naked eye and in an analytical way by means of RS and Raman imaging. The temperature that marks the start of the transformation progress seems to be 200°C, because (i) in the RS classification model the group of the fragment aged at 200°C was placed at the same PC1 values than original yellow and (ii) at this temperature a transformation of only 0.5% was determined. At 225 °C a transformation of 26.9% was registered. Nevertheless, the highest transformation variation was observed in the transit from 225 up to 275°C. Thus, taking into account the results obtained, the temperature of 250°C can be assumed as the inflection temperature for the dehydration process of goethite. As quantitative values obtained by Raman imaging pointed out, at 275°C the

transformation of goethite is completed because from this temperature up to 400°C a transformation of 100% was registered. Moreover, in the RS classification model the groups of fragments aged from 275°C up to 400°C were placed together and with same PC1 values than original red fragments, suggesting the complete transformation. In this sense, the quantitative results and classification model obtained by the two different techniques came totally in agreement.

It is important to remark that the RS classification model is able not only to discriminate yellow ochres transformed into red (negative PC2 values) from original ochres (positive PC2 values), but it can also classify transformed fragments that have been exposed from the initial transformation temperature (200°C) up to the temperature at which the transformation is complete (275°C). In this sense, it can be predicted at which temperature a certain yellow ochre pictorial layer has been transformed depending on the PC1 value in which it is placed in the model. It must be remarked that this is the first time that an analytical methodology based on the use of a molecular technique is able to discriminate both red colored pigments (original and transformed one)

Moreover, it has been proven that the most important factor that promotes the thermal transformation is the temperature and not the exposure time, since the fragment aged at 200 °C did not show any additional transformation when the ageing time was increased up to 7 hours.

To obtain faithful transformation values, the adequateness of the standard to be used for the quantification Raman imaging method had to be evaluated. It was corroborated that, in this case, it was better to use a thermally aged Pompeian goethite standard than pure hematite standard because more accurate and realistic results were obtained since its composition is more similar to the pictorial layer in real wall painting fragment.

Finally, although the Raman imaging analysis has been carried out using a benchtop instrument, considering that in the last years new developments and possibilities in the in situ Raman mapping field using portable instruments will took place[15], it is feasible to think that in the near future quantitative Raman imaging methodologies will be applicable on site. Thus, this last instrumental development will permit to this methodology be transferable to a totally non-destructive perspective which will allow determining, without extracting any painting fragment, the temperature at which each goethite painted wall was impacted according to its position and orientation in the Archeological Park of Pompeii and in additional archaeological sites which suffered the impact of 79 AD eruption such as Herculaneum.

11.7 REFERENCES

1. Artioli, G. *et al.* Red/yellow pigments in Pompeii and Herculaneum: which is which?. *Acta Cryst. A*, **70**, C1401 (2017).

2. Ruan, H. D. *et al.* Infrared spectroscopy of goethite dehydroxylation: III. FT-IR microscopy of in situ study of the thermal transformation of goethite to hematite. *Spectrochim. Acta. A. Mol. Biomol. Spectrosc.* **58**, 967–981 (2002).

3. Romero Gómez, P. *et al.* Estudio in-situ de la transformación térmica de limonita utilizada como pigmento procedente de Perú. *Boletin Soc. Espanola Ceram. Vidr.* **52**, 127-131 (2013).

4. Pomies, M. P. *et al.* TEM observations of goethite dehydration: application to archaeological samples. *J. Eur. Ceram. Soc.* **19**, 1605–1614 (1999).

5. Prasad, P. S. R. *et al.* In situ FTIR study on the dehydration of natural goethite. *J. Asian Earth Sci.* **27**, 503–511 (2006).

6. de Faria, D. L. A. *et al.* Heated goethite and natural hematite: can Raman spectroscopy be used to differentiate them? *Vib. Spectrosc.* **45**, 117–121 (2007).

7. Gonçalves, Í. G. *et al.* Quantification of hematite and goethite concentrations in kaolin using diffuse reflectance spectroscopy: a new approach to Kubelka-Munk theory. *Clays Clay Miner.* **60**, 473–483 (2012).

8. Lugassi, R. *et al.* Reflectance spectroscopy of soils post-heating—Assessing thermal alterations in soil minerals. *Geoderma* **213**, 268–279 (2014).

9. Lugassi, R. *et al.* A spectral-based method for reconstructing spatial distributions of soil surface temperature during simulated fire events. *Remote Sens. Environ.* **114**, 322–331 (2010).

10. https://blogs.helsinki.fi/pompeii-project/. (Accessed: 8th October 2019)

11. Cioni, R. *et al.* Temperatures of the AD 79 pyroclastic density current deposits (Vesuvius, Italy). *J. Geophys. Res. Solid Earth* **109**, B02207 (2004).

12. Sherman, D. M. *et al.* Electronic spectra of Fe^{3+} oxides and oxide hydroxides in the near IR to near UV. *Am. Mineral.* **70**, 1262–1269 (1985).

13. Cornell, R. M. *et al.* The iron oxides: structure, properties, reactions, occurrences and uses. (John Wiley & Sons, 2003).

14. Cioni, R. *et al.* Temperatures of the AD 79 pyroclastic density current deposits (Vesuvius, Italy). *J. Geophys. Res. Solid Earth* **109**, B02207 (2004).

15. Lauwers, D. *et al.* In situ Raman mapping of art objects. *Philos. Trans. R. Soc. Math. Phys. Eng. Sci.* **374**, 20160039 (2016).

12. FINAL CONCLUSIONS AND FUTURE WORKS

In this final chapter an integrated discussion is presented, leading to the overall conclusions extracted from the work developed inside this PhD Thesis.

The works presented in this manuscript have contributed to acquire knowledge about the colors used in the ancient Pompeii. Some colors of the palette used by the Pompeian artists have been revealed thanks to the analysis of the powdered pigments recovered from the burial. In addition, the application of these pigments on different supports, such as tesserae to create mosaics, or walls to create wall paintings, has been also studied. In this sense, the most evident and noteworthy alteration of Pompeian pigments that can be appreciated nowadays in the wall paintings is the transformation of yellow ochre into red. In this PhD Thesis different methodologies capable to identify this transformation, and therefore, to differentiate original red areas from the current red areas that were originally painted in yellow have been developed. Moreover, thanks to the stable isotopes analysis, preliminary information about the alteration of the calcium carbonate acting as the binder of the wall paintings of Pompeii has been also obtained in this PhD Thesis.

To attain the proposed goals, the selected analytical techniques were able to offer the required elemental and molecular information about the composition of both, the powdered pigments and those applied on different supports (walls or floors using tesserae). In this sense, the combined use of spectroscopic techniques (handheld and/or laboratory instrumentation in each case) to characterize the studied pigments offered a deep overview about the materials that were used by the artists in the ancient city of Pompeii to create the magnificent wall paintings and mosaics. Concretely, portable/handheld spectrometers have been successfully employed to achieve this purpose. Indeed, thanks to the use of two portable Raman spectrometers, provided by 532 and 785 nm excitation lasers, and a HH-EDXRF spectrometer, the composition of the color palette used by the ancient Pompeian artists has been determined. Moreover, the results obtained with the portable instruments can be considered completely conclusive in most of the cases, offering also a cost effective instrumental option to achieve the proposed objectives. A clear example of this last, is the usefulness of portable Raman spectrometers to carry out SERS analysis, offering appropriate spectral information comparable to the one achievable with benchtop instruments such as confocal Raman microscopes.

Regarding the composition of the pigments, most of the analyzed samples revealed the use of materials of natural origin, such as clays or minerals. Indeed, red and yellow ochre pigments, together with the green malachite, the brilliant red cinnabar or white dolomite were identified in the performed in situ characterization. Apart from that, Egyptian Blue, a synthetic pigment, has been also identified. More sophisticate pigments such as madder lake pink pigment, obtained dying clays with a colorant extracted from the roots of *Rubia* plant, was also characterized. In this case, a sample treatment for the subsequent SERS analysis was optimized, including the solvent to use and its volume, the wavelength of the laser, or the lowest amount of mass to obtain conclusive results. The proposed optimized sample treatment can be used with the purpose of identifying the organic colorant present in this type of pigment. Apart from the dye, thanks to the analysis of the

inorganic mordant, it was proven that its composition was based on local clays of volcanic origin, mainly allophane.

Apart from the characterization of the inorganic and organic composition of the pigment powders, during the multi-analytical study, it was possible to verify in the ochre pigments the presence of mineral phases of volcanic origin, suggesting the local origin of most of the ochre pigments analyzed. Moreover, specific contaminations coming from other pigments detected in the analyzed ochre pigments suggest that the containers or bowls used by the artists to store the pigments were probably reused.

Most of the Pompeian pigments recovered from the burial in their original containers and studied in this PhD Thesis showed high lead concentrations, suggesting that the origin of this metal is not natural in those pigments. Thanks to the isotopic ratio analysis, it was determined that the unexpected high concentrations were related to the leaching of lead coming from the lead pipes used in the ancient water system of Pompeii. In previous works, high concentrations of lead were also detected in sediments from the area, suggesting that during the 79 AD volcanic eruption, the water system of Pompeii suffered a collapse, allowing in this sense the transfer of lead-rich waters to the ground level. Moreover, groundwater would be also able to promote subsequent leaching processes in the buried lead pipes during almost 2000 years of exposure.

The original Pompeian pigments stored in their containers were recovered from the burial in the ground level, thus according to the experimental evidences presented in this PhD Thesis, a lead enrichment of these pigments in the burial took place. These results suggest that special care should be taken with the extraction of conclusions related to the analysis of lead in these pigments. Example of this last is the lead isotope study carried out with the red and yellow ochre pigments. This study demonstrated that possible contaminations in the pigments modify the real isotopic ratio value, offering erroneous conclusions regarding the provenance of archaeological materials, such as pigments in

this case. However, to the author knowledge, the soils from the area do not show high levels of elements such as W and Sn. The identification of both metals in some specific red ochre pigments recovered from the burial could suggest the possible use of hematite ores coming from Elba Island, which show characteristic levels of both metals. Therefore, these elements in the mentioned red pigments can be considered geochemical markers that allow tracing the provenance of the mineral ore used to create specific hematite red pigments from Pompeii. However, in the future, it will be recommendable to perform W and Sn isotopic analysis with those pigments to confirm this conclusion. The obtained results should be compared with those obtained from hematite ores coming from Elba Island.

Regarding the use of pigments in mosaics, for white tesserae limestone pieces were used, without the application of any pigment. On the contrary, in the case of red and orange tesserae, hematite pictorial layer was applied over the white tesserae. In this sense, the orange color was achieved lightening the hematite with calcite. However, the black tesserae did not present pictorial layer. In fact, they were composed by silicate-bearing materials from local black colored volcanic rocks. Thus, the identification of this material in this PhD Thesis has showed the exploitation of the natural resources that ancient Pompeian artist performed to obtain the materials used for their artworks.

Isotopic studies of stable elements (carbon, oxygen and sulfur) allowed to obtain preliminary results related to the identification of degradation processes of the carbonate-based binder of the pigments of the Pompeian wall paintings by means of C and O isotopic analysis. However, in the future the C and O isotopic composition of the water extracted from the original wells of Pompeii will be conducted to confirm the contribution of the carbonates/bicarbonates of the waters in the deviation of the values extracted in real mortars and wall painting from Pompeii.

In this PhD Thesis, sulfur isotopic analysis allowed also to extract preliminary conclusions related to the origin of the sulfate salts crystallizations in the walls and wall paintings from Pompeii. In this case also, it will be crucial to establish the S isotopic value in the waters from the original wells of Pompeii, to determine if the groundwater that can migrate to the walls and wall paintings could contribute to the sulfate salts crystallizations. It is expected that this waters could be enriched in sulfates because of the leaching of the volcanic deposits from the area. Moreover, if possible, the S isotopic ratio of the SO_x present in the atmosphere of Pompeii will be also evaluated. The final experiment proposed for the near future will be also to evaluate the concentration of sulfates that can be leached from the volcanic or tephra deposits which could migrate to the walls. This experiment will allow confirming better the real input of sulfates and other ions that can migrate to the walls of Pompeii contributing in this sense to the crystallization of new salts.

With all the information extracted from the stable isotope analysis conducted in the PhD Thesis and the additional experiments that will be conducted in the near future, unequivocal conclusions about the degradation of the calcite in the mortars of Pompeii and the sources that contribute to the crystallization of sulfates in the walls will be obtained.

In the final part of this PhD Thesis, the transformation of the yellow ochre into red in the wall paintings of Pompeii has been studied. Concretely, two discrimination models have been created. On the one hand, PCA has been applied to the results obtained by a HH-EDXRF spectrometer, which allowed to identify arsenic as the elemental marker that allow to differentiate if a red area was originally painted in red (presence of As) or yellow (absence or no detection of As in yellow areas transformed into red). On the other hand, an additional discrimination model using PCA applied to the results obtained with field reflectance spectroscopy has been developed. This discrimination model not only differentiates among original red ochre and transformed yellow ochre into red painted

areas, but also is useful to predict the temperature at which the transformation took place. Therefore, two different alternatives have been proposed in this PhD Thesis for the discrimination of the original red areas and those obtained from transformation, using both elemental and molecular techniques and applying chemometrics to the results. These discrimination/prediction models can be used not only for their application to the analysis of wall paintings of Pompeii, but also for other archaeological sites that suffer the same thermal transformation such as Herculaneum. In addition, a quantitative methodology based on Raman imaging microscopy has been also developed. With this methodology it was possible not only to confirm the temperature range of yellow ochre transformation, but also to determine quantitatively the percentage of transformation of the yellow ochre as a function of the temperature impact. In this sense, the application of this methodology in the walls that present the mentioned transformation can provide useful information about the thermal impact that suffered each specific wall in the 79 AD Mount Vesuvius eruption. This information can be valuable also to extract additional information about the volcanic events that took place in the 79 AD.

Although in this PhD Thesis the proposed objectives have been covered, new ones came up during the course of this research work.

Regarding the characterization of the colorants in the Pompeian pink lake pigments using SERS, in this PhD Thesis a destructive methodology based on its extraction from the inorganic mordant has been proposed. However, considering the current restrictions in the sampling process inside the Archaeological Park of Pompeii, it could be beneficial to develop a non-invasive methodology, useful to determine the nature of the pink colorants in lake pigments used directly on wall paintings from Pompeii. In fact, during the research stay in the group *Espectroscopías de Superficie y Fotónica de Plasmones Superficiales* from the *Instituto de Estructura de la Materia* of the *Consejo Superior de Investigaciones Científicas (CSIC)*, the first steps have been taken towards the development of a SERS based-hydrogel microsampler. The firsts tests have been

demonstrated a potential ability of this kind of microsamplers to extract the colorant without modifying the polychromy of the wall paintings. In the future, additional materials for the creation of the microsamplers and tests should be conducted to verify the complete usefulness and innocuousness for the artwork.

In the discrimination model of the yellow ochre transformation into red developed using a field reflectance spectrometer, wall painting fragments thermally aged in the laboratory have been used for the creation of the model. In the next expedition of IBeA research group in 2020, the applicability of this model will be verified measuring directly different Pompeian wall paintings that show this color transformation.

APPENDIX.

SCIENTIFIC PUBLICATIONS

This PhD Thesis is based on the results presented in the scientific ISI publications that are listed below. Some of the results presented in chapters 9 and 11 will be published in the future.

- ✓ Marcaida, I., Maguregui, M., Morillas, H., García-Florentino, C., Knuutinen, U., Carrero, J. A., Fdez-Ortiz de Vallejuelo, S., Pitarch, A., Castro, K., Madariaga, J. M. Multispectroscopic and isotopic ratio analysis to characterize the inorganic binder used on Pompeian pink and purple lake pigments. *Anal. Chem.* **88**, 6395-6402 (2016).

- ✓ Marcaida, I., Maguregui, M., Morillas, H., García-Florentino, C., Pintus, V., Aguayo, T., Campos-Vallette, M., Madariaga, J. M. Optimization of sample treatment for the identification of anthraquinone dyes by surface-enhanced Raman spectroscopy. *Anal. Bioanal. Chem.* **409**, 2221-2228 (2017).

- ✓ Marcaida, I., Maguregui, M., Fdez-Ortiz de Vallejuelo, S., Morillas, H., Prieto-Taboada, N., Veneranda, M., Castro, K., Madariaga, J. M. In situ X-ray fluorescence-based method to differentiate among red ochre pigments and yellow ochre pigments thermally transformed to red pigments of wall paintings from Pompeii. *Anal. Bioanal. Chem.* **409**, 3853-3860 (2017).

- ✓ Marcaida, I., Maguregui, M., Morillas, H., Prieto-Taboada, N., Fdez-Ortiz de Vallejuelo, S., Veneranda, M., Madariaga, J. M., Martellone, A., De Nigris, B., Osanna, M. In situ non-invasive characterization of the composition of Pompeian pigments preserved in their original bowls. *Microchem. J.* **139**, 458-466 (2018).

- ✓ Marcaida, I., Maguregui, M., Morillas, H., Veneranda, M., Prieto-Taboada, N., Fdez-Ortiz de Vallejuelo, S., Madariaga, J. M. Raman microscopy as a tool to discriminate mineral phases of volcanic origin and contaminations on red and yellow ochre raw pigments from Pompeii. *J. Raman Spectrosc.* **50**, 143-149 (2019).

- ✓ Marcaida, I., Maguregui, M., Morillas, H., Prieto-Taboada, N., Veneranda, M., Fdez-Ortiz de Vallejuelo, S., Martellone, A., De Nigris, B., Osanna, M., Madariaga, J. M. In situ non-invasive multianalytical methodology to characterize mosaic tesserae from the House of Gilded Cupids, Pompeii. *Her. Sci.* **7**, 3 (2019).

- ✓ Marcaida, I., Maguregui, M., Morillas, H., Perez-Diez, S., Madariaga, J. M. Raman imaging to quantify the thermal transformation degree of Pompeian yellow ochre caused by the 79 AD Mount Vesuvius eruption. *Anal. Bioanal. Chem.* DOI: 10.1007/s00216-019-02175-5